



Faculty of Engineering & Information Technology

# Performance of New Diffuser Design for an Axial Flow Pump

By; Robert F Rosier

Masters in Engineering (Research) C03017

Supervisor: Dr Phuoc Huynh





## ***CERTIFICATE OF ORIGINAL AUTHORSHIP***

*I certify that the work in this thesis has not previously been submitted for a degree nor has it been submitted as part of requirements for a degree except as fully acknowledged within the text.*

*I also certify that the thesis has been written by me. Any help that I have received in my research work and the preparation of the thesis itself has been acknowledged. In addition, I certify that all information sources and literature used are indicated in the thesis.*

*Signature of Student:*

*Date:*



# Abstract

In an axial-flow pump unit, energy is lost from the pump system due to the swirl of the liquid between the vanes and leaving the stator. A combined stator-diffuser has been designed for the purpose to reduce this swirl and the corresponding loss of energy. Previous experimental investigations indicated that the new stator-diffuser design does reduce the swirl still present in the flow exiting from the pump unit when compared with a conventional design wherein the stator is followed by a separate diffuser. However the efficiency of the modified pump unit was slightly reduced. One of the reasons for this reduction in efficiency has been identified where a sudden enlargement at the outlet of the diffuser introduces secondary flow creating large fluid swirl.

To reduce the secondary flow dimensional, theoretical, computational fluid dynamics (CFD) and experimental measurements have been performed to determine the performance effects of the new design diffuser combined with an additional tail piece. The tail piece is fitted to the outlet of the new diffuser to eliminate the sudden enlargement. Theoretical calculations determined that the five vane impeller did not match the new diffuser, whereas the eight vane impeller did match the new diffuser design. Impellers with five and eight vanes were used during laboratory testing.

CFD and laboratory experiments were performed to verify that the tail piece addition would produce improved performance. The theory was confirmed from the experiments that the five vane impeller is not the correct impeller for use with the new diffuser with the tail piece however testing with the eight vane impeller efficiency improved by 3.9%, when compared to the standard pump test.



# Acknowledgments

Firstly I would like to thank Bruce Mackay who not only encouraged me but gave me the opportunity to return to and take up studies at university.

It has been from working with pump engineers such as Ron Palgrave, Vic Kinder, Peter Smith and David Manson whose combined engineering knowledge always encouraged me to want to know more about hydraulic design.

Thank you to Dr Phuoc Huynh who offered and gave me the opportunity to take up this research. I have learnt so much and improved my engineering capabilities during the course of this work. Thanks also to Vahik Avakian who helped with the laboratory testing, numerous test rig repairs and advice. Also thanks to Florin Voicu and Dr. Luis Moscoso from Weir for their help and advice.

Finally, thanks for the support and patience from my wife Merrin and our children Ella and Taj.



# Nomenclature

Symbol	Description	Unit
Q	Flowrate	L/s
H	Head	m
H <sub>p</sub>	Pumping head	m
H <sub>L</sub>	Head loss	m
p	Pressure	Pa
NPSH	Net Positive Suction Head	m
v	Velocity	m/s
v <sub>r</sub>	Velocity reduced	m/s
C	Absolute velocity	m/s
C <sub>m</sub>	Axial velocity	m/s
C <sub>u</sub>	Tangential absolute velocity	m/s
W	Relative velocity	m/s
W <sub>u</sub>	Tangential relative velocity	m/s
L	Lift	
C <sub>L</sub>	Lift coefficient	
D	Drag	
C <sub>D</sub>	Drag coefficient	
ρ	Density	kg/m <sup>3</sup>
g	Gravity	m/s <sup>2</sup>
η	Efficiency	
N	Rotational Speed	rpm
Ns	Specific speed	
A	Area	m <sup>2</sup>
d	Diameter	m
E	Energy	J
Re	Reynolds number	
P	Power	W
P <sub>p</sub>	Pump input power	W
P <sub>w</sub>	Pump output power	W
t	Time	s
T	Torque	Nm
U	Mean velocity	m/s
V	Volume	m <sup>3</sup>
z	Height above reference plane	m

$\lambda$	Pipe friction loss coefficient	
$\omega$	Angular velocity	rad/s
$L_r$	Impeller radial length	m
$l$	Length	m
$b$	Outlet width	m
BEP	Best efficiency point	
$F$	force	N
$m$	mass	kg
$\beta$	Outlet angle	°
$\alpha$	Inlet angle	°
$\sigma$	Solidity	



# Table of Contents

1	Introduction.....	1
2	Literature Review.....	3
2.1	General Pump Introduction .....	3
2.1.1	Pump Classification .....	3
2.1.1.1	Pump Specific Speed .....	4
2.1.2	Axial Flow Pumps.....	6
2.1.3	Axial Pump Capabilities .....	6
2.1.4	Axial Pump Assembly .....	8
2.1.4.1	Axial Flow Pump Major Components .....	10
2.1.4.1.1	Suction Bell.....	10
2.1.4.1.2	Impeller .....	11
2.1.4.1.3	Bowl (Stator) and Diffuser.....	13
2.1.5	Axial Pump Performance .....	16
2.1.5.1	Calculating Pump Performance.....	17
2.1.5.1.1	Pump Pressure.....	17
2.1.5.1.2	Pump Input Power ( $P_p$ ).....	18
2.1.5.1.3	Pump Output Power ( $P_w$ ) .....	18
2.1.5.1.4	Pump Efficiency.....	18
2.2	Theoretical Axial Pump Design .....	19
2.2.1	Velocity Triangles.....	20
2.2.2	Streamlines.....	22
2.2.3	Boundary Layer.....	22
2.2.4	Impeller Vane Shape.....	23
2.2.5	Turbulent and Secondary Flow .....	25
2.2.6	Vane Tip Clearance.....	26
2.2.7	Pump Stall.....	27
2.2.8	Impeller Design.....	29
2.2.8.1	Impeller Hub Ratio.....	29
2.2.8.2	Number of Impeller Vanes.....	30
2.2.8.3	Impeller Vane Length .....	30

2.3	Pump Stator and Diffuser.....	31
2.3.1	Diffuser Design.....	31
2.3.2	Diffuser Vane Design Theory.....	32
2.3.2.1	Diffuser Guide Vanes .....	33
2.3.2.2	Diffuser Efficiency .....	34
2.3.2.2.1	Axial Distance .....	35
2.3.2.2.2	Diffuser Vane Length and Number of Vanes .....	35
2.4	Previous Research Review .....	36
2.4.1	Previous Test Comparisons .....	36
3	Component Investigation .....	39
3.1	Part Measurement.....	39
3.1.1	Coordinate Measuring Machine (CMM).....	39
3.1.1.1	Hard Probe Measurement .....	41
3.1.1.2	Laser Probe Measurement .....	41
3.1.2	CMM Measurement Results .....	42
3.1.2.1	Original Impeller .....	42
3.1.2.2	New Impeller .....	44
3.1.2.3	Bowl Ring.....	46
3.1.2.4	New Diffuser .....	48
3.2	New Diffuser Design.....	51
3.2.1	New Diffuser Exit Profile.....	53
3.2.2	New Diffuser Design Investigations.....	55
3.2.2.1	Diffuser Efficiency .....	55
3.2.2.1.1	Axial Distance .....	55
3.2.2.1.2	Diffuser Vane Length .....	58
3.2.2.2	Diffuser Inlet Angle.....	59
3.2.2.3	Pump Speed Investigations.....	63
3.2.2.4	Increase of Impeller Blades .....	64
3.2.2.5	Flow Passage .....	65
3.3	Repair of New Diffuser .....	67
3.3.1	Diffuser Inspection .....	67
3.3.2	Flow Passage Surface Repair .....	69
3.3.3	Tail Piece Addition .....	70

3.3.3.1	Tail Piece Manufacture .....	73
3.3.3.1.1	3D Printing Process.....	73
3.4	Eight Vane Impeller Repair .....	75
3.4.1	Preliminary CMM Check.....	75
3.4.2	Paint Removal .....	77
3.4.3	Vane Repair .....	78
3.4.4	Vane Polishing .....	79
3.5	Chapter Conclusion .....	79
4	Computational Fluid Dynamics (CFD) .....	82
4.1	CFD Nomenclature .....	82
4.2	CFD Introduction.....	83
4.2.1	Continuity Equation (Mass Transfer).....	83
4.2.2	Momentum Equations .....	83
4.2.3	Total Energy Equations.....	83
4.2.4	Turbulence Equations .....	84
4.3	Research Parameters .....	85
4.3.1	Analysis Type .....	85
4.3.2	Grid Selection .....	85
4.3.2.1	Mesh Size Determination.....	88
4.3.3	Model Boundary Parameters.....	89
4.3.3.1	Boundary Inlet Input .....	89
4.3.3.2	Boundary Outlet Input .....	89
4.3.3.3	Pump Wall Boundary.....	90
4.3.4	Domains .....	90
4.4	CFD Analysis and Results .....	91
4.4.1	Five Vane Impeller Pump Configuration.....	91
4.4.1.1	Standard Pump Configuration Analysis.....	92
4.4.1.2	New Diffuser Configuration Analysis .....	95
4.4.1.3	Tail Piece Angle Analysis.....	99
4.4.1.4	Predicted Pressure Rise.....	104
4.4.2	Eight Vane Impeller Pump Configuration .....	107
4.4.2.1	Standard Pump Configuration Analysis.....	107
4.4.2.2	New Diffuser Configuration Analysis .....	109

4.4.2.3	Tail Piece Analysis .....	111
4.4.2.4	Predicted Pressure Rise .....	114
4.4.3	Analysis at Stall Flow.....	116
4.5	Further Analysis .....	117
4.5.1	Inlet Hub Modification .....	117
4.6	Alternative Diffuser Design Analysis .....	119
4.7	Chapter Conclusion .....	126
5	Experimental Investigation .....	128
5.1	Pump Testing.....	128
5.1.1	Laboratory Test Rig Layout.....	129
5.1.1.1	Original Pump Test Rig.....	129
5.1.1.2	Upgraded Refurbishment of Test Rig.....	133
5.1.2	Pump Test Configurations .....	134
5.1.2.1	Configurations A and B.....	134
5.1.2.2	Configurations C and D.....	135
5.1.2.3	Configurations E and F.....	136
5.1.3	Test Schedule.....	136
5.1.4	Test Procedure .....	137
5.1.5	Test Measurements .....	139
5.1.5.1	Flow Measurement .....	141
5.1.5.2	Measurement of Pump Power Input .....	141
5.1.5.2.1	Torque Measurement.....	141
5.1.5.3	Pump Total Head.....	143
5.1.5.4	Pump Speed .....	144
5.2	Test Results .....	144
5.2.1	Determine Test Base Results .....	145
5.2.1.1	Five Vane Impeller Test: Standard Pump.....	145
5.2.1.2	Possible Reasons for Reduced Test Performance Results .....	149
5.2.1.2.1	Impeller Bowl Ring Leakage.....	149
5.2.1.2.2	Reduced Impeller Cord Length .....	149
5.2.1.3	Eight Vane Impeller Test: Standard Pump.....	150
5.2.2	Pump Test with New Diffuser .....	154
5.2.2.1	Five Vane Impeller tests .....	155

5.2.2.2	Eight Vane Impeller Tests.....	157
5.2.3	Pump Test with Tail piece Addition .....	159
5.2.3.1	Five Vane Impeller Tests .....	159
5.2.3.2	Eight Vane Impeller Tests.....	163
5.3	Chapter Conclusion .....	166
6	Summary, Findings and Future Work .....	168
6.1	Research Summary .....	168
6.2	Research Findings.....	169
6.3	Future Work.....	171
7	Bibliography .....	172
Appendix A.	Detailed Calculations .....	175
A.1.	Detailed Calculations.....	175
A.2.	Five Vane Impeller Velocity Calculations .....	175
A.2.1.	Velocity Calculations for Five Vane Impeller .....	176
A.2.2.	Velocity Triangles for Five Vane Impeller .....	177
A.2.3.	Comparisons of Impeller Outlet Angles to New Diffuser Inlet Angles .....	178
A.3.	Six Vane Impeller Velocity Calculations .....	179
A.3.1.	Velocity Calculations for Six Vane Impeller .....	180
A.3.2.	Velocity Triangles for Six Vane Impeller.....	181
A.3.3.	Comparisons of Impeller Outlet Angles to New Diffuser Inlet Angles.....	182
A.4.	Eight Vane Impeller Velocity Calculations.....	182
A.4.1.	Calculations for Eight Vane Impeller .....	184
A.4.2.	Velocity Triangles for Eight Vane Impeller.....	185
A.4.3.	Comparisons of Eight Vane Impeller Outlet Angles to New Diffuser Inlet Angles	186
A.5.	Speed Increase .....	187
A.5.1.	Results.....	187
Appendix B.	Test Rig Assembly and Disassembly .....	191
B.1.	Initial Pump Rig Observations .....	191

B.2. Pump Disassembly Steps .....	191
B.2.1. Complete Pump Disassembly .....	191
B.2.2. Impeller Change Over .....	193
B.3. Pump Assembly Steps .....	194
B.3.1. Pump Reassembly Steps .....	194
B.3.2. Installation of Impeller only .....	196
B.4. Test Rig Tool Improvements .....	196
B.4.1. Opening and Closing the Pump .....	196
B.4.2. Impeller Installation and Removal .....	197
B.5. Pump Laboratory Issues .....	198
B.5.1. Rubber Gaskets and Debris .....	199
B.5.2. Pump Sealing and Leaking .....	199
B.5.3. Test Rig Straightening Tubes .....	200
B.5.4. Pump Assembly .....	200
Appendix C. Ultrasonic Flow Meter .....	202
C.1. Sound Path .....	204
C.2. Flow Measurement Recording .....	205
Appendix D. Laboratory Test Data .....	207
D.1. Pump Tests 1 .....	207
D.1.1. Tests 1.01 and 1.02 .....	207
D.1.2. Test 1.03 .....	208
D.1.3. Tests 1.04 and 1.05 .....	210
D.1.4. Tests 2.02 and 2.03 .....	213
D.1.5. Tests 3.01 and 3.02 .....	215
D.1.6. Tests 4.01 and 4.02 .....	218
D.1.7. Tests 4.03 and 4.04 .....	220
D.1.8. Tests 5.01 and 5.02 .....	223
D.1.9. Tests 6.01, 6.02 and 6.03 .....	225
Appendix E. CFD Models .....	228
E.1. Standard Pump Initial CFD Analysis .....	228

E.2. New Diffuser with Elongated Tail piece .....	230
E.3. Complete Diffuser Design .....	231
Appendix F. Coordinate Measurement Machine .....	237
Appendix G. Coating Data Sheet .....	239
Appendix H. Tachometer Technical Sheet .....	241
Appendix I. 3D Printer Data Sheet .....	243
Appendix J. Drawings .....	245
C163 – Impellers all Sizes, General Blade Forms	
C168 – Thin Blade Impellers Section Dimensions	
C269 – No. 8 impeller Blade Section Dimensions	
C277 – Bowl Vane Dimensions type 3-4-5-6	
C400 – Bowl Vane 6-7-8	
UTS0001 – Exit Profile Addition	
UTS0002 – Adaptor	
UTS0003 – Assembly Cone Piece	
UTS0004 – Proposed Modification (New Diffuser)	
UTS0005 – Collet Drive	
UTS0006 – Tail Piece, Base	
UTS0007 – Tail Piece, Top	
UTS0008 – Tail Piece Assembly	

## List of Figures

Figure 1 – Pump Classification Tree.....	3
Figure 2 – Specific Speed vs. Efficiency (Australian Pump Handbook, 2004) .....	4
Figure 3- Specific Speed Graph (Stepanoff, 1957) pg76 .....	5
Figure 4 – Flow Direction Axial Flow Pumps .....	6

Figure 5 – 450AX ‘Ornel’ pump, for water transfer (Installation by Weir Minerals Australia) ...	7
Figure 6 - 400AX ‘Ornel’ pump, for water transfer (Installation by Weir Minerals Australia)....	7
Figure 7 – Portable Ornel 300AX pump (Manufactured by Weir Minerals Australia).....	8
Figure 8– Typical Arrangement of an Ornel Axial Flow Pumps (Nelson, n.d.) .....	9
Figure 9 – Existing pump used in this research.....	10
Figure 10 – Suction Bell used in the research .....	10
Figure 11 – Recommended Bell Diameter (Institute, 1994) pg30.....	11
Figure 12 – Five vane open impeller used in the research .....	12
Figure 13 – Vane Angle .....	12
Figure 14 – Stator and Diffuser arrangement .....	14
Figure 15 – Original Pump Curve for a 300AX ‘Ornel’ pump running at a speed of 1465rpm (Weir Minerals Australia 1990).....	15
Figure 16 – Typical Axial Flow Pump performance curve - sourced from (Lazarkiewicz, 1965) pg404 .....	16
Figure 17 – One-dimensional flow through an Axial Flow Pump impeller (Lazarkiewicz, 1965) pg222 .....	19
Figure 18 – Development of an Ornel five vane impeller .....	20
Figure 19 – Velocity triangles for single pump stage (Kovats, 1964) pg91 .....	20
Figure 20 – Velocity triangle at impeller inlet and outlet (Kovats, 1964) pg91 .....	21
Figure 21 – (a) Flow of a streamline in plane xz (b) Streamline coordinates (Munson, 2013) pg100 .....	22
Figure 22 – Airfoil description (Stepanoff, 1957) pg140 .....	23
Figure 23 – Pressure generated on impeller blade surfaces.....	24
Figure 24 – Forces acting on an airfoil Blade (Stepanoff, 1957) pg140 .....	24
Figure 25 – Turbulence Formation.....	26
Figure 26 – Secondary flow within an Axial Flow Pump Impeller (Brennen, 1994) pg71 .....	26
Figure 27 – Flow field at vane tip (Farrell, 1989) pg4 .....	27
Figure 28 – Impeller to bowl ring leakage (Stepanoff, 1957) pg202 .....	27
Figure 29 – Pump stall.....	28



Figure 30 – Pump curve stall line .....	28
Figure 31 – Hub ratio for number of vanes and l/t ratio (Stepanoff, 1957) pg145 .....	29
Figure 32 – Extended hub ratio chart showing pump used in this research.....	30
Figure 33 – Vane length reduction (Dicmas, 1987) pg108.....	31
Figure 34 – Change in pump performance (Dicmas, 1987) pg109.....	31
Figure 35 – Original Ornel pump design of a stator followed by diffuser.....	32
Figure 36 – Loss coefficient for a diffuser (Munson, 2013) pg435 .....	32
Figure 37 – Velocity triangle at impeller outlet at a streamline.....	33
Figure 38 – Detail of velocity triangle at impeller outlet and angle of guide vane inlet.....	33
Figure 39 – Diffuser design variables (Stepanoff, 1957) pg159 .....	34
Figure 40 – Velocity diagram at diffuser inlet (Stepanoff, 1957) pg157.....	34
Figure 41 – Recommended impeller vane outlet to guide vane inlet, design distance .....	35
Figure 42 – Comparison of two identical pumps with different diffusers (Lazarkiewicz, 1965)	36
Figure 43 – Previous research five vane impeller test results.....	37
Figure 44 – Comparison of test configuration ‘A’ of previous and current research of a five vane impeller standard pump (error bars set at 8%).....	38
Figure 45 – CMM (Faro arm) .....	40
Figure 46 – CMM measurement of new impeller.....	40
Figure 47 – Centre of probe to surface contact (Hi-Tech, 2010) pg3 .....	41
Figure 48 – Field of view of laser probe (FARO Technologies, 2008) .....	41
Figure 49 – Scan of Impeller.....	42
Figure 50 – 3D Model of scanned impeller .....	43
Figure 51 – Overlay of scan onto design model .....	43
Figure 52 – Comparison of impeller scan to model of original design impeller. ....	44
Figure 53 – Reduction distance of trailing edge .....	44
Figure 54 – New impeller set-up and laser scanned image.....	45
Figure 55 – Measurement of new impeller outside diameter.....	45
Figure 56 – Bowl ring CMM measurements .....	46
Figure 57 – Bowl ring runout checks.....	47

---

Figure 58 – Scan image of new diffuser .....	48
Figure 59 – 3D CAD model of diffuser.....	49
Figure 60 – Comparison Inlet Vane Tip .....	50
Figure 61 – Comparison Outlet Vane Tip .....	50
Figure 62 – New diffuser design, stator and diffuser combined.....	51
Figure 63 – Velocity streamline in a standard design ‘Ornel’ pump at midstream line, showing recirculation between diffuser vanes. ....	52
Figure 64 – Mixed flow pump flow direction .....	52
Figure 65 – New diffuser flow direction .....	53
Figure 66 – Sudden enlargement (Munson, 2013) pg435 .....	54
Figure 67 – Area measurement of diffuser outlet.....	54
Figure 68 – New diffuser CFD velocity streamline on single plane .....	54
Figure 69 – Comparison of dimensions.....	55
Figure 70 - Original standard 300AX pump configuration .....	56
Figure 71 – Measured axial distance during pump assembly between original stator and the five vane impeller .....	56
Figure 72 – Pump arrangement with new diffuser. ....	57
Figure 73 – Suction case spacer addition .....	57
Figure 74 – Possible modifications to new diffuser .....	58
Figure 75 – Diffuser vane distance from impeller centre for original pump.....	58
Figure 76 - Diffuser vane distance from impeller centre for new diffuser design.....	59
Figure 77 – Blade profiles for a five vane impeller.....	59
Figure 78 – New diffuser vane profile.....	60
Figure 79 – Mid stream velocity triangles for 6 vane impeller and standard ‘Ornel’ type VII bowl (stator).....	60
Figure 80 – Mid streamline velocity triangles for five vane impeller and new diffuser .....	61
Figure 81 – Mid stream velocity triangles for 6 vane impeller and new diffuser.....	62
Figure 82 – Performance curve showing speed increase at 1465, 1495 and 1525 rpm using a five vane impeller .....	64

Figure 83 - Mid stream velocity triangles for eight vane impeller and new diffuser.....	65
Figure 84 – Original Ornel type 5 bowl flow passage measurements .....	66
Figure 85 – New diffuser flow passage measurements.....	66
Figure 86 – Flow passage area comparison .....	67
Figure 87 – Removed diffuser pre-repairs .....	68
Figure 88 – Rust build-up and paint flaking on guide vane inlet.....	68
Figure 89 – Diffuser surfaces after sand blasting.....	69
Figure 90 – Coating being applied to surface .....	70
Figure 91 – Completed coated diffuser internals .....	70
Figure 92 – New diffuser exit area.....	71
Figure 93 – CFD comparison of pump with and without 20° tail piece .....	72
Figure 94 – Tail Piece addition to diffuser exit profile.....	72
Figure 95 - Stages of the build process (Hiemenz, 2014) pg2 .....	73
Figure 96 – 3D printed tail piece .....	74
Figure 97 – 3D print surface before sanding.....	74
Figure 98 – Sanding 3D print surface .....	74
Figure 99 – Painted eight vane impeller .....	75
Figure 100 – Damage to outlet vane tips. ....	75
Figure 101 – CMM scan of eight vane impeller vane.....	76
Figure 102 – Overlay of scan to 3D model.....	76
Figure 103 – Overlay showing vane profile.....	77
Figure 104 – Bead blasting the impeller to remove paint. ....	77
Figure 105 – Uncovered vane face damage .....	78
Figure 106 – Repair of damaged vane tips .....	78
Figure 107 – SST model blend for accurate turbulence prediction (ANSYS Inc, 2013) pg18	
Lecture 7 .....	85
Figure 108 – Types of mesh elements (ANSYS, 2013) lecture 10 pg. 33.....	86
Figure 109 – Split plane of model’s flow area mesh .....	86
Figure 110 – Grid inflation at wall boundary (Tu, 2008) pg.239 .....	87

---

Figure 111 – Internal mesh zoomed view .....	87
Figure 112 – Mesh sizing check .....	89
Figure 113 – Model domains .....	90
Figure 114 – Rotating frame of reference (ANSYS Inc, 2013) pg34.....	91
Figure 115 - CFD model of original pump configuration with five vane impeller .....	91
Figure 116 - CFD analysis of original pump configuration with five vane impeller .....	92
Figure 117 - Enlarged view of blade outlet area from Figure 116 .....	93
Figure 118 – Original pump stator design (from Weir Engineering drawing) .....	93
Figure 119 - Original pump configuration 3D streamline .....	93
Figure 120 – Original five vane pump total pressure prediction .....	94
Figure 121 – Predicted pressure rise through std. diffuser .....	94
Figure 122 - CFD analysis of new diffuser pump configuration with five vane impeller.....	95
Figure 123 - Enlarged view of blade outlet area from Figure 122 .....	96
Figure 124 – New diffuser pump configuration 3D streamline.....	96
Figure 125 – Comparison of standard pump and new diffuser design .....	97
Figure 126 – 300AX impeller drawing (Weir Minerals Australia) .....	97
Figure 127 – Addition of open area to impeller model .....	98
Figure 128 – Modified model 2D streamline .....	98
Figure 129 – New Diffuser five vane pump total pressure prediction.....	99
Figure 130 – Determination of start angle for analysis .....	100
Figure 131 – The different CFD models analysed. Range from the new diffuser with tail piece added at various angles.....	100
Figure 132 – 2D streamlines of tail piece angle analysis .....	101
Figure 133 – CFD analysis of tail piece addition configuration with five vane impeller.....	102
Figure 134 – Enlarged view of blade outlet area from Figure 133.....	103
Figure 135 – Comparison of new diffuser and tail piece addition 3D streamline .....	103
Figure 136 - Predicted outlet pressure for tail piece addition, plane plot at probe point.....	104
Figure 137 – Planes created for pressure section measurements.....	105
Figure 138 - Predicted pressure through new diffuser with five vane impeller .....	105

Figure 139 - Predicted pressure rise through new diffuser .....	106
Figure 140 – Predicted pressure rise through new diffuser with tail piece .....	106
Figure 141 - CFD analysis of original pump configuration with eight vane impeller .....	107
Figure 142 - Enlarged view of blade outlet area from Figure 141 .....	107
Figure 143 - Original pump configuration 3D streamline .....	108
Figure 144 – Overlay of velocity streamline and total pressure .....	108
Figure 145 – Original eight vane pump pressure prediction.....	109
Figure 146 - CFD analysis of new diffuser pump configuration with eight vane impeller .....	109
Figure 147 - Enlarged view of blade outlet area from Figure 146.....	110
Figure 148 - New diffuser pump configuration 3D streamline.....	110
Figure 149 – Predicted pressure at new diffuser outlet.....	111
Figure 150 - CFD analysis of tail piece addition configuration with eight vane impeller .....	112
Figure 151 - Enlarged view of blade outlet area from Figure 150.....	112
Figure 152 - Predicted outlet pressure for tail piece addition .....	112
Figure 153 – Comparison of new diffuser and tail piece addition 3D streamline .....	114
Figure 154 - Predicted pressure rise through new diffuser .....	114
Figure 155 - Predicted pressure rise through new diffuser with tail piece.....	115
Figure 156 - Predicted pressure through new diffuser with eight vane impeller .....	115
Figure 157 – Test comparison 2D velocity streamlines at 234 L/s.....	116
Figure 158 – Test comparison total pressure at 234 L/s .....	117
Figure 159 – Impeller hub face open area model modification .....	118
Figure 160 – Impeller hub face open area model modification 3D streamline.....	118
Figure 161 – Layout of diffuser re-design number 1 .....	120
Figure 162 - Layout of diffuser re-design number 2.....	120
Figure 163 – Layout of diffuser re-design number 3 .....	121
Figure 164 – Layout of diffuser re-design number 4 .....	121
Figure 165 – Flow passage area measurements.....	122
Figure 166 – 2D velocity streamlines of re-designed diffuser .....	123

Figure 167 – Total pressure plots for re-designed diffuser.....	124
Figure 168 – 3D velocity streamline plots for re-designed diffuser.....	125
Figure 169 – Refurbished hydraulics laboratory pump test rig at UTS.....	129
Figure 170 – Test Rig Layout.....	130
Figure 171 – Straightener pipe section.....	130
Figure 172 – Pipe internals showing straightener section .....	131
Figure 173 – Pump installation arrangement for Test no.1 .....	131
Figure 174 – Main air release valve chamber.....	132
Figure 175 – Throttle Valve .....	133
Figure 176 – Upgraded test rig.....	134
Figure 177 – New control panel .....	134
Figure 178 – Pump assembly configurations A & B.....	135
Figure 179 – Pump assembly configuration C & D .....	135
Figure 180 – Pump assembly configuration E & F .....	136
Figure 181 – Pressure release valve .....	137
Figure 182 – Valve notch indicator (a) full notch (b) half notch.....	138
Figure 183 – Conducting test 5.01.....	139
Figure 184 – Blank pump test sheet .....	140
Figure 185 – Plummer block supports.....	141
Figure 186 – Arm and force gauge .....	142
Figure 187 – Test rig VSD .....	142
Figure 188 – Digital pressure gauges .....	143
Figure 189 – Mercury manometer and replacement hand held manometer .....	144
Figure 190 – Comparison of Pump Tests 1.04 and 1.05 .....	147
Figure 191 - Test 1.04 Pump Test Performance Curve .....	148
Figure 192 – Difference in impeller chord length .....	149
Figure 193 – Difference in impeller shape .....	150
Figure 194 – Original pump assembly .....	152

Figure 195 - Test 2.02 pump test performance curve .....	153
Figure 196 – Impeller running gap check, new diffuser installation .....	154
Figure 197 – Installed pump with new diffuser .....	154
Figure 198 – Five vane impeller base test to new diffuser comparison.....	156
Figure 199 - Pump test results 4.03.....	157
Figure 200 - Eight vane impeller base test to new diffuser comparison .....	158
Figure 201 – Preassembly of tail piece, in two steps .....	159
Figure 202 – Tail piece assembly .....	159
Figure 203 – Impeller running gap check for five vane impeller.....	160
Figure 204 - Test 5.02 performance curve .....	161
Figure 205 - Five vane impeller, base test to new diffuser and tail piece comparison .....	162
Figure 206 - Test 6.01 performance curve .....	164
Figure 207 - Eight vane impeller, base test to new diffuser and tail piece comparison.....	165
Figure 208 – Impeller streamlines .....	175
Figure 209 - Overlay of five vane impeller AA, BB & CC streamlines .....	175
Figure 210 – Velocity Triangle, Streamlines AA, BB & CC, Five Vane Impeller Inlet .....	177
Figure 211- Velocity Triangle, Streamlines AA, BB & CC, Five Vane Impeller Outlet .....	177
Figure 212 – Streamline AA of five vane impeller and new diffuser inlet.....	178
Figure 213 - Overlay of impeller no.6 AA, BB & CC streamlines.....	179
Figure 214 - Velocity Triangle, Streamlines AA, BB & CC, Six Vane Impeller Inlet.....	181
Figure 215 - Velocity Triangle, Streamlines AA, BB & CC, Six Vane Impeller Outlet .....	181
Figure 216 – Streamline AA of Six vane impeller and new diffuser inlet.....	182
Figure 217 - Overlay of Eight Vane Impeller AA, BB & CC streamlines .....	183
Figure 218 – Velocity Triangle, Streamlines AA, BB & CC, Eight Vane Impeller Inlet.....	185
Figure 219 - Velocity Triangle, Streamlines AA, BB & CC, Eight Vane Impeller Outlet.....	185
Figure 220 - Streamline AA of eight vane impeller and new diffuser inlet.....	186
Figure 221 – Comparison of velocity triangles running at 1465 rpm and 1525 rpm. ....	188
Figure 222 – Performance curve showing speed increase at 1465, 1495 and 1525 rpm .....	189

Figure 223 – Open dismantling joint.....	191
Figure 224 – Pump assembly.....	192
Figure 225 – Attachment of cable winch.....	192
Figure 226 – Removal of suction case.....	193
Figure 227 – Impeller Removal.....	193
Figure 228 – Diffuser and tail piece installation .....	194
Figure 229 – Impeller installation .....	195
Figure 230 – Lever to close pump assembly .....	195
Figure 231 – Assembled dismantling joint.....	196
Figure 232 – Stud and nut collet removal.....	197
Figure 233 – Backing plate modification .....	197
Figure 234 – Collet drive.....	198
Figure 235 – Damaged sealing face of bowl ring.....	199
Figure 236 – Leakage and repair at spool piece .....	200
Figure 237 – Impeller installation with no running gap .....	201
Figure 238 – Damage to new diffuser .....	201
Figure 239 – Path of Ultrasonic Signal (User Manual UMF601V1-1EN Ultrasonic Flowmeter, 2008).....	202
Figure 240 – Transit time difference (User Manual UMF601V1-1EN Ultrasonic Flowmeter, 2008).....	202
Figure 241 – Ultrasonic flowmeter installation .....	203
Figure 242 – Flowmeter transducer sound path .....	204
Figure 243 – Mounting of transducer .....	205
Figure 244 – Flow data for test 1-01. ....	205
Figure 245 – Test point 1, test 1-01 .....	205
Figure 246 – Flow results test points for test 1-01 .....	206
Figure 247 – Test curve, Tests 1-01 and 1-02 .....	208
Figure 248 – Pump test curve 1.03 .....	210
Figure 249 - Comparison of pump tests 1.04 and 1.05.....	212



Figure 250 - Comparison of pump tests 2.02 and 2.03 .....	214
Figure 251 - Comparison of pump tests 3.01 and 3.02 .....	216
Figure 252 - Test 3.02 performance curve compare to original design. ....	217
Figure 253 - Comparison of pump tests 4.01 and 4.02 .....	219
Figure 254 - Comparison of pump tests 4.03 and 4.04 .....	221
Figure 255 - Test 4.03 performance curve compared to original design curve .....	222
Figure 256 – Comparison of pump tests 5.01 and 5.02 .....	224
Figure 257 - Comparison of pump tests 6.01, 6.02 and 6.03 .....	227
Figure 258 – STT analysis, fine mesh, inlet: mass flow rate, outlet: 90 kPa, probe pressure point suction: 23.6 kPa, discharge: 94.1 kPa.....	228
Figure 259 – k-e analysis, medium mesh, inlet: mass flow rate, outlet: 90 kPa, point probe point suction: 27 kPa, discharge: 93 kPa.....	228
Figure 260 - k-e analysis, coarse mesh, inlet: mass flow rate, outlet: 90 kPa, point probe point suction: 27.5 kPa, discharge: 93.5 kPa.....	229
Figure 261 - SST analysis, fine mesh, inlet: mass flow rate, outlet: mass flow rate, point probe point suction: -48.5 kPa, discharge: 22.6 kPa .....	229
Figure 262 - SST analysis, fine mesh, inlet: mass flow rate, outlet: 90 kPa, point probe point suction: 23.6 kPa, discharge: 94.14 kPa.....	229
Figure 263 - SST analysis, fine mesh, inlet: 100 kPa, outlet: mass flow rate, point probe point suction: 100 kPa, discharge: 172.1 kPa.....	230
Figure 264 – Elongated tail piece 2D velocity streamlines.....	230
Figure 265 –Elongated tail piece total pressure and 2D velocity streamlines .....	231
Figure 266 – 2D velocity streamline plot for new design number 1 .....	231
Figure 267 – Total pressure plot for new design number 1 .....	231
Figure 268 – New design number 1, shroud and hub outline .....	232
Figure 269 – Vane profile for new design number 1 .....	232
Figure 270 – Vane profile alignment design number 1.....	233
Figure 271 - New design number 2, shroud and hub outline .....	233
Figure 272 - 2D velocity streamline plot for new design number 2 .....	234
Figure 273 – Total pressure plot for new design number 2 .....	234

---

Figure 274 – Zoom view of Figure 273.....	234
Figure 275 - New design number 3, shroud and hub outline.....	235
Figure 276 - Vane profile for new design number 3 .....	235
Figure 277 - 2D velocity streamline plot for new design number 3 .....	236
Figure 278 – Total pressure plot for new design number 3 .....	236
Figure 279 - Zoom view of Figure 278 .....	236
Figure 280 – Coating data sheet .....	240

## List of Tables

Table 1 – Impeller to stator assembly.....	13
Table 2 – Comparison of five vane impeller outlet velocity to new diffuser inlet .....	61
Table 3 - Comparisons of 6 vane impeller outlet velocity to new diffuser inlet .....	62
Table 4 – Comparison of an eight vane impeller to the new diffuser.....	65
Table 5 - Standard CFX medium mesh parameters.....	88
Table 6 – Re-designed diffuser predicted total pressure .....	122
Table 7 – Pump test configurations .....	128
Table 8 – Pump test schedule .....	136
Table 9 – Pump Test Results 1.04 .....	146
Table 10 - Pump test results 2.02 .....	151
Table 11 - Pump test results 3.02 .....	155
Table 12 - Pump test results 5.02 .....	160
Table 13 - Pump test results 6.01 .....	163
Table 14 –Five vane impeller pump test comparison to base test .....	166
Table 15 - Eight vane impeller pump test comparison to base test .....	167
Table 16 – Five vane impeller velocity calculations .....	176
Table 17 – Six Vane Impeller inlet velocity calculations.....	180
Table 18 – Eight Vane Impeller inlet velocity calculations.....	184
Table 19 - Calculations of number eight impeller angles $\alpha_2$ and $\beta_3$ at 1465rpm .....	186

Table 20 – Calculations of angles $\alpha_2$ and $\beta_3$ at 1465, 1495 and 1525 rpm.....	187
Table 21 – Calculations for an increase in pump speed, for 1465, 1495, 1525 and 2000 rpm .	190
Table 22 – Pump test 1.01.....	207
Table 23 – Pump test 1.02.....	207
Table 24 – Pump test 1.03.....	209
Table 25 – Pump test results 1.04 .....	211
Table 26 – Pump test results 1.05 .....	211
Table 27 - Pump test results 2.02.....	213
Table 28 - Pump test results 2.03.....	213
Table 29 - Pump test results 3.01 .....	215
Table 30 - Pump test results 3.02.....	215
Table 31 - Pump test results 4.01 .....	218
Table 32 - Pump test results 4.02.....	218
Table 33 - Pump test results 4.03.....	220
Table 34 - Pump test results 4.04.....	220
Table 35 - Pump test results 5.01 .....	223
Table 36 - Pump test results 5.02.....	223
Table 37 - Pump test results 6.01 .....	225
Table 38 - Pump test results 6.02.....	225
Table 39 - Pump test results 6.03.....	226



# 1 Introduction

During the 1990's Mr Hugh Nelson designed a new type of diffuser for an Ornel axial flow type pump. It was designed for the purpose to introduce improved performance to Axial Flow Pumps. This type of pump is used for high flow with low head applications. It was hoped that the new diffuser design would reduce the fluid swirl which is developed within the conventional pump stator's flow passages. This swirl introduces energy losses, hence a loss in pump efficiency.

Previous laboratorial research performed using the new diffuser showed there is a hydraulic pressure increase from the inlet to the outlet of the diffuser when compared to the conventional stator, hence a possible reduction in the fluid's swirl. However the overall pump performance was less than the original equipment's manufactures (OEM) pump configuration. This was believed to be due to a sudden enlargement at the outlet of the new diffuser where swirling angle measurements were observed.

In order to determine the bottleneck of the overall performance and some possible methods that could be improved in the new class off diffuser, further work such as dimensional investigation, computational fluid dynamics (CFD) analysis and rigorous experimental procedure were necessary. Applying the three types of investigation are the purpose of this thesis to assess and improve the performance.

Due to no dimensional drawings being available to investigate the new diffusers design parameters, a coordinate measurement machine (CMM) is used to laser scan and accurately measure the critical pump components used for this research. The recorded measured data is then used to create 3D models of the components where the dimensions are compared to original design drawings of the impellers for compatibility. The models dimensions are also checked against theoretical design literature to determine the components designed parameters and define their suitability to perform with pump components.

The 3D models are required to build a number of different model configurations for CFD analysis. For this thesis, CFD turbulence modelling is being used to predict the fluid flow patterns and turbulence through the Axial Flow Pump. The predicted total pressures created within the pump are compared to OEM performance curves to assess the accuracy of the models to proven pump capacities. A tail piece component is to be designed and installed at the outlet of the new diffuser to reduce the previously measured fluid swirl. A CFD analysis of this area is used to predict the extent of the swirl. This information is applied with theory to create design parameters for the tail piece, which is also CFD tested before the manufacture of the piece, to evaluate the benefits of the design.

Once the tail piece design is confirmed it will be manufactured and installed into the pump. The method of manufacture of this item will be 3D printing as this will supply a component with accurate sizing and a suitable material for strength, non-corrosive properties and surface smoothness required for pump flow applications. There is also an ease of manufacture with this method, as items with complicated internals do not require core patterns for casting, difficult machining and welded fabrications.

Experimental laboratory testing is performed using the test rig located at the *University of Technology* in Sydney. Due to the out dated measurement equipment and worn pump components the test will undergo a full refurbishment. By using new pump components, upgraded measurement equipment to industry standards, as well as being installed as per Australian Standards for Performance Testing, the final performance results will produce accurate data for final assessment.'

Section 2 of this thesis gives a general introduction to pumps, theoretical pump design parameters specific to this research and a comparison of the previous research test results, to the test results of this research. The pump component investigation is examined in Section 3 where the critical dimensions of the pump items are compared to the design theory of Section 2. The detailed calculations are found in Appendix A. This will show the new diffusers compatibility with the corresponding pump components and issues with some of the design parameters of the new component. This section also outlines the repairs and repair methods required to be made to the new diffuser and existing pump components. The design of the tail piece addition is also covered. The CFD introduction, methodology and analysis results are covered in Section 4. This section also looks at the flow path and created pressures of possible concept modifications and re-designs to the new diffuser. Appendix E contains CFD models analysed which were not used for final results but needed to determine analysis parameters. A complete re-design for a diffuser to match a five vane impeller is also detailed. Section 5 discusses the hydraulics laboratory set-up, the test rig refurbishment, testing procedures and test results analysis. The pump assembly, disassembly, equipment improvements and testing issues are found in Appendix B. Detailed manufacturing, concept and reference drawings applicable to this research are found in Appendix J.

## 2 Literature Review

This chapter provides a review of literature which is relevant to this research. The topics covered are the pump characteristics such as pump classification, capabilities, assembly, performance and design theory. The design theory covered in this thesis only looks at the pump components which are relevant to this research of Axial Flow Pumps. The theory which is discussed is used in the following chapters to review the design of the components being tested. A brief review of previous research conducted on the existing pump has been added as some of the new test results are compared to the old. Previous research recommendations are also detailed in this research.

### 2.1 General Pump Introduction

The definition of a pump is a device which transports fluids to hydraulic systems by converting mechanical power to fluid power. The power is added to the fluid via an impeller, located on a shaft, which is usually driven by a motor.

#### 2.1.1 Pump Classification

Pumps fall under two main categories of: rotodynamic pumps and positive displacement pumps. Under the rotodynamic category falls the group of centrifugal pumps where the axial flow type of pump is found. A single stage axial flow is the design of pump under examination in this research.

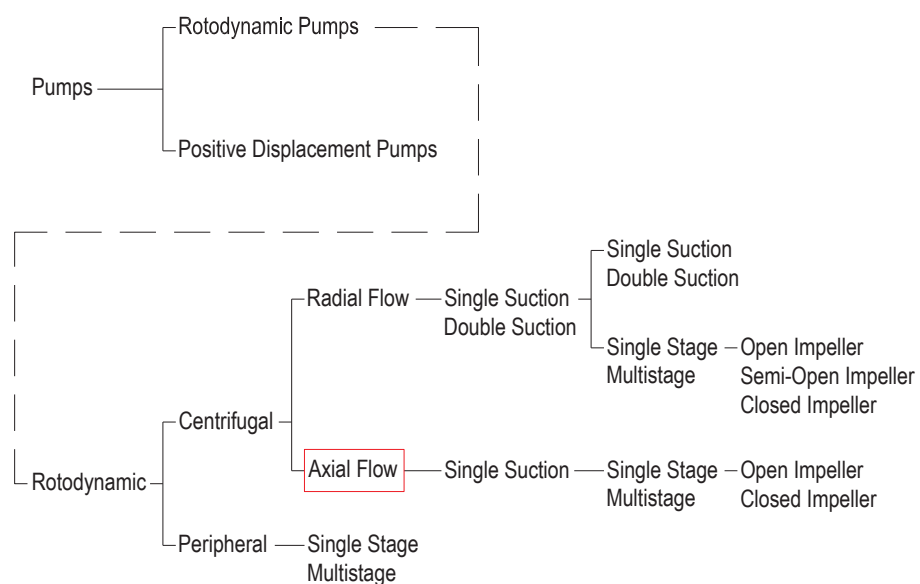


Figure 1 – Pump Classification Tree

Figure 1 is a graph which outlines the classification and where the Axial Flow Pump is positioned in the makeup of different pump designs.

Kinsky defines that centrifugal pumps use the principle that a centrifugal force is generated, whenever a body rotates in a circular path. In a centrifugal pump the centrifugal force is added to fluid by the impeller creating an increase in the fluids kinetic energy, causing the fluid to move from the inlet to the outlet of the impeller. As the fluid moves through the impeller's flow passage, its velocity increases and it is known as velocity head. The high kinetic energy is converted into pressure head by reducing the fluid's velocity being passed through the pumps diffuser or volute. The diffuser does this by the fluid moving gradually from a small sectional area to the larger sectional area, of the pump discharge.

To determine which type of pump to select from the rotodynamic group shown in Figure 1 the specific speed for the required systems duty must be firstly determined.

### 2.1.1.1 Pump Specific Speed

The specific speed is a dimensionless number used to give an indication of the type of impeller that may be used for a required head, flow and speed (the pump's duty). This is what determines what type of pump will be selected for the required system duty. Specific speed will also show the approximate shape of the pump curve as shown in Figure 3. The specific speed will remain constant for a pump design regardless of its rotating speed (Karassik, 2001).

Figure 3 shows as the specific speed increases, the angle of the pump head curve becomes steeper. Also, as the specific speed increases the efficiency of the pump increases (see Figure 2). This is because of leakage losses between the impeller and casing are less, as the flow increases (Norrie, 1963).

For example Figure 16 also shows that for an Axial Flow Pump, when at maximum power the flow is at its minimum. This means that an axial flow type of pump cannot be used under zero flow condition, as this will result in motor damage due to such factors as overheating.

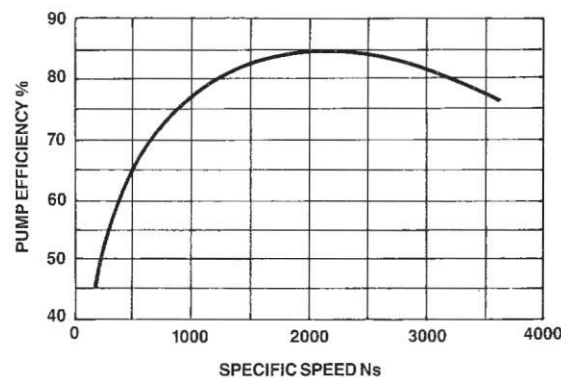


Figure 2 – Specific Speed vs. Efficiency (Australian Pump Handbook, 2004)



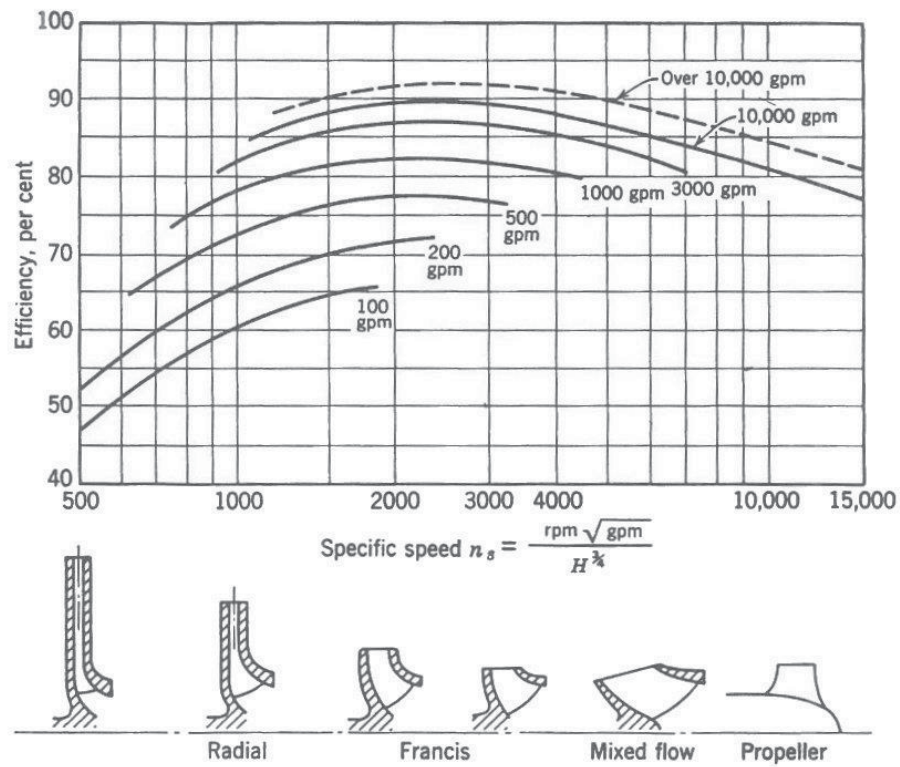


Figure 3- Specific Speed Graph (Stepanoff, 1957) pg76

The specific speed is calculated by using the following formula:

$$N_s = \frac{N\sqrt{Q}}{(gH)^{0.75}}$$

Equation 1

Where:  $N_s$  = Specific speed  
 $N$  = shaft speed (rpm)  
 $Q$  = flow (m<sup>3</sup>/s)  
 $H$  = Head (m)  
 $g$  = gravity (m/s<sup>2</sup>)

*Note: for the specific speed used in Figure 3, the numbers are not dimensionless. The dimensions used are shaft speed (rpm), flow (usgpm), head (ft) and gravity is ignored.*

As an example, the five vane impeller pump being used in this research, it's specific speed is:

$$N_s = \frac{1465\sqrt{5040.4}}{(29.2)^{0.75}}$$

$$N_s = 8280$$

This has been determined by using the best efficiency point (BEP) from the original pump curve (Figure 15) of 8.9m at 318L/s (29.2 ft at 5040.4 usgpm).

This result is consistent with the specific speed theory where a specific speed of 8280 rpm would result with selecting an Axial Flow Pump for the calculated duty.

### 2.1.2 Axial Flow Pumps

Axial Flow Pumps are also known as propeller pumps due to the impeller being open, the same as a propeller. This pump is called axial flow due to the fluid flow through the impeller in an axial direction as per Figure 4.

The pump has a basic unit known as a ‘stage’. One stage is made up of an impeller surrounded by the bowl ring, followed by a stator, then a diffuser, before being discharged into the piping system. The pump assembly configuration is detailed in Section 2.1.4.

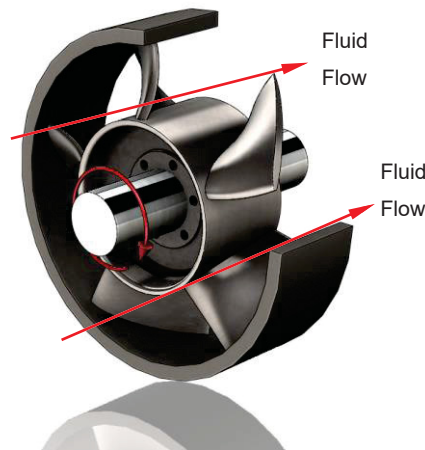


*Figure 4 – Flow Direction Axial Flow Pumps*

Unlike a centrifugal pump with less specific speed, where the impeller is generally closed and uses centrifugal force to create head pressure, the head is generated by the tangential force developed by the impeller blades. This operation creates less head, yet higher flows. Therefore to increase the head in this type of pump, an extra stage is required to be added to the pump configuration. The multiple stages operate in series as the fluid flows from the outlet from one stage into the next stage. Each added stage develops a rise in pressure but the flow remains constant. Any number of stages can be added together to achieve the required system head.

### 2.1.3 Axial Pump Capabilities

The capabilities of an Axial Flow Pump are different to that of a radial impeller type pump. Due to an axial flow type pump having high flow at a low head, compared to a radial flow impeller which has a higher head at a lower flow. Axial Flow Pumps have a maximum

efficiency when using a large diameter impeller rotating at low speeds. The flow discharge from this pump can vary from 15 L/s to 90000 L/s ( $90\text{m}^3/\text{s}$ )<sup>1</sup>.

In industry, due to its high flow capabilities, Axial Flow Pumps are widely used for water transfer purposes mostly in agricultural applications, such as irrigation from rivers or bores and drainage where pressure is not regarded as critical as the flow.

Having worked on these pumps for more than nineteen years, the author has been involved in a number of installations of both new and serviced pump assemblies for a number of different applications. Some are shown in Figure 5 to Figure 7.



*Figure 5 – 450AX 'Ornel' pump, for water transfer (Installation by Weir Minerals Australia)*



*Figure 6 - 400AX 'Ornel' pump, for water transfer (Installation by Weir Minerals Australia)*

---

<sup>1</sup> Dependent on the size of impeller and number of blades.



*Figure 7 – Portable Ornel 300AX pump (Manufactured by Weir Minerals Australia)*

### 2.1.4 Axial Pump Assembly

Figure 8 shows two typical arrangements of Axial Flow Pumps. The pump impeller is driven by a motor connected to the shaft. As the impeller rotates, fluid is sucked into the impeller's inlet via the suction bell (see Section 2.1.4.1.1) and forced through the impeller's flow passage into the stator, which has fixed guide vanes (2.1.4.1.3). This process is repeated for each stage of the pump. From the final stage stator, the fluid travels through the diffuser (2.1.4.1.3) into the column pipe leading to the discharge head, where it is delivered into the pipe system.

Figure 8 and Figure 9 show the sectional arrangement of an Ornel<sup>2</sup> 300AX pump which is being used for this research. The open line shaft or product lube pump is the arrangement assembled in the university's hydraulic laboratory. An open line shaft arrangement is where the bearings are held in place by spider couplings, resulting in the bearings being exposed to the product being pumped. Therefore, bearings are being lubricated by the fluid being pumped. Product lubricated pumps must have pre-lubrication of bearings before start-up<sup>3</sup> to prevent seizing.

The enclosed tube arrangement, also shown in Figure 8, is the preferred option when the fluid being pumped contains abrasive solids. The bearings are installed within a tube, which is fed with oil to lubricate the bearings, preventing contamination and bearing damage from the abrasives.

Figure 9 is the pump configuration of the five vane impeller with the new diffuser fitted which is assembled in the hydraulics laboratory.

---

<sup>2</sup> Brand of axial flow type pump.

<sup>3</sup> The test pump for this research is installed in a horizontal position with a fully filled closed loop constantly filled with water therefore pre-lubrication of the bearings is not required.



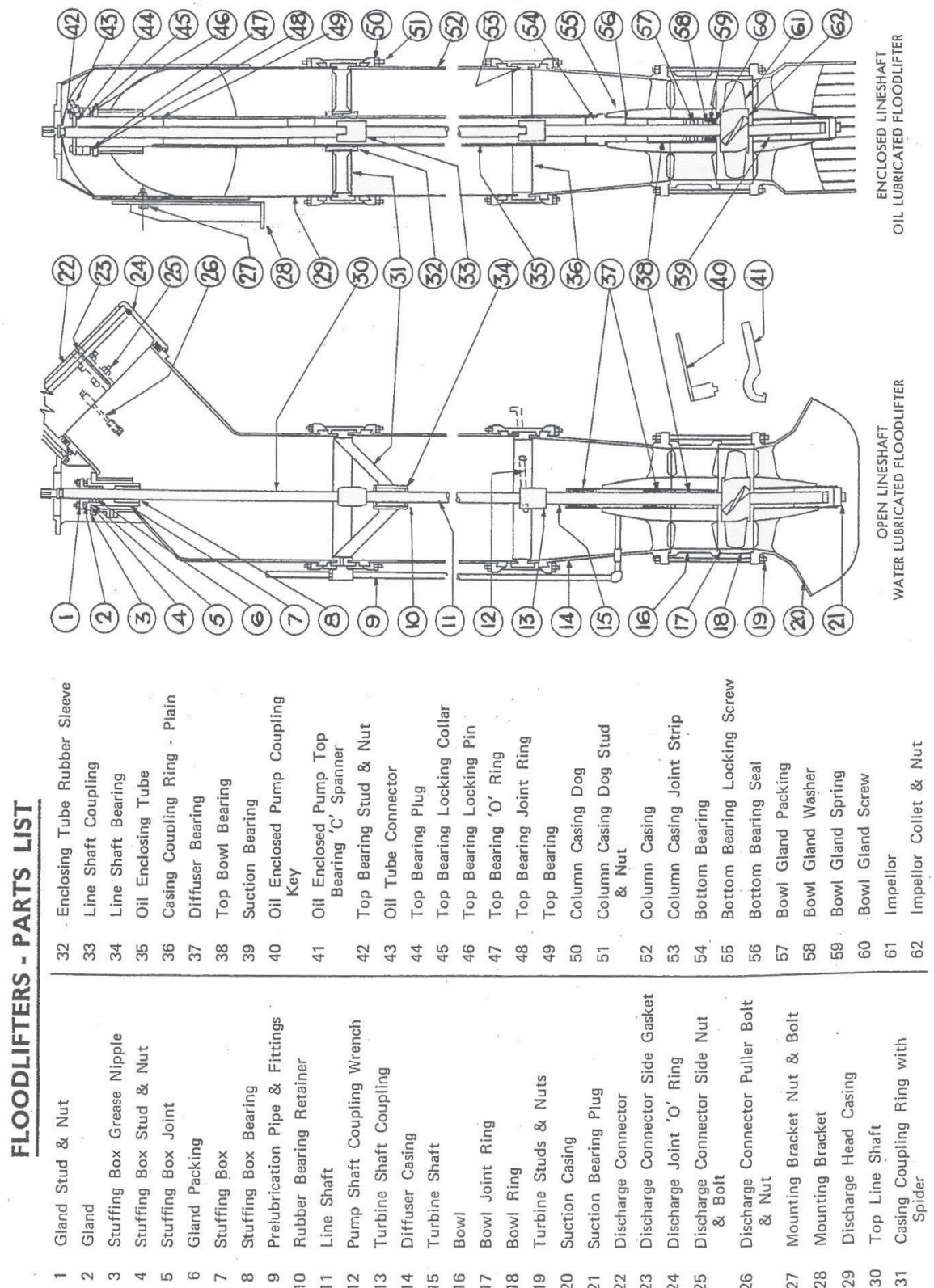
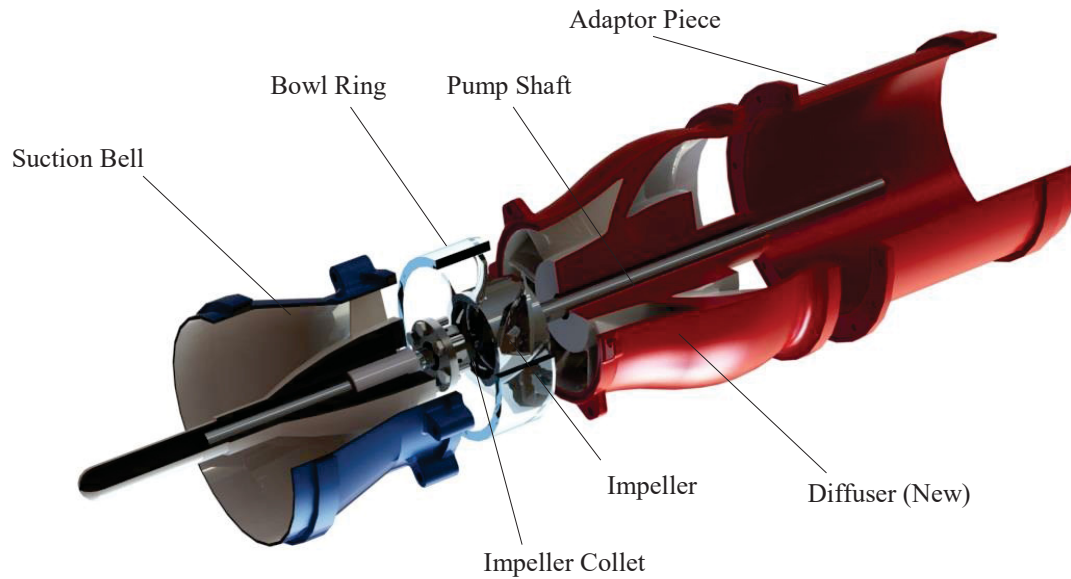


Figure 8– Typical Arrangement of an Ornel Axial Flow Pumps (Nelson, n.d.)



*Figure 9 – Existing pump used in this research.*

#### 2.1.4.1 Axial Flow Pump Major Components

The following sections give a brief description of the major components which make up the standard design of an Axial Flow Pump.

##### 2.1.4.1.1 Suction Bell

The suction bell is designed to direct fluid flow into the pump as well as to reduce the possibility of vortexes generating in the pump's suction. The bell has guide vanes which not only support the bearing housing but direct and straighten the fluid flow into the impeller. By straightening the flow direction, fluid pre-rotation into the impeller is prevented.

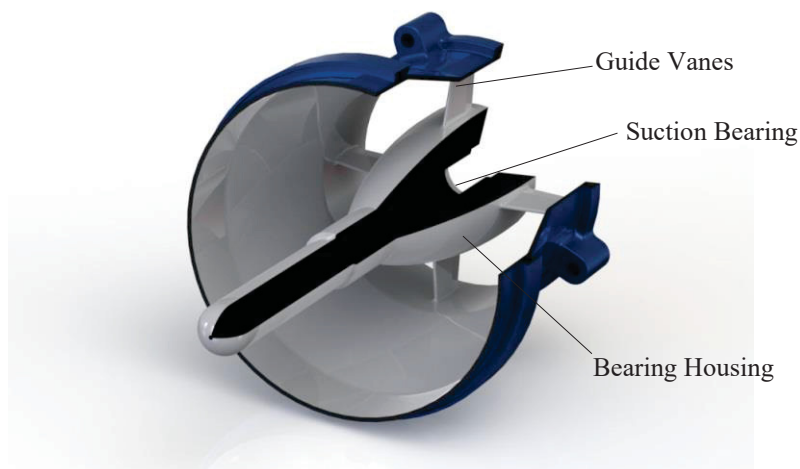


*Figure 10 – Suction Bell used in the research*

Generally the suction case is a bell shape, where the diameter is sized to ensure the fluids inlet velocity is controlled to be at a recommended tolerance to restrict the introduction of a vortex forming. The *Hydraulic Institute* recommends that for a pump operating between 315 to 1260L/s the inlet velocity should be between 0.9 to 2.4 m/s. Figure 11 is a chart showing the recommended bell diameters for the above mentioned flow rates.

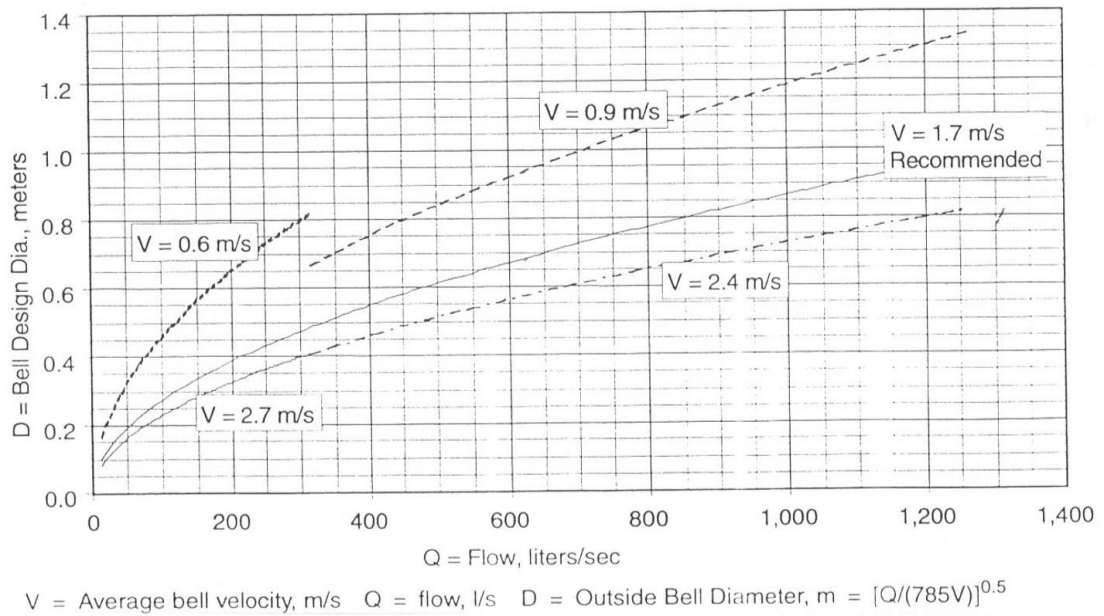


Figure 11 – Recommended Bell Diameter (Institute, 1994) pg30

However in the case of this research, the laboratory pump is installed horizontally within a closed loop, therefore it is constantly flooded and with the required NPSH controlled during testing, the required velocity is maintained and no inlet vortex is present.

#### 2.1.4.1.2 Impeller

As mentioned in previous sections, the axial flow impeller is an open type impeller, therefore not having an outer shroud to enclose the flow passage area. The open impeller rotates within a casing, or in the case of this brand of pump, a bowl ring. There is a small clearance between these two components which is looked at in detail in Section 2.2.6.

The rotating impeller adds energy to the fluid via the vanes. The fluid's velocity is increased as it is forced through the impellers flow passages.



*Figure 12 – Five vane open impeller used in the research*

The vanes of an axial-flow pump impeller are an airfoil shape (see Section 2.2.8) consisting of equally shaped and equally spaced blades on the circumference of the hub, which are inclined at an angle to the direction of rotation (Kinsky, 1982). The vane angle varies from being steep at the hub diameter ( $A^\circ$ ), to less steep at the outside diameter ( $B^\circ$ ), to give the impeller maximum efficiency, as shown in Figure 13. The number of blades determines the pump flow. It is shown in Figure 15 in the original pump curve that an increase in number of impeller vanes from three to eight, will increase the amount of flow as well as head for the pump whilst running at a constant speed, in this case 1465rpm. As the number of vanes increase, the required power to rotate the impeller will increase, resulting in a slight drop in efficiency. This is due to a larger number of vanes that reduce the impellers flow passage areas.

The impeller vane profile has little curvature which results in slight deflection of the relative velocity vector of fluid particles as it flows through the rotating passages (Logan, 1993). This is discussed in more detail in Section 2.2.

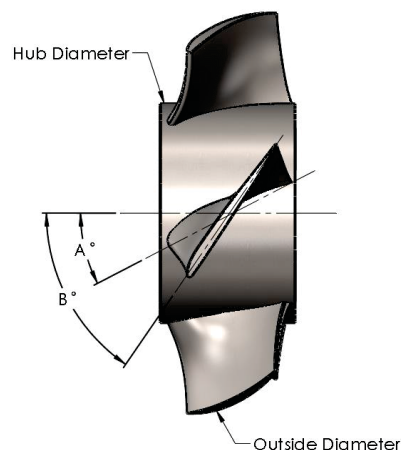


*Figure 13 – Vane Angle*

Many tests on ‘Ornel’ pumps have proven that this range of pump has a successful design by demonstrating very high efficiencies (up to 90% for a multistage 24” pump and 86% in a single



stage) (Nelson, N.D.). These tests have also proven the effectiveness of the airfoil shaped blade sections in minimising cavitation. This is done by the low pressure zone being spread over the whole lower surface of each impeller blade and not concentrated near the leading edge. This results in pumps being able to run at higher speeds and greater flow rates without cavitation (Nelson N.D.).

For the research being conducted, two different types of ‘Ornel’ impellers have been used. Both impellers are for a 300AX size pump. The types being used are types no.5 and no.8. The type number corresponds to the number of impeller blades. For the pump to run as per the supplier’s recommendations, indicated the pump head verse flow curve (Figure 15), the impeller is to be matched with the corresponding bowl as per Table 1.

Impeller to Stator; Match	
Impeller Type	Stator Type
2 & 3	Low Flow (III)
3, 4, 5, 6	Medium Flow (V)
6, 7, 8	High Flow (VII)

*Table 1 – Impeller to stator assembly*

#### 2.1.4.1.3 Bowl (Stator) and Diffuser

The pump stator is positioned after each impeller. The combination of impeller, bowl ring and stator make up one pump stage.

The purpose of the bowl or stator is to redirect the fluid leaving the impeller. The camber line of the vanes in the stator is usually an arc of a circle. The stator vane, like the impeller vane, is an airfoil shape where the inlet tip is rounded and the outlet tip is sharp. However, it has been discussed by Lazarkiewicz and Troskolanski that experiments conducted by B.Eckert showed that thin even blades with a constant thickness and rounded tips have similar results for efficiency and head as the airfoil blades.

In the Ornel range of pumps there are three types of stators. From low flow (type III) to high flow (type VII). Table 1 shows the match up for impeller to stator. The information for this table was compiled from original design drawings for Ornel bowls and impellers (Ornel, 1953).

As shown in Table 1 impellers with three and six vanes can be used with different stator types. One must ensure that when building a multi staged pump that the same impeller and stator type is used at each stage.

The efficiency is influenced by the shape of the flow passage area of the diffuser. The vane’s axial length, the number of vanes and the distance between the impeller blades and the bowl vanes are all factors which determine the flow passage (refer to Section 2.3.1).

In the pump's assembly after the final stage bowl is the diffuser. It is within the diffusers conical shape that the fluids velocity energy, converts the fluids velocity energy into pressure energy as the fluid leaves the pump. Refer to Section 2.3.1 for greater detail of the diffuser design.

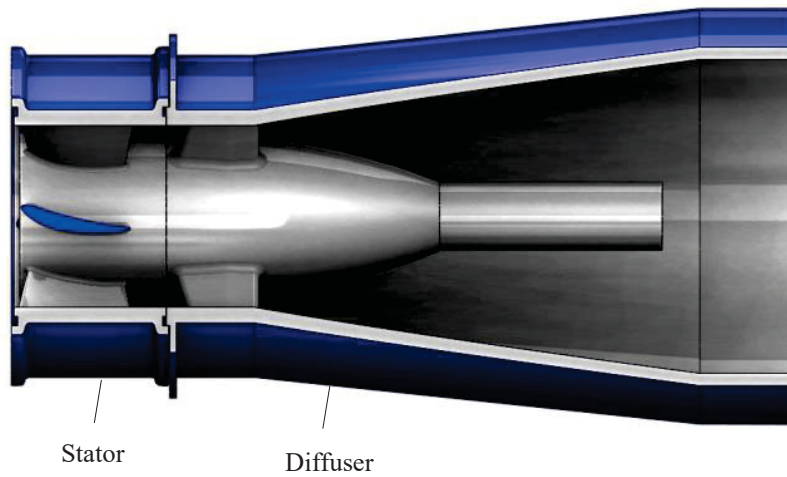
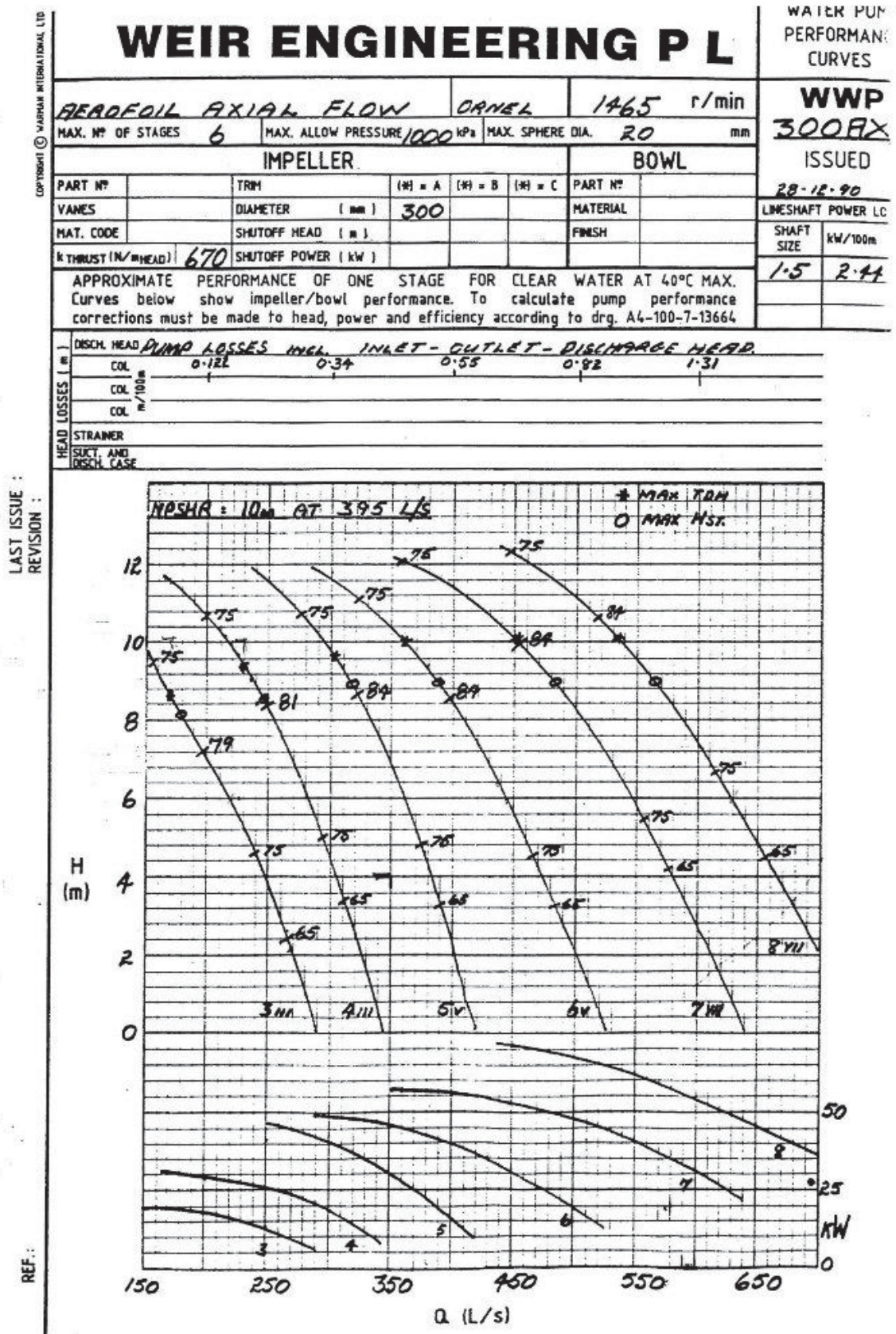


*Figure 14 – Stator and Diffuser arrangement*



### 2.1.5 Axial Pump Performance

Performance characteristics are displayed by a plot of the pump head, flow, efficiency, speed and power referred to as a pump performance curve. Pump performance curves are used to determine the pumps suitability to perform at the required systems conditions. The performance curve indicates the head, power, efficiency and NPSH for the pump measured against flow at a set speed. This curve is also known as a head verse flow curve (H-Q curve). For example, Figure 15 shows the pump curve for a 300AX ‘Ornel’ pump running at 1465 rpm. Each impeller variation performance is shown. In the case of this research, impellers numbers five and eight are being used. By looking at the curves, the best efficiency point (BEP) for the five vane impeller is 8.9m head at 318 L/s flow and for the eight vane impeller 564 L/s at 9m head.

The pump performance curve is produced by testing the pump in a controlled environment<sup>4</sup>. By measuring data during the test for the head and power consumption at various flow points at a constant speed, a curve is produced. Changing the flow or head is achieved by throttling a valve located in the discharge line of the pump. The performance curve is used to select the pump which has a BEP closest to the point where the system curve intersects with the head flow curve.

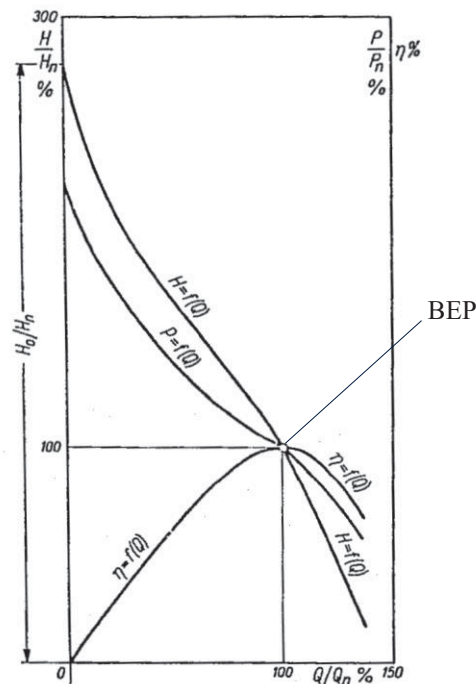


Figure 16 – Typical Axial Flow Pump performance curve - sourced from (Lazarkiewicz, 1965) pg404

The BEP is determined by the where the efficiency is at the highest point of the plotted efficiency curve in Figure 16 this is indicated as 100%. The pump can be run at a certain

<sup>4</sup> Pump testing in industry is conducted as per AS2417 which is also used in this research.

percentage above and below the 100%, which is known as the operating range of the pump. For example, an operating range of 70% to 150% means the pump can run between 70% and 150% of the BEP (100%). When the pump is run outside the operating range problems such as high vibrations due to stall, cavitation and fluid recirculation can reduce the pumps operation life, therefore it is best to operate a pump as close as possible to the BEP. For an Axial Flow Pump the stall line is the lowest flow point for the pump therefore considered the low percentage point for the operating range. Pump stall is discussed in more detail in Section 2.2.7.

### 2.1.5.1 Calculating Pump Performance

To calculate the pump performance a number of different requirements are to be determined during laboratory testing. Pump pressure, power input and output and efficiency are the major requirements for determining pump performance. The following calculations are used when putting together the data to determine the performance curve.

#### 2.1.5.1.1 Pump Pressure

Pump pressure or pump head is expressed by Australian Standard AS2417 as a height of pumped liquid column, it represents the energy transmitted by the pump per unit weight of liquid.

Pump pressure or pump head is calculated using the Bernoulli equation:

$$z_1 + \frac{p_1}{\rho g} + \frac{v_1^2}{2g} + H_P = z_2 + \frac{p_2}{\rho g} + \frac{v_2^2}{2g} + H_L \quad \text{Equation 2}$$

Where:  $H_P$  = pumping head

$H_L$  = head loss

$p$  = pressure

$v$  = velocity

$\rho$  = density

$g$  = gravity

$z$  = gauge height above datum

The above equation can be rearranged to suit the laboratory test loop by:

$$H_P = z_2 - z_1 + \frac{p_1}{\rho g} - \frac{p_2}{\rho g} + \frac{v_1^2}{2g} - \frac{v_2^2}{2g} + H_L \quad \text{Equation 3}$$



Broken into terms:

$$H_P = \overset{\text{Term 1}}{(z_2 - z_1)} + \overset{\text{Term 2}}{\left(\frac{p_1}{\rho g} - \frac{p_2}{\rho g}\right)} + \overset{\text{Term 3}}{\left(\frac{V_1^2}{2g} - \frac{V_2^2}{2g}\right)} + H_L$$

The suction and discharge pipework in the test loop construction have the same nominal bore size. This will also eliminate Term 3 from the equation, as the velocity in these pipes will be the same due to the flow in the loop being constant.

Finally, the systems head losses ( $H_L$ ) will also be eliminated. By having the suction and discharge, pressure gauges positioned at the required distance from the pump's suction and discharge (2 times the inlet and outlet's diameter), the pump losses are only measured and the losses through the rest of the loop are removed from the results. This is the case with most pump test facilities using AS2417.

$$H_P = \frac{\Delta p}{\rho g} + z \quad \text{Equation 4}$$

#### 2.1.5.1.2 Pump Input Power ( $P_p$ )

The Pump Input Power used for calculating performance is the shaft input power. It is determined by the following equation:

$$P_p = T \times \omega \quad \text{Equation 5}$$

#### 2.1.5.1.3 Pump Output Power ( $P_w$ )

Pump Output Power is the power added to the pumped fluid by the pump. This is determined by:

$$P_w = \rho \times g \times H \times Q \quad \text{Equation 6}$$

#### 2.1.5.1.4 Pump Efficiency

The Pump Efficiency is expressed by (Institute, 1994) as the ratio of the output power to the input power:

$$\eta = \frac{P_w}{P_p} \times 100 \quad \text{Equation 7}$$

The overall pump efficiency is another value in determining the performance of a pump. The mechanical and volumetric losses are factors within the pump which affect the overall efficiency. In an Axial Flow Pump, an example of the volumetric losses is the clearance between the outside diameter of the impeller and the bore of the bowl ring. As this clearance increases, due to pump wear, the leakage is increased which is part of the volumetric losses.

Also mechanical losses are found in the bearings, seals and surface finish of the impeller and diffuser vanes.

The overall pump efficiency is a combination of the mechanical efficiency  $\eta_m$ , hydraulic efficiency  $\eta_h$  and volumetric efficiency  $\eta_v$ , resulting in the equation below:

$$\eta = \eta_m \eta_h \eta_v$$

Equation 8

## 2.2 Theoretical Axial Pump Design

Due to its unsteadiness and three-dimensional properties, the flow parameters in a pump are very complex to calculate. Therefore a basic one-dimensional theory has been developed to approximately determine the average forces developed during a pumps operation. It uses manipulated energy and Euler equations to determine the performance parameters. When using the theory for one-dimensional flow, the following assumptions can be made:

- The streamlines in the impeller within the impellers flow passage are similar with each other and the fluid particles follow the same profile as the rotating impeller vanes. (Lazarkiewicz, 1965).
- The flow of liquid through an impeller passage may be regarded as a flow of liquid particles along the centre line of the flow passage (Lazarkiewicz, 1965).

To determine the existing impeller parameters for one-dimensional theory, the vanes are laid out as a development of the hub diameter as shown in Figure 18. Figure 17 shows diagrammatically the one-dimensional theory of an Axial Flow Pump impeller where the velocity triangles location is on the centre line of the flow passage, as per the assumption above.

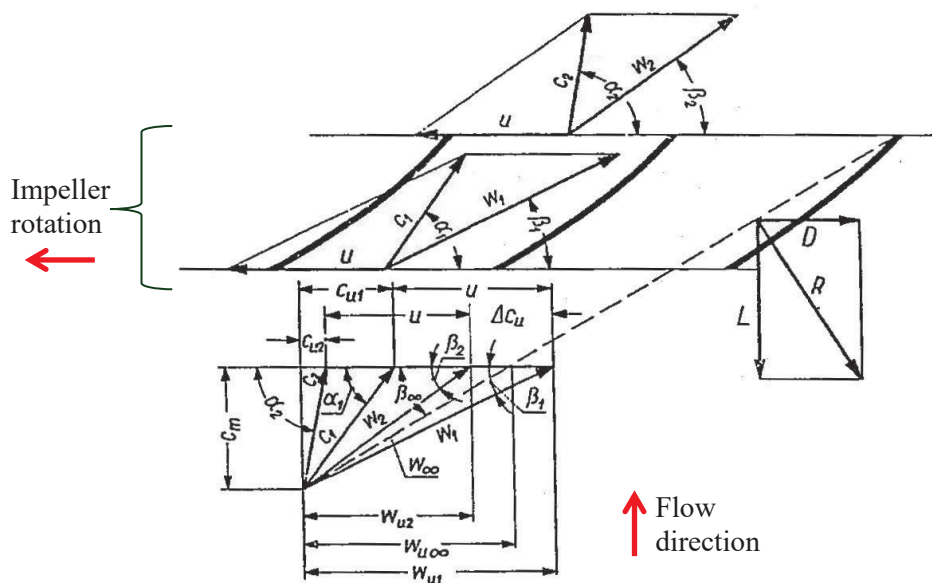


Figure 17 – One-dimensional flow through an Axial Flow Pump impeller (Lazarkiewicz, 1965) pg222

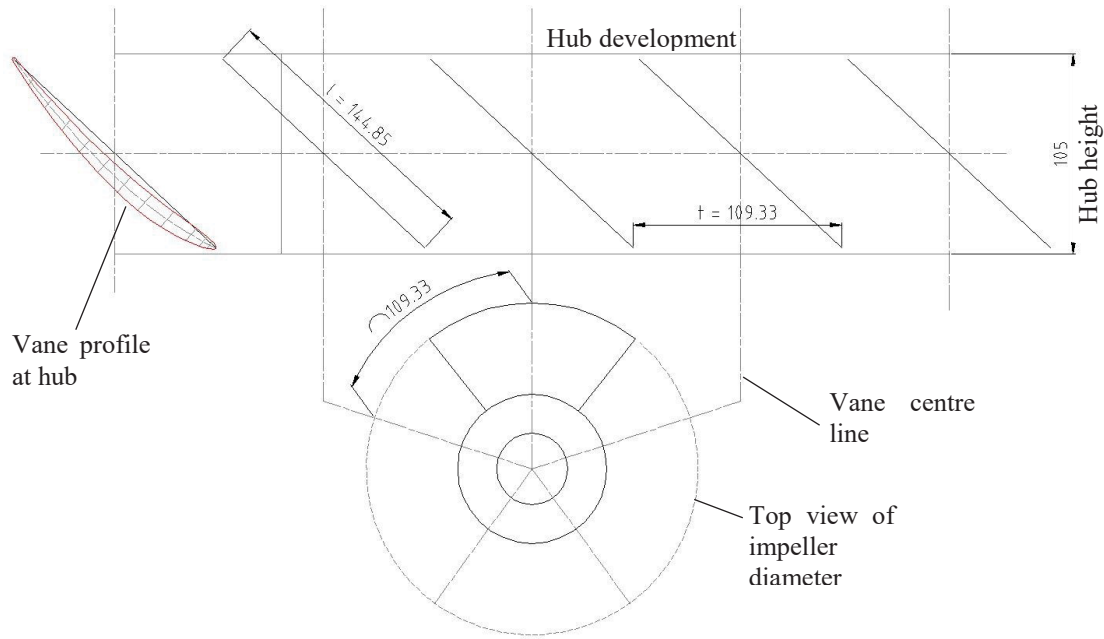


Figure 18 – Development of an Ornel five vane impeller

### 2.2.1 Velocity Triangles

The calculation of velocity vectors through an impeller can best be determined graphically by using Velocity Triangles. Velocity Triangles for this thesis have been calculated by using the existing inlet and outlet vane angles, even though they can be calculated at any point within the fluids flow path.

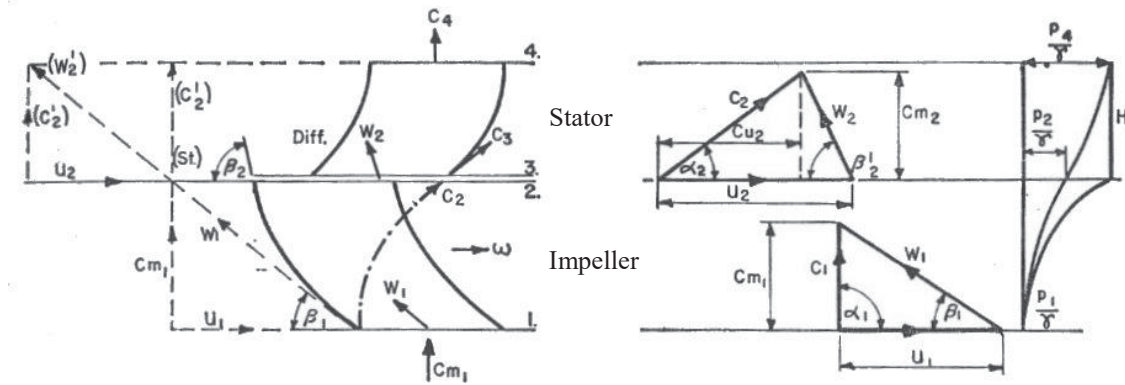


Figure 19 – Velocity triangles for single pump stage (Kovats, 1964) pg91

Figure 19 shows the velocities for a single stage Axial Flow Pump<sup>5</sup>. Due to the axial flow of this type of pump, the fluid particles enter and leave the pump impeller with the same blade tip velocity ' $U$ ' therefore  $U_1 = U_2$ .

<sup>5</sup> A single Axial Flow Pump stage is made up of an impeller and stator.



The tip velocity is calculated by:

$$U = \frac{\omega d}{2} \quad \text{Equation 9}$$

Where:

- $\omega$  = the pump shaft speed in rad/s
- $d$  = the impeller diameter

$$\omega = N \frac{\pi}{30} \quad \text{Equation 10}$$

To determine a velocity triangle, the fluids relative velocity ' $W$ ' is added to the vane tip velocity ' $U$ ', to determine the absolute velocity ' $C$ ' (also referred to as ' $V$ ')<sup>6</sup>.

$$C = U + W \quad \text{Equation 11}$$

The relative velocity ' $W$ ' is the fluid velocity relative to the direction or angle ' $\beta$ ' of the impeller.

$$W = \sqrt{U^2 + C_m^2} \quad \text{Equation 12}$$

Where the axial velocity ' $C_m$ ' which is perpendicular to the tip velocity ' $U$ ', is found by:

$$C_m = \frac{4Q}{\pi(d_2^2 - d_1^2)} \quad \text{Equation 13}$$

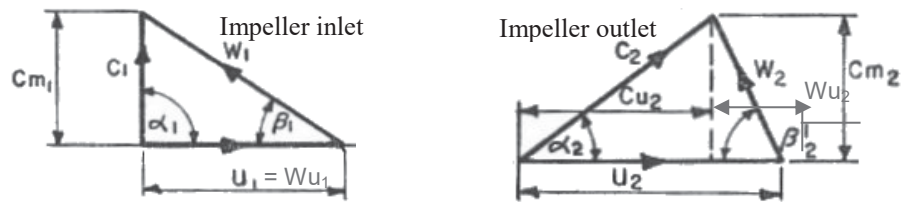


Figure 20 – Velocity triangle at impeller inlet and outlet (Kovats, 1964) pg91

Tangential component of relative velocity ' $W$ ':

$$W_u = C_m \times \tan \beta \quad \text{Equation 14}$$

Tangential component of the absolute velocity ' $C$ ':

$$C_u = U - W_u \quad \text{Equation 15}$$

---

<sup>6</sup> In some texts absolute velocity is also referred to as ' $V$ ', in the majority of reference texts used for this research the absolute velocity is referred to as ' $C$ '

The absolute velocity of fluid can also be determined from the tangential of the relative and absolute velocities by:

$$C = \sqrt{C_u^2 + C_m^2} \quad \text{Equation 16}$$

### 2.2.2 Streamlines

Newton's Second Law of Motion (equation 17) is used to determine the flow path of a fluid particle due to the particle being subjected to acceleration and mass in a number of different directions as it passes through a flow passage.

$$F = ma \quad \text{Equation 17}$$

Therefore, to be able to predict the flow path of the particle, a coordinate system is applied with Newton's law resulting in a flow streamline being produced. The streamline is the path that is tangent to the flows velocity vector.

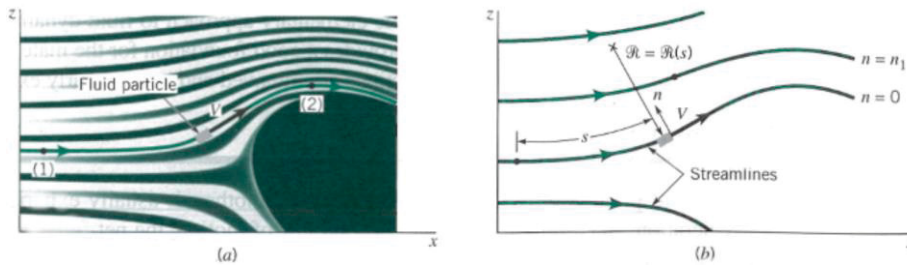


Figure 21 – (a) Flow of a streamline in plane  $xz$  (b) Streamline coordinates (Munson, 2013) pg100

As stated in the previous sections one-dimensional theory is used to determine the average forces developed during a pumps operation. However with the use of computational fluid dynamics (CFD) the dimension streamlines can be predicted in the direction of the fluid particles at a point in time by integrating the three dimensional velocity components of 'u', 'v' and 'w' where:

- $dx/dt = u,$
- $dy/dt = v$
- $dz/dt = w$

### 2.2.3 Boundary Layer

The Boundary Layer is a thin layer of shear stress created where the fluids connect with the component's surface. Because the surface has zero velocity, the velocity of the fluid passing

over the surface is a rapid change in velocity due to surface friction, resulting in a high layer of shear stress on the surface.

### 2.2.4 Impeller Vane Shape

The impeller vanes of an Axial Flow Pump are usually an airfoil design. This design is used to add strength to the vanes and also help to maintain pump efficiency. This streamlined shape of the airfoil is designed to produce low drag at high lift at an inclined angle. The hydraulic properties of an airfoil are determined by the mean line. A mean line is the curvature of the vane based on the required inlet angle ' $\beta_1$ ' and outlet angle ' $\beta_2$ ' for the required duty determined by velocity triangles. The vane thicknesses are of equal distance from the mean line and vary in length along the line. This thickness determines the strength of the vane where the maximum section from the cord length to the mean line is known as the camber. The maximum camber distance is a percentage of the cord length expressed as ' $c/l$ ' where the chord length ' $l$ ' is the straight line distance from the vane inlet and outlet tips.

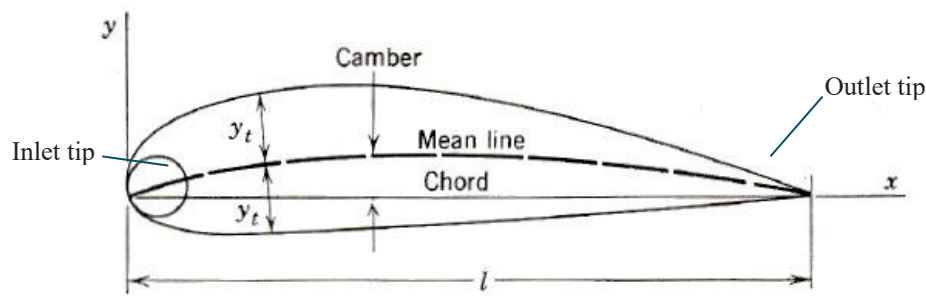


Figure 22 – Airfoil description (Stepanoff, 1957) pg140

When a fluid stream passes an airfoil, the convex side creates a drop in pressure and the concave side creates a rise. Figure 23 is a CFD image of an axial flow impeller showing the pressures applied to the impellers surfaced during operation. The pressure difference on each side of the airfoil creates a lift force ' $L$ '. The lift force is perpendicular to the direction of flow ' $w_{ave}$ '. A drag force ' $D$ ' is a combination of the surface friction drag (smoothness of the vane surface) and the pressure drag and is created in the flow direction. A thicker airfoil design increases the drag due to larger eddies formed in the vane wake. To help reduce the drag produced by eddies, a rounded inlet tip and sharp outlet tip is used in the vane design. The resultant of the lift and drag forces is the total dynamic thrust ' $P$ '. The lift force being much higher than the drag force is one characteristic feature of an airfoil design (Logan, 1993).

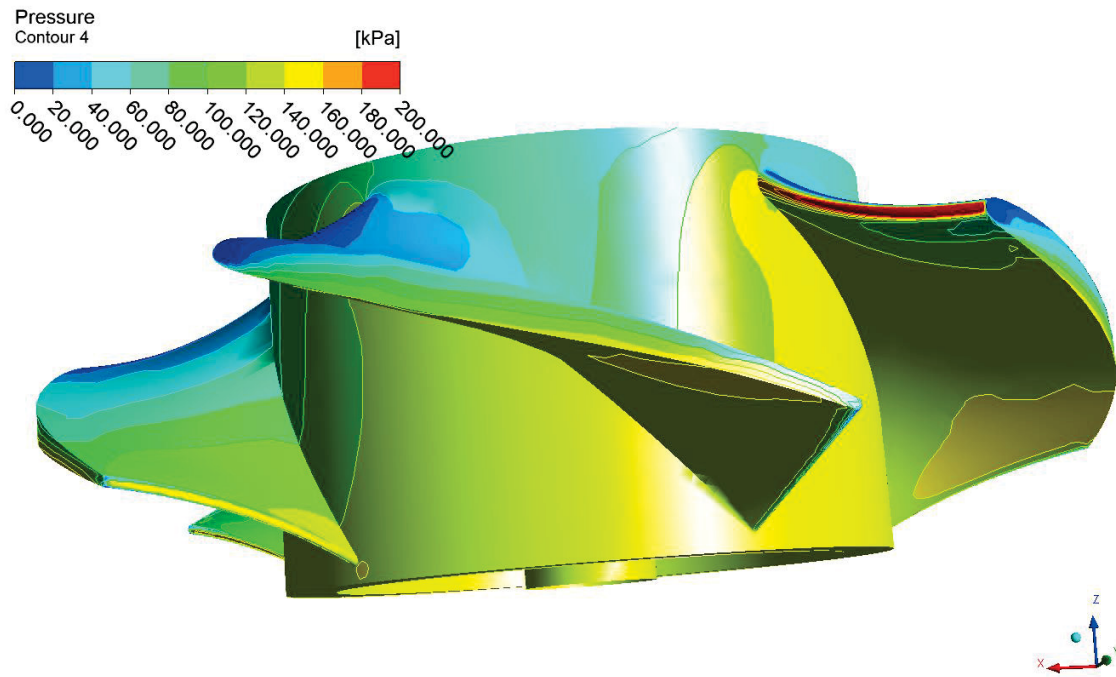


Figure 23 – Pressure generated on impeller blade surfaces

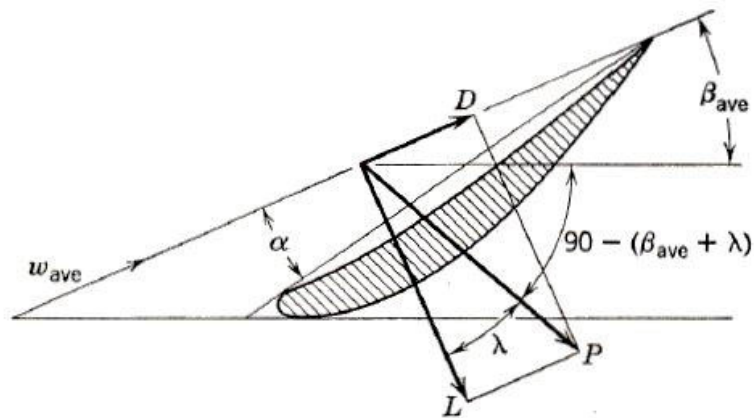


Figure 24 – Forces acting on an airfoil Blade (Stepanoff, 1957) pg140

The lift and drag can be calculated by the following:

$$L = C_L b l \rho \frac{w_{ave}^2}{2} \quad \text{Equation 18}$$

$$D = C_D b l \rho \frac{w_{ave}^2}{2} \quad \text{Equation 19}$$

Where;

- $C_L$  and  $C_D$  = lift and drag coefficient
- $b$  = airfoil width
- $l$  = chord length

The lift coefficient is dependent on the shape of the vane and the angle of attack.

$$C_L = \frac{2\cos\beta_m(\tan\beta_1 - \tan\beta_2)}{\sigma} = \frac{L}{0.5\rho U^2 A} \quad \text{Equation 20}$$

Where,  $\sigma = \text{Solidity}^7$  is determined by:

$$\sigma = \frac{l}{t} \quad \text{Equation 21}$$

Where,  $t = \text{distance between vane tip}$   $t = \frac{\pi \times \text{Diameter}}{\text{number of vanes}}$

The drag coefficient is a combination of both the shear stress and pressure forces applied to the vane profile as well as the Renolds number or surface roughness.

$$C_D = \frac{D}{0.5\rho U^2 A} \quad \text{Equation 22}$$

$$\lambda = C_D / C_L \quad \text{Equation 23}$$

The vane curvature mean line increases from  $\beta_1$  to  $\beta_2$ . This gradual increase is the factor which pushes the fluid through the impeller.

### 2.2.5 Turbulent and Secondary Flow

The majority of losses within a pump are due to a combination of turbulence and secondary flow. In pump flow passage areas, the flow is almost always turbulent. The turbulence is caused when the shear force created by the fluid's viscosity is relative to the difference in the fluid's velocity. The velocity difference occurs when a higher velocity of a flow path passes a lower velocity flow path, resulting in the creation of eddies which mix into the current direction of the flow. The lower velocity path is not limited to a fluid, it can also be the surface of pump component where the boundary layer has a lower pressure. Therefore, the higher the surface roughness the more turbulent flow will be, due to the boundary layer being thicker and crossing into the main flow area creating larger eddies.

---

<sup>7</sup> Solidity is the amount of fluid particles available within the impellers flow passage. Where, the flow passage is the volume area between the impeller blades.

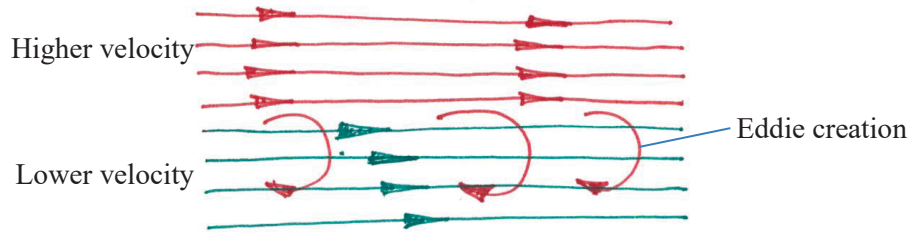


Figure 25 – Turbulence Formation

Secondary flow occurs when a minor flow pattern is created by separating from the primary flow. In an Axial Flow Pump impeller there are a number of different types of secondary flow as indicated in Figure 26. This figure is a cross section view of the impeller looking from the suction end. The vane tip leakage is discussed in the section below and contributes to the radial flow as it increases due to wear. The radial flow is created between the pressure and suction surfaces as the flow follows the impeller blades rotation.

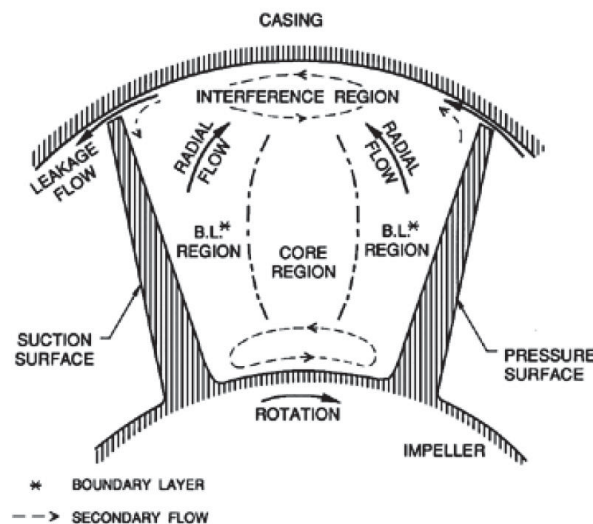


Figure 26 – Secondary flow within an Axial Flow Pump Impeller (Brennen, 1994) pg71

### 2.2.6 Vane Tip Clearance

Due to the axial flow impeller being an open type impeller design, the flow passage area is enclosed by a stationary bowl ring taking the place of an outer shroud. There is a small clearance between the impeller vane tips and the stationary bowl ring. Figure 27 shows that as the flow passes over the vane tips through the clearance, some of the fluids velocity collides with the fluid being pushed up the face of the following blade, creating a small vortex region in the flow passage and secondary flow along the blade surfaces. As the clearance is increased, the resulting greater leakage past the impeller tip into the radial flow increases the vortex and pump

losses, resulting in a reduction in pump head, efficiency and increased power. The graph in Figure 28 shows how the increase of the tip clearance will affect the pumps performance.

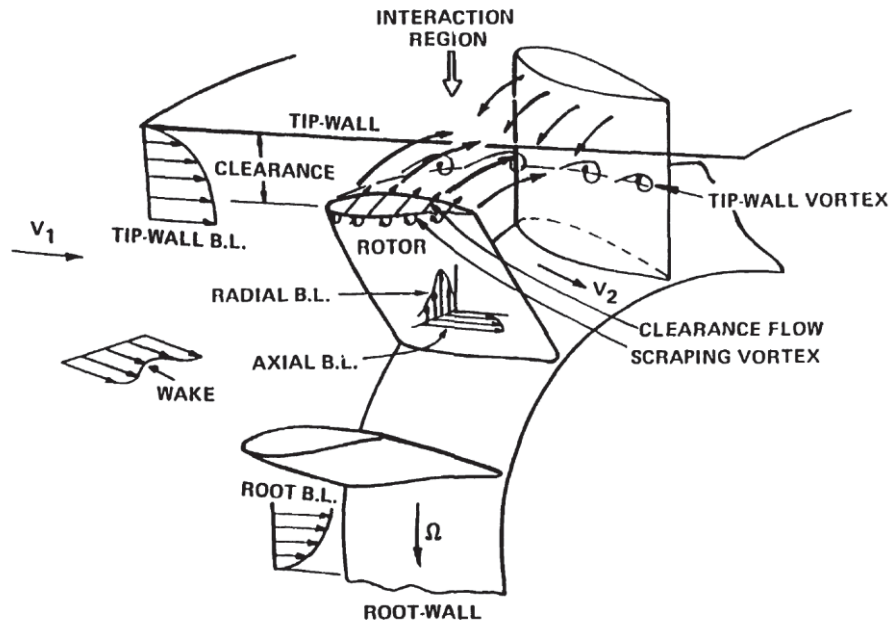


Figure 27 – Flow field at vane tip (Farrell, 1989) pg4

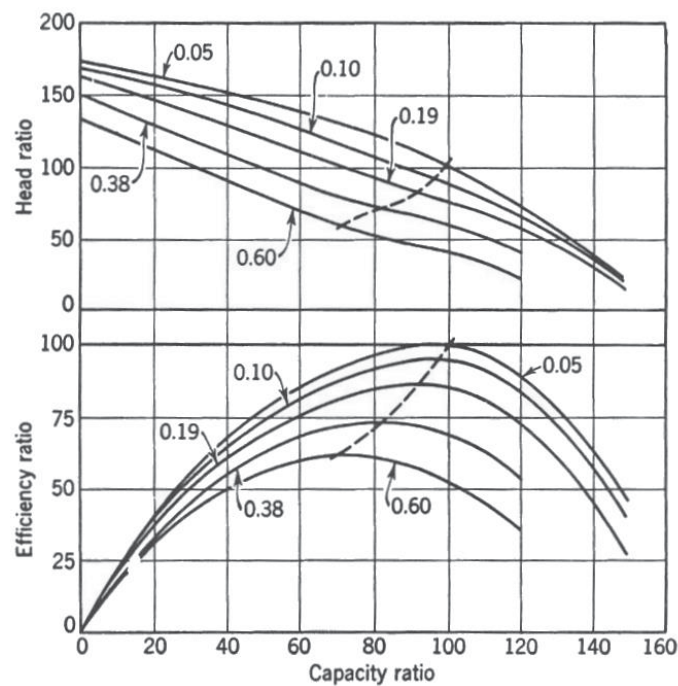


Figure 28 – Impeller to bowl ring leakage (Stepanoff, 1957) pg202

### 2.2.7 Pump Stall

As mentioned in Section 2.1.5 in an Axial Flow Pump the stall line is considered the limit for the pump's lower operating range. Pump stall is caused when the low fluid flow reduces the

absolute velocity ' $v$ ' of the fluid entering the impeller's inlet vane tips. The reduced absolute velocity ' $v_r$ ' changes the fluids approach angle  $\theta$  resulting in a greater amount of the fluid passing the pressure side of the vane, creating fluid separation from the surfaces, resulting in reverse flow on the vanes trailing edge. This creates a blockage in the flow passage stalling the pump flow.

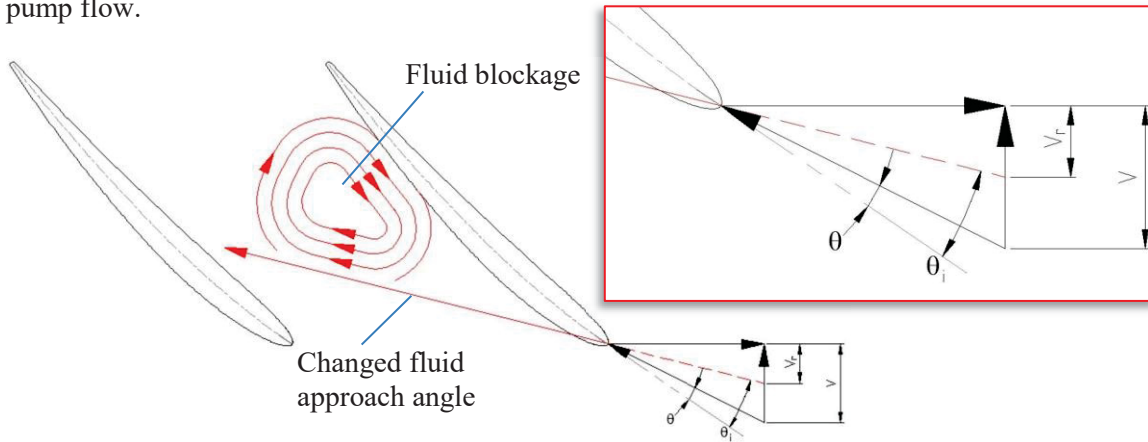


Figure 29 – Pump stall

During pump stall, high vibrations cause stresses on the impeller vanes which, over time, can result in damage and eventual pump failure. The stall line is visible on the pump performance curve as the head curve flattens out then raises again creating a dip where the blockage stalls the pump head.

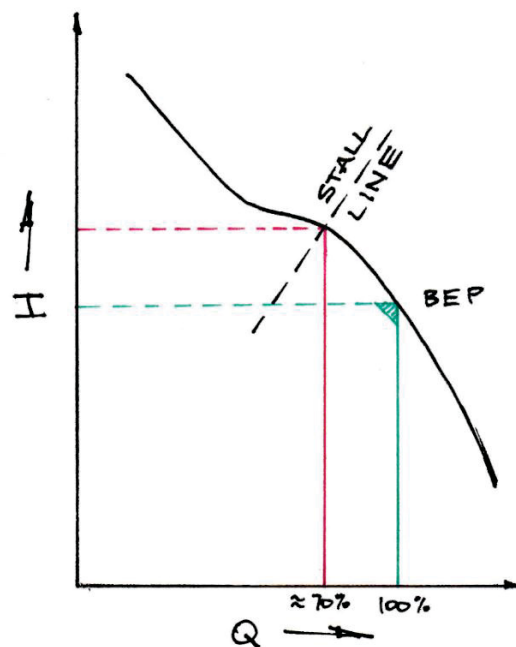


Figure 30 – Pump curve stall line



## 2.2.8 Impeller Design

The actual design of the impeller is not the main focus of this thesis, however a brief review of the design factors have been studied for an understanding of how the impeller dimensions can affect the flow follow on into the stator and how a change of some of the design factors can affect pump's performance. Design factors such as impeller hub ratio, number of impeller vanes, vane length and pump stator and diffuser design (see Section 2.3.1) are critical in the design of the pump's wet end components. Further on in this thesis, it is proven that a slight change in some of these factors affect the pump's performance.

### 2.2.8.1 Impeller Hub Ratio

The Impeller Hub Ratio is the ratio of the outside diameter to the hub diameter. This can be determined by the pumps specific speed as smaller hub diameters are associated with higher specific speed. With a smaller hub diameter, the flow area will be larger, which will result in larger flow capacity. The ratio is selected from figure 31 which has been determined from years of testing on numerous Axial Flow Pumps.

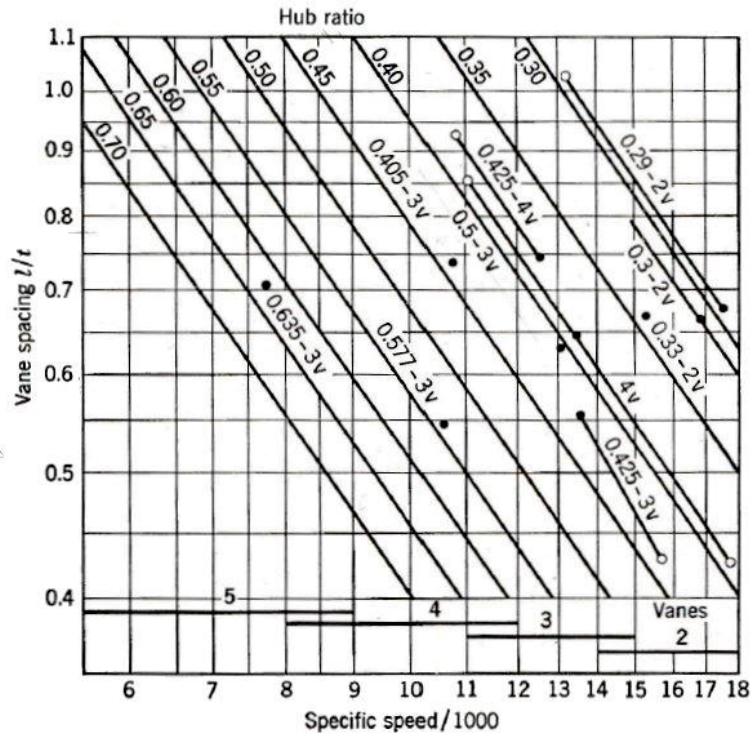


Figure 31 – Hub ratio for number of vanes and  $l/t$  ratio (Stepanoff, 1957) pg145

The graph confirms that at higher specific speeds, the hub ratio decreases (smaller diameter hub) as well as the number of blades decrease.

Calculations of the five vane impeller being used in this research and having the results of vane spacing  $l/t = 1.325$ , specific speed of  $N_s/1000 = 5.2$  and hub ratio ' $d_2/d_1$ ' of 0.6 do not lie within

the data shown on Figure 31. However, by making an assumption by extending the hub ratio chart, Figure 32 shows that the results are consistent to that of the recommended values.

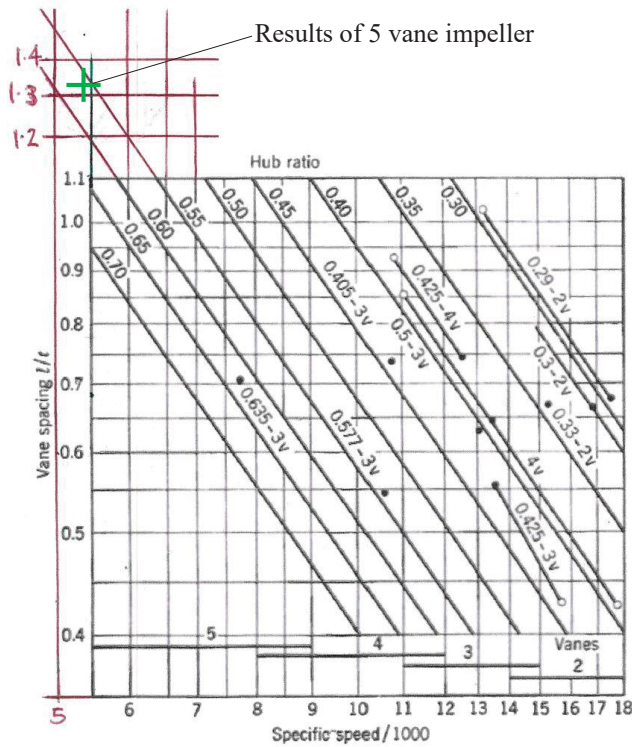


Figure 32 – Extended hub ratio chart showing pump used in this research

### 2.2.8.2 Number of Impeller Vanes

The number of impeller vanes is critical to the pump's performance as the number of vanes determine the amount of fluid flow. As the number of impeller vanes increase, so will the flow at a set speed. However, a higher number of vanes will also increase the power required to rotate the impeller, due to a higher flow rate. This can be observed in Figure 15, which shows the research pump's design performance curves for impellers with three to eight vanes, when the number of vanes increase, so does the power and flow but the head remains similar.

### 2.2.8.3 Impeller Vane Length

To control the head produced by the Axial Flow Impeller the vane chord length is modified. If the vane length is reduced at the trailing edge from the original design, there will be a drop in head and efficiency. This is due to the change of the outlet angle ' $\beta_2$ ' and the increase to the axial distance (see Section 2.3.2.2.1). If the leading edge is reduced, the flow will be increased however the pump will stall at a higher flow reducing the operating limit and efficiency. Figure 34 is a chart developed to show how the difference in vane lengths can affect the performance

characteristics of the pump. A reduced length is highlighted in red and shows the drop in head and power for a reduced vane length.

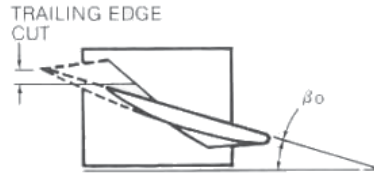


Figure 33 – Vane length reduction (Dicmas, 1987) pg108

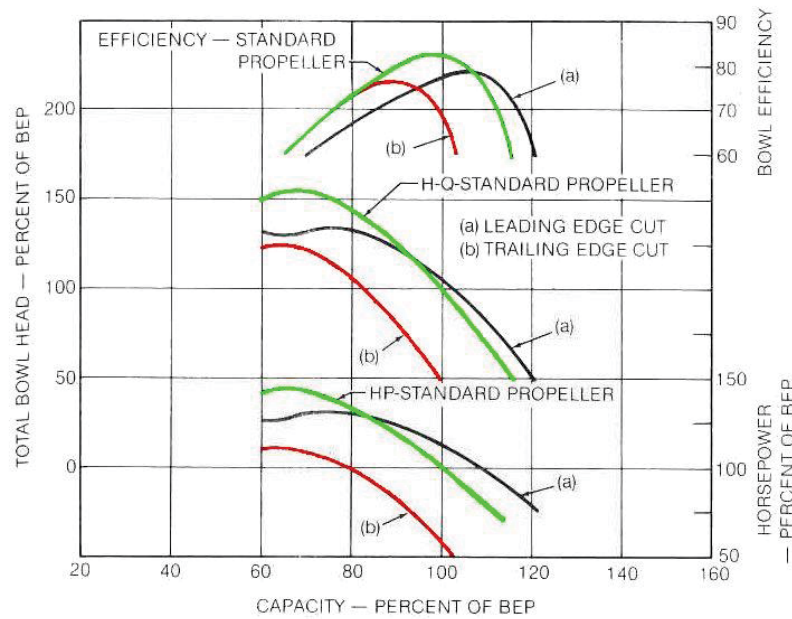


Figure 34 – Change in pump performance (Dicmas, 1987) pg109

The impeller chord length comparison between the five vane original designed impeller and the new impeller used for this thesis is detailed in Section 5.2.1.2.2, which found the new manufactured component has a reduced trailing edge.

## 2.3 Pump Stator and Diffuser

This section discusses the design theory of the stator and diffuser. The theories reviewed in this section are applied to the new diffuser design in Section 3.2.

### 2.3.1 Diffuser Design

In the original Ornel pump design, the stator and diffuser are assembled as two separate components as shown in Figure 35. The stator has eight guide vanes which are designed to redirect and straighten the flow coming from the impeller discharge and to return it to an axial flow direction. As stated in Section 2.1.4.1.3, the straightened flow moves into the diffuser

which converts the fluid's kinetic energy into pressure energy. This is achieved by reducing the fluid's velocity as the flow moves into the expanding conical shape. As recommended by Stepanoff, the conical shape of the diffuser shroud should not exceed an angle of 4 to 5° radially (see Figure 39).

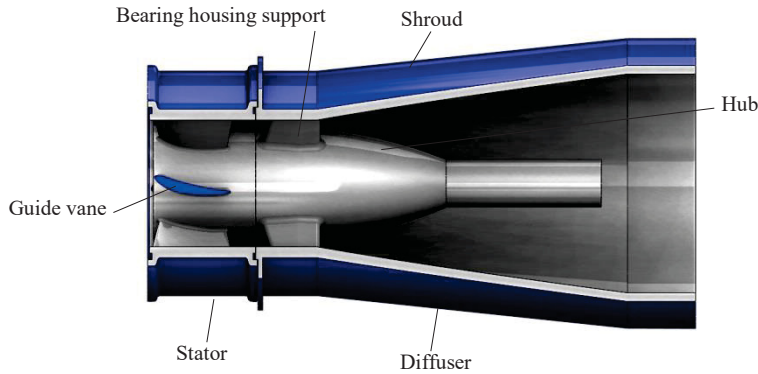


Figure 35 – Original Ornel pump design of a stator followed by diffuser

This angle recommendation will result in the minimum loss coefficient as indicated in Figure 36. With a smaller angle, the fluid stays in contact with the diffuser's walls as the velocity decreases. As the angle increases the fluid separates from the wall introducing secondary flow and greater losses. This is shown in detail in Section 3.2.1.

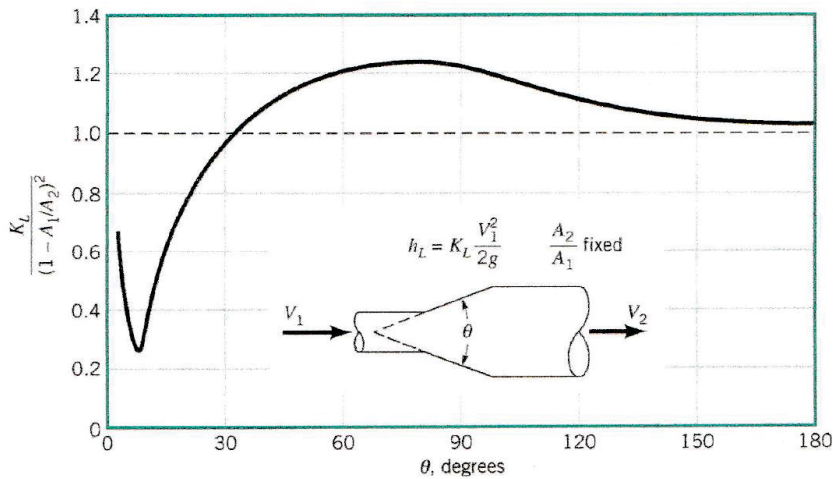


Figure 36 – Loss coefficient for a diffuser (Munson, 2013) pg435

### 2.3.2 Diffuser Vane Design Theory

As with the impeller vanes, the guide vanes of the diffuser are designed with the same one-dimensional based theory. The majority of design calculations for the guide vanes are based on the velocity triangles of the impeller outlet. An airfoil shape can be used for the vanes to add strength to the component.

### 2.3.2.1 Diffuser Guide Vanes

The curvature of the diffuser vane is designed to ensure that the fluid enters the diffuser at an angle which will introduce minimum flow losses, as well as ensuring the fluid leaves with an axial flow direction. To do this, the guide vane inlet angle  $\beta_3$  is calculated to determine a starting point from which to design the curve. To calculate the inlet angle, the velocity triangle for a streamline at the impeller outlet at a number of radial positions is used. Angle  $\alpha_2$  taken from the impeller velocity triangle is used as a reference to determine the angle of  $\alpha_3$  by using a tolerance of  $\pm 5^\circ$  (Lazarkiewicz, 1965). This is the recommended angle which results in a minimum of losses within the pump.

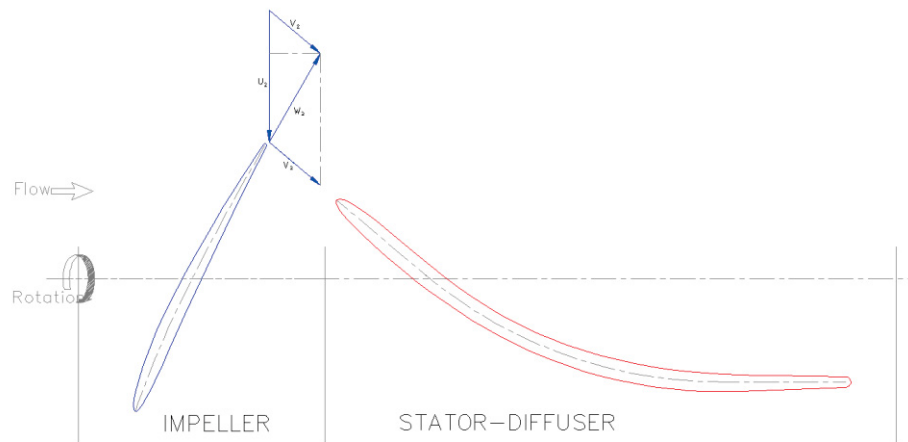


Figure 37 – Velocity triangle at impeller outlet at a streamline

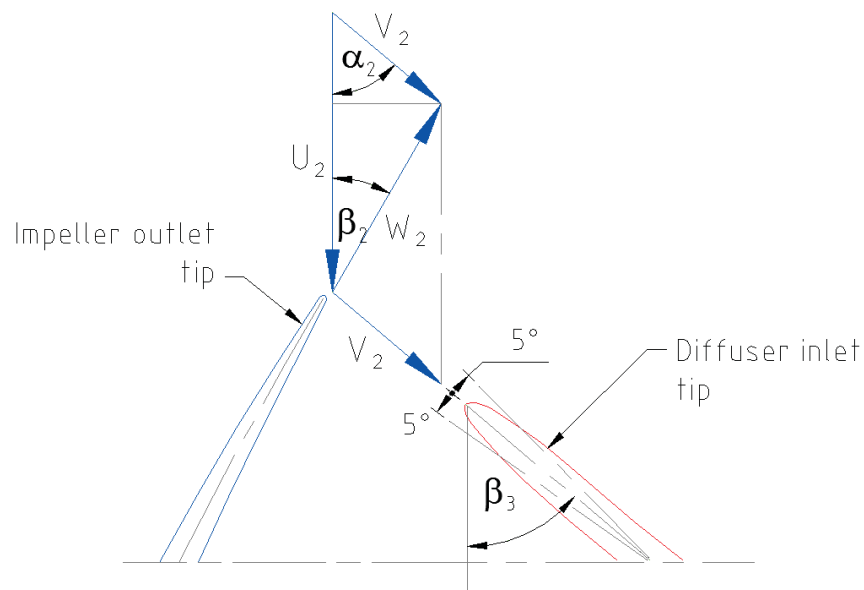


Figure 38 – Detail of velocity triangle at impeller outlet and angle of guide vane inlet

From the inlet angle ' $\alpha_3$ ', the vane camber line will follow a curve to the outlet angle ' $\alpha_4$ ' of  $0^\circ$ , to re-introduce the fluid flow to an axial direction.

The inlet angle at each streamline should result in a constant pitch to ensure that the flow velocity leaving the impeller remains constant. A constant pitch ' $P_3$ ' as shown in Figure 40 of the velocity diagram, is used to determine the selected angles are sufficient.

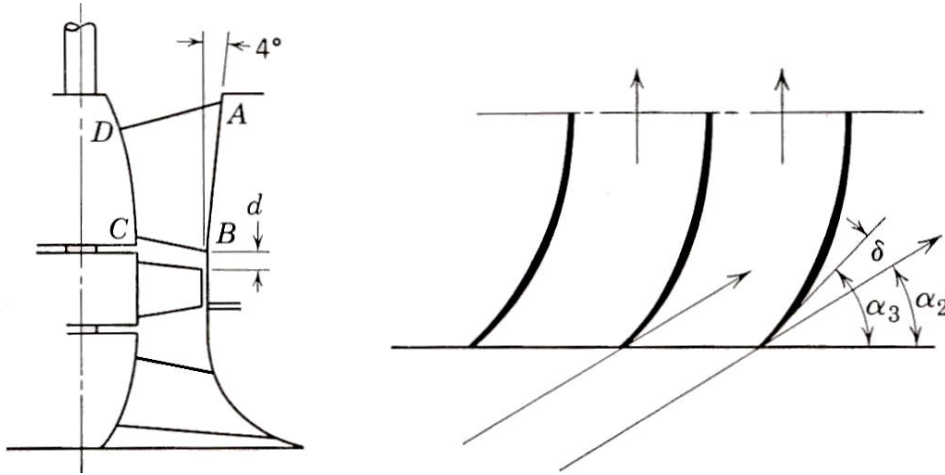


Figure 39 – Diffuser design variables (Stepanoff, 1957) pg159

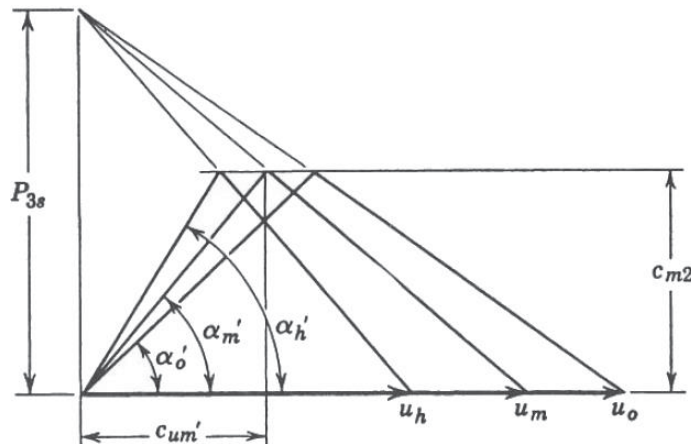


Figure 40 – Velocity diagram at diffuser inlet (Stepanoff, 1957) pg157

### 2.3.2.2 Diffuser Efficiency

The shape of the diffuser influences the efficiency to a certain degree. Efficiency can depend on design features including the number of vanes, their axial length and the axial distance between the impeller vane outlet and the guide vane inlet.

### 2.3.2.2.1 Axial Distance

Lazarkiewicz & Troskolanski recommend that the axial distance design ‘ $d$ ’ should be approximately  $0.2 L_r$  (where  $L_r$  is the impeller vane radial length) to eliminate a drop in efficiency. This is due to the high degree of reaction of an Axial Flow Pump operation. This theory was earlier outlined by Stepanoff, where the axial distance to be the ratio of  $d/D_o$  should approximately equal 0.05. Both of these methods have a similar result as shown in Section 3.2.2.1.1.

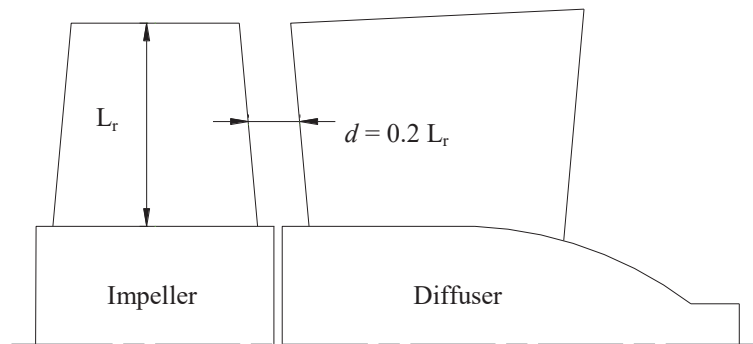


Figure 41 – Recommended impeller vane outlet to guide vane inlet, design distance

### 2.3.2.2.2 Diffuser Vane Length and Number of Vanes

The vane length is measured from the mid-way point of the impeller to the end on the stator vane where it intersects with the shroud. An example of the effects of different guide vane numbers and length have on efficiency is shown in Figure 42. This shows the test results from two Axial Flow Pumps made by the *Escher Wyss Company*. The type II diffuser has shorter, yet double the vanes, of a type I diffuser. The results show that type II diffuser has approx. 3% higher efficiency than type I diffuser when both diffusers have identical flow and head. This difference in efficiency is due to the boundary friction on the blade face. The larger surface area resulting in increased friction and a drop in efficiency.



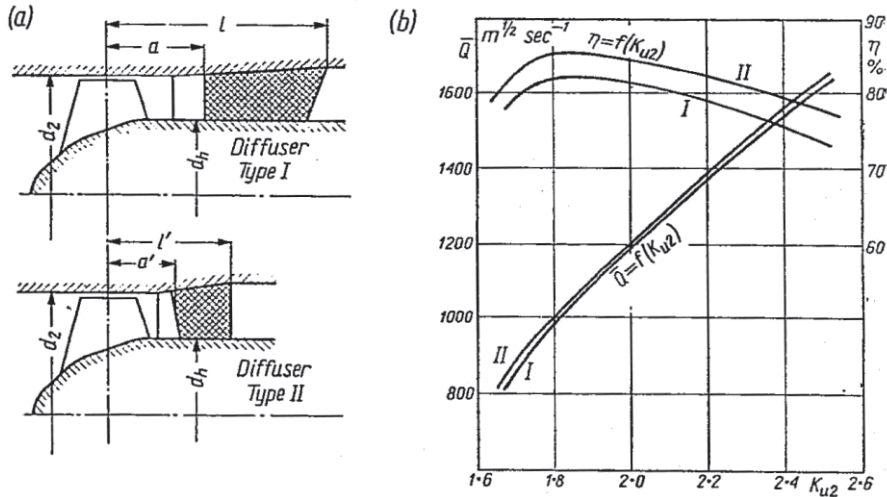


Figure 42 – Comparison of two identical pumps with different diffusers (Lazarkiewicz, 1965)

Generally a larger diameter pump will have a greater number of vanes than a smaller diameter pump. The number of vane would normally be from five to eight vanes.

The vane length at the hub streamline can be less than the vane length at the outside diameter due to the larger spacing between the vanes at the outside diameter (see Figure 39 where  $DC < AD$ ).

## 2.4 Previous Research Review

Previous research conducted at the university using the new diffuser design has been used in this research to compare with current results. During the current research, different measurement equipment has been used to obtain test data, therefore the comparisons of test results have been used to access the accuracy and practicality of the previous results, so some theories are not required to be repeated.

### 2.4.1 Previous Test Comparisons

Test configurations for the current research are detailed in Section 5 Table 7. Test configuration 'A' (five vane impeller and medium flow stator) is to be used as the base test to compare with all other test configurations. Test configuration 'A' results have been compared to test results from previous research, tested with the same pump configuration.

Figure 44 indicates that the tests points for this current research and previous research lay within 2% of each other. The current results are also lower than the previous results, which may be due to the different instruments used for measuring data (refer to Section 5.1.4). Both sets of testing points, (current and previous), are approximately 8% lower than the original design curve which is investigated in Section 5.2.1.2.



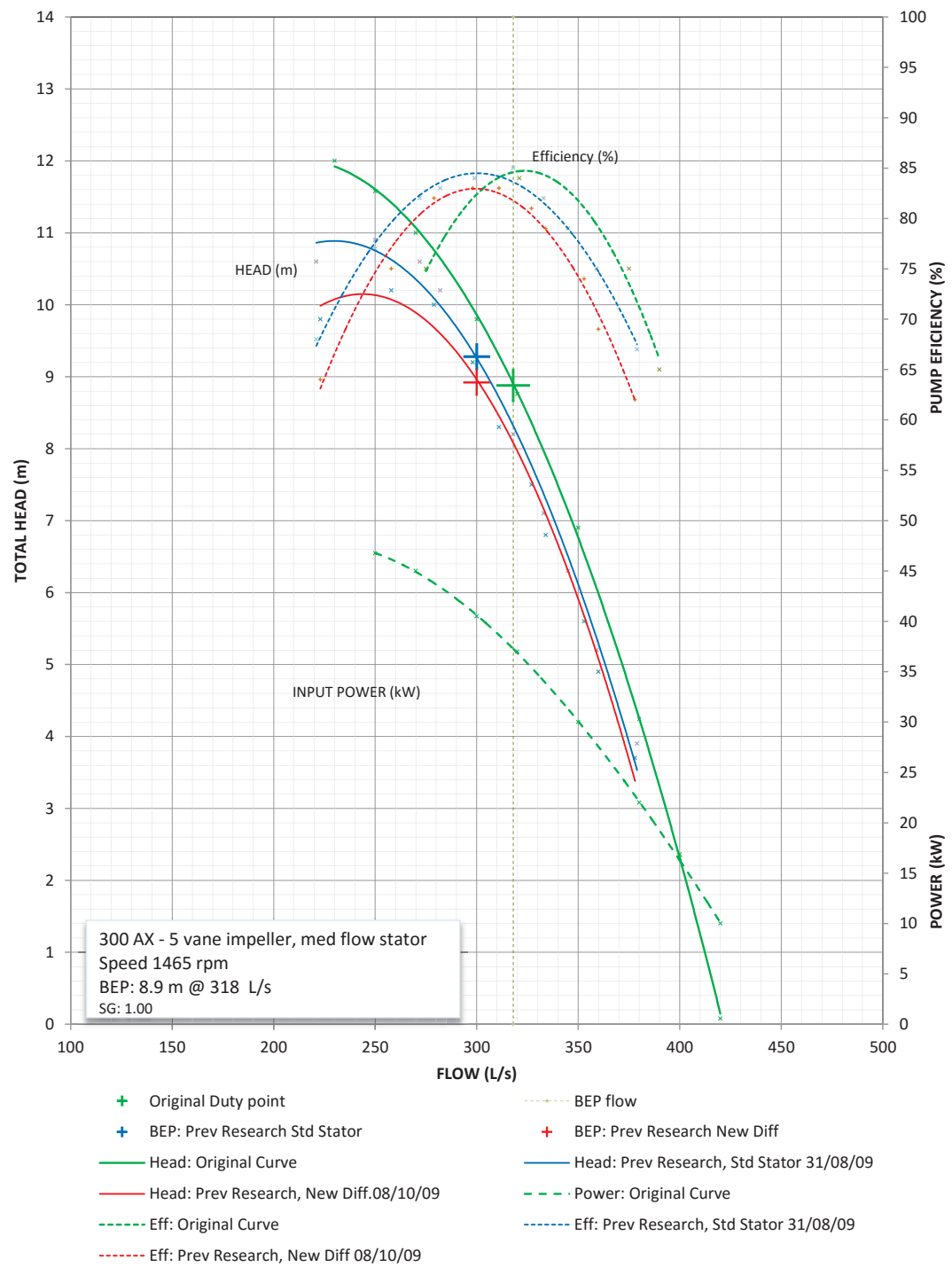


Figure 43 – Previous research five vane impeller test results

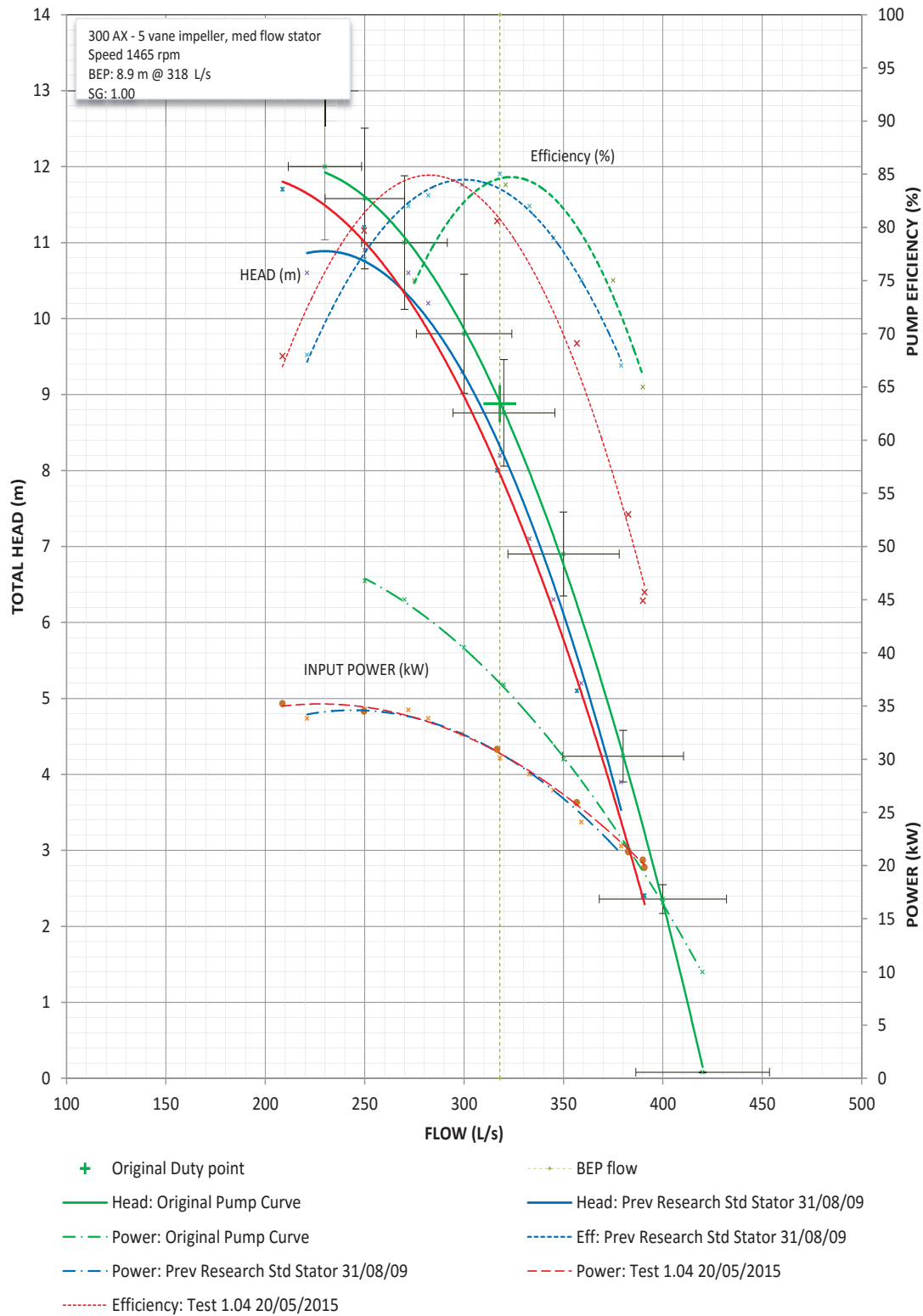


Figure 44 – Comparison of test configuration 'A' of previous and current research of a five vane impeller standard pump (error bars set at 8%)

# 3 Component Investigation

This chapter looks in detail at the design of the pump components utilised for this research. The method and equipment used to determine the components manufactured dimensions are explained. These dimensions are used with the theory from the previous chapter to review the component's design. This chapter also reviews the physical state of the components and, where required, the process in which they were repaired.

## 3.1 Part Measurement

To be able to make an assessment of the pump being used for this research, accurate measurements of the pump's parts is required to be carried out. The original drawings for the impellers and original design for stator are available and were used to model these items. However, for the new diffuser, the design drawings were not available. Therefore, a coordinate measurement machine (CMM) was used to measure the part.

The CMM was also used to scan the impellers to ensure the manufactured items are compatible with the original drawings. To do this, the scanned image is overlaid onto the 3D model of the original component design.

The CMM used for this research was a 6ft FaroArm® platinum 7 Axis Machine (see Appendix B for technical data sheet). This CMM has an accuracy of  $\pm 0.026\text{mm}$  and for this research was calibrated to 0.051mm accuracy. Both a 6mm hard probe and a laser probe were used for the measurements.

The software being used with the CMM to record the data is *Polyworks*.

### 3.1.1 Coordinate Measuring Machine (CMM)

The CMM measures points on the surface of an item. The CMM measures these points via the two probes which touch (hard probe) or scan (laser probe) the surface of the component. These points have x, y and z coordinates which are related to a 0,0,0 origin location. The origin location is determined by the most appropriate position of the component from which all measurements are based from. This position would normally be based on a machined area of the component comprising of a flat plane, centre hole or an axis. The selection of origin points for the components that were measured are detailed in Sections 3.1.2.1 and 3.1.2.4.



*Figure 45 – CMM (Faro arm)*

The CMM uses microscopic grating patterns to record its location on the surface using 3 axis. This information is sent to the measurement processor where the coordinates generate the component being measured.



*Figure 46 – CMM measurement of new impeller*

### 3.1.1.1 Hard Probe Measurement

The hard probe consists of a sphere of a specific diameter. As the probe touches a selected position on the surface, a point (x, y and z coordinate) is measured at the centre of the sphere then shifted back to the actual contact point as per Figure 47. Therefore, due to a 6mm probe being used, 3mm is automatically added or removed from the measurement, depending on the compensation selection. Linear encoders built into the axis of the arm track the movement of the probe with very high precision (FARO, 2008).

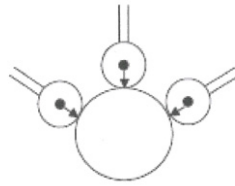


Figure 47 – Centre of probe to surface contact (Hi-Tech, 2010) pg3

### 3.1.1.2 Laser Probe Measurement

The laser probe is an attachment added to the arm and will digitise the shape and position of an object that is in its field of view. A laser line is generated by “fanning” out a laser light beam into a sheet-of-light. When that sheet-of-light intersects an object, a bright stripe of light can be seen on the surface of the object. By using a triangulation process, a built-in camera, in the laser probe head, views that stripe at an angle and the observed distortions can be translated into height variations (FARO, 2008). As the laser stripe is swept across an object, hundreds of cross-sections are instantly captured. They are then rendered in a CAD environment, the end result is a full 3D digital representation of the object. The collection of point data is commonly referred to as a “point cloud”. The laser probe has the ability to measure up to 19000 points per second but it is not as accurate as the hard probe which has an accuracy of  $\pm 0.05\text{mm}$ .

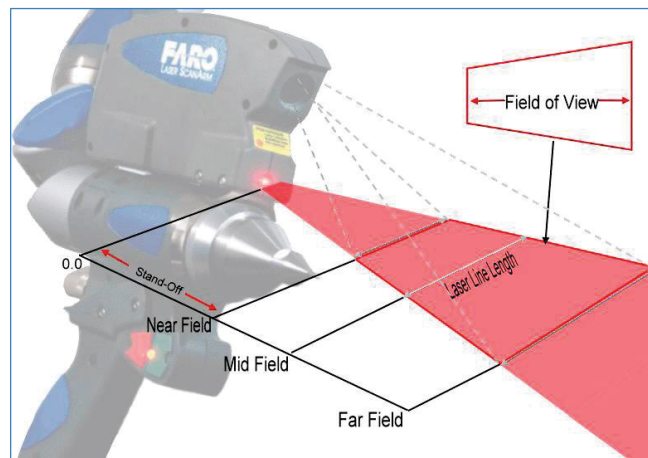


Figure 48 – Field of view of laser probe (FARO Technologies, 2008)

The point cloud is generated by using the *Polyworks* program. These are combined with the hard probe measurements to produce an accurate image of the component as per Figure 49.

Dimensions, cross sections, nurb surfaces, points etc. are exported from the image as iges files and imported into *SolidWorks* CAD program to produce the 3D model of the component. *SolidWorks* is the program that was used to create all the models for this research.

### 3.1.2 CMM Measurement Results

The major pump components both new and existing were measured and assessed using the CMM. The process and findings of each component analysis is found in the following data.

#### 3.1.2.1 Original Impeller

The origin used for the impeller is the face of the retaining plate and the centre point of the impeller trim diameter. Hard and laser probes are both used to measure the surfaces of the impeller.

Once enough of the impeller area has been scanned<sup>8</sup>, a 3D model of the impeller can be produced. In this case, as with most impellers, if there is minimal damage to the impeller blades, only one of the blades and only a section of the hub area is required to be scanned.

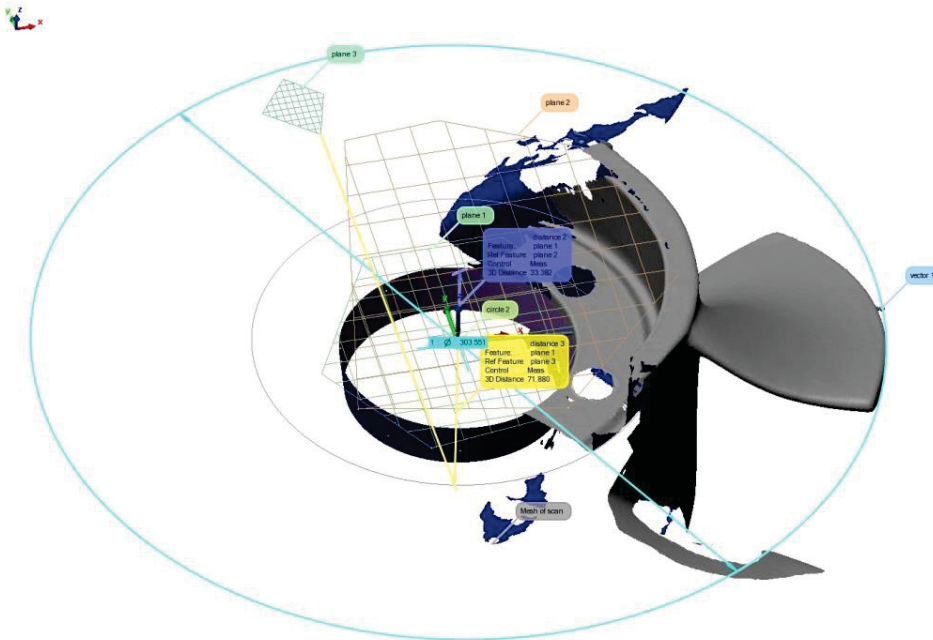
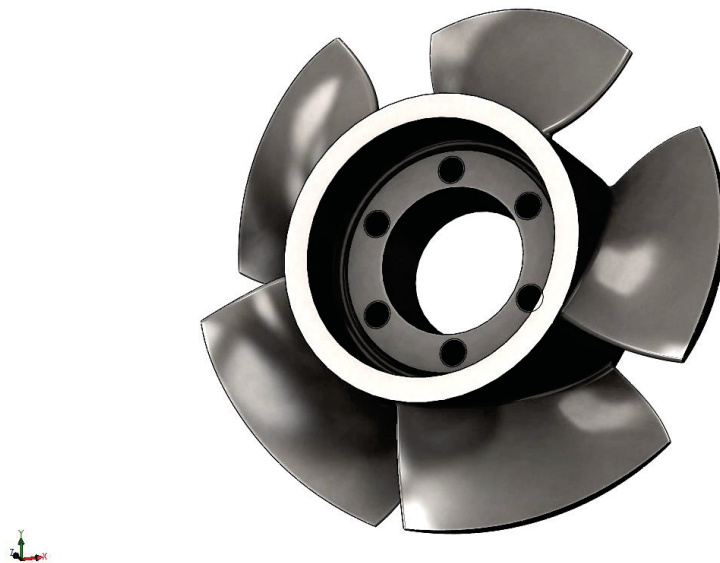


Figure 49 – Scan of Impeller

<sup>8</sup> Only a section of the component requires to be scanned when an item is symmetric.



*Figure 50 – 3D Model of scanned impeller*

Because the original design drawings are available for the impeller, it was possible to use the drawings to produce a CAD model of the component and then overlay the scanned image onto the model of the original design. This comparison proved that the outlet angle of the manufactured component matched the original design dimensions. This also showed there is a slight variation with the inlet angle.

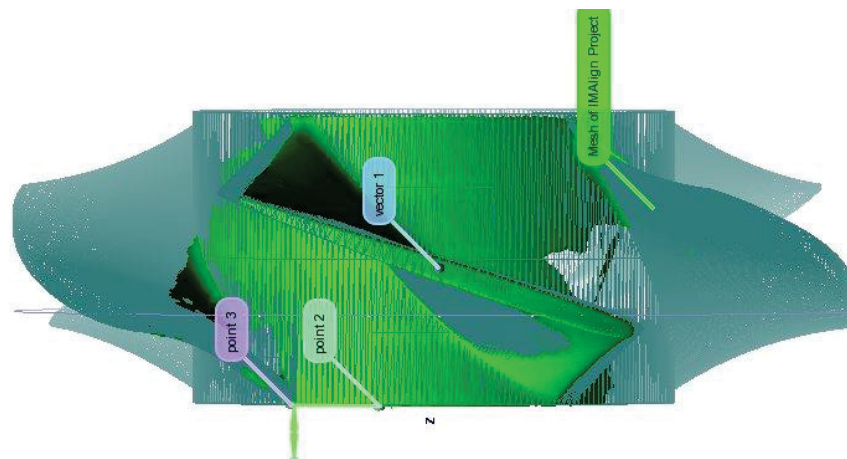


*Figure 51 – Overlay of scan onto design model*



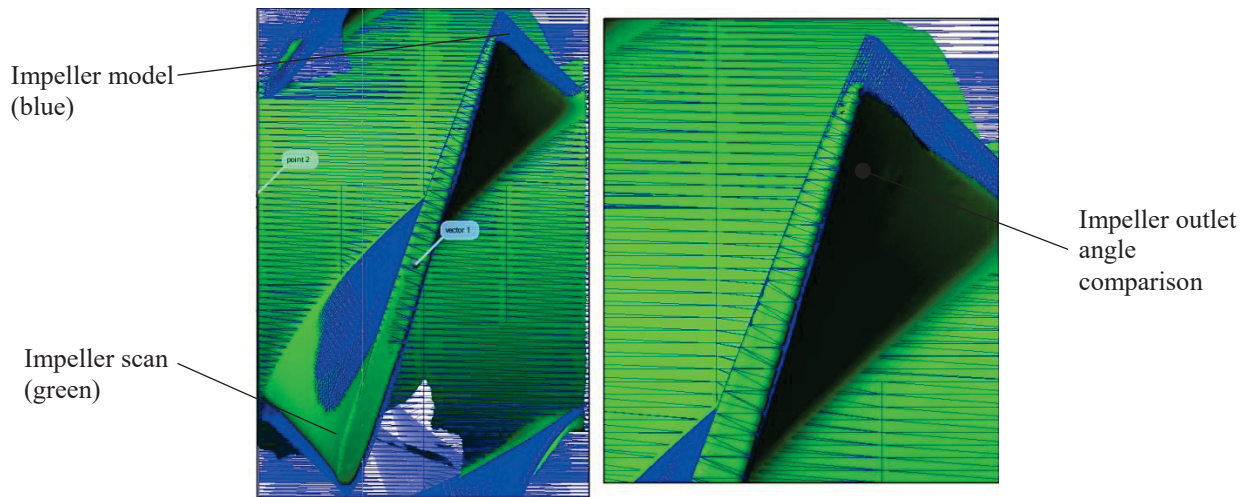


Figure 52 – Comparison of impeller scan to model of original design impeller.

It was also found that there is a reduction in the impeller chord length on average of 8mm (see Figure 53). This length reduction has an effect on the pump’s performance. The performance issues are further investigated in Section 2.2.8.3.

For the ease of modelling, it was decided for this research that the original design dimensions are used for the theoretical calculations and CFD analysis of the pump components.

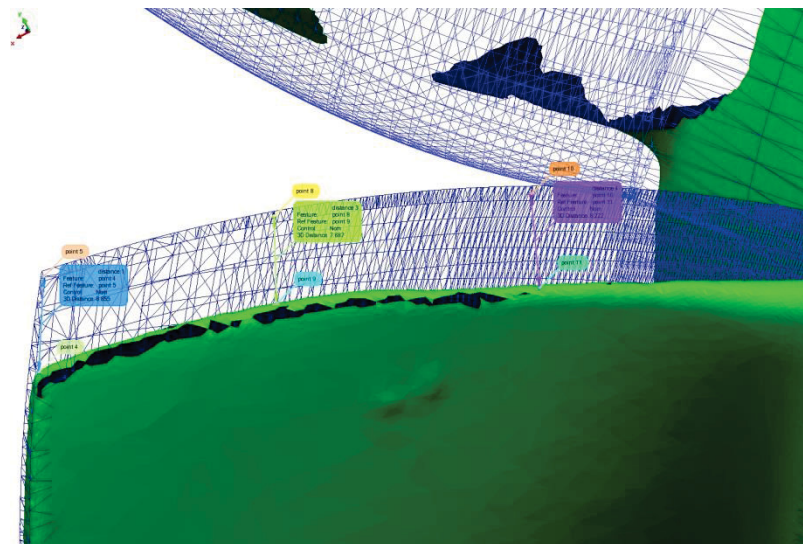


Figure 53 – Reduction distance of trailing edge

### 3.1.2.2 New Impeller

During the refurbishment of the laboratory test rig, a new five vane impeller was purchased. To determine if this impeller was compatible with the original design drawings, a CMM inspection was conducted as per the same procedure as the existing impeller.





*Figure 54 – New impeller set-up and laser scanned image*

On initial inspection of this impeller, it was obvious that it had been fabricated and not cast as per standard. With the vanes being welded to the hub, the roughness of this surface will contribute to a greater turbulence and increased losses within the pump.

It was discovered, via the scan being overlaid onto the 3D model, that even though the vanes have a consistent profile at the inlet tip curvature, the vane chord length is also reduced which is further investigated in Section 5.2.1.2.2.

The impeller outside diameter dimension measurement is 304.304mm which is within the design dimension of 304.39 / 304.09mm.

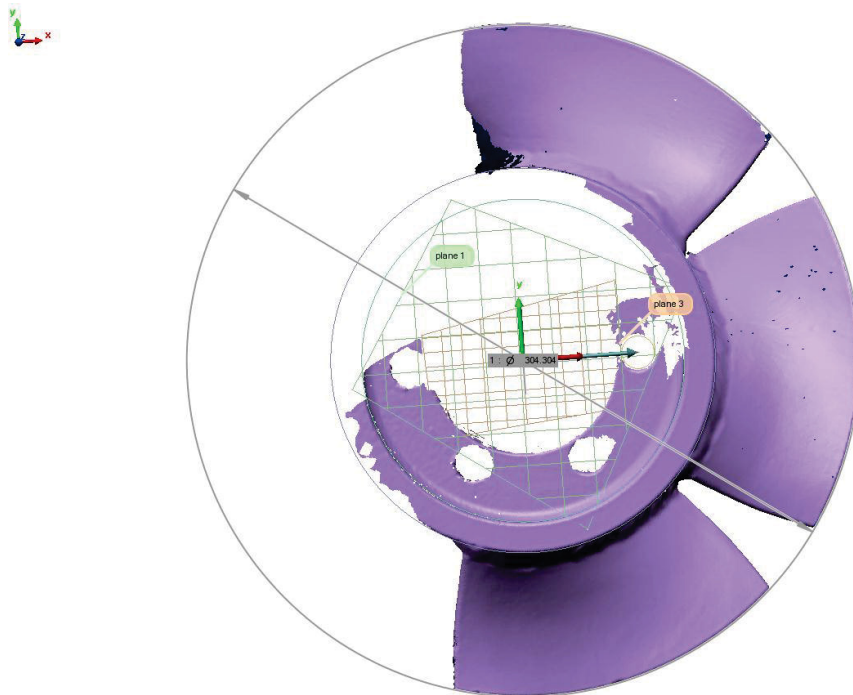


*Figure 55 – Measurement of new impeller outside diameter*

### 3.1.2.3 Bowl Ring

A CMM inspection of the pump bowl ring was undertaken to investigate the concentricity and if the bore was still within the original design tolerance.

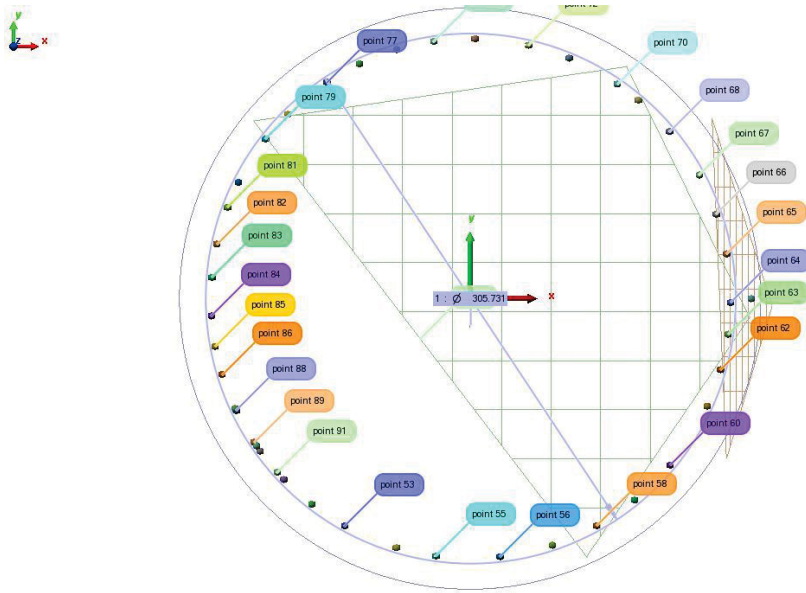


*Figure 56 – Bowl ring CMM measurements*

The set-up for the bowl ring inspection is to probe one of the connecting faces as the initial plane and the spigot<sup>9</sup> face as the centre point position to set the origin point. From this point a vector is created perpendicular to the initial plane. This created the centre line axis of the component.

To determine the concentricity, a point probe is used and a number of positions are selected on the internal surface of the components bore. Each point is then measured to the axis line and a table was created showing the distance. It should be noted that a 6mm probe was used for the measurements, therefore, because the probe measures from the centre, 3mm should be added to the recorded data to achieve the true dimension.

<sup>9</sup> The spigot face aligns one component to another during assembly therefore a spigot face is always used for a CMM set-up. As it is not a moving part it would be assumed that a spigot face would not have wear and is therefore maintained its concentricity.

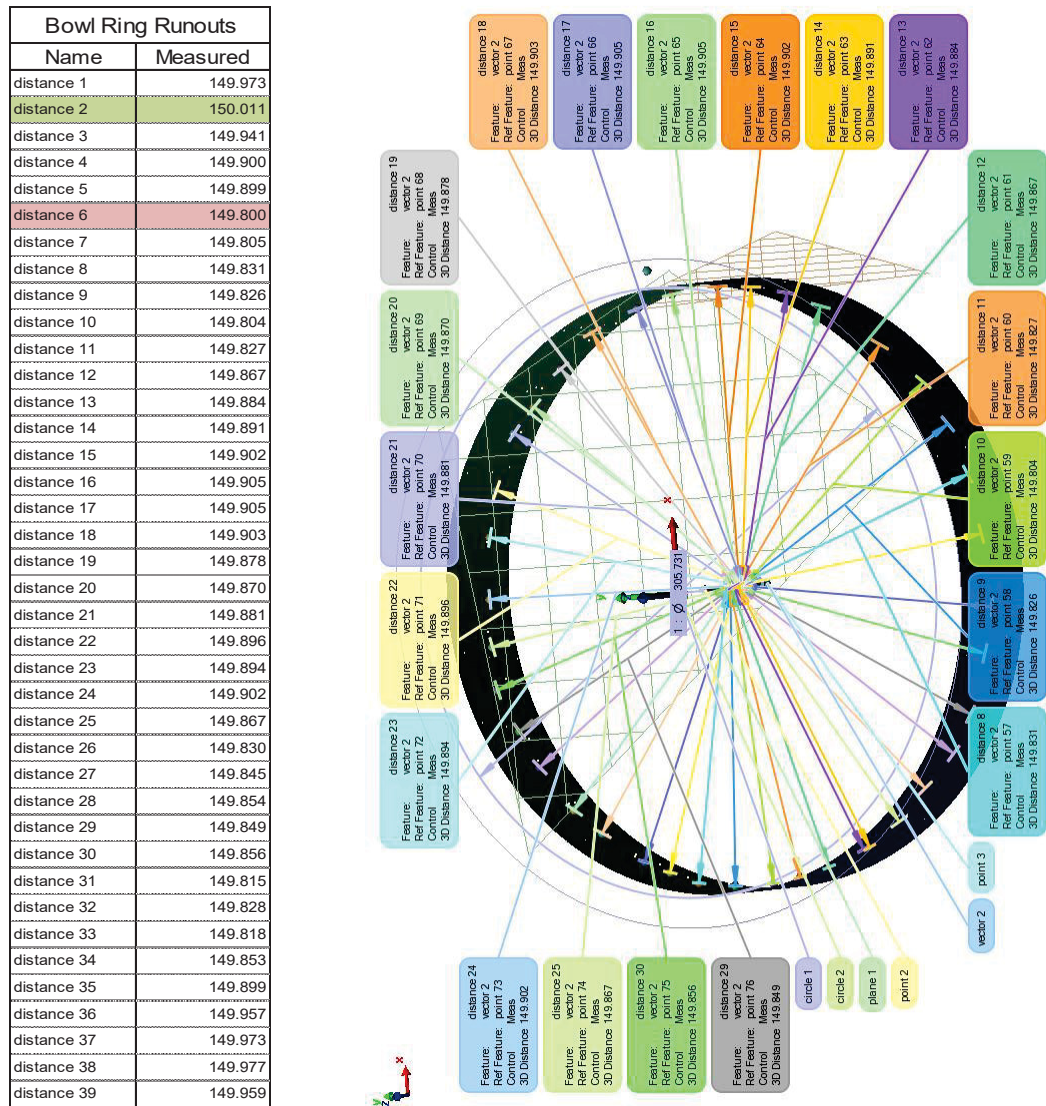


Figure 57 – Bowl ring runout checks

From the results in Figure 57 the maximum and minimum dimensions are highlighted with a result of the bowl ring check having 0.2mm runout when compared to the axis.

To measure the bore size again, a number of points are measured and an average of the points creates a diameter which is measured. The measurement of the bore is 305.7mm.

From the bowl ring drawing the bore diameter is 305.05mm and machining tolerance is  $\pm 0.05\text{mm}$  (total of 305.10 / 305.00) with a required concentricity of 0.05mm to the spigot face. Therefore, from the measured results the bowl ring is 0.6mm oversize and it would be assumed that this component is also considered to be oval with the concentricity being 0.2mm over tolerance. But as the highest and lowest measurements are close together it could be assumed that the bore may be damaged in this area.

Results from the measurements of the new impeller and bowl ring are:

$$305.7 - 304.3 = 1.4 \text{ mm clearance}$$

Where the design clearance is:

$$305.10 - 304.09 = 1.01 \text{ mm}$$

$$305.00 - 304.39 = 0.61 \text{ mm}$$

Therefore, the bowl ring has worn 0.4mm during use over many years. This excessive will contribute to increased losses in the pump as discussed in Section 2.2.6.

### 3.1.2.4 New Diffuser

As with the impeller the new diffuser was measured by using CMM hard and laser probes. The selected origin point is the mating face and the location spigot of the bowl ring.



Figure 58 – Scan image of new diffuser



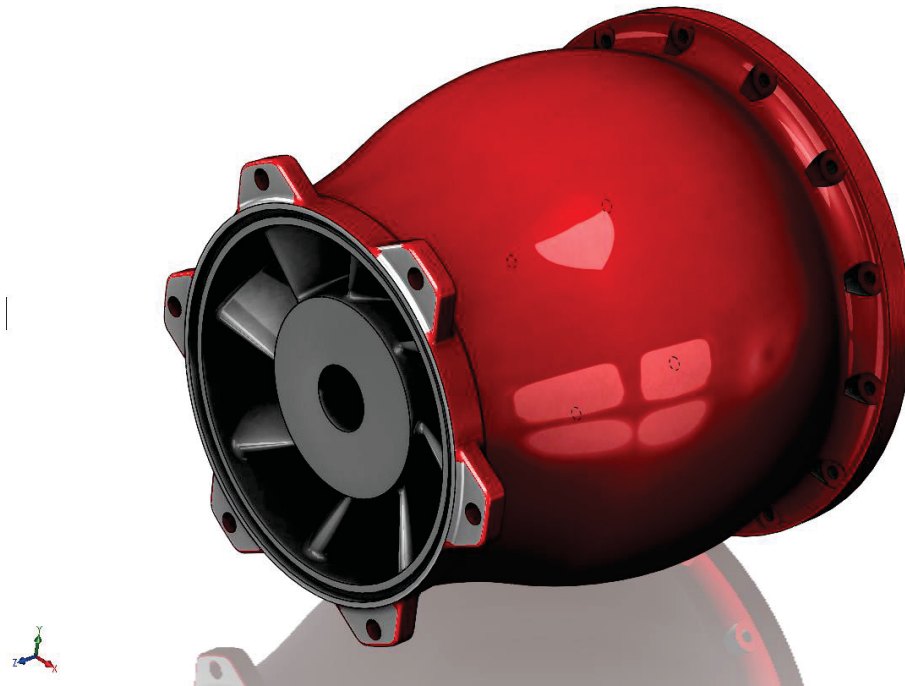


*Figure 59 – 3D CAD model of diffuser*

Unlike the impellers, the design drawing was not available for the new diffuser; therefore measurements from the scanned image were used to produce the CAD model.

When the CAD model was complete, the accuracy was checked. To check the accuracy, the CAD model is overlaid into the scan and a comparison of points is run. A comparison map shows the difference between the points of the model and scan. Figure 60 shows the results of the comparison map. Colours on the scan and the table on the side of the screen indicate the distance between the scan and CAD model (green is 0 mm red is 4 mm). The model can be adjusted to best match the scan. It must be noted that the actual casting will have inconsistencies, therefore a best fit mentality is adopted.

---

50

## 3.2 New Diffuser Design

The new diffuser is designed to combine the two functions of the standard design stator and diffuser configuration as described in Section 2.2.8.1. The new diffuser prototype, used in the laboratory experiments, was designed and patented in 1982 by Mr Hugh Nelson.

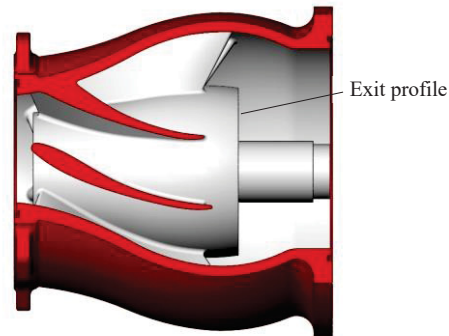
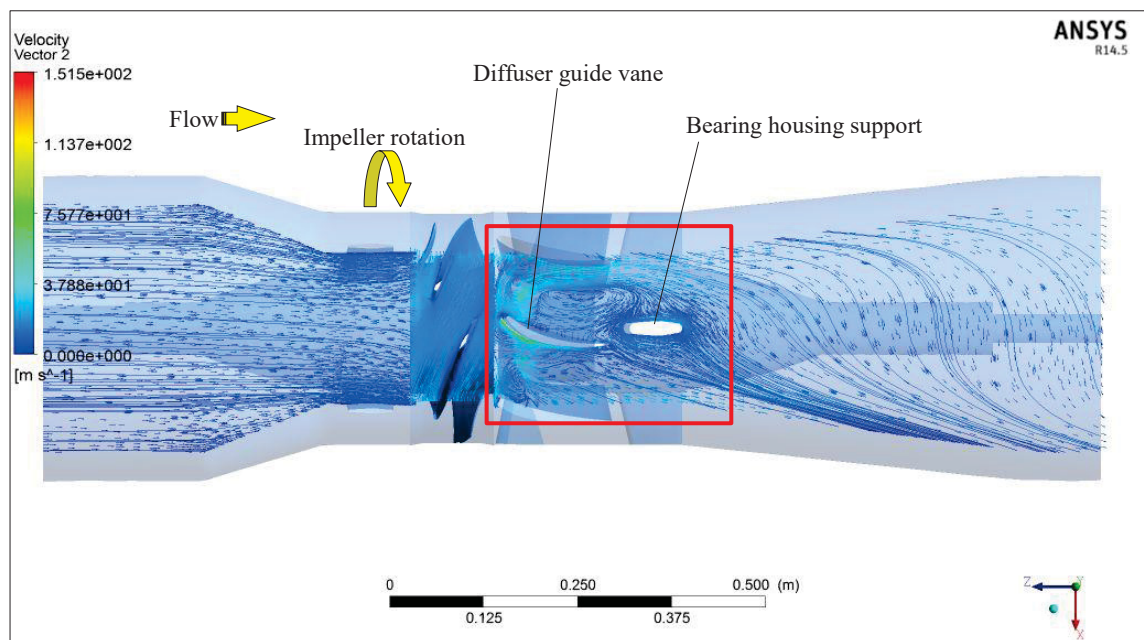


Figure 62 – New diffuser design, stator and diffuser combined.

Mr Nelson claims that the original design of a stator followed by a diffuser configuration, introduces reverse flow between the vanes on the discharge side of the stator. This internal recirculation contributes to cavitation and swirling in the flow entering the diffuser, making the kinetic energy recovery process less efficient (Nelson, H.D).

Computational fluid dynamics (CFD) analysis of the original bowl's flow passages indicates that Mr Nelson's theory is plausible (see Figure 63).





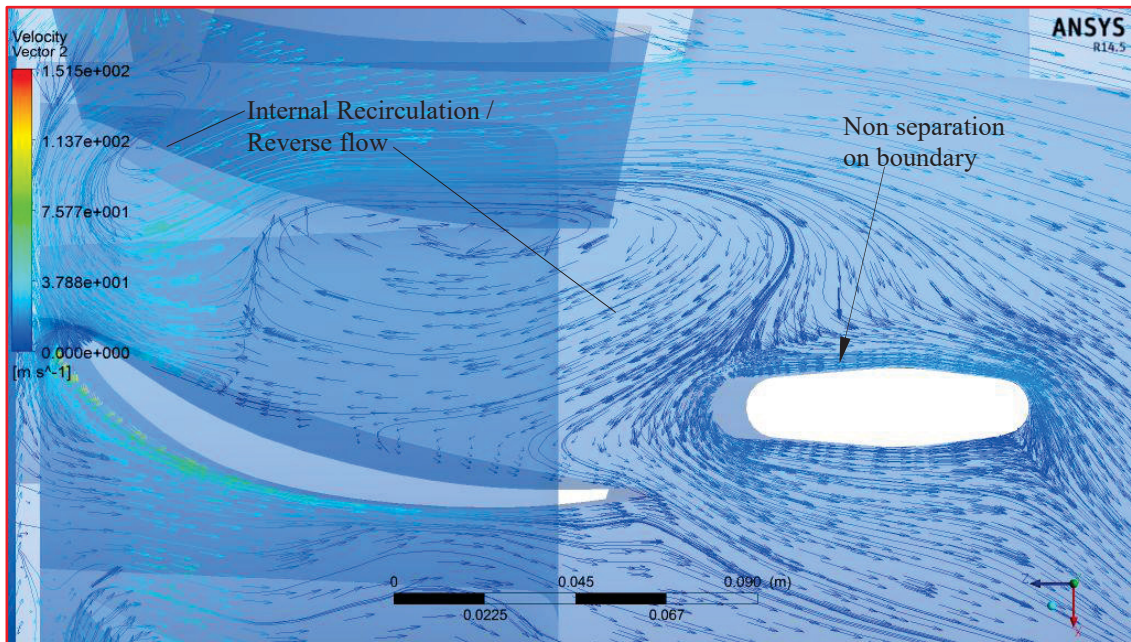


Figure 63 – Velocity streamline in a standard design ‘Ornel’ pump at midstream line, showing recirculation between diffuser vanes.

However the shape of the new diffuser is similar to that of a diffuser bowl for a vertical mixed flow type pump. As with the Axial Flow Pump, a mixed flow pump bowl is designed to direct the flow to an axial direction. But the outlet direction for a mixed flow impeller is at an angle, not an axial direction, hence the bell shape is required to redirect flow from the impeller outlet.

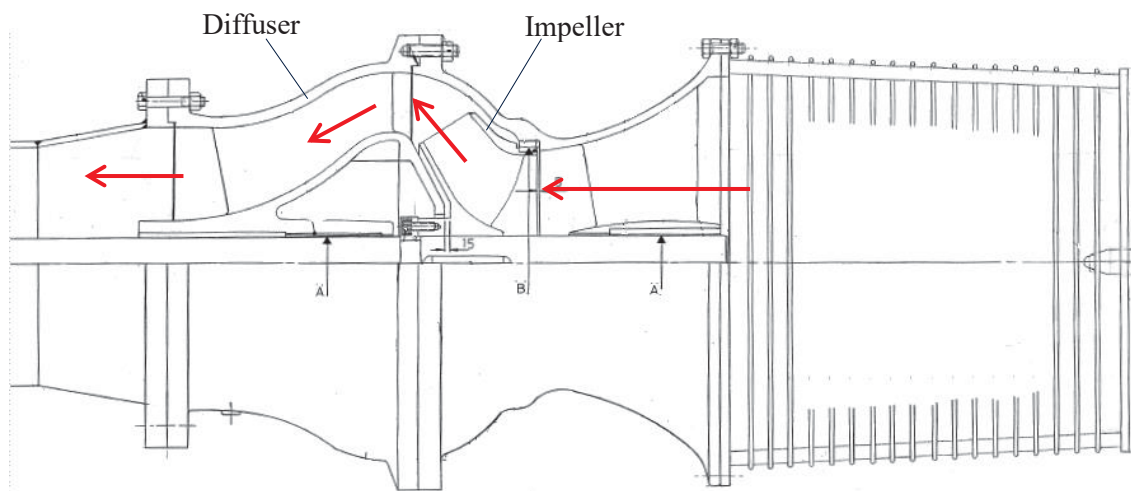


Figure 64 – Mixed flow pump flow direction

It is the belief of the author that by using this bell shape in the new diffuser design the axial flow direction will be redirected and redirection will increase the turbulence at the outlet of the new diffuser.



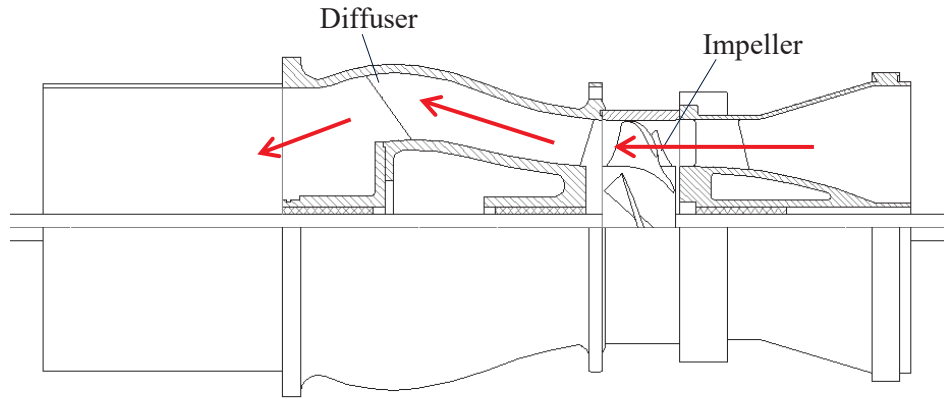


Figure 65 – New diffuser flow direction

### 3.2.1 New Diffuser Exit Profile

Previous experimental investigations indicated that the new diffuser design does reduce the swirl between the guide vanes when compared to the original stator design. However, the pump efficiency is slightly reduced. This is assumed to be partly due to the sudden enlargement of the exit profile which causes recirculation in the outlet flow area. A sudden flow area enlargement has a  $C$  value of 1.0. The ' $C$ ' value is used in the formula below to determine head loss ' $h_l$ '.

$$h_l = C \frac{(v_1 - v_2)^2}{2g} \quad \text{Equation 24}$$

$$v_1 = \frac{Q}{A} = \frac{0.318}{0.105} = 3.02 \text{ m/s} \quad v_2 = \frac{Q}{A} = \frac{0.318}{0.146} = 2.17 \text{ m/s}$$

$$h_l = 1 \frac{(3.02 - 2.17)^2}{2 * 9.81} = 0.04\text{m}$$

The ' $C$ ' value in an enlargement is close to double that of a sudden reduction ( $C = 0.4$  to  $0.5$ ). For the new diffuser it is estimated that the head loss through this Section is  $0.04\text{m}$  ( $0.4 \text{ kPa}$ ).

Figure 66 is a diagram showing the theory of how the sudden enlargement introduces secondary flow behind the faces (a) and (c). Even though the sudden enlargement in the new diffuser design has the smaller flow passage area at the outer faces, (not around the centre as per the diagram) secondary flow occurs and is directed towards the centre of the outlet flow area. This is shown in Figure 68 by using CFD to simulate the original recommended design flow of  $318\text{L/s}$  at  $1465\text{rpm}$ . The CFD results showed a drop in the flow velocity, as well as flow recirculation in the area where expected.

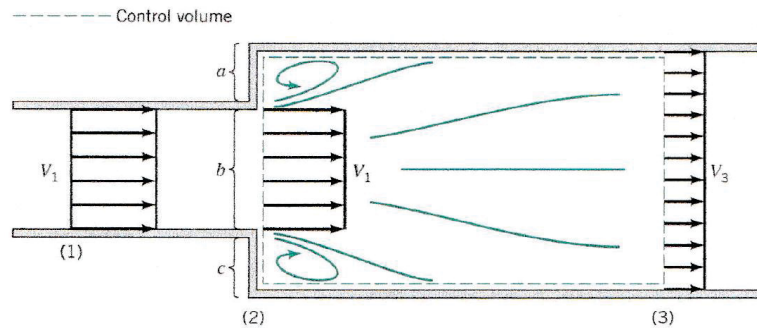


Figure 66 – Sudden enlargement (Munson, 2013) pg435

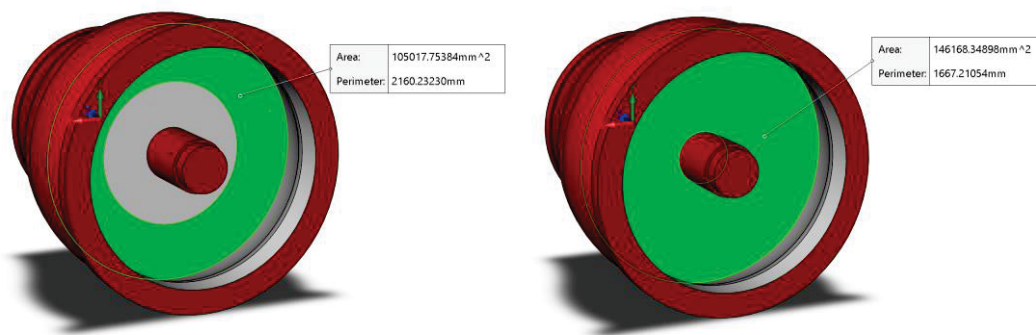


Figure 67 – Area measurement of diffuser outlet

By extending the exit profile by gradually reducing the profile towards the pump centre line, the rapid enlargement can be eliminated and the amount of recirculation reduced. Section 3.3.3 further investigates the design of a tail piece to extend the exit profile.

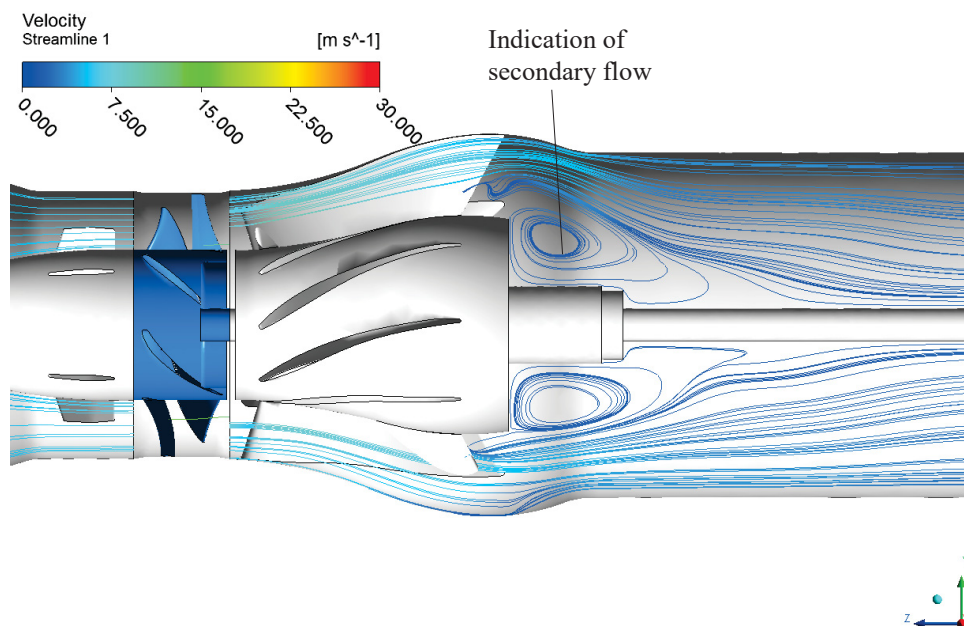


Figure 68 – New diffuser CFD velocity streamline on single plane

### 3.2.2 New Diffuser Design Investigations

The design theory discussed in Section 2.3.2 was used to investigate the design parameters of the new diffuser. The components physical dimensions were measured by CMM, as detailed in Section 3.1.

Figure 69 outlines the difference in dimensions and design configuration between the original pump design and the new diffuser design. The area above the centre line outlines the original pump design, where the new diffuser design is portrayed in the area below the centre line.

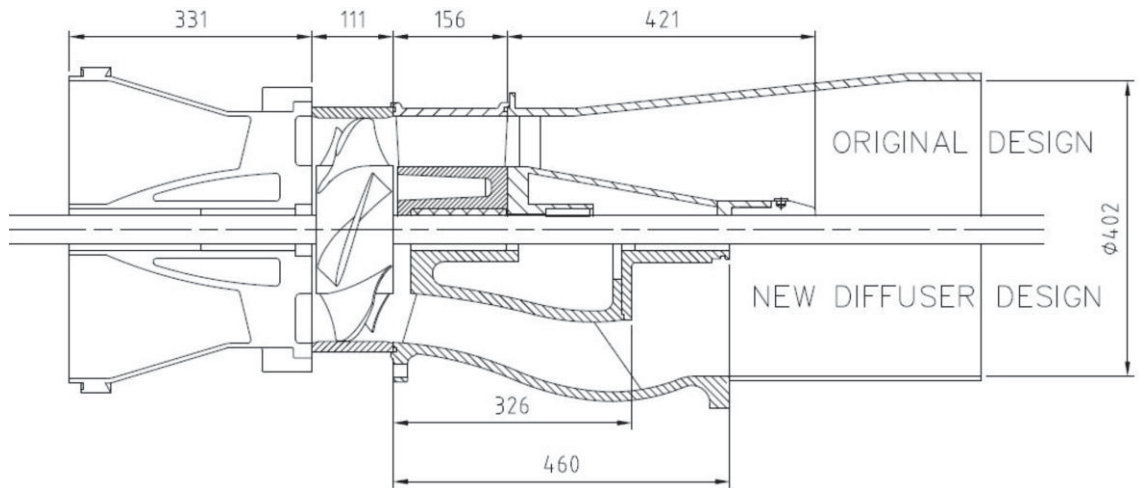


Figure 69 – Comparison of dimensions

#### 3.2.2.1 Diffuser Efficiency

To try to understand the drop in tested pump efficiency some of the design factors that affect the efficiency as mentioned in Section 2.3.2.2 were looked at in detail.

##### 3.2.2.1.1 Axial Distance

When looking at the original pump configuration, using the recommended design distance between the impeller outlet vane and the diffuser inlet vane of  $0.2 L_r$ , the distance should be approximately 13mm ( $0.2 * 65 = 13$ )<sup>10</sup>. But due to the difference in angle between the vanes, this dimension is only relevant to approximately 1/3 of the area closest to the impeller hub (see Figure 70).

<sup>10</sup> When this calculation is checked as per Stepanoff recommendation; where  $d/D_o \approx 0.05$   
( $13 / 304.24 = 0.04$ ).

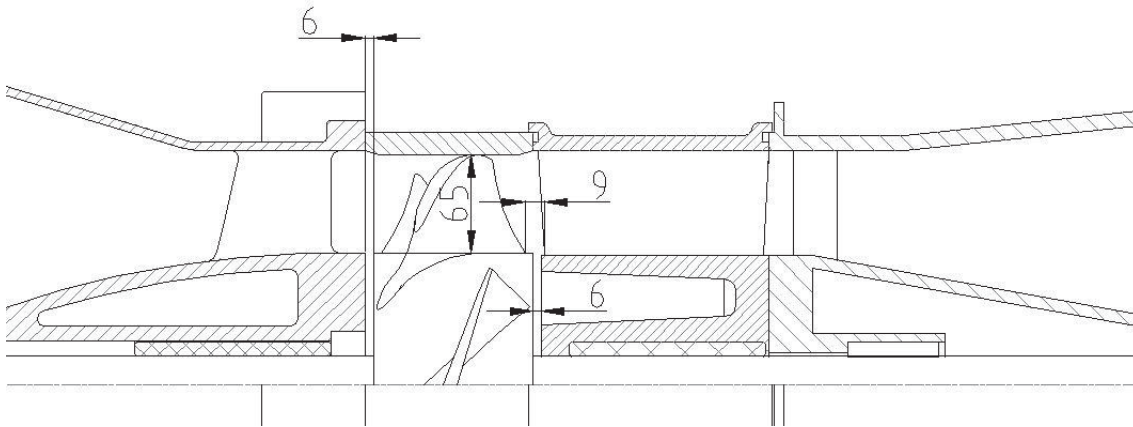


Figure 70 - Original standard 300AX pump configuration

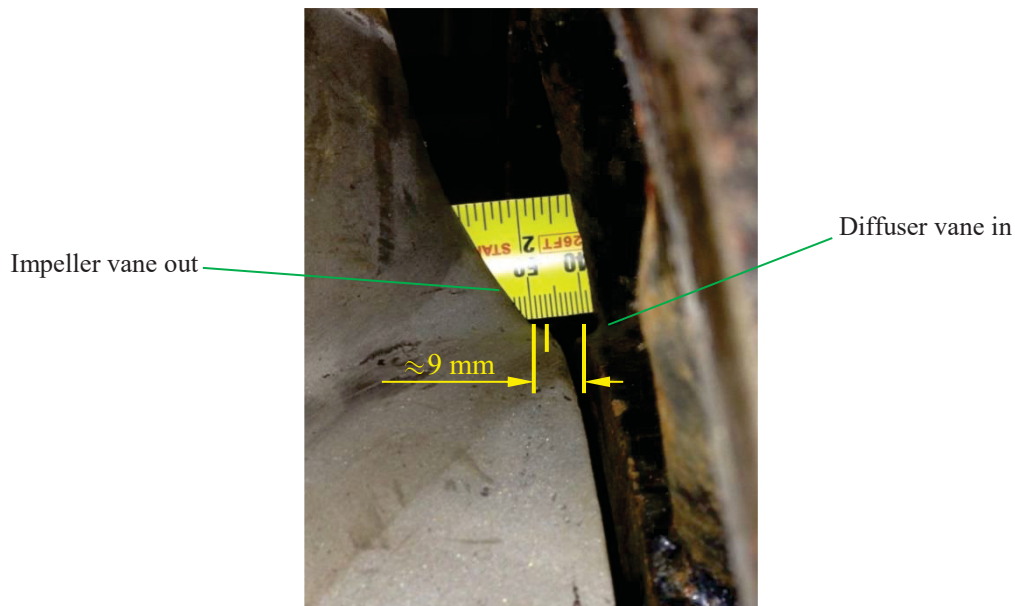


Figure 71 – Measured axial distance during pump assembly between original stator and the five vane impeller

In the case of the new diffuser, the distance of 13mm is far off being achieved with a minimum distance of 36mm (see Figure 72). This is assumed to be one of the contributing factors to the reduction of efficiency of this new diffuser design. To try to achieve the required axial distance, a spacer piece is installed at the rear of the suction case. By adding the spacer the required running gap is returned, however the axial has been reduced but is still over the recommended distance. To reduce the axial gap further, modifications such as removing 10mm from the hub face<sup>11</sup>, could be made to the new diffuser as shown in Figure 74.

<sup>11</sup> This modification was not done as the new diffuser is a one of a kind, therefore no physical modifications were allowed to be made.

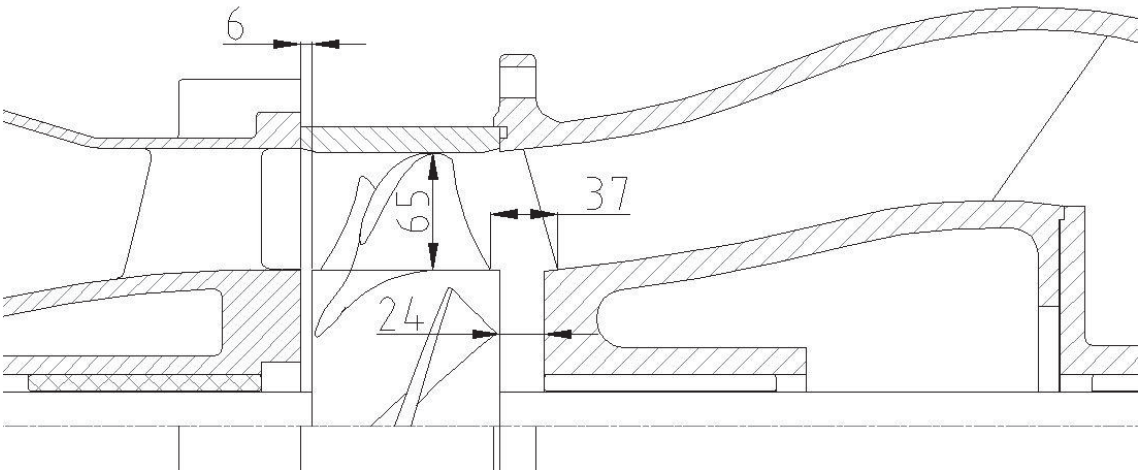


Figure 72 – Pump arrangement with new diffuser.

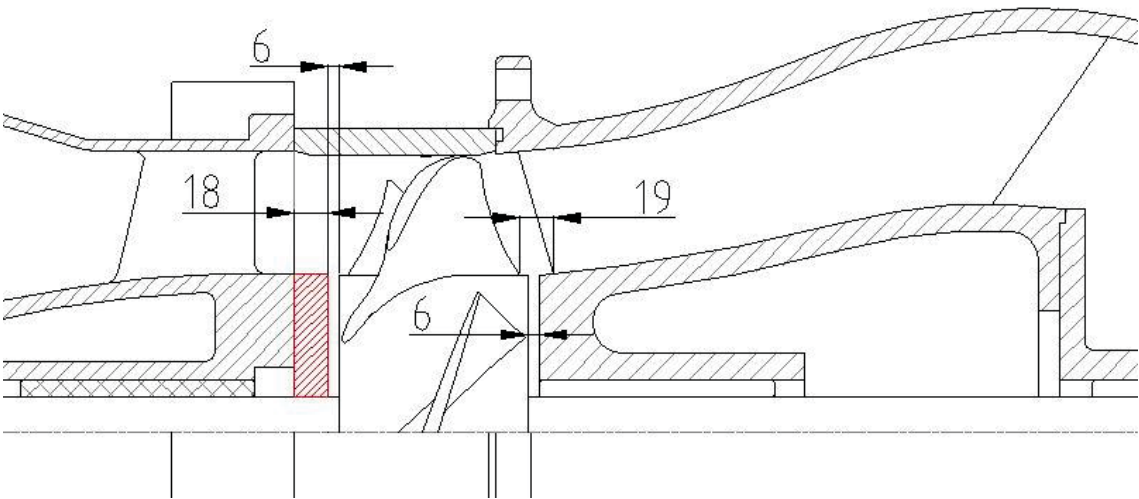


Figure 73 – Suction case spacer addition

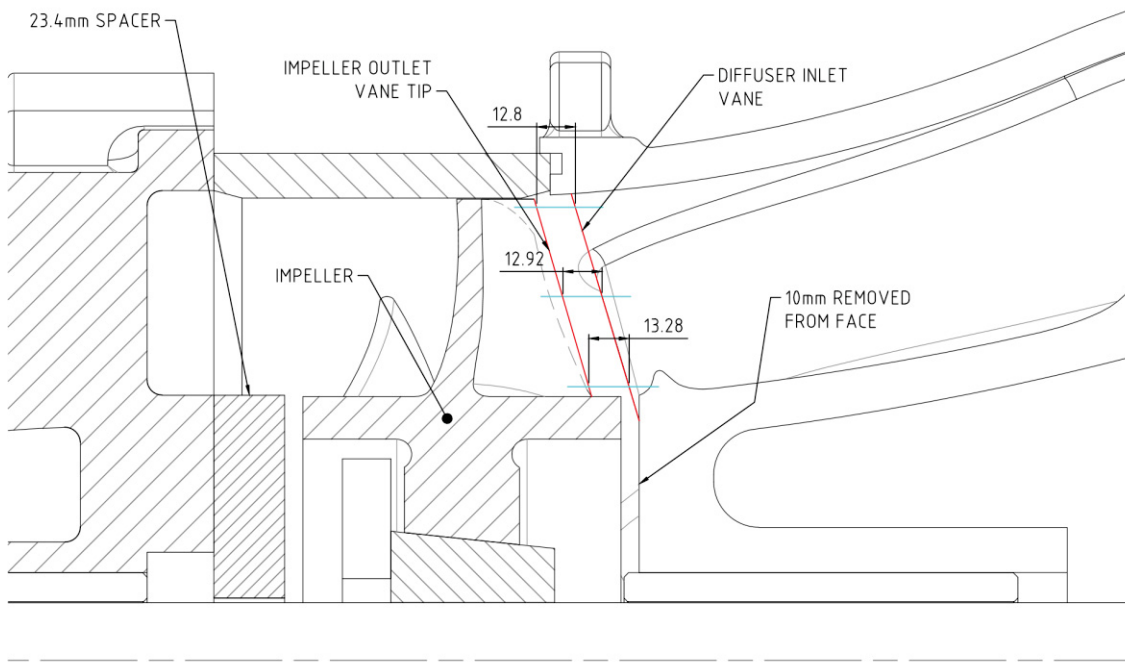


Figure 74 – Possible modifications to new diffuser

### 3.2.2.1.2 Diffuser Vane Length

To apply the same theory to the new diffuser design, as the tests mentioned in Section 2.3.2.2.2, measurements from the impeller centre to the diffuser vane inlet and outlet were taken (see Figure 75 and Figure 76). The results show the new diffuser lengths are larger than that of the original pump design. It can therefore be assumed that, as per the axial distance results, when comparing these results with the test completed by the *Wyss Company*, the new diffuser will have lower efficiency than the original design.

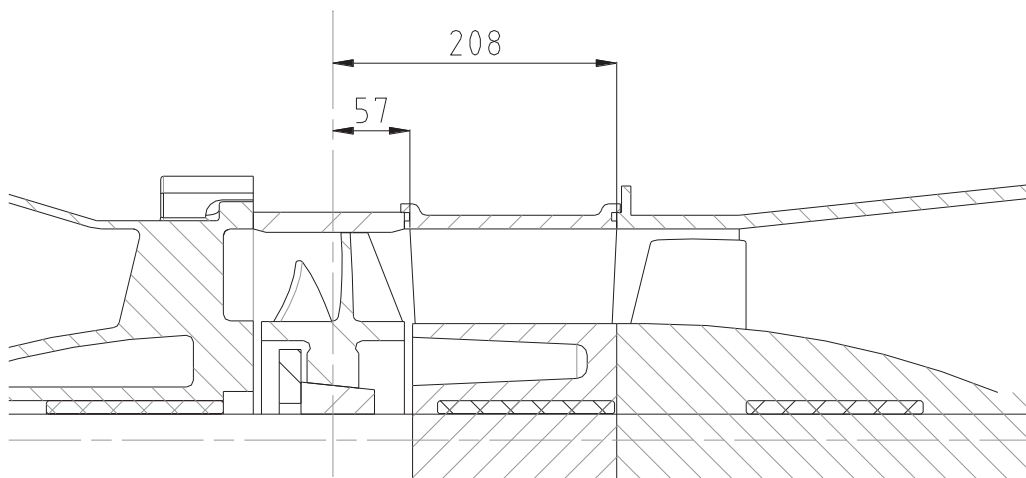


Figure 75 – Diffuser vane distance from impeller centre for original pump



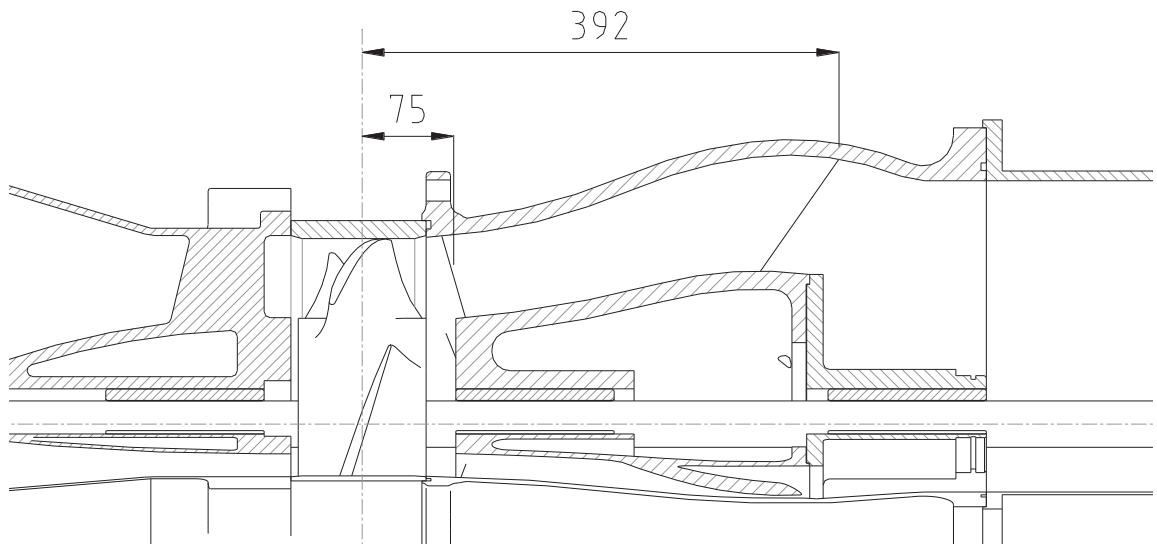


Figure 76 - Diffuser vane distance from impeller centre for new diffuser design

### 3.2.2.2 Diffuser Inlet Angle

As outlined in Section 2.3.2.1 the angle  $\alpha_2$  is used as a reference angle to match the inlet angle for the diffuser's guide vanes  $\alpha_3$ .

To calculate the velocity triangles, the impeller blade angle is required. To determine the angles, the impeller blade profiles were drawn to scale by using the dimensions from the original 'Ornel' impeller drawings. This was completed for the five, six and eight vane impellers as well as the original designed stators for the medium and high flow types.

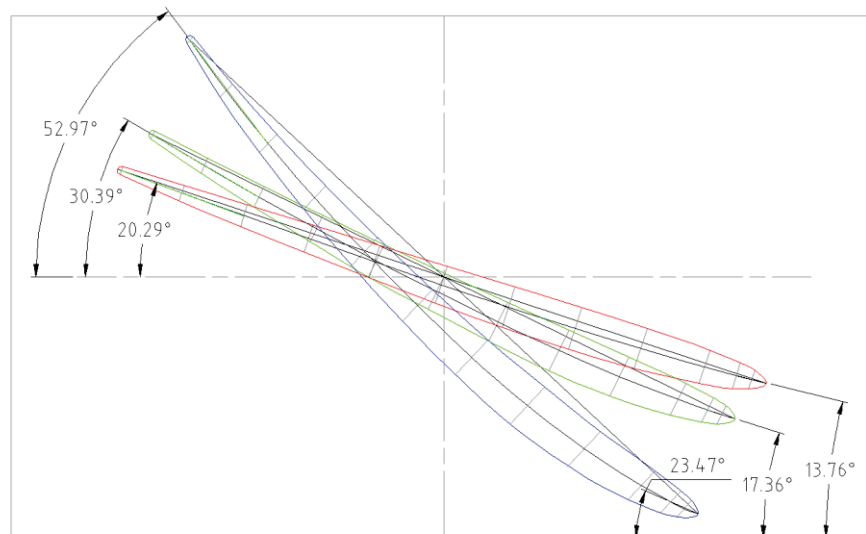


Figure 77 – Blade profiles for a five vane impeller

The vane profiles for the new diffuser were also drawn to scale from the dimensions determined via CMM shown in Section 3.1.2.4.

After the vane angles were determined, the velocity triangles could be calculated. Details of the velocity triangle calculations for each impeller can be found in Appendix A.

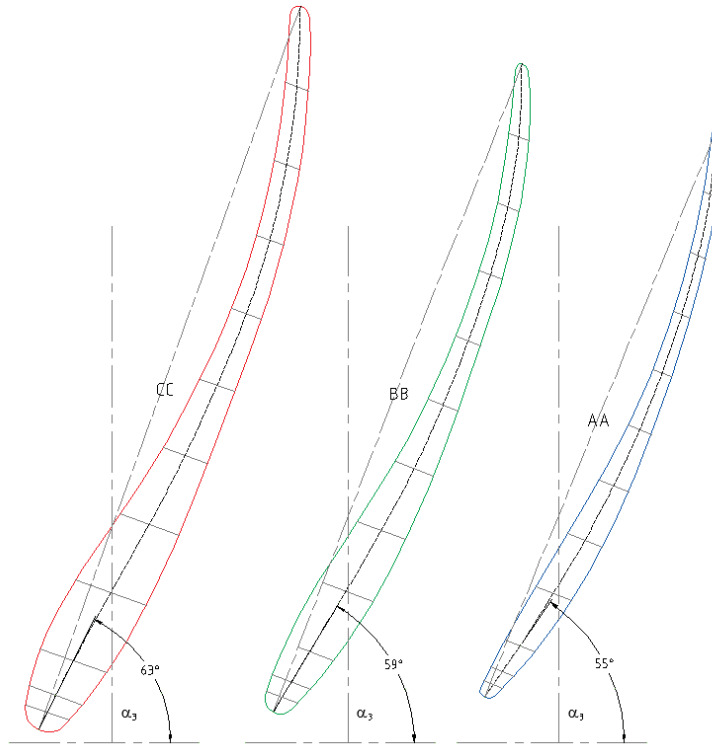


Figure 78 – New diffuser vane profile

Figure 79 shows the velocity triangles for the original standard design of a six vane impeller and a type VII bowl (stator). The results indicate there is a  $4^\circ$  difference between angles  $\alpha_2$  and  $\alpha_3$  which is within the recommended tolerance, as discussed in Section 2.3.2.1.

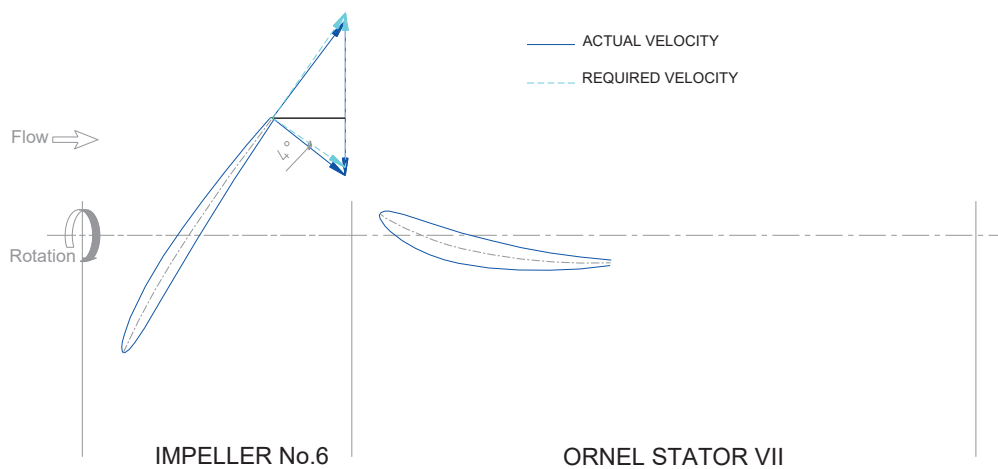


Figure 79 – Mid stream velocity triangles for 6 vane impeller and standard 'Ornel' type VII bowl (stator)



After calculating the impeller's outlet velocity triangle, the angle  $\alpha_2$  can be determined. The angle  $\alpha_3$  is also calculated using the same method.

Table 2 shows the comparison of the actual velocity (impeller outlet) to the required velocity (diffuser's actual velocity triangle) for the mid streamline measurement of the impeller and new diffuser (refer to A.2.3 for each streamline comparison).

Angle	Unit	Streamline		
		AA	BB	CC
$\alpha_2$	deg.	33	34	36
$\alpha_3$	deg.	55	59	63
difference	deg.	22	25	27

Table 2 – Comparison of five vane impeller outlet velocity to new diffuser inlet

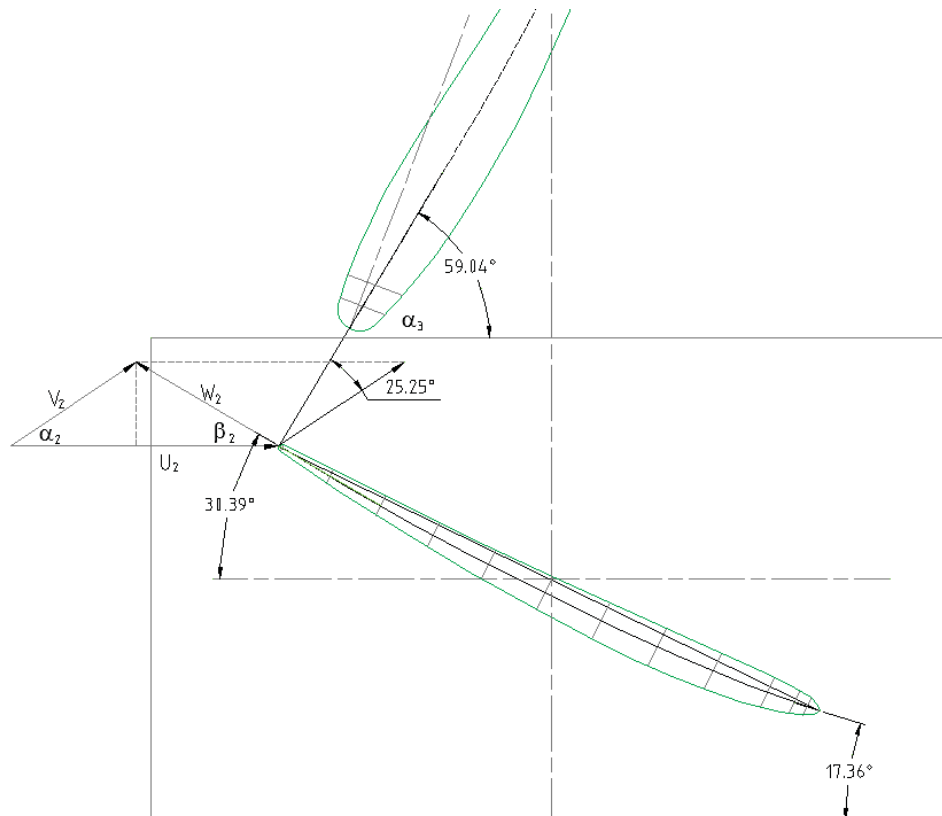


Figure 80 – Mid streamline velocity triangles for five vane impeller and new diffuser

The results show that angle  $\alpha_2$  does not fall within the recommended  $\pm 5\text{mm}$  tolerance. Therefore, the inlet angle  $\alpha_3$  of the diffuser guide vanes for use with a five vane impeller would be required to be modified to improve the match with the impeller's outlet velocity angle  $\alpha_2$ .

Angle	Unit	Streamline		
		AA	BB	CC
$\alpha_2$	deg.	44	51	49
$\alpha_3$	deg.	55	59	63
difference	deg.	11	8	14

Table 3 - Comparisons of 6 vane impeller outlet velocity to new diffuser inlet

As with the five vane impeller, the comparisons between a six vane impeller's outlet angles  $\alpha_2$  and new diffuser angles  $\alpha_3$  reveals the difference for streamlines AA, BB and CC are also outside the recommended tolerance of  $\pm 5^\circ$  however are much closer to than the five vane impeller with streamline AA. This would account for the improved efficiency results than that of the five vane impeller, shown in the previous and this new research.

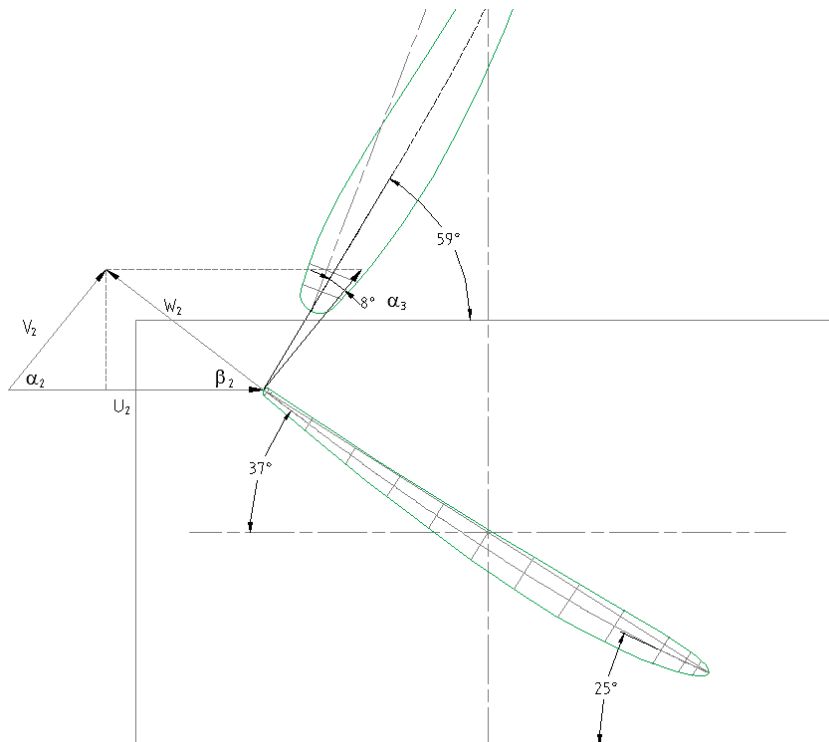


Figure 81 – Mid stream velocity triangles for 6 vane impeller and new diffuser

Due to the mismatch between angles  $\alpha_2$  and  $\alpha_3$  for the five and six vane impellers, further calculations have been made to investigate different options of increased pump speed and increased number of impeller vanes to help achieve the correct velocity angles between the impeller and diffuser inlet.

### 3.2.2.3 Pump Speed Investigations

Calculations were conducted to investigate how an increase in pump speed would affect the angles of  $\alpha_2$  and  $\alpha_3$ . By applying similitude to the original pump curve data, new curve points were produced for an increase of 30 rpm in speed (refer to Appendix A.4 for detailed calculations).

Typically, an increase in pump speed means an increase in flow and head, which is what the calculation results confirmed by the pump curves shown in Figure 82.

An increase in flow means an increase in flow velocity. As the flow velocity is a constant in many of the formulas used to calculate the velocity angles, there is no change in the velocity angles, just an increase in velocity.

Therefore, theoretically an increase in pump speed will not change the velocity angles resulting in no change in the angle mismatch between angles  $\alpha_2$  and  $\alpha_3$ .

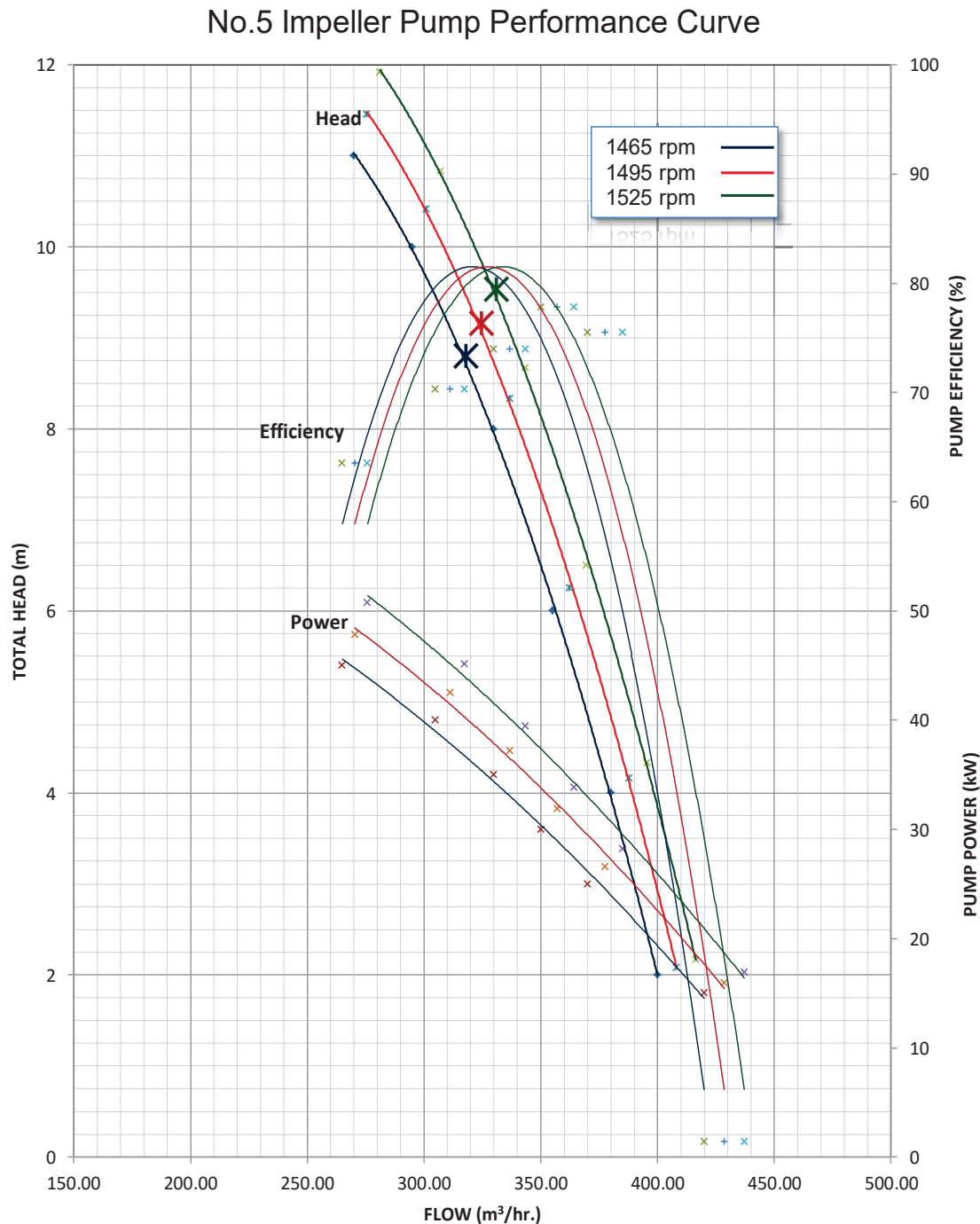


Figure 82 – Performance curve showing speed increase at 1465, 1495 and 1525 rpm using a five vane impeller

### 3.2.2.4 Increase of Impeller Blades

Calculations have been made to assess the compatibility of an eight vane impeller to the new diffuser. The BEP for the eight vane impeller was derived from the original 'Ornel' pump performance curve (see Figure 15). From the curve it was determined that the BEP for a pump running at 1465 rpm is 8.9 m head at 564 L/s flow.

The blade profiles were drawn to scale by using the dimensions from the original ‘Ornel’ impeller drawings. From the blade profile drawings the inlet and outlet blade angles could be determined.

Angle	Unit	Streamline		
		AA	BB	CC
$\alpha_2$	deg.	51	56	61
$\alpha_3$	deg.	55	59	63
difference	deg.	4	3	2

Table 4 – Comparison of an eight vane impeller to the new diffuser

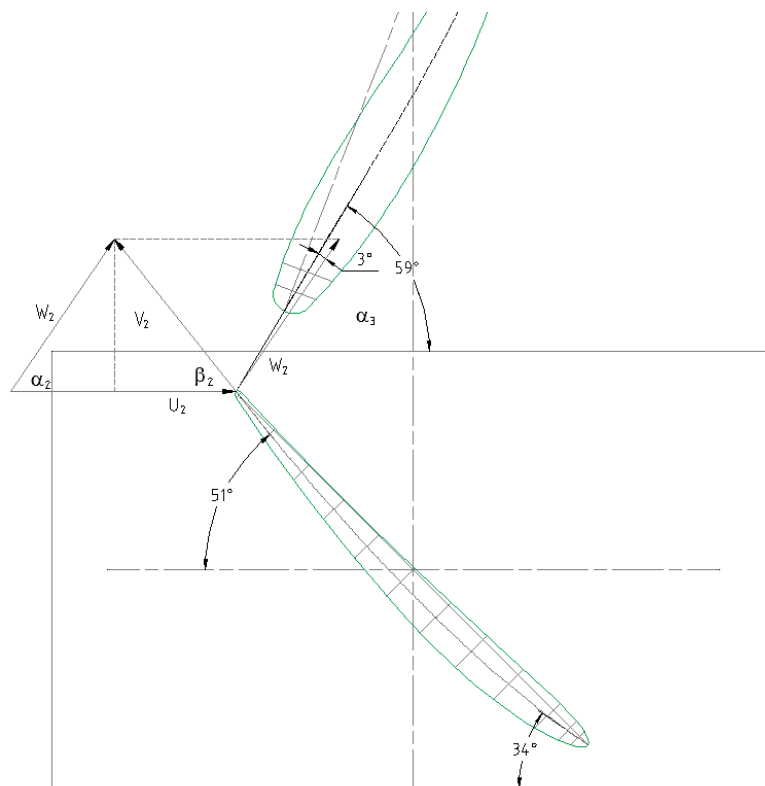


Figure 83 - Mid stream velocity triangles for eight vane impeller and new diffuser

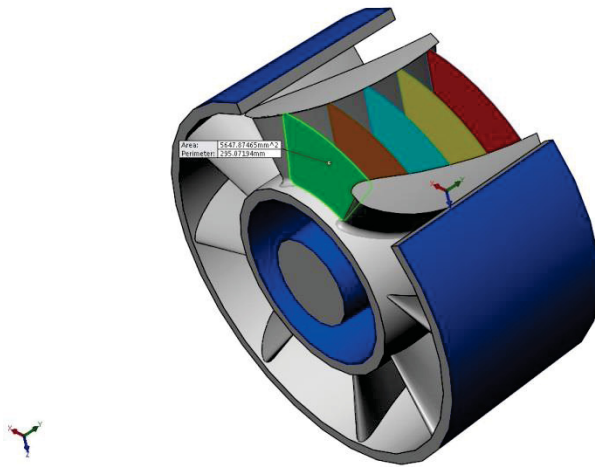
The results showed that the eight vane impeller is the most compatible to the new diffuser.

Table 4 shows that each of the streamlines lie within the recommended tolerance of  $\pm 5^\circ$ . Refer to appendix A.4 for detailed calculations.

### 3.2.2.5 Flow Passage

Cross sectional areas at a set distance were measured through the flow passage of the new diffuser (see Figure 85). The same measurements were also taken from the original Ornel

bowls. The results were plotted and compared to analyse the difference in flow passage profile increase.



*Figure 84 – Original Ornel type 5 bowl flow passage measurements*

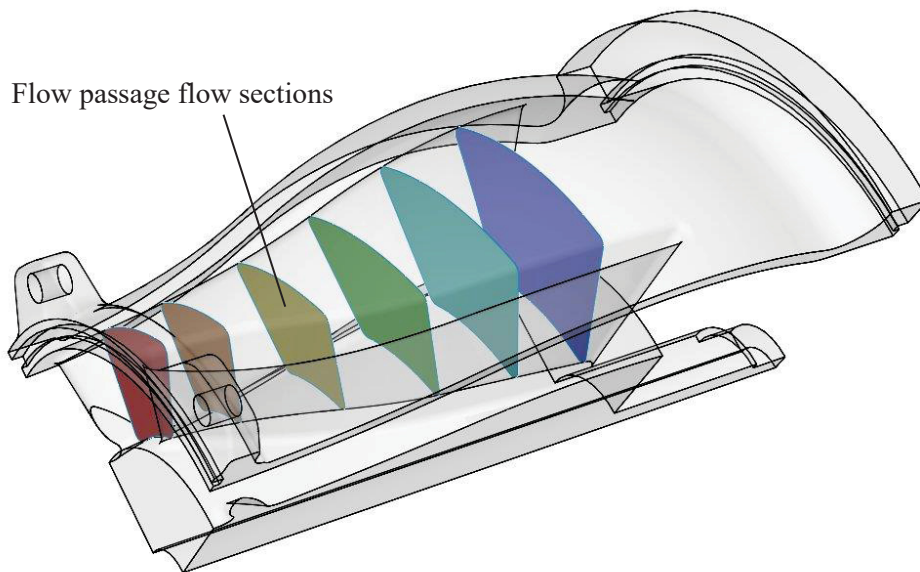


*Figure 85 – New diffuser flow passage measurements*

Figure 86 shows a graph of the plotted flow passage area section increase of the original Ornel bowl designs compared to the new diffuser. The graph shows that the section areas of the Ornel stators have a steady increase, whereas the new diffuser has a mostly steady increase but has a slight area decrease towards the discharge end of the flow passage. Also the vane length is double that of the original stators which will increase the surface friction losses through the component.

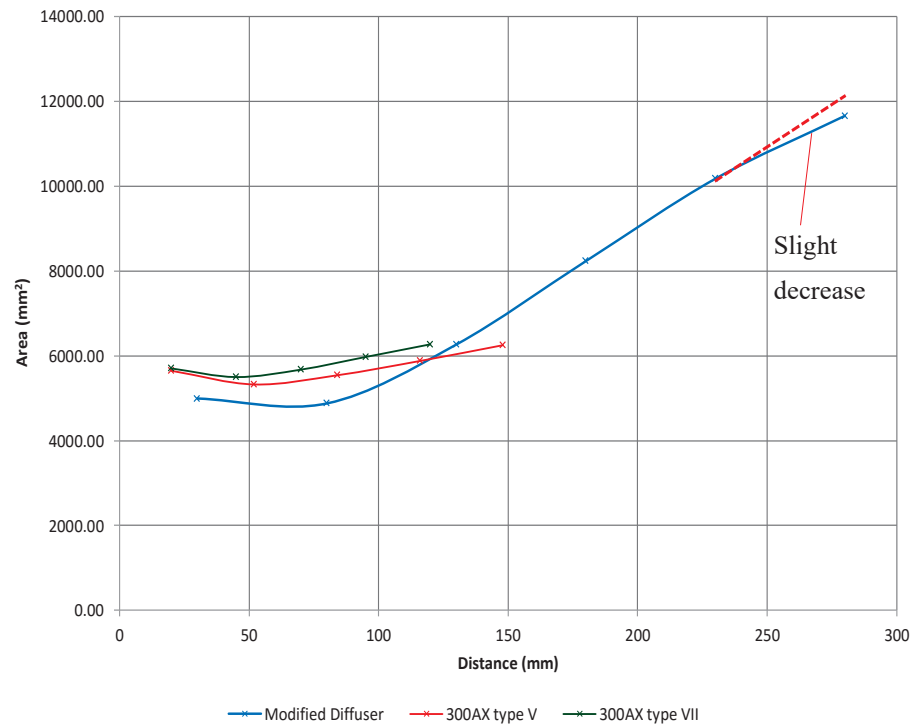


Figure 86 – Flow passage area comparison

## 3.3 Repair of New Diffuser

Due to the many years the laboratory pump had been assembled and sitting with water within the pump components, upon being dismantled, it was observed that the pump components were required to be cleaned and in some cases repaired, to ensure the components were suitable for pump testing.

### 3.3.1 Diffuser Inspection

During the removal of the pump from the test loop, the initial visual inspection of the new diffuser revealed a high level of rust build-up within the flow passages. The poor condition of the surface would require repairs.

The surface showed signs of previously being painted, which had started to peel and flake off. There is a large possibility that the paint flakes are being passed through the test loop system. As this is for test purposes only, a small amount of debris can be tolerated. However, during some of the tests performed, the debris would find its way into the vane tip clearance and would require removal during disassembly.

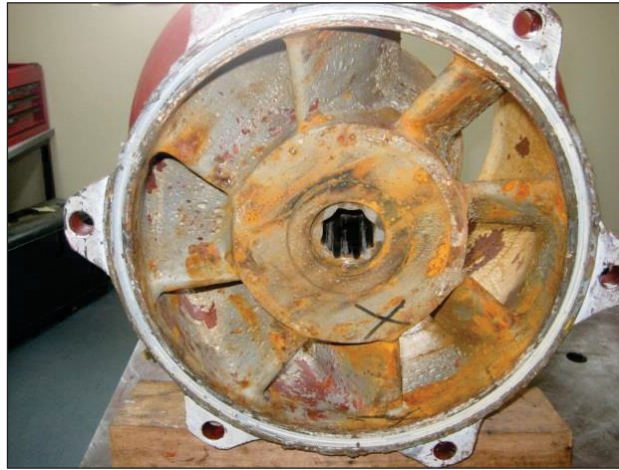


*Figure 87 – Removed diffuser pre-repairs*



*Figure 88 – Rust build-up and paint flaking on guide vane inlet*

The rust and paint also contribute to an increase in surface roughness which will increase the friction boundary layer of the flow passage way. This contributes to turbulent flow increasing reduced efficiency in the pump.

To reduce the turbulence within the flow passages, the rust and paint must be removed and a smoothed surface finish introduced.



### 3.3.2 Flow Passage Surface Repair

The diffuser was sand blasted to remove the rust damage and paint from the internal surfaces. The results of sandblasting were satisfactory but uncovered pitting damage from the rust erosion.

To repair the pitted internal surface of the diffuser, a coating was applied. The coating used is a two part epoxy ceramic coating which is reinforced with abrasion resistant fillers<sup>12</sup>. This coating will give better surface protection than the previously used paint which will result in a longer life of the diffuser. With the smooth surface of the coating and also having less surface friction resistance than steel, the efficiency will also be improved by coating the surface.

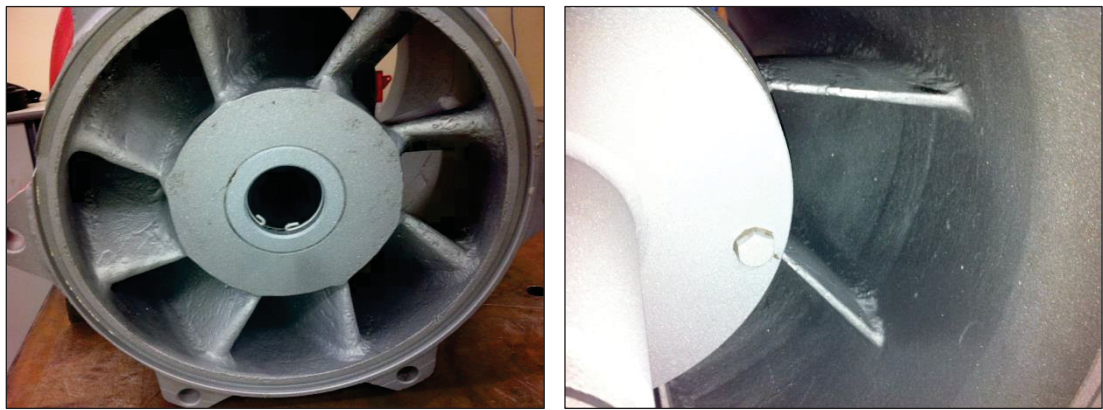


*Figure 89 – Diffuser surfaces after sand blasting*

In 1987 an investigation conducted by *Weir Minerals Australia*, demonstrated that the coating of the internal surfaces of a centrifugal pump, with efficiency coating, not only prolonged the life of a pump, it also increased the pump efficiency by, in some cases, 6%. The majority of this investigation was carried out during pump overhauls where the internals were coated and monitored once they were returned to service. This was carried out on more than 300 pumps. A testing rig was also used to determine which type of coating would be best suited to the pumps application.

The coating used in this research was applied using only two coats. This was done to keep the coating thickness to a minimum as to not reduce the cross sectional area of the flow passage. By reducing the sectional area the flow velocity will increase more so than the original velocities making the recorded data inaccurate compared to previous research. The final coating thickness of the new diffuser is approximately 0.40mm.

---

<sup>12</sup> Refer to Appendix B for coating data sheet indicating the required surface preparation and coating application techniques.



*Figure 90 – Coating being applied to surface*

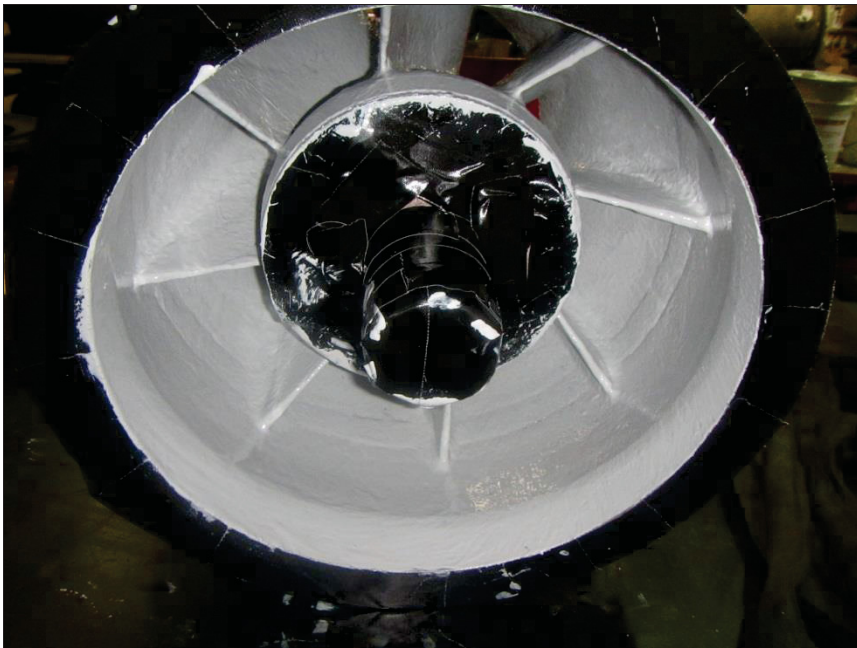


*Figure 91 – Completed coated diffuser internals*

Spigots and flange faces are covered to ensure that they are not coated. The final result is a smoother surface and protection to extend the new diffuser's life.

### 3.3.3 Tail Piece Addition

To achieve the required exit profile reduction (refer to Section 3.2.1), an attachment piece was designed. Due to the new diffuser not being able to be physically modified, as it is the only one

of its kind, it was decided that a cone shaped attachment piece was to be designed that would slide onto the existing bearing support area and bolt onto the existing back plate.

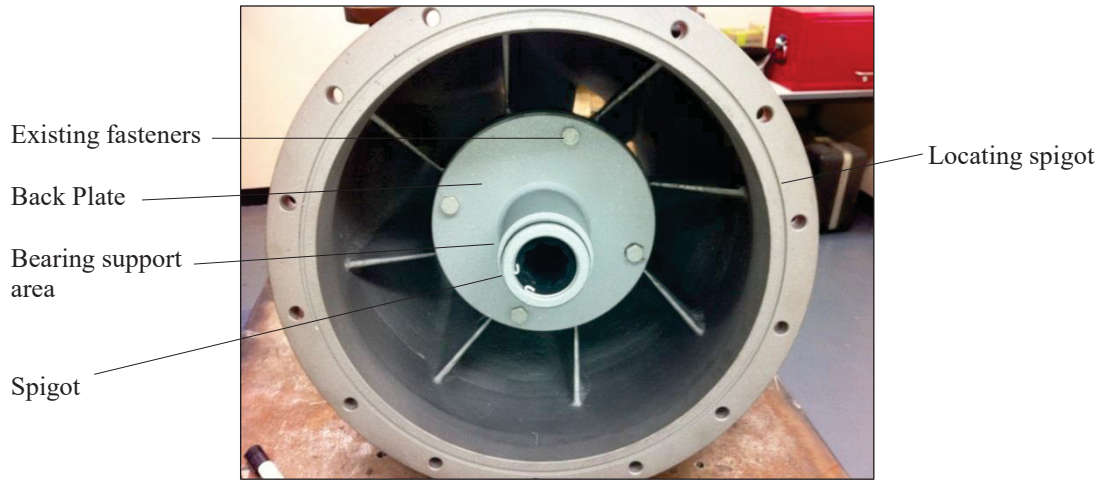


*Figure 92 – New diffuser exit area*

The design of the tail piece is based on the original design for the fabricated diffuser for an ‘Ornel’ pump. This will allow for a more gradual cross sectional transition from the new diffuser discharge to the column pipe. By the design being able to be fabricated it gave more option in the manufacturing process of the tail piece.

By not removing the back plate of the diffuser, minimal manufacturing requirements for the additional tail piece design could be achieved. For a more appropriate design, this area should be replaced, however, to reduce manufacturing cost a simple method of adding a tail piece is being used.

Due to a rough surface finish, the spigot diameter was cleaned up. This will not only give a clean mating surface but also make sure this diameter can be checked for concentricity to the locating spigots on the flanges (checked by using the CMM). This diameter also has an O-ring area which is also cleaned and the O-ring is to be replaced.

Computational fluid dynamic (CFD) analysis was conducted on various cone models to achieve the most suitable angle for reducing the flow swirl (see Section 4.4.1.3). The angle of 20° was selected due to CFD results indicating the least amount of recirculation close to the diffusers outlet vane tips and the following flow area. This is shown by comparing the CFD 2D streamline results of the new diffuser model to the tail piece model as shown in Figure 93.

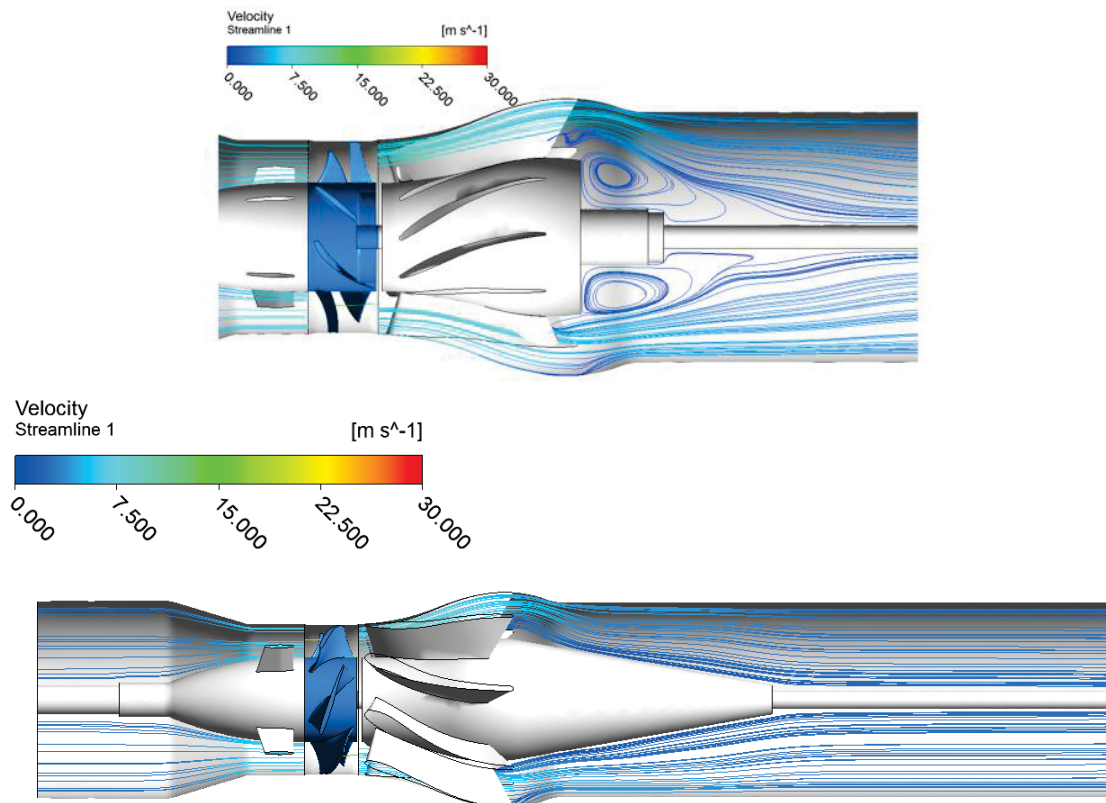


Figure 93 – CFD comparison of pump with and without 20° tail piece

The tail piece is designed to be located onto the spigot of the back plate where the bearing is held. This will ensure that the component is concentric to mating components as well as an even flow passage area through the pump. The tail piece is held in place by four socket head set screws located on the back plate. There are original tapped positions being reused for the new fasteners to secure the cone onto the back plate (see Figure 94).

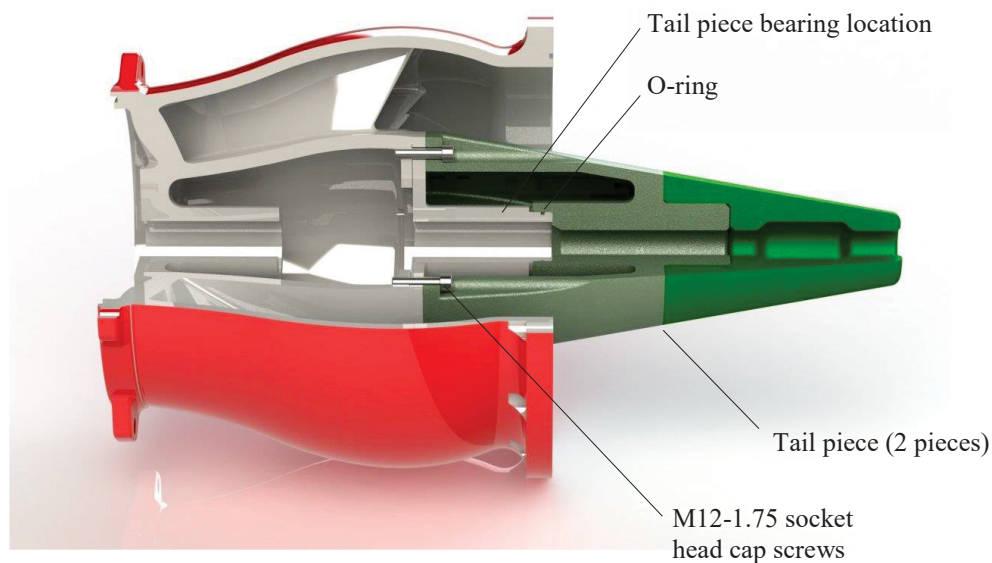


Figure 94 – Tail Piece addition to diffuser exit profile



### 3.3.3.1 Tail Piece Manufacture

To manufacture the tail piece a 3D printer was used. This method was selected over casting and fabrication due to the following reasons: casting the piece was of greater cost and it was also difficult to find a foundry which would be interested in casting a one off item. A pattern would be required to be made or printed. Once the piece is cast, it must then be machined to ensure a flat mating face and locating spigot concentricity as well as the removal of risers. A fabricated piece may be a cheaper option but similar to the cast piece would be required to be machined. Welding introduces the problem of warping which may result in the tail piece shape not being round to the axis. Both of the above methods take a great amount of man hours. The 3D printer is mostly used in industry for component prototypes, models, casting patterns etc. Therefore, for a one off item requiring high accuracy it was the perfect choice. The material used to print the tail piece is Acrylonitrile Butadiene Styrene (ABS) has a high impact resistance and corrosion resistance and is a common material used in the manufacture of clear water piping and fittings.

The printer used was a *Fortus 400mc* (see Appendix I for the data sheet) which is situated at *Weir Minerals Australia*.

#### 3.3.3.1.1 3D Printing Process

The process to produce the 3D print started with the final design model file being converted to a relevant file, in this case a 'stl' file, being transferred to the software used for the printer. The printer works by melting a fine ribbon of plastic through the computer-controlled extrusion head of the printer. The plastic ribbon is deposited in layers which build up to produce the required component.

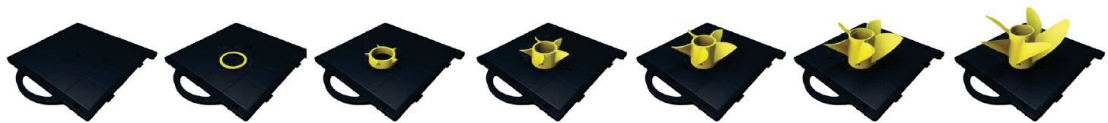


*Figure 95 - Stages of the build process (Hiemenz, 2014) pg2*



*Figure 96 – 3D printed tail piece*



*Figure 97 – 3D print surface before sanding*



*Figure 98 – Sanding 3D print surface*

## 3.4 Eight Vane Impeller Repair

Upon visual investigation of the eight vane impeller which is available for testing, it was found that the impeller has been both painted and dropped or similar. The latter was determined due to the damage found on the bottom edge of the outlet vane tip on five vanes.

Theoretical investigations have indicated that the eight vane impeller may be the most suitable impeller to run with the new diffuser (see Section 3.2.2.4). Previous research was unable to be conducted using this impeller due to the damage, therefore it was determined to repair the impeller to be used for testing.



*Figure 99 – Painted eight vane impeller*

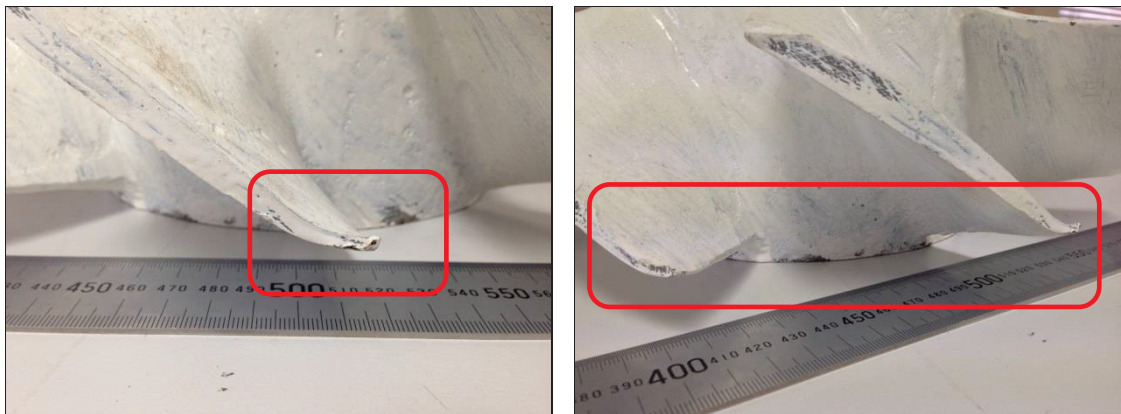


*Figure 100 – Damage to outlet vane tips.*

### 3.4.1 Preliminary CMM Check

Firstly before any repairs were to be made, the eight vane impeller was scanned using the CMM and 3D modelled using the original design drawing. The CMM scan was then overlayed on to the 3D model to determine if the damaged impeller vane profile matched the original design.



This was to determine that the impeller was suitable to use for this research and matched the model to be used for CFD analysis.

The results showed that the vane inlet tip area of the impeller matched the original design. The mid vane profile also matches the original design. The impeller outlet tip is as expected, due to damage slightly away from the design face profile.

The overall assessment indicates that the impeller is suitable for this research, as the profile matches the original design.

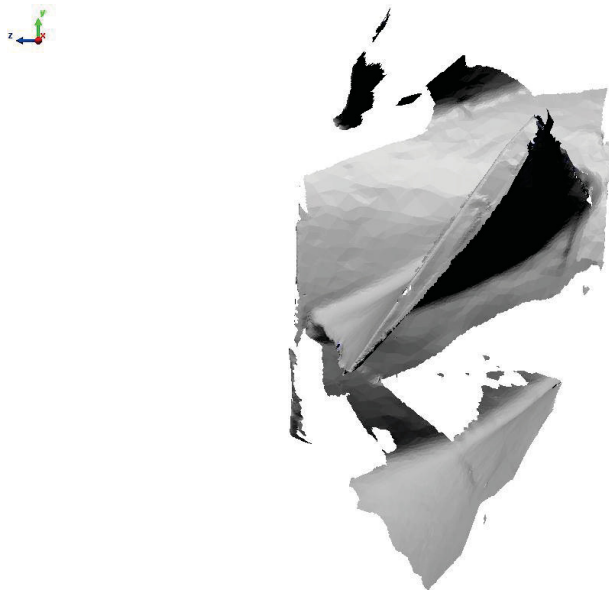


*Figure 101 – CMM scan of eight vane impeller vane*

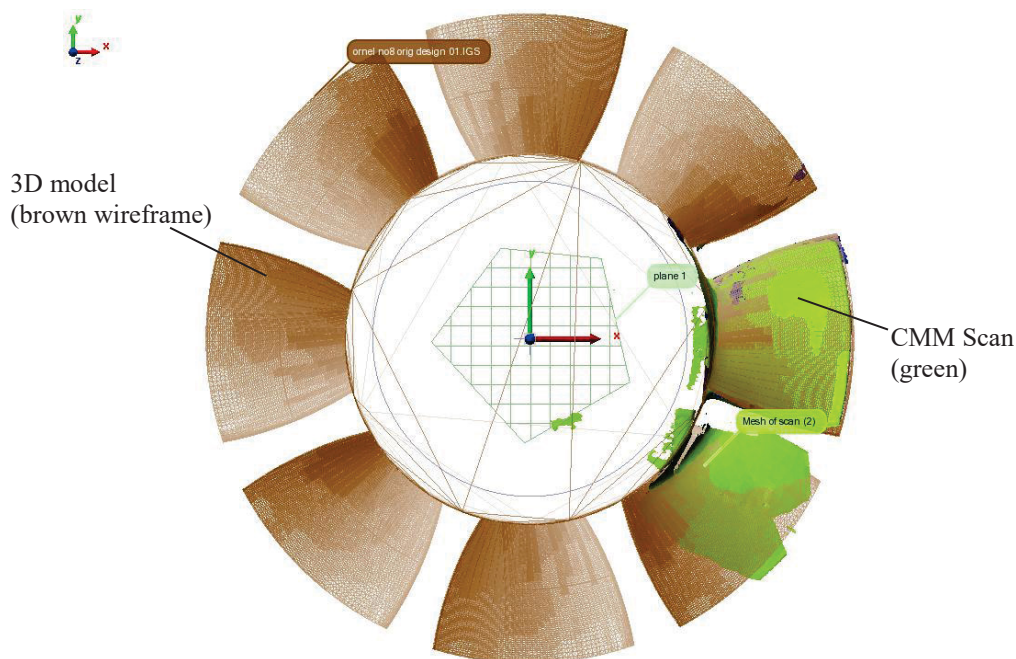


*Figure 102 – Overlay of scan to 3D model*



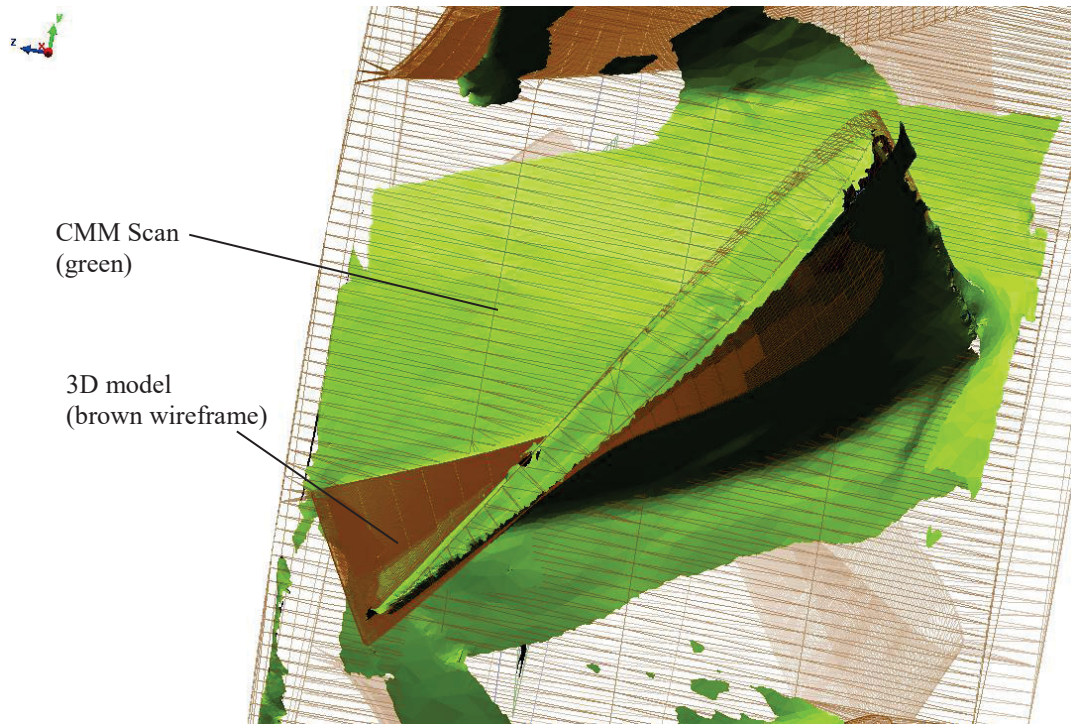


*Figure 103 – Overlay showing vane profile*

### 3.4.2 Paint Removal

The painted vane surface is uneven and patchy, which can result in adding higher losses in the pump due to the high surface friction. For best results, the paint must be removed and the impeller polished.

To remove the paint the impeller was blasted using 3 sizes of glass beads as not to damage the soft 316 stainless steel material. Sand or grit blasting is too abrasive for this material and may cause greater surface damage.



*Figure 104 – Bead blasting the impeller to remove paint.*

Upon removal of the paint it was discovered there was more damage than was originally visible.

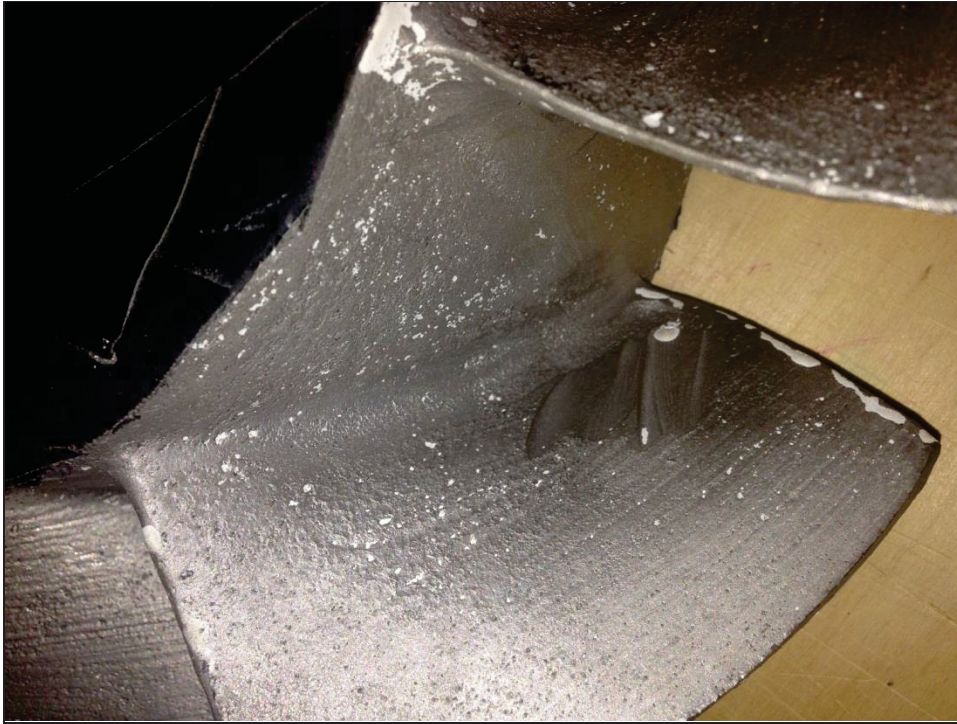


*Figure 105 – Uncovered vane face damage*

### 3.4.3 Vane Repair

To repair the damaged vane tips the areas were ‘panel beaten’ back to the original position. Due to the 316 material being soft, the damaged vane tips were easily repaired.



*Figure 106 – Repair of damaged vane tips*

### 3.4.4 Vane Polishing

After the damaged areas were repaired the impeller vanes and hub surfaces were polished using different grades of emery wheels and completed with a metal polishing compound. The surfaces of the impeller vanes were in poor condition, as shown in Figure 106 and could not be fully repaired. The polishing did improve the majority of the surfaces, which would help the testing results by having a smoother surface finish.

The final check required was the balance. The impeller was installed on a dummy shaft and placed between two rollers for a static balance. The impeller was turned a number of times and left to freely rotate until resting. The low area of the hub is marked. This was repeated a number of times. It was surprising that the impeller did not rest at the same position, therefore is assumed to be in suitable balance for testing.

## 3.5 Chapter Conclusion

To determine that the manufactured dimensions for the new diffuser and laboratory pump components comply with theoretical design parameters, a CMM was used to measure the surfaces. By using the CMM 3D scans and comparing them to the design drawings, it was discovered that:

- The 2 manufactured, five vane impellers used for the laboratory tests have a reduced chord length when compared to the original impeller design. This will result in a reduction of overall pump performance as shown in Section 2.2.8.3.
- The new five vane impeller used in the laboratory testing, is within design tolerance by having a dimension of 304.3mm on the vane tip outside diameter.
- The bowl ring bore is worn oversize with dimension of 305.7mm, which is an increase in the component design of 0.6 mm.
- The running clearance between the bowl ring and impeller vane tip is 1.4 mm which is oversize by 0.4 mm. This will also result in a slight increase of mechanical losses, hence a small added reduction to the pump performance as discussed in Section 2.2.6.

From the surface scan a 3D model of the new diffuser was created. It was calculated from the 3D model that the sudden area enlargement at the diffuser outlet increased by  $41150.6\text{mm}^2$  over a distance of 0mm creating a small mechanical loss of 0.04m head.

The measured dimensions from the components were used to determine the new diffuser design against diffuser design theory with the following results:

- The axial distance between the impeller outlet vanes and diffuser inlet vanes is 23 mm over the recommended distance of 13 mm. It is assumed that this distance increase is



one of the issues affecting the pump efficiency. To reduce this distance a spacer is installed at the suction case outlet.

- Diffuser vane length is longer than the original design. With a longer vane the increased surface friction will add mechanical losses to the pump.

From the 3D model created, the dimensions of the blade profiles were produced at three streamline sections through the vanes AA (hub), BB (midsection) and CC (shroud) to determine the vanes profiles specifically the inlet angle  $\alpha_3$ . The impellers relative and absolute velocities were calculated at the same streamline diameters and the outlets absolute velocity angle  $\alpha_2$  compared to the diffuser's vane inlet angle  $\alpha_3$ . The results indicated that the five vane impeller was not a suitable match to the new diffuser, as the velocity angle difference at each streamline is above the recommended tolerance angle of  $\pm 5^\circ$  to the vane inlet angle. The same analysis was used with a six and eight vane impeller (the only impellers available to the laboratory) and the results were that the eight vane impeller was the most suitable match to the new diffuser design with a difference between  $\alpha_2$  and  $\alpha_3$  at each streamline are within the  $\pm 5$  tolerance. The following results were attained from the collected data:

- The new diffuser does not match the five vane impeller with the measured angles as per the Table 2 from Section 3.2.2.2.

Angle	Unit	Streamline		
		AA	BB	CC
$\alpha_2$	deg.	33	34	36
$\alpha_3$	deg.	55	59	63
difference	deg.	22	25	27

- The six vane impeller does not match the new diffuser with the measured angles as per the Table 3 from Section 3.2.2.2.

Angle	Unit	Streamline		
		AA	BB	CC
$\alpha_2$	deg.	44	51	49
$\alpha_3$	deg.	55	59	63
difference	deg.	11	8	14

- The eight vane impeller is a match for the new diffuser with the measured angles as per the Table 4 from Section 3.2.2.4.

Angle	Unit	Streamline		
		AA	BB	CC
$\alpha_2$	deg.	51	56	61
$\alpha_3$	deg.	55	59	63
difference	deg.	4	3	2

From the data collected it is shown that the new diffuser design is for a high flow impeller application (7 to 8 vane) not the original medium flow impellers (3 to 6 vane).

It was also observed that there are a number of small mechanical losses throughout the components which when added together accumulate to produce significant losses affecting the pump's performance.

Therefore, the dimensional inspection results shown in this chapter prove that the new diffuser design theoretically does not fall within theoretical design parameters. Also the five vane impellers with a reduced chord length will not reach the OEM pump capacity as per the performance curves.

# 4 Computational Fluid Dynamics (CFD)

Computational Fluid Dynamics (CFD) is the science of using algebraic equations to predict fluid flow, heat and mass transfer, chemical reactions and other flow related trends. It is used as one of the design stages for the concept design and development for products, as well as component troubleshooting and redesign.

For this research CFD is being used in conjunction with laboratory pump testing to analyse predicted swirl and flow velocities within the pump's components.

This section provides an outline of the parameters used to analyse the fluid flow patterns through the Axial Flow Pump, as well as a brief description of the governing equations and the type of modelling used to best establish the desired results. This section tests a number of different designs for the tail piece addition to determine the most appropriate shape. By comparing the flow patterns of the original bowl/diffuser design to the new diffuser design, the effectiveness of additions to the new diffuser to reduce the swirl recirculation can be predicted. Possible modifications to the new diffuser and a diffuser re-design were also analysed.

## 4.1 CFD Nomenclature

Symbol	Description
$\rho$	Density
$t$	time
$U$	Vector of velocity
$u$	Fluctuating velocity component in turbulent flow
$\tau$	Shear stress
$S_M$	Momentum stress
$S_E$	Energy source
$\delta$	Identity matrix or Kronecker delta function
$\lambda$	Thermal conductivity
$T$	Static temperature
$h$	Specific static enthalpy
$h_{tot}$	Specific total enthalpy
$p$	Static pressure
$\mu$	Molecular (dynamic) viscosity

$k$	Turbulence kinetic energy per unit mass
$\nabla$	Vector operator = $\frac{\partial}{\partial x}, \frac{\partial}{\partial y}, \frac{\partial}{\partial z}$

## 4.2 CFD Introduction

To calculate the many different aspects of the fluid flow passing through the pump, certain differential equations are applied to a particle of the fluid to determine the required results. The fluid particle is described as a point. The equations that are applied to the point to determine its motion are highly complicated and cannot be solved exactly. To analyse the fluid motion through a pump there are millions of points created. Therefore CFD is used to be able to resolve these multiple equations.

CFD analyses the fluid flow patterns through computer modelled components. The CFD solver used for this research is based on finite volume method (FVM). This method uses integral formulations to express the conservation laws, allowing calculation of discontinuous functions. FVM requires dividing the physical flow area of the model into cells by creating mesh with certain characteristics as detailed in Section 4.3.2. The solver discretises the integral form of the governing flow equations and applies variables in discrete points of the mesh called nodes. This integral formulation is prone to uncertainties; therefore, FVM will use artificial viscosities to produce stable results. These equations are solved numerically to render the solution field.

Navier-Stokes equations in their conservation form are the governing equations used, as they determine the momentum, mass transfer and heat.

### 4.2.1 Continuity Equation (Mass Transfer)

$$\frac{\partial \rho}{\partial t} + \nabla \cdot (\rho U) = 0 \quad \text{Equation 25}$$

### 4.2.2 Momentum Equations

$$\frac{\partial(\rho U)}{\partial t} + \nabla \cdot (\rho U \otimes U) = -\nabla p + \nabla \cdot \tau + S_M \quad \text{Equation 26}$$

Where stress is related to strain by

$$\tau = \mu \left( \nabla U + (\nabla U)^T - \frac{2}{3} \delta \nabla \cdot U \right) \quad \text{Equation 27}$$

### 4.2.3 Total Energy Equations

$$\frac{\partial(\rho h_{tot})}{\partial t} - \frac{\partial p}{\partial t} + \nabla \cdot (\rho U h_{tot}) = \nabla \cdot (\lambda \nabla T) + \nabla \cdot (U \cdot \tau) + U \cdot S_M + S_E \quad \text{Equation 28}$$



Where  $h_{tot}$  is the total enthalpy.

$$h_{tot} = h + \frac{1}{2}U^2 \quad \text{Equation 29}$$

## 4.2.4 Turbulence Equations

As this thesis is investigating the flow of fluid around the pump components, turbulence modelling is used to achieve satisfactory analysis of the flow regions. Fluid turbulence modelling is defined in (ANSYS Inc, 2013) as consisting of fluctuations in the flow region in time and space. Being turbulence is three dimensional and unsteady; trying to calculate its properties can be complex. Therefore CFD uses turbulence models to account for the effects of fluid turbulence.

Turbulence model equations substitute average quantities into the fluctuating sections of the Navier stokes equations to eliminate the high degree of time and velocity variations which occur with fluid turbulence, due to the Reynolds factor. These equations are known as Reynolds Averaged Navier-Stokes (RANS).

By substituting the average quantity the Continuity equation translates into:

$$\frac{\partial \rho}{\partial t} + \frac{\partial}{\partial x_j} \cdot (\rho U_j) = 0 \quad \text{Equation 30}$$

The RANS equation for momentum substitutes the Reynolds stress  $\rho \overline{u_i u_j}$  therefore changing the equation to:

$$\frac{\partial(\rho U_i)}{\partial t} + \frac{\partial}{\partial x_j} \cdot (\rho U_i U_j) = -\frac{\partial p}{\partial x_i} + \frac{\partial p}{\partial x_j} (\tau_{ij} - \rho \overline{u_i u_j}) + S_M \quad \text{Equation 31}$$

The RANS energy equation is:

$$\frac{\partial(\rho h_{tot})}{\partial t} - \frac{\partial p}{\partial t} + \frac{\partial p}{\partial x_j} (\rho U_j h_{tot}) = \frac{\partial}{\partial x_j} \left( \lambda \frac{\partial T}{\partial x_j} - \rho \overline{u_j h} \right) + \frac{\partial}{\partial x_j} [U_i (\tau_{ij} - \rho \overline{u_i u_j})] + S_E \quad \text{Equation 32}$$

The viscous work part of the equation is  $\frac{\partial}{\partial x_j} [U_i (\tau_{ij} - \rho \overline{u_i u_j})]$  and the total enthalpy  $h_{tot}$  is determined by:

$$h_{tot} = h + \frac{1}{2}U_i U_j + k \quad \text{Equation 33}$$

Where the kinetic energy is determined by:

$$k = \frac{1}{2} \overline{u_i^2} \quad \text{Equation 34}$$

## 4.3 Research Parameters

The computational fluid dynamics program being used for this research is *ANSYS CFX*. A number of models of different pump configurations with different parameters were run to determine best suitable results.

The most appropriate set of parameters were selected as a base for every CFD model to be formatted to. To determine the final parameters various simulations were conducted to prove which setup had the closest outcome to the actual laboratory test results for pressure at the pump's BEP flow rate.

However, some of the CFD's research setup selections were restricted by the amount of processing time and computer capacity which was available. The approximate process running time for each model was around 10 hours.

The following headings indicate the parameter selections made.

### 4.3.1 Analysis Type

The type of analysis selected was Shear Stress Transport (SST). Shear Stress Transport is a variant of  $k-\omega$  and  $k-\varepsilon$  models. The  $k-\varepsilon$  models are the standard for predicting fully turbulent flows but studies conducted by Dr Menter concluded that the prediction of boundary layer separation was not accurate, whereas a  $k-\omega$  model will give a more accurate prediction of fluid turbulence close to the wall. SST modelling was developed for the accurate turbulence prediction, particularly for airfoils. It does this by combining the best parts of both  $k-\omega$  and  $k-\varepsilon$  models to predict more accurate turbulence results.

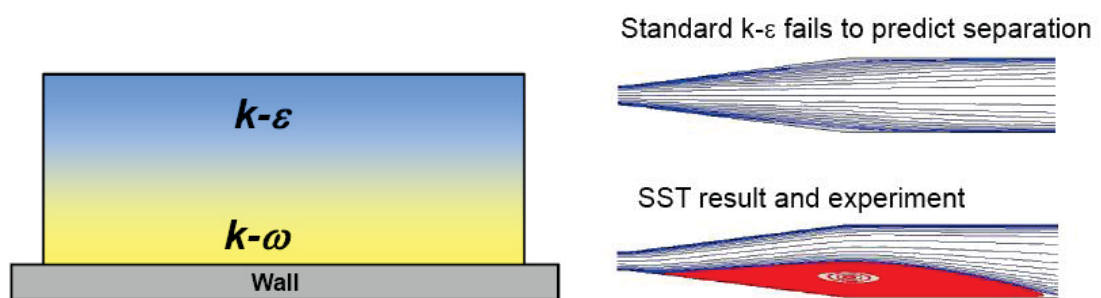


Figure 107 – SST model blend for accurate turbulence prediction (ANSYS Inc, 2013) pg18 Lecture 7

### 4.3.2 Grid Selection

Creating the mesh for the CFD model is an essential part of the computation process. Meshing divides the flow area of the model into the cells required for the computation to take place. The correct mesh selection is critical to attain accurate results.

There are four different types of elements used to create the mesh: hexahedron, tetrahedron, prism and pyramid as shown in Figure 108. With each element having both advantages and disadvantages depending on the results required.

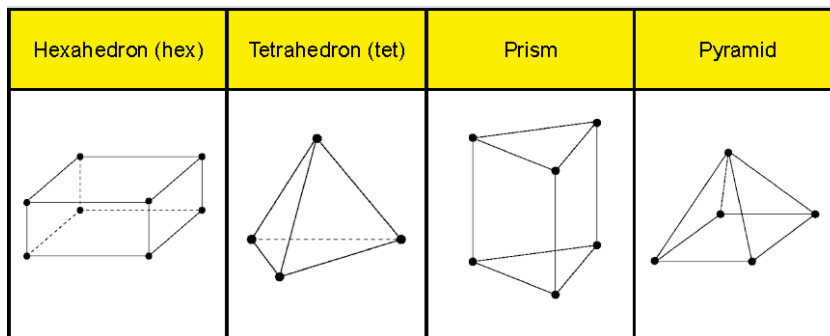


Figure 108 – Types of mesh elements (ANSYS, 2013) lecture 10 pg. 33

The type of mesh used to attain the most accurate results required for turbulence analysis is an unstructured mesh consisting of a combination of tetrahedron, hexahedron and pyramid elements. Figure 109 shows in detail the elements used in the mesh for this research. The grid consists of the hexahedron elements along the boundary walls which then converge into unstructured tetrahedron elements in the flow area.

The combinations of these different elements give the mesh the flexibility to match the boundary wall to the inner flow area which is of complex construction. The hexahedron elements are used at the boundary wall as the regular shape of the element, which can adjust to the requirements of wall modelling for turbulence.

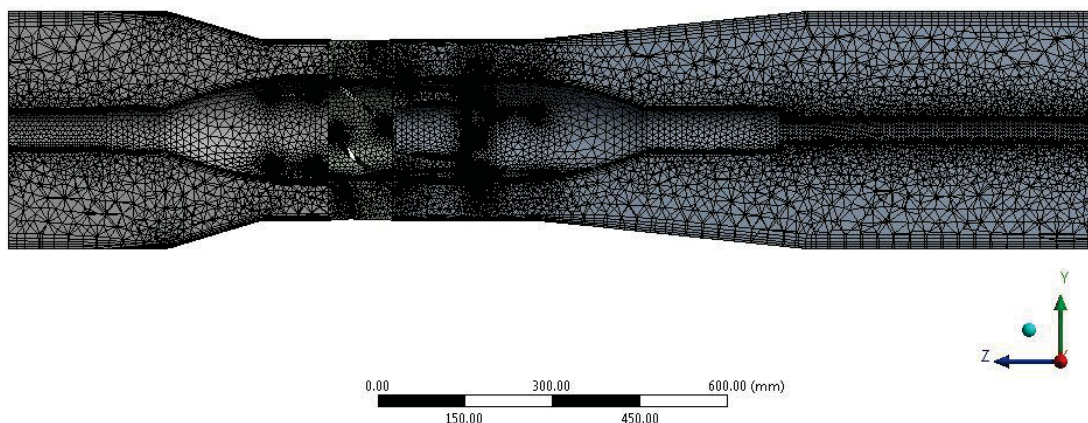


Figure 109 – Split plane of model's flow area mesh

The wall boundary condition was set as inflation to introduce finer grid patterns at the wall for more accurate turbulence results at the surface boundary layer. The inflation setting used, was 5 grids at an expansion rate of 1.2. Figure 110 shows how by using a finer grid pattern along the

wall boundary, a higher number of nodes are introduced within the physical boundary layer, resulting in higher computation, hence achieving more accurate results.

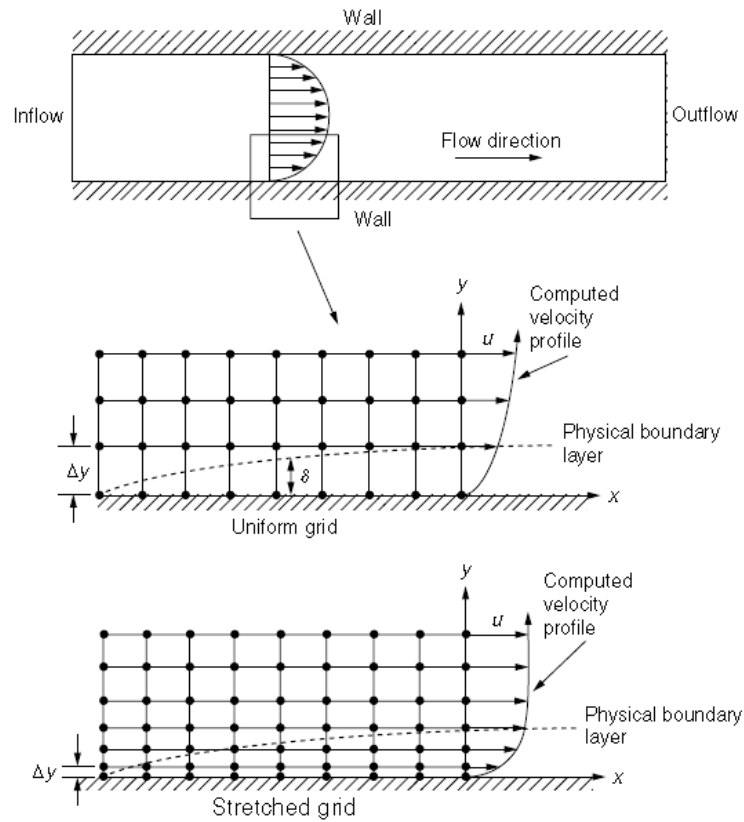


Figure 110 – Grid inflation at wall boundary (Tu, 2008) pg.239

Figure 111 is a cross section from the research model showing the inflation grid pattern merging into unstructured grids of the flow area.

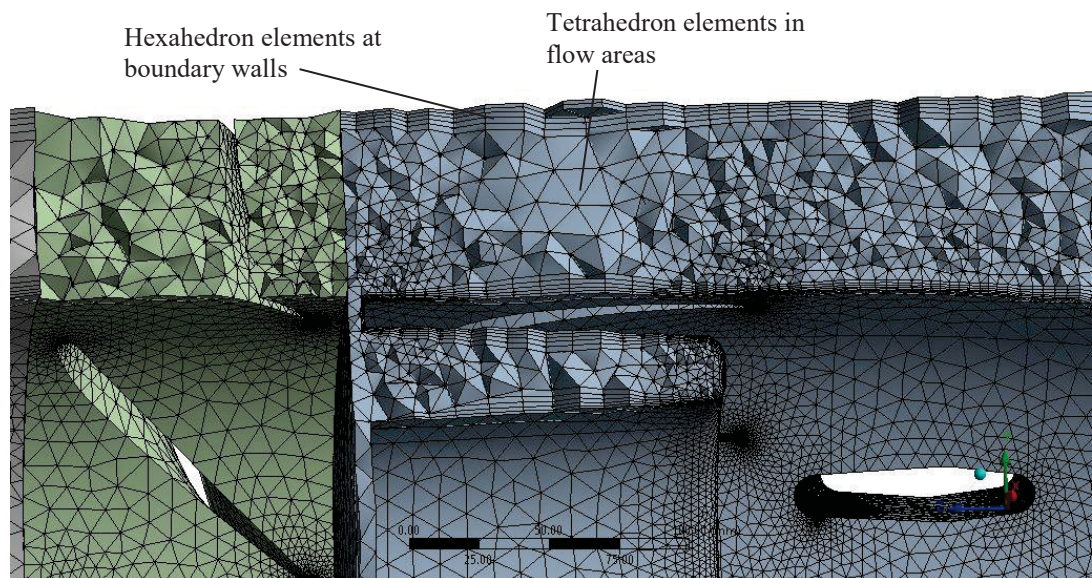


Figure 111 – Internal mesh zoomed view

### 4.3.2.1 Mesh Size Determination

To determine the mesh sizing to be used, five computations of the same model was run with different mesh sizing. The CFX program's standard mesh sizing's are: coarse, medium and fine. Another size to be 50% of the medium and fine was calculated to be 25% of the medium values. The results for the total pressure, velocity and velocity  $U$  were recorded at the same point in the model of each computation and plotted (see Figure 112).

From the plotted graph, it shows when the grid numbers are between 3,100,000 and 4,250,000 elements the curves become stable. However, when the number of elements reaches 5,000,000 or greater, the results steeply increase for velocity  $U$ , this would indicate that the accumulated errors increase for this parameter.

Therefore, it was decided to use medium mesh (4,265,525 elements) as it is the standard grid size selection which shows the best stable results. The factors for the fine mesh are shown in the table below.

CFX Mesh Description	Selection
Smoothing	Medium
Relevance	Medium
Transition	Slow
Span angle	Fine
Min size	0.486820
Max face size	48.6820
Max size	97.3650
Nodes	1,056,027
elements	4,265,525

*Table 5 - Standard CFX medium mesh parameters*

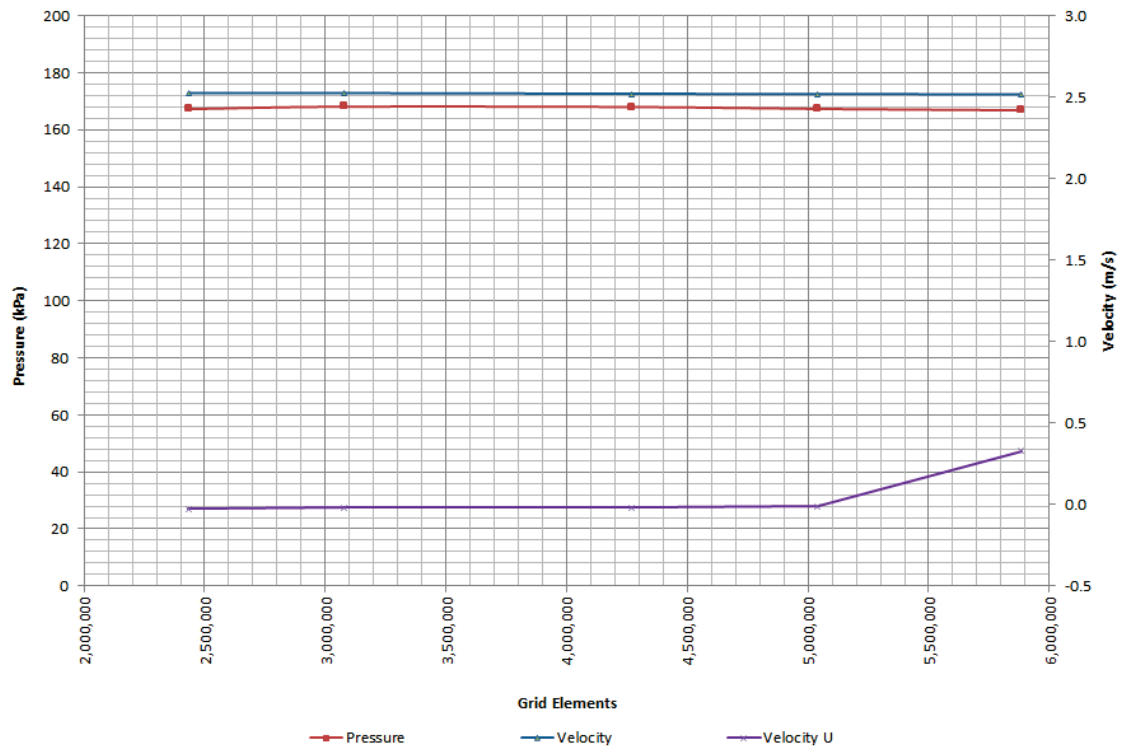


Figure 112 – Mesh sizing check

### 4.3.3 Model Boundary Parameters

The pump boundary parameters that have been selected are based on the conditions the pump is designed for, as per the original pump curves, shown in Figure 15. The pumps BEP for each of the different impellers was used to input the required pump flow data.

The recommended boundary parameters by the *ANSYS* reference guide (ANSYS Inc, 2013) for liquid pumps and turbines is to set the inlet with a total pressure and the outlet with a mass flow rate. The total pressure is assumed to be the most stable for pump analysis.

#### 4.3.3.1 Boundary Inlet Input

A total pressure of 100 kPa was applied to the inlet boundary. This is based on the pump having a NPSHR of 10 m, as indicated on the original pump curve in Figure 15.

#### 4.3.3.2 Boundary Outlet Input

The boundary outlet was set to have a mass flow rate of 318 kg/s, which is the flow for the pumps BEP for a five vane impeller pump. For the eight vane impeller pump the mass flow rate is increased to 564 kg/s.



### 4.3.3.3 Pump Wall Boundary

The ‘no slip wall’ boundary condition is applied to the walls of the pump model. This sets the wall velocity as zero, which in turn transfers to the fluid directly located on the wall. The pipes of the laboratory test rig have been blasted and epoxy coated, where the pump components have been epoxy ceramic coated, therefore it is assumed that the Reynolds number will be low, hence a smooth wall setting was selected. The impeller vanes surface roughness was measured with an average impeller  $R_a$  of approximately  $7.3\mu\text{m}$ . This roughness was set in the parameters however there was no difference in the CFD analysis results when compared to a ‘smooth wall’ setting (see Appendix E).

### 4.3.4 Domains

A domain is used to define the properties of the model’s fluid area where the equations are solved. For this research two domains were created to separate the stationary components from the components with a rotating motion.

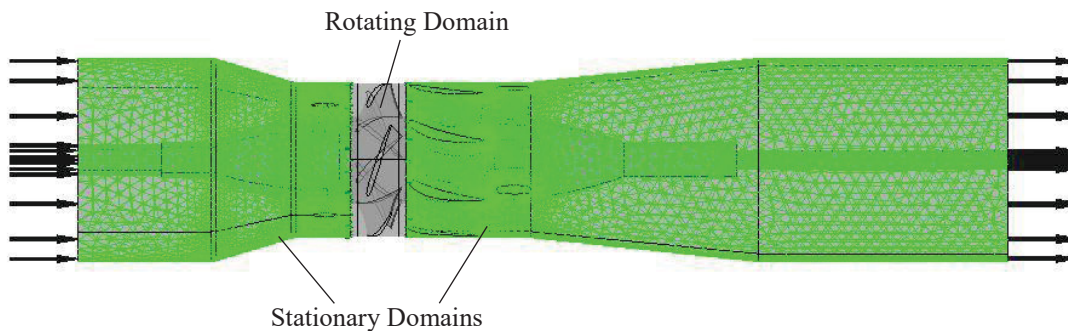


*Figure 113 – Model domains*

The different domains are joined using the general connections interface, where each connecting face was set as a ‘frozen rotor’. With a frozen rotor setting, the grid pitch is changed however the components each side of the interface are fixed. This results in, when there is a change in the reference frame, the suitable equation transforms as required. This connection is suitable for a steady state solution.

The rotating domain of the model includes the impeller and bowl ring. The impeller is set as ‘rotating’ with an angular velocity of  $-1465\text{rpm}$  from the pump curve. The angular velocity is negative as per the ‘right hand rule, shown in Figure 114. The ‘wall velocity’ for the wall which is bounding the impeller, (pump bowl ring area) is set to ‘counter rotating wall’. By having the wall velocity as counter rotating, this section of the domain remains stationary.



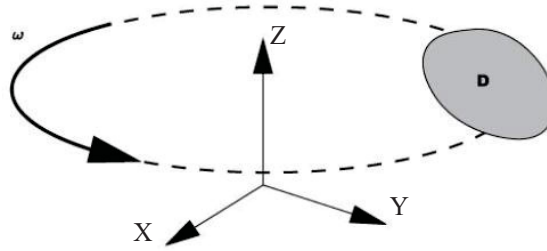


Figure 114 – Rotating frame of reference (ANSYS Inc, 2013) pg34

## 4.4 CFD Analysis and Results

CFD analysis was conducted on a number of different model variations of the pump being used during laboratory testing for this research.

The final parameters applied to the CFD models are as the details outlined in Section 4.3. The standard pump configuration is shown in the figure below. The analysis of the flow path of the fluid particles through the pump is the main focus for this research. It was found that plotting the velocity streamlines, produced the information required (see Section 2.2.2 for detailed explanation).

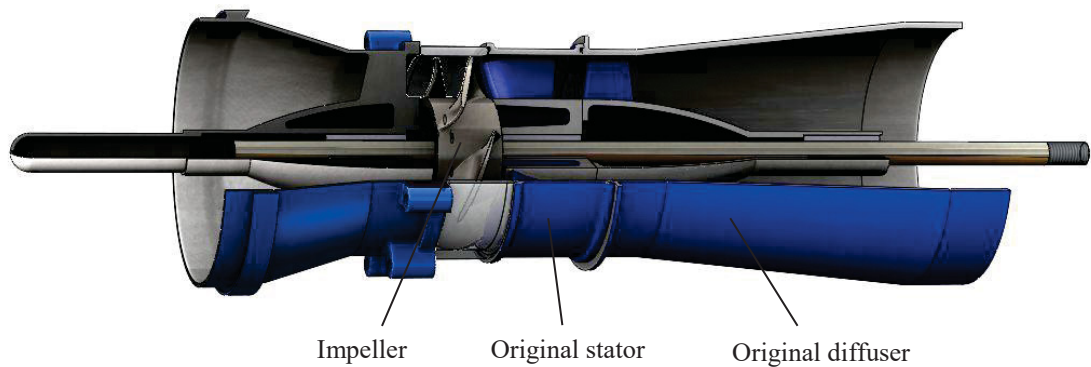


Figure 115 - CFD model of original pump configuration with five vane impeller

### 4.4.1 Five Vane Impeller Pump Configuration

Three different pump configurations using a five vane impeller were analysed and compared to each other, as well as the laboratory test results for each of the configurations. The configurations modelled were the (a) standard pump design (b) the new diffuser and (c) the new diffuser with tail piece added. In the case of the tail piece CFD has been used to determine the design.

#### 4.4.1.1 Standard Pump Configuration Analysis

The first of the CFD analysis performed was the standard pump design.

Figure 116 shows the 2D velocity streamlines results of the flow along the YZ plane through the standard pump configuration. The analysis indicates that the flow has very little turbulence in the major flow areas of the pump. This is also shown in Figure 119 which is the 3D velocity streamlines of the same pump, showing the prediction of the fluid straightening back to an axial flow from the stator.

There is a small amount of swirl that can be seen in Figure 117 on the stator internals. This is the hollow section at the front of the stator and can be ignored for this research as it does not affect the area of interest. The area is detailed in Figure 118.

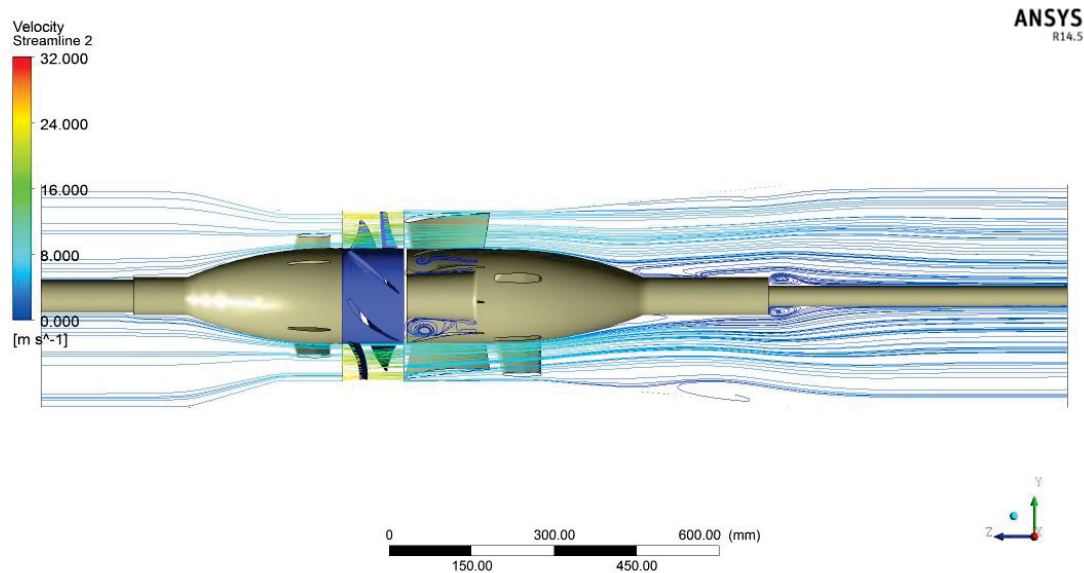


*Figure 116 - CFD analysis of original pump configuration with five vane impeller*

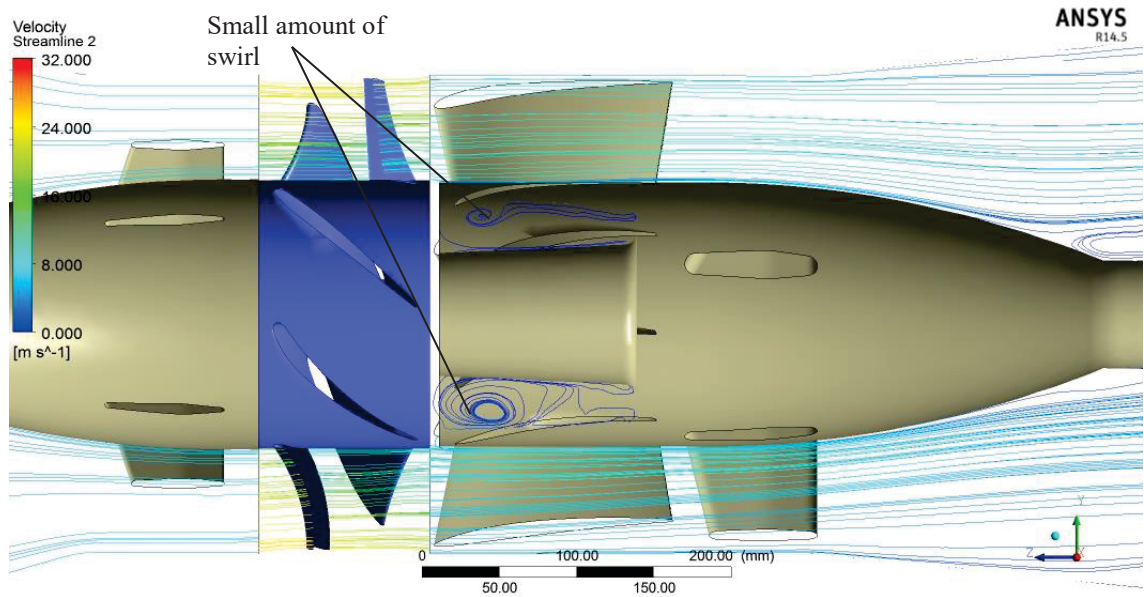


Figure 117 - Enlarged view of blade outlet area from Figure 116

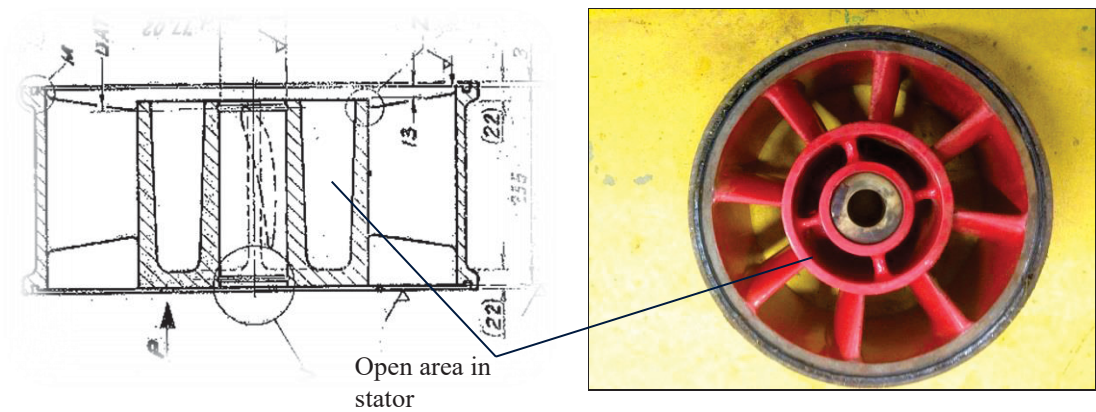


Figure 118 – Original pump stator design (from Weir Engineering drawing)

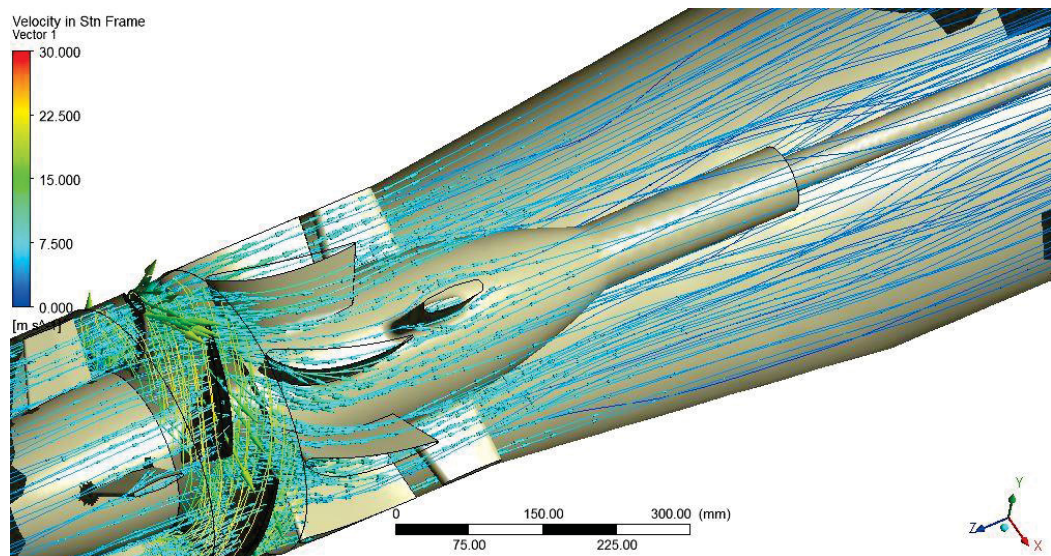


Figure 119 - Original pump configuration 3D streamline

To determine the predicted pump pressure, a probe point was selected at a position in the flow passage two times the pipe diameter<sup>13</sup> past the impeller, to compare the CFD analysis to the laboratory pump tests for the same pump configuration. The probe point selected indicated the total pressure is 172.3 kPa. To calculate the actual head pressure at this point, equation 4 is used:

$$H_p = \frac{\Delta p}{\rho g} + z = \frac{172.3 - 100}{9.81 \times 1} + 0 = 7.4 \text{ m} \quad \text{Equation 35}$$

From the laboratory pump test curve shown in Figure 191 the pressure is approximately 8 m at 318 L/s flow<sup>14</sup>. The result is a difference of 7.5% between tests (approximately 5.9 kPa).

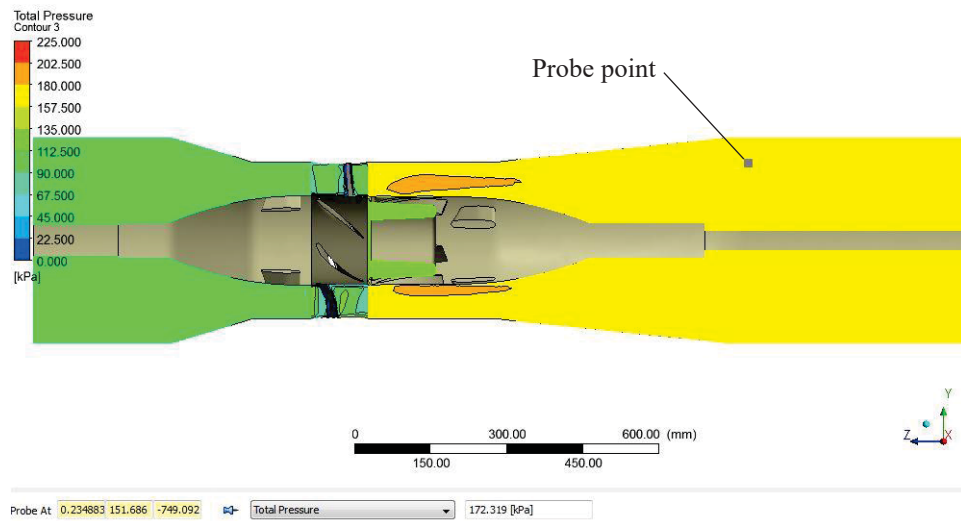


Figure 120 – Original five vane pump total pressure prediction

Two probe points were placed within the diffuser to determine the predicted pressure rise within the diffuser. Figure 121 shows the probe points and that the predicted pressure rises in the standard diffuser, from inlet to outlet, to approximately 9 kPa.

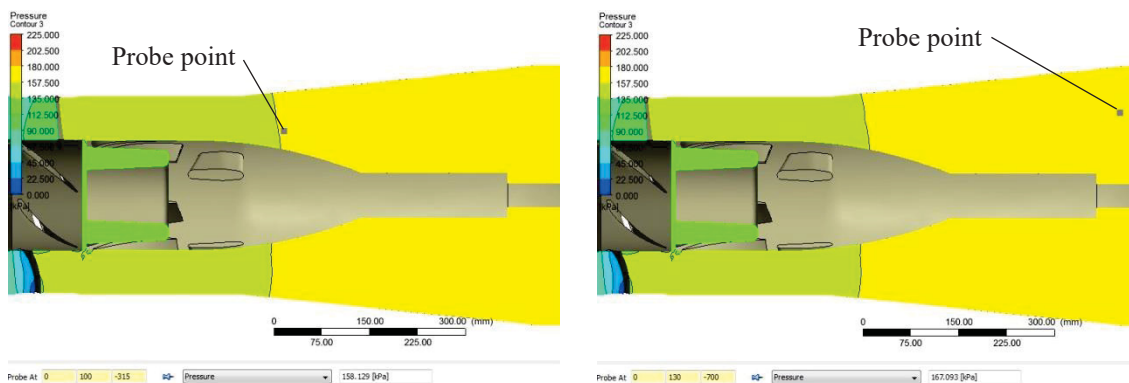


Figure 121 – Predicted pressure rise through std. diffuser

<sup>13</sup> Recommended position to measure pump pressure as per AS2417.

<sup>14</sup> 318 L/s is the flow for the original pump BEP which is the programmed flow for the CFD model.



#### 4.4.1.2 New Diffuser Configuration Analysis

As with the standard pump analysis, (Section 4.4.1.1), the model for the new diffuser pump configuration uses the same set-up as indicated in Section 4.3. The 2D velocity streamlines for the new diffuser configuration predicted that there is not only high turbulence at the back face of the diffuser, but also high velocity at the vane inlet tip of the diffuser. This is shown in Figure 122 and Figure 123. The diffuser inlet turbulence may be due to a number of factors: the axial distance between the impeller vane outlet tip and the diffuser vane inlet, the mismatch of the impeller outlet and diffuser vane inlet angles, or the running gap between the impeller and diffuser. Figure 125 compares the new diffuser to the standard stator design which has an open area at the stator hub, which may dampen and reduce this high velocity.

The streamline turbulence shown at the diffuser outlet is the result of the sudden flow passage enlargement as explained in Section 3.2.1.

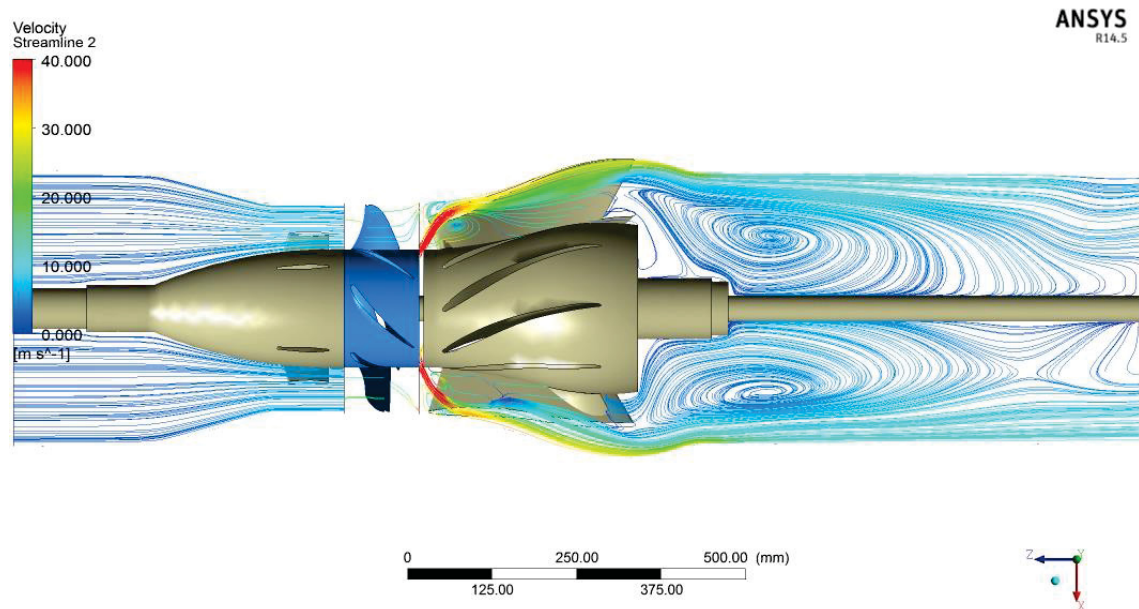


Figure 122 - CFD analysis of new diffuser pump configuration with five vane impeller

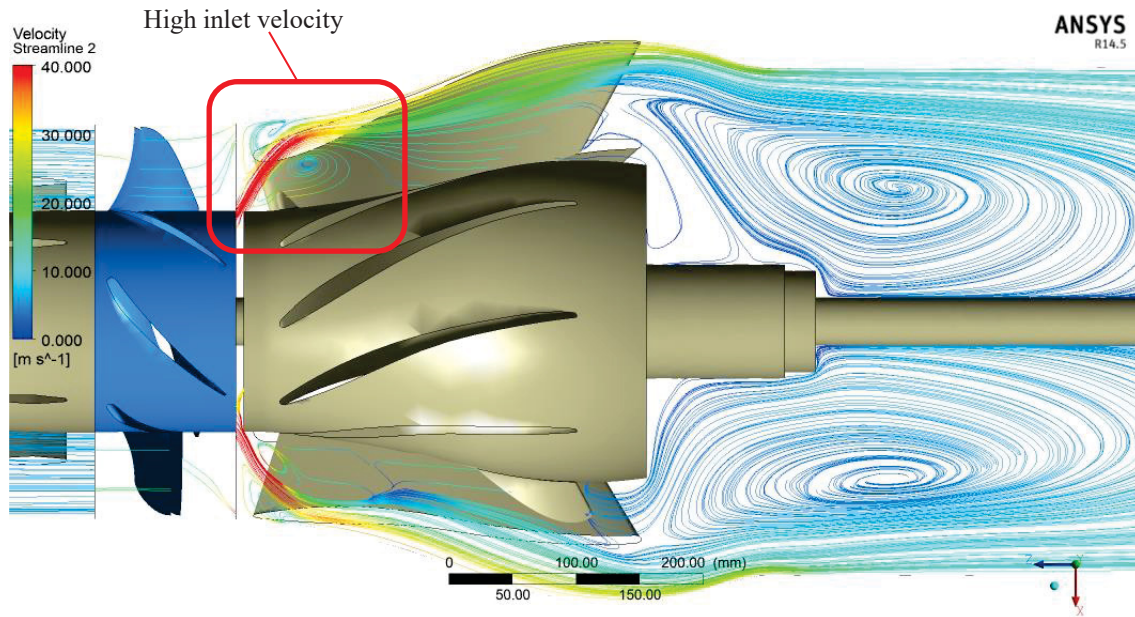


Figure 123 - Enlarged view of blade outlet area from Figure 122

Figure 124 shows the predicted 3D streamlines of the new diffuser. Unlike the standard design stator, the streamlines indicate that the flow from the new diffuser does not return to an axial flow straight away. It also illustrates the high velocity at the running gap between the impeller hub back face and the diffuser hub.

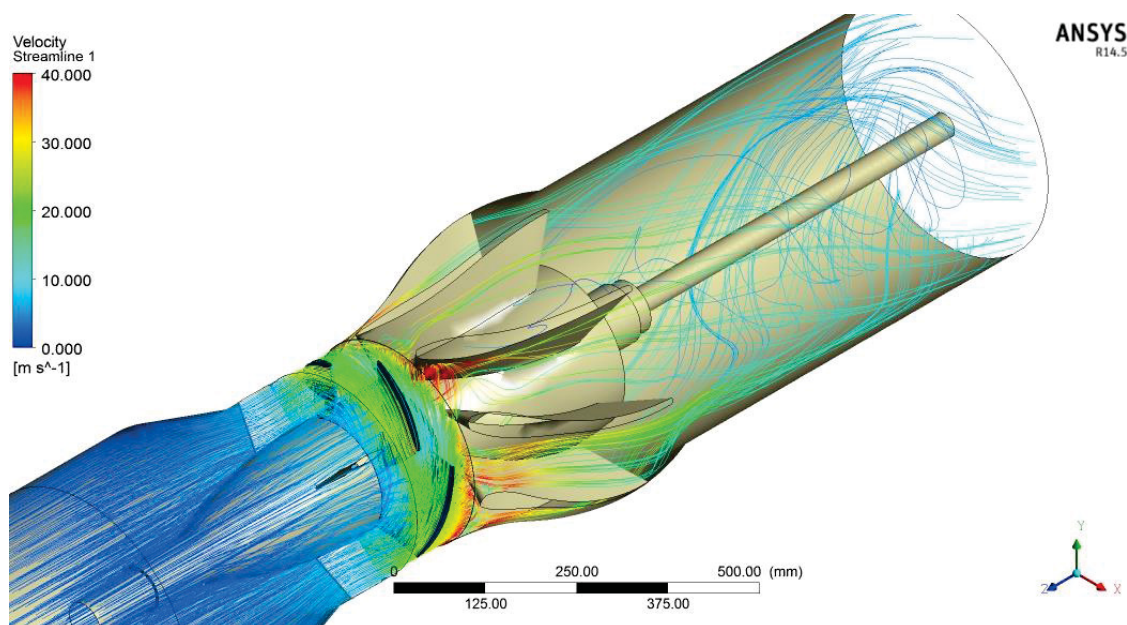


Figure 124 – New diffuser pump configuration 3D streamline

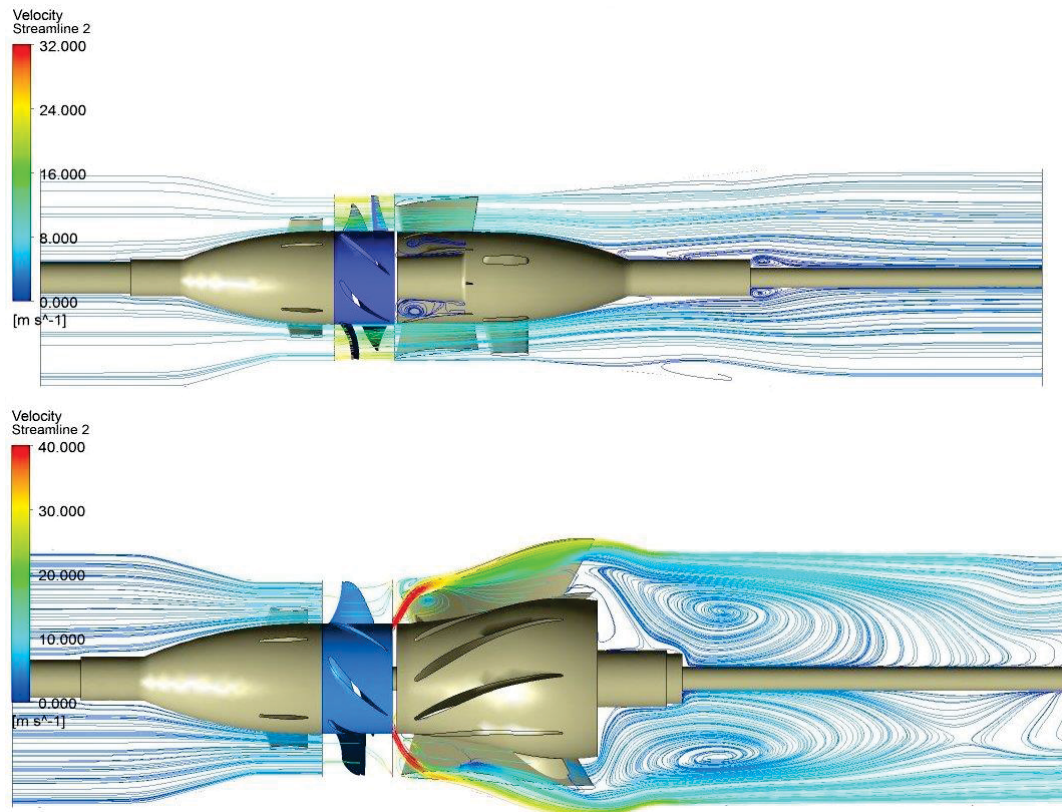


Figure 125 – Comparison of standard pump and new diffuser design

It was found that the high velocity at the diffuser's inlet affected the original pressure predictions by redirecting the flow away from an axial direction resulting in secondary flow in the flow passage. Due to this problem the CFD impeller model was changed and the open area that is found on impeller hub was added to the model (Figure 127). This was previously left from the model, as it was thought that as the area was away from the primary flow path, it would not affect the results. However, the remodelled CFD analysis indicated that the flat face of the impeller was the cause of the high velocity streamlines at the inlet. And due to the outlet turbulence remaining with some flow deviation at the diffuser outlet shroud area, the modification to the model would provide the required results. For further detailed investigation into the high inlet velocity refer to Section 4.5.1.

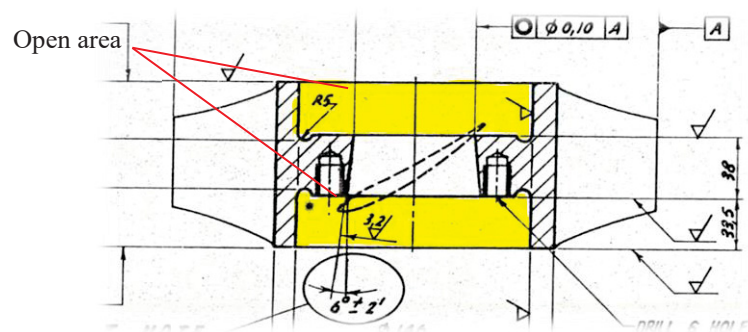


Figure 126 – 300AX impeller drawing (Weir Minerals Australia)



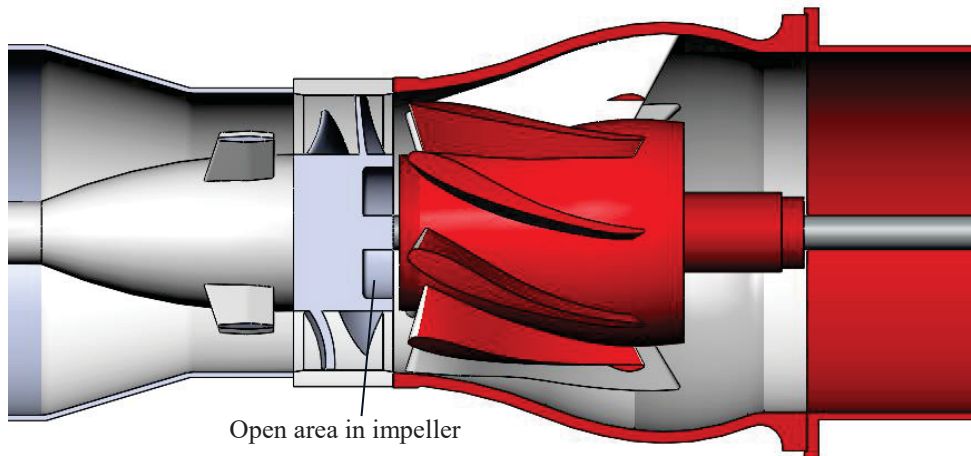


Figure 127 – Addition of open area to impeller model

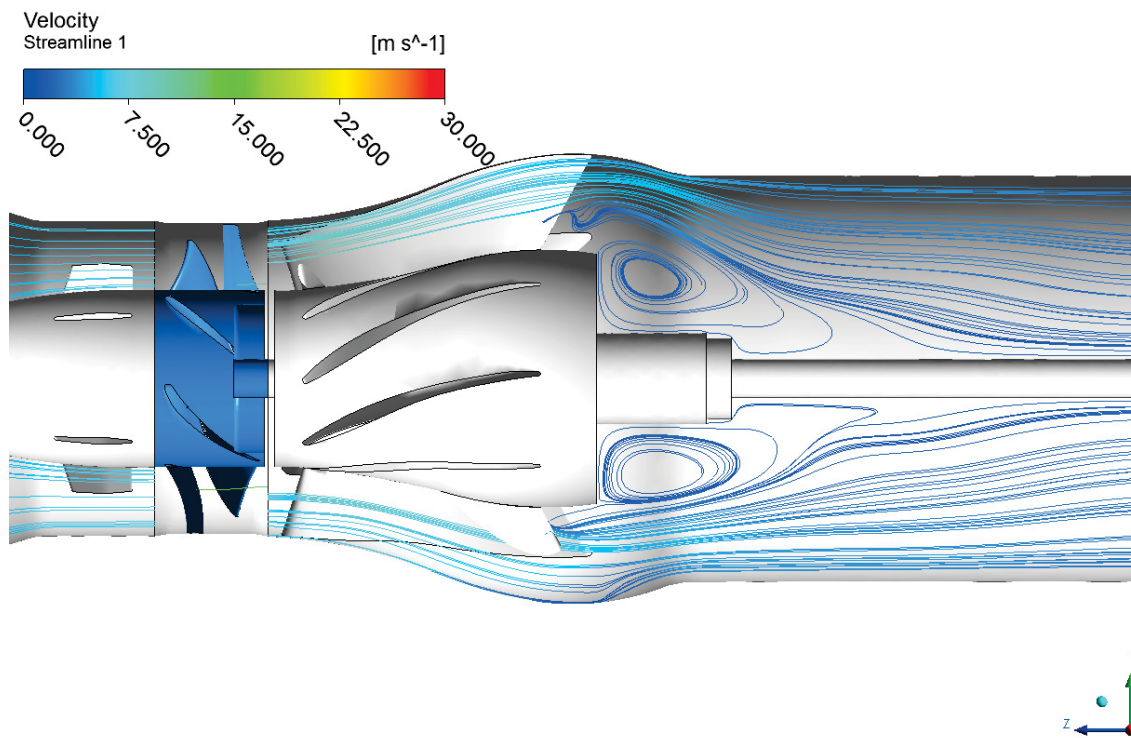


Figure 128 – Modified model 2D streamline

The predicted outlet pressure indicated in Figure 129 is 159.24 kPa resulting in a head pressure of 6.0 m.

$$H_P = \frac{\Delta p}{\rho g} + z = \frac{159.2 - 100}{9.81 \times 1} + 0 = 6.0 \text{ m} \quad \text{Equation 36}$$

This prediction is lower than the pump laboratory test results<sup>15</sup> of 7.5 m (refer to Section 5.2.2.1). The image does show that there is low pressure behind the back face of the new diffuser which is consistent with the predicted secondary flow.

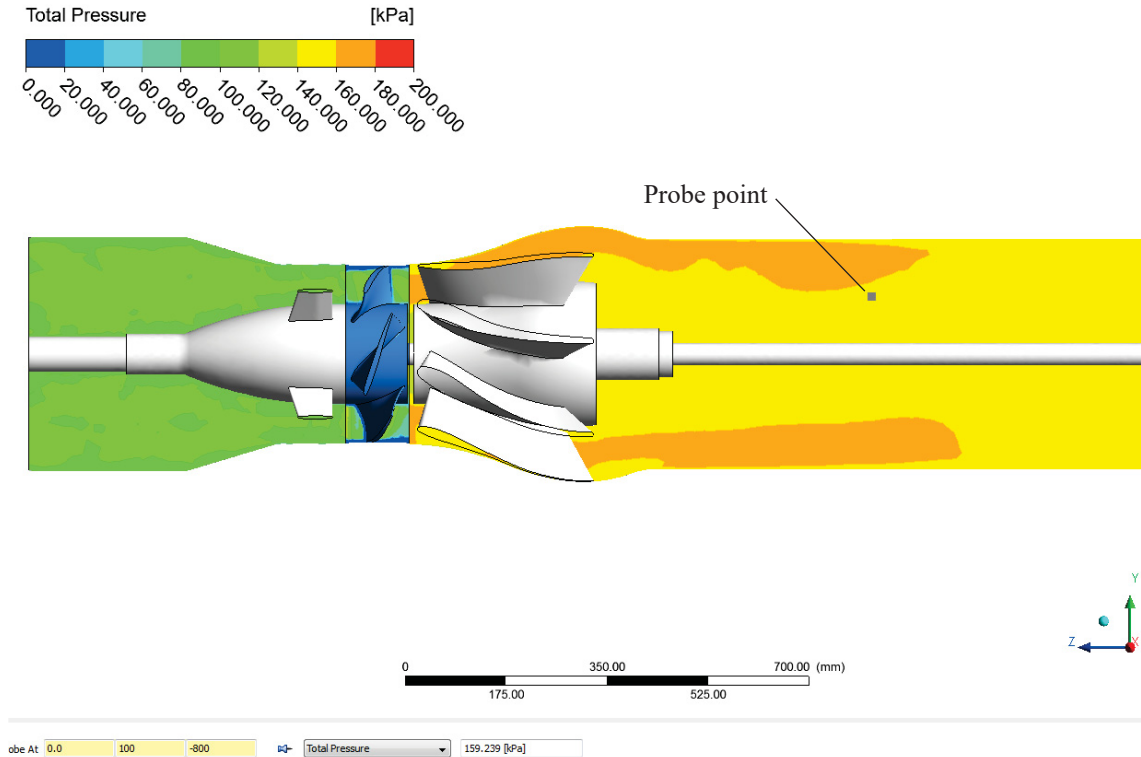


Figure 129 – New Diffuser five vane pump total pressure prediction

#### 4.4.1.3 Tail Piece Angle Analysis

Section 3.3.3 details the theory of the addition of a tail piece to the back face of the new diffuser to introduce a more controlled flow area reduction. In theory, this will help to reduce to turbulence at the rear of the diffuser, improve the flow direction and improve efficiency.

A number of CFD models with different angles have been analysed to determine the appropriate angle for the tail piece component to attain the most amount of swirl reduction. The figure below outlines the different angles modelled for the analysis. The angles used were 64°, 40°, 30° and 20°.

Initially it was thought that by roughly drawing lines onto the print out of the 2D streamline analysis to determine the angle that followed internal lines of the streamline (refer to Figure 130), the secondary flow would be reduced. It was also thought that the bell shape of the

<sup>15</sup> The pressure result is determined from the pressure indicated on the laboratory tested pump curve at the flow of 318 L/s (flow setting for CFD analysis).

diffuser's shroud would direct the outer flow downwards towards the pump's centre and a component with a low angle would result with more swirls due to the flow directed towards it.

However, when looking at the 2D streamline results in Figure 132(a) the calculated angle of  $64^\circ$  only slightly reduces the swirl. This was not the result which was estimated.

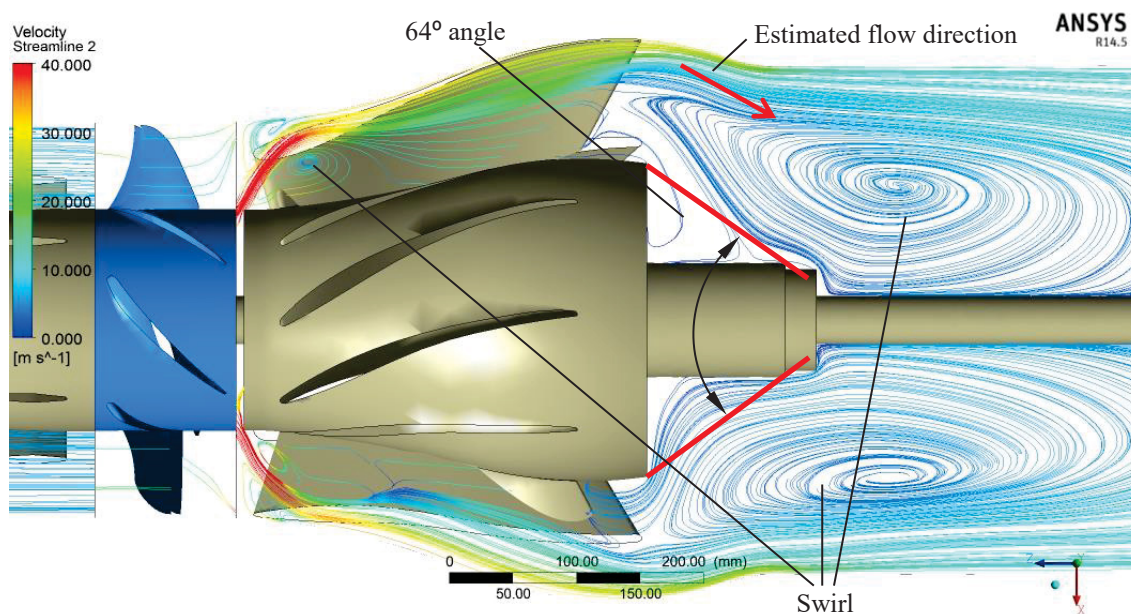


Figure 130 – Determination of start angle for analysis

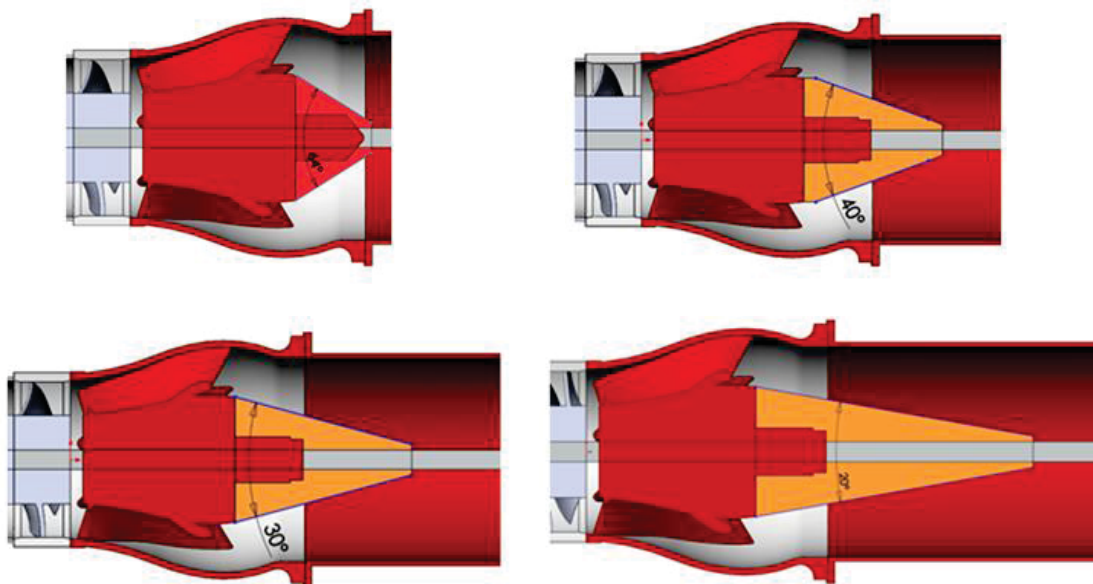


Figure 131 – The different CFD models analysed. Range from the new diffuser with tail piece added at various angles.

Therefore, it was decided to analyse a number of reduced angles to achieve the desired results. By decreasing the angle each time by  $10^\circ$  to the angles of  $40^\circ$ ,  $30^\circ$  and  $20^\circ$  the number of analysis required would be at a minimum. An angle of  $20^\circ$  is the smallest possible angle that

could be achieved because as the angle reduces, the length of the component increases, resulting with the tail piece interfering with the lineshaft coupling.

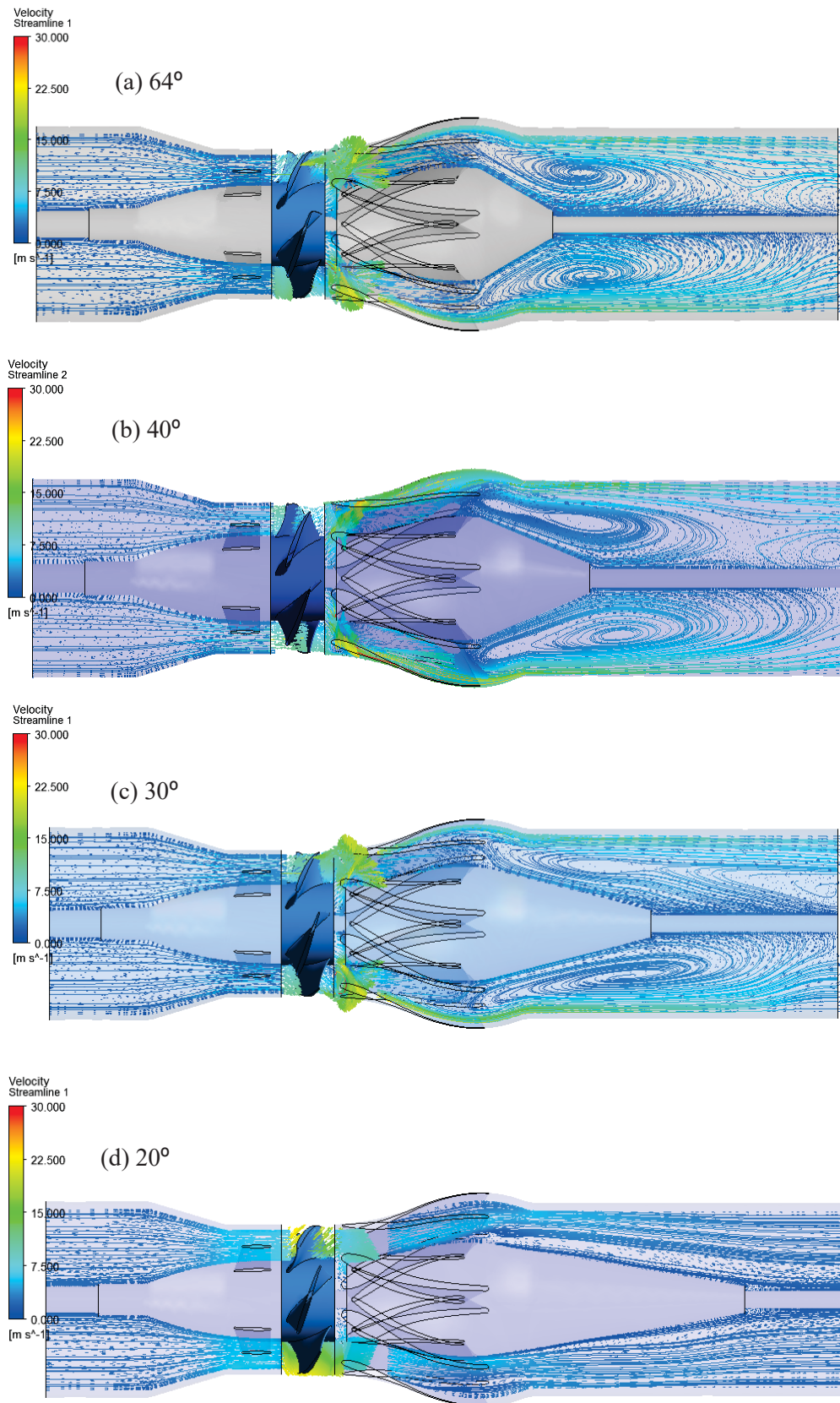
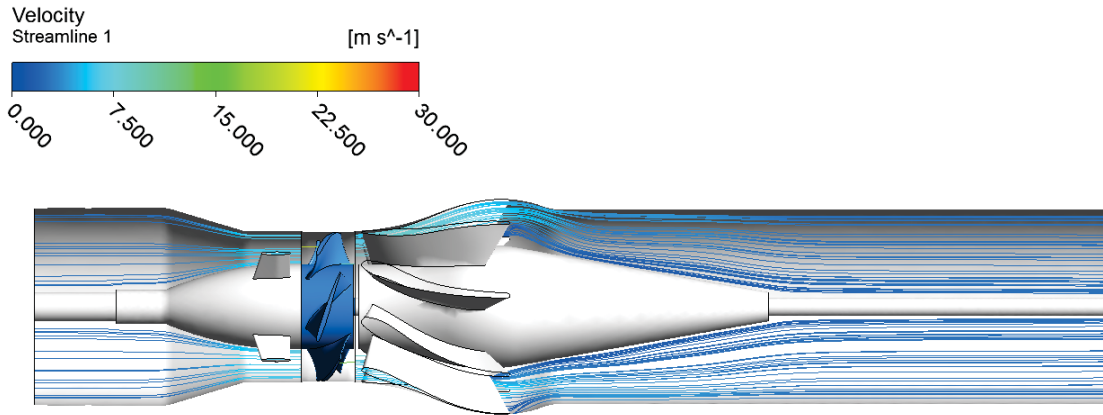


Figure 132 – 2D streamlines of tail piece angle analysis



The 2D streamline results in Figure 132 (b), (c) and (d) show that as the angle is decreased, the swirl is elongated and reduced until the smallest angle of  $20^\circ$  is where it is predicted that the swirl is at its minimal. Therefore, it was decided that this angle may achieve the desired results for the tail piece design.



*Figure 133 – CFD analysis of tail piece addition configuration with five vane impeller*

The enlarged view of the 2D velocity streamline (Figure 134) indicates there is a small flow path deviation at the outlet. This is due to the slight twist in the outlet vane, as well as the bell shape of the shroud directing flow inwards towards the pump centre and away from any axial flow path.

Figure 135 compares the two 3D velocity streamlines of the tail piece addition to the new diffuser. It illustrates that the tail piece may reduce the rotational swirl and introduces some axial direction flow to the fluid with a less turbulent swirl path, which can be seen in the image of the new diffuser around the shaft at the back face area.

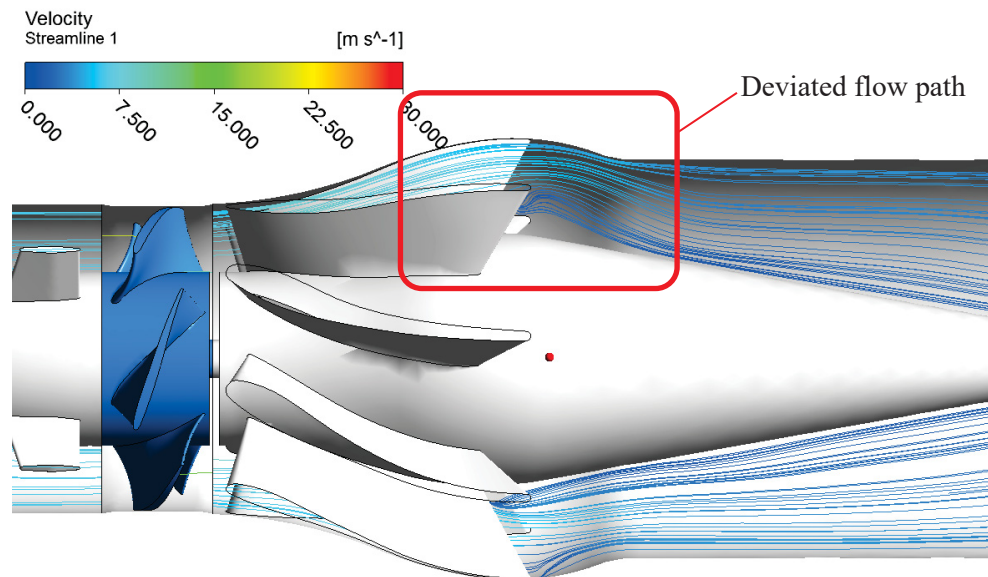


Figure 134 – Enlarged view of blade outlet area from Figure 133

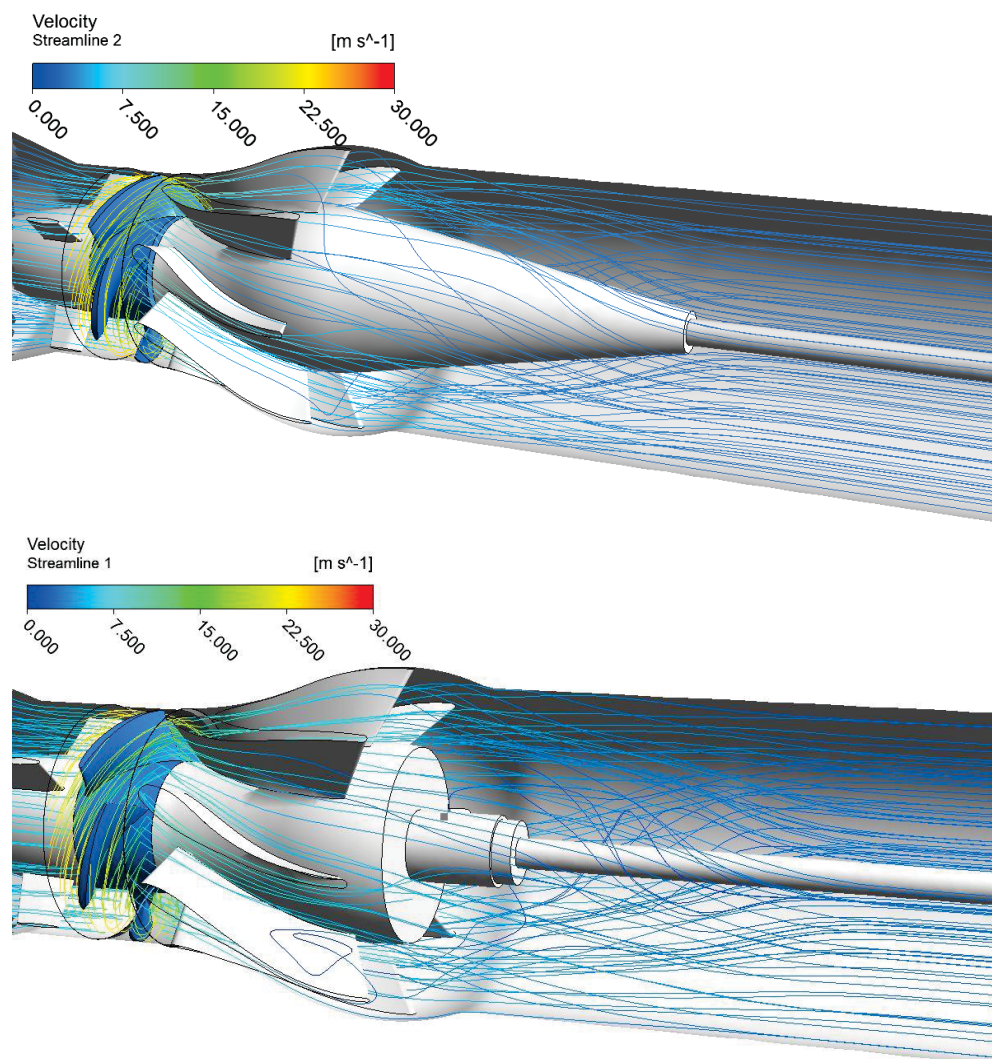


Figure 135 – Comparison of new diffuser and tail piece addition 3D streamline



The predicted outlet pressure indicated in Figure 136 is 160.2 kPa resulting in 6.1 m.

$$H_p = \frac{\Delta p}{\rho g} + z = \frac{160.2 - 100}{9.81 \times 1} + 0 = 6.1 \text{ m}$$

Again this prediction is 16% lower than the base pump test results of 7.2 m (refer to Section 5.2.3.1) and there is no pressure increase when compared to the new diffuser design for the five vane pump configuration. The image does show that area of lower pressure is along the surface of the tail piece with an increase of the high pressure area in the flow passage. This would suggest that this component addition will greatly reduce the possibility of turbulence in the pump.

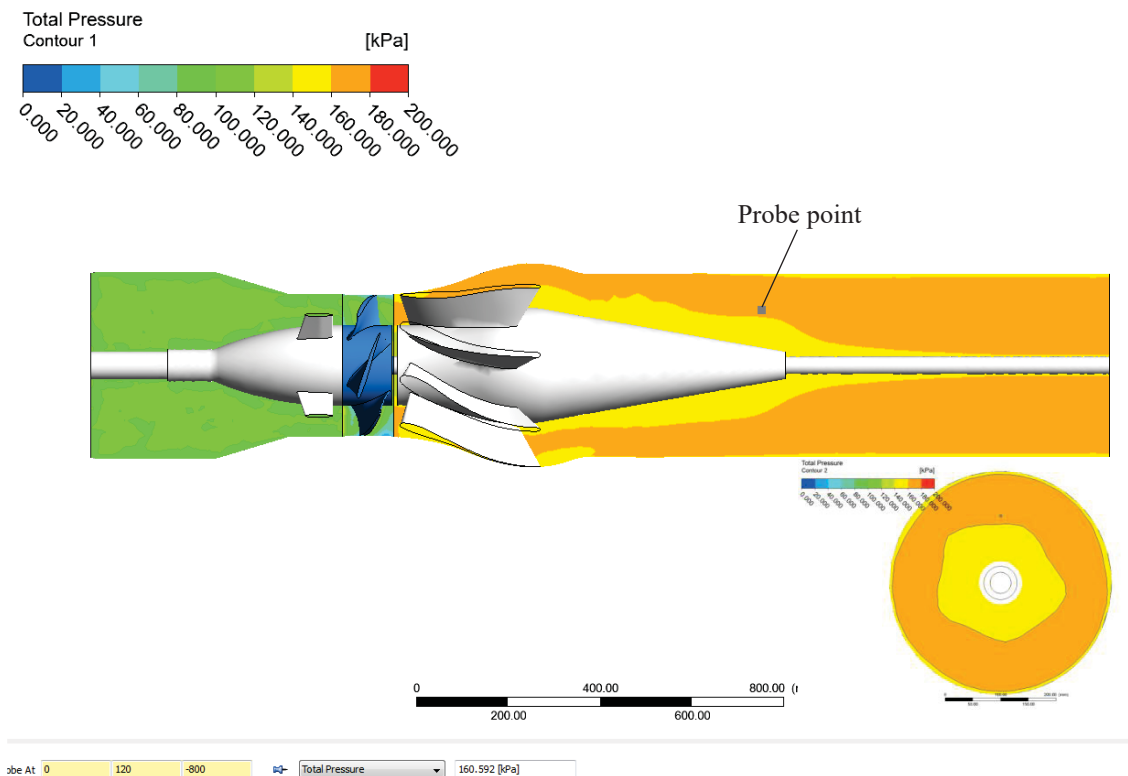


Figure 136 - Predicted outlet pressure for tail piece addition, plane plot at probe point

#### 4.4.1.4 Predicted Pressure Rise

Figure 140 shows the comparison of the pressure rise between the new diffuser and the new diffuser with the tail piece addition. To measure the pressure through the diffuser, seven planes were constructed and spaced 100mm apart starting from the inlet of the new diffuser continuing downstream. A total pressure plot was created at each of the planes to analyse the pressure progression through the diffuser and tail piece sections. The results are shown in Figure 139 and Figure 140.

A probe point for total pressure measurement was taken in the midpoint area of the hub and outer shroud and plotted in Figure 138 to compare the pressure difference through the diffuser

section. It shows that there is only a slight overall difference in the pressure rise with the new diffuser. However with the introduction of the tail piece, the pressure has a more stable path than that of the new diffuser alone.

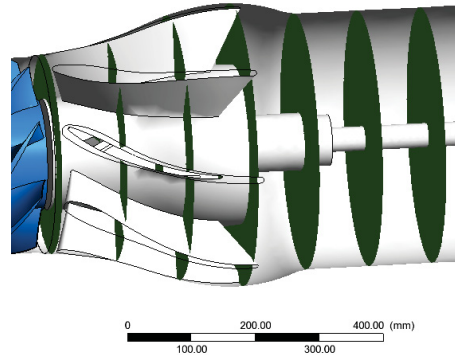


Figure 137 – Planes created for pressure section measurements

However even though the pressure increase is minimal (0.4%), when comparing the two sets of results in Figure 139 and Figure 140, a greater percentage of the cross sectional area has a higher pressure in the tail piece addition. This would suggest that the gradual reduction of the cross sectional area of the flow passage introduces the sustainability of higher pressure for a prolonged distance through the pump's flow area. This is proven during the laboratory testing, where the pump stall occurs at a lower flow, hence a higher pressure when the tail piece is fitted. Therefore, increasing the pump's operating range.

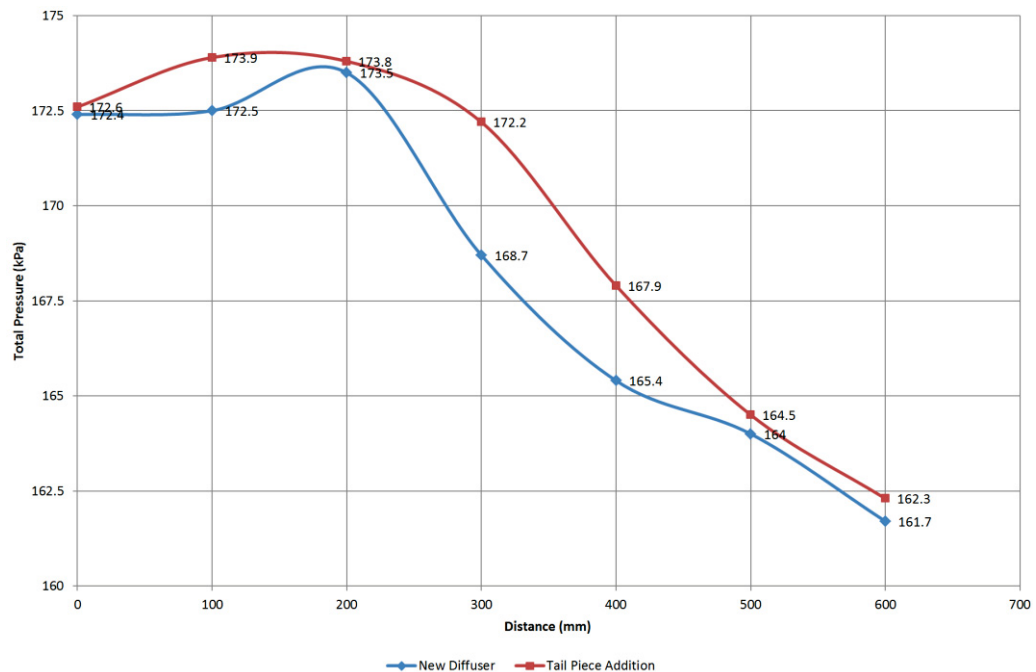


Figure 138 - Predicted pressure through new diffuser with five vane impeller

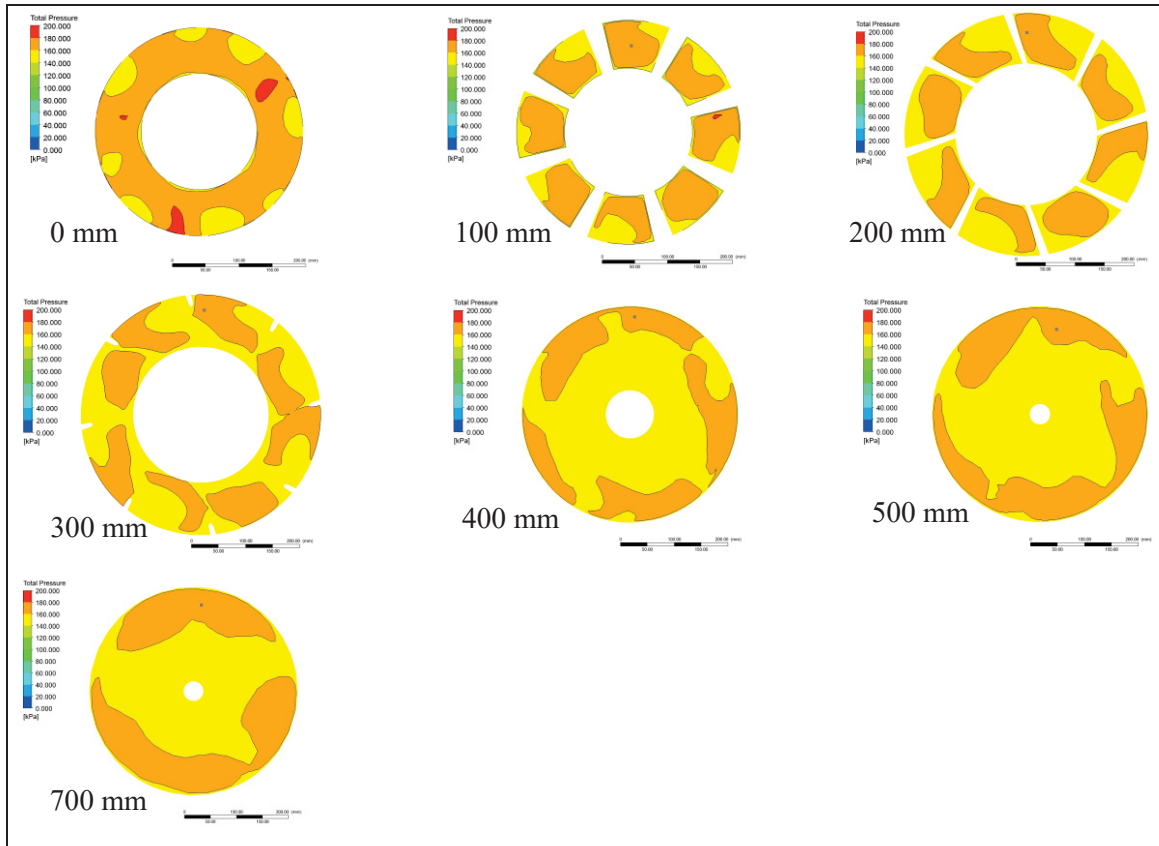


Figure 139 - Predicted pressure rise through new diffuser

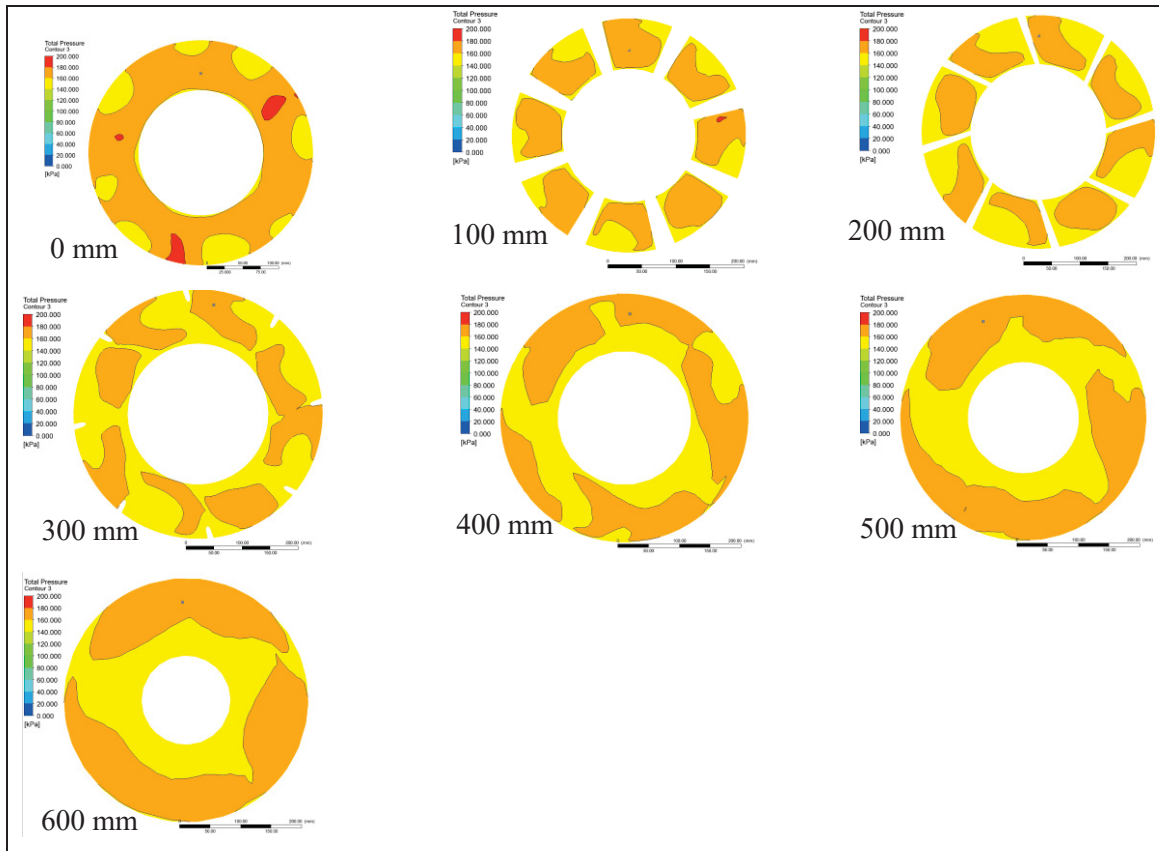


Figure 140 – Predicted pressure rise through new diffuser with tail piece

## 4.4.2 Eight Vane Impeller Pump Configuration

As with the five vane impeller, three different pump configurations using an eight vane impeller were analysed and compared to each other as well as the laboratory test results for each of the configurations. Again the configurations modelled were the (a) standard pump design (b) the new diffuser and (c) the new diffuser with tail piece added.

### 4.4.2.1 Standard Pump Configuration Analysis

The results for the standard pump configuration with an eight vane impeller are shown below. As with the five vane impeller standard pump configuration, the 2D and 3D velocity streamlines have a mostly straight flow path through the pump. There is however a small amount of swirl present at the diffuser hub area, where the hub transitions to the bearings housing outside diameter.

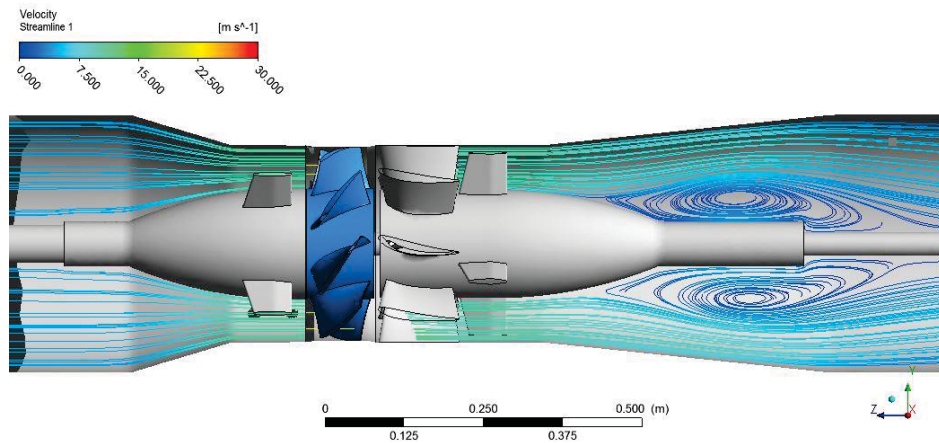


Figure 141 - CFD analysis of original pump configuration with eight vane impeller

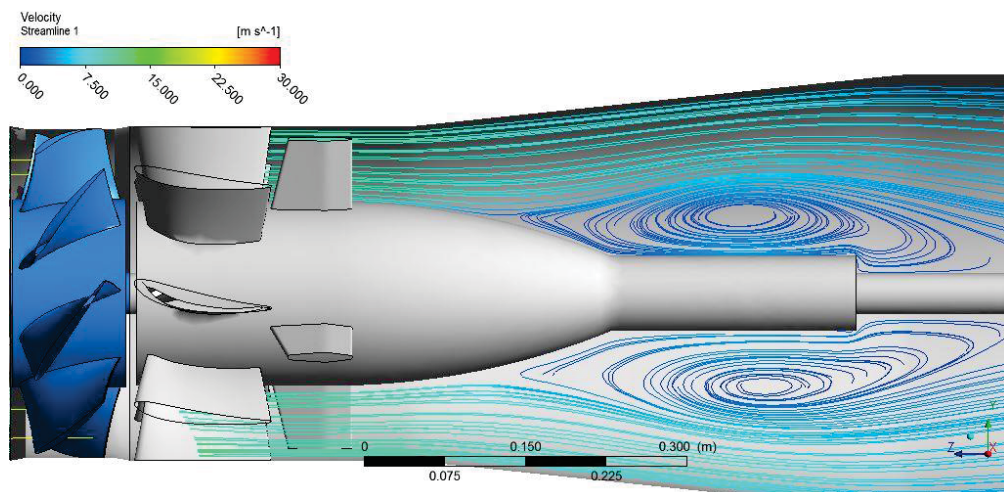


Figure 142 - Enlarged view of blade outlet area from Figure 141



The 3D velocity streamline image indicates that the flow using the eight vane impeller is mostly axial.

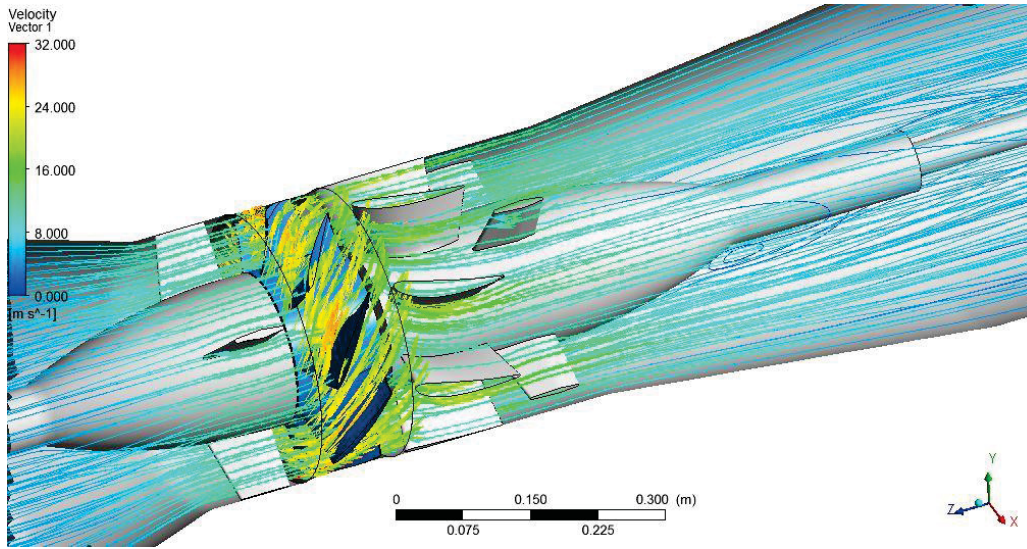


Figure 143 - Original pump configuration 3D streamline

Figure 144 is an overlay of the 2D velocity streamlines onto the total pressure. The results indicate that the turbulent area is at the low pressure area of the flow passage. The higher pressure area has straight axial flow closer to the shroud area. This is a result of the higher flow rate from the impeller vane.

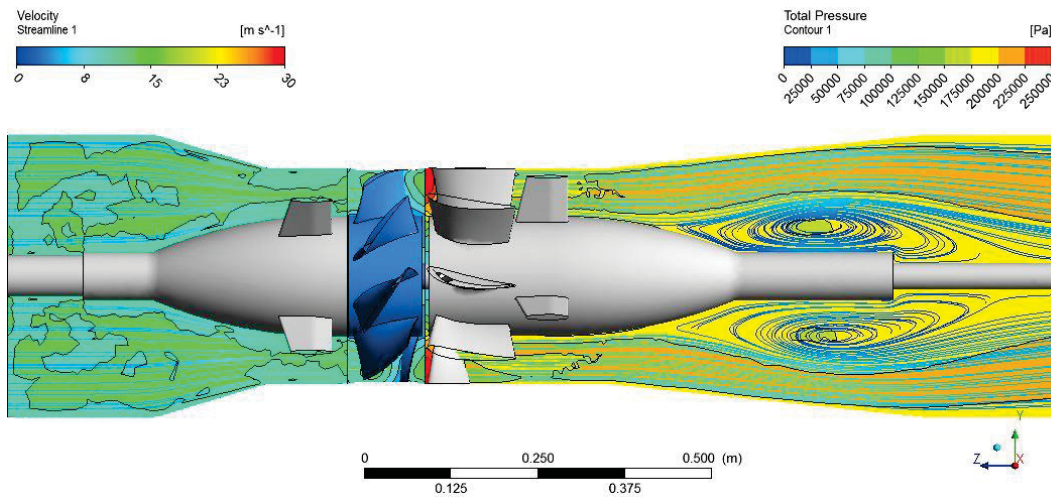


Figure 144 – Overlay of velocity streamline and total pressure

The probe point selected indicated the total pressure is 190.3 kPa.

$$H_P = \frac{\Delta p}{\rho g} + z = \frac{190.3 - 100}{9.81 \times 1} + 0 = 9.2 \text{ m}$$

From the physical laboratory pump test curve shown in Figure 195, the pressure is approximately 7.2 m at the BEP. The 2m difference is not the ideal result as the CFD data may

not give the correct predictions for the flow path, velocities, pressure etc. However, the CFD results are similar to the original pump design curve Figure 15 having a head of 9m at 564L/s flow.

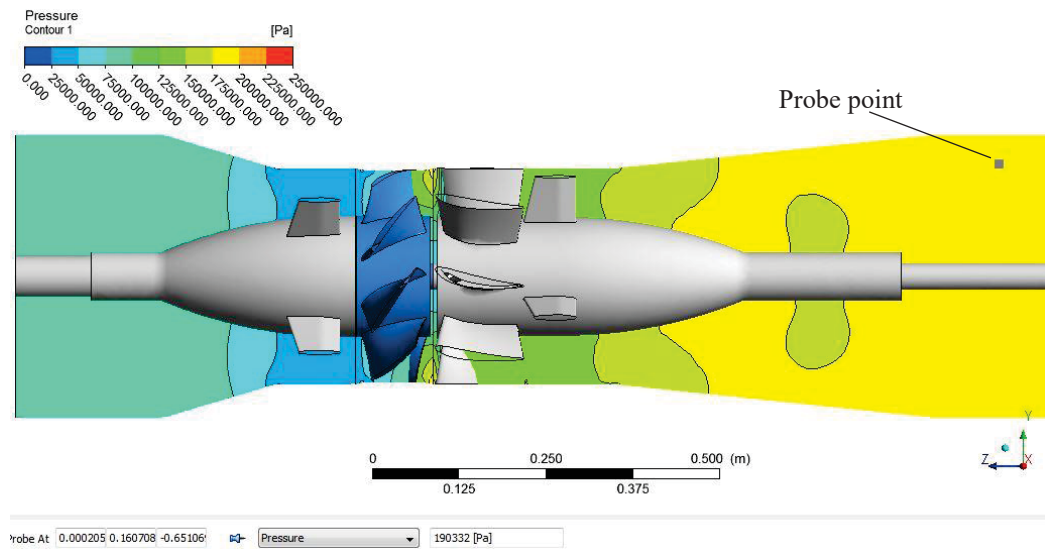


Figure 145 – Original eight vane pump pressure prediction

#### 4.4.2.2 New Diffuser Configuration Analysis

With the eight vane impeller the higher flow causes the swirl area to be elongated behind the new diffuser. When reviewing Figure 149, there is a large lower pressure in this area with a much larger pressure passing over close to the shroud creating this larger secondary flow.

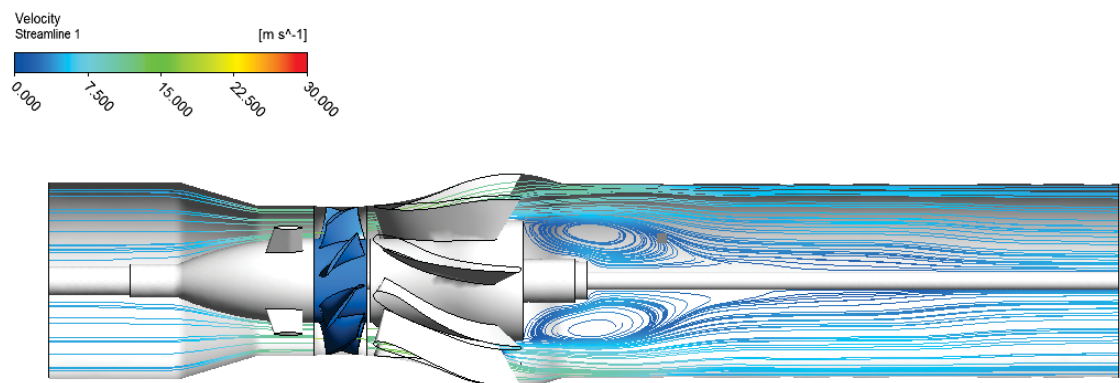


Figure 146 - CFD analysis of new diffuser pump configuration with eight vane impeller



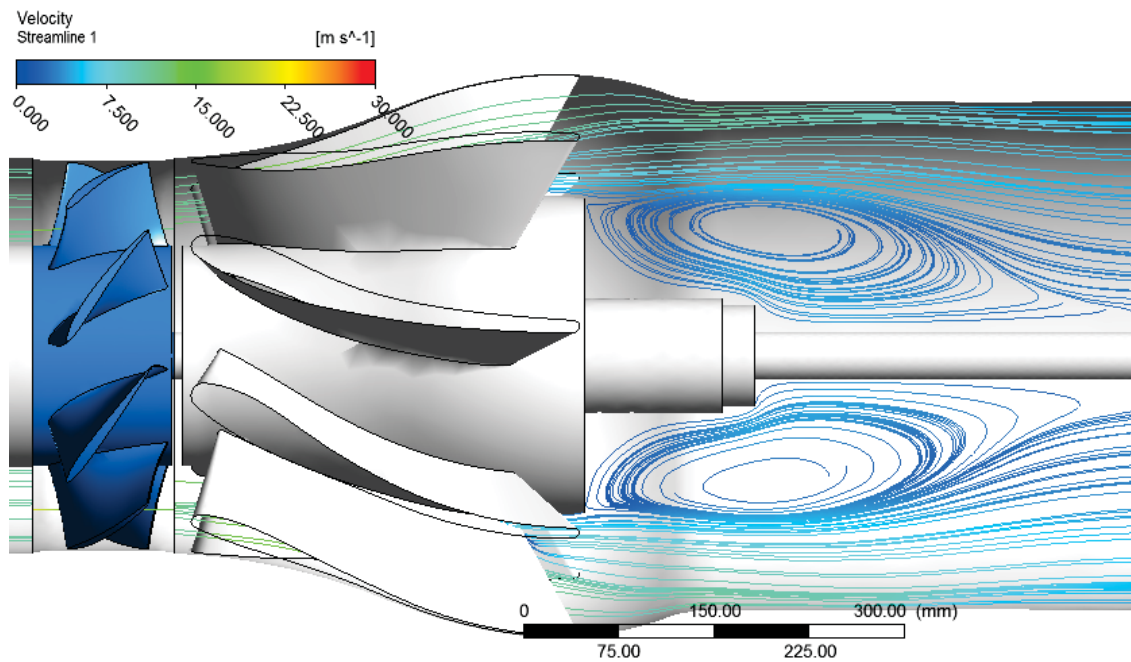


Figure 147 - Enlarged view of blade outlet area from Figure 146

As with the analysis using the five vane impeller, the 3D streamlines indicate the flow towards the centre of the discharge is turbulent and redirected from the axial flow direction.

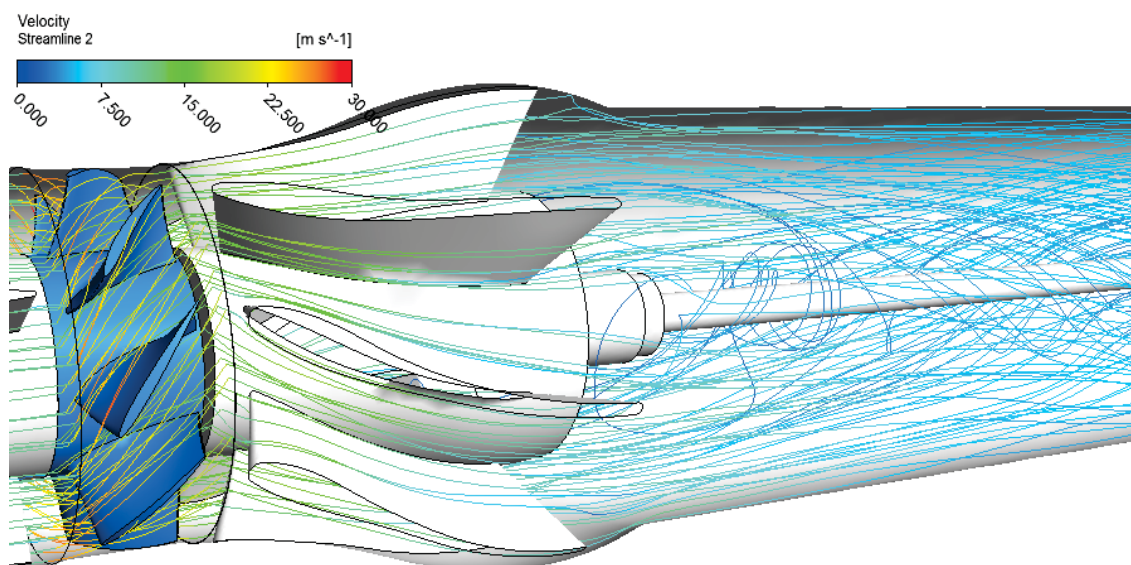


Figure 148 - New diffuser pump configuration 3D streamline

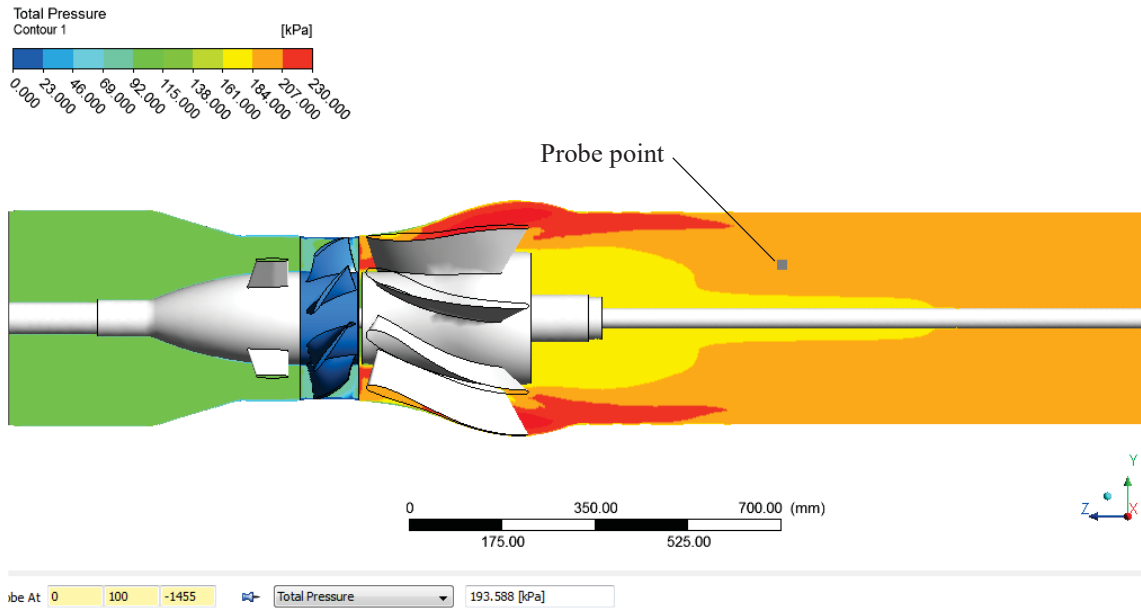


Figure 149 – Predicted pressure at new diffuser outlet

The probe point selected indicated the total discharge pressure is 193.6 kPa.

$$H_P = \frac{\Delta p}{\rho g} + z = \frac{193.6 - 100}{9.81 \times 1} + 0 = 9.54 \text{ m}$$

This result predicts that the pump head with the new diffuser fitted is an improvement from the original designed pump by approximately 0.34m (3.6%). However, when compared to the laboratory pump test 4.03 at the set flow<sup>16</sup> of 564 L/s the head pressure is 5.82m. Again the CFD prediction is much higher than actual laboratory testing.

#### 4.4.2.3 Tail Piece Analysis

Section 4.4.1.3 determined the most suitable design for the tail piece. This same design was used for the following analysis using the eight vane impeller. This was to conclude the design is suitable to reduce the secondary flow from the new diffuser design.

The 2D velocity streamlines shown are in mainly axial flow direction; however there is a small amount of separation causing secondary flow midway along the surface of the tail piece. This result is better understood with the total pressure prediction shown in Figure 152, where there is an area of lower pressure along the surface to the midway area where a higher pressure is viewed along the remaining surface. As previous theory would suggest, this change in pressure, results in the introduction of secondary flow.

<sup>16</sup> The actual BEP for laboratory test 4.03 is 11.3m at 475 L/s.

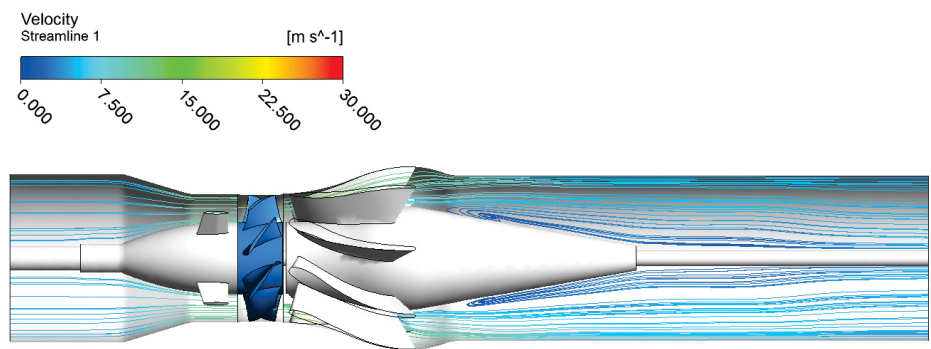


Figure 150 - CFD analysis of tail piece addition configuration with eight vane impeller

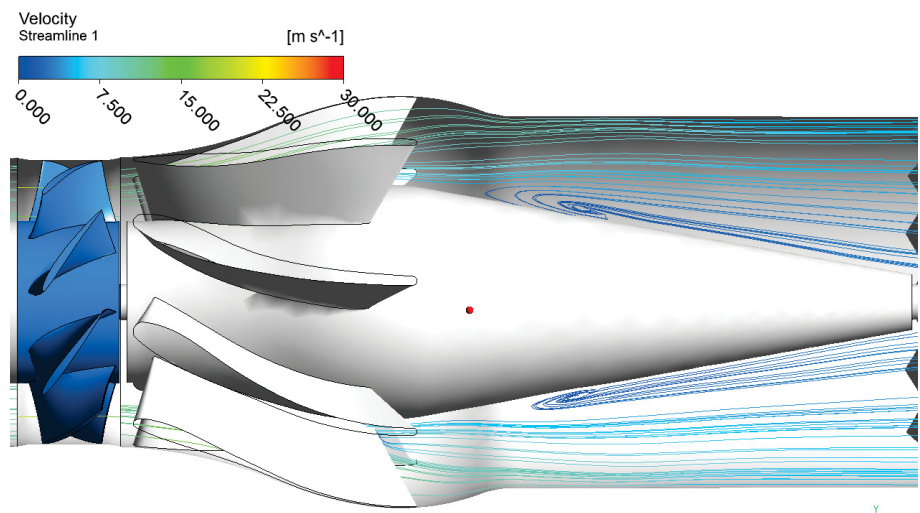


Figure 151 - Enlarged view of blade outlet area from Figure 150

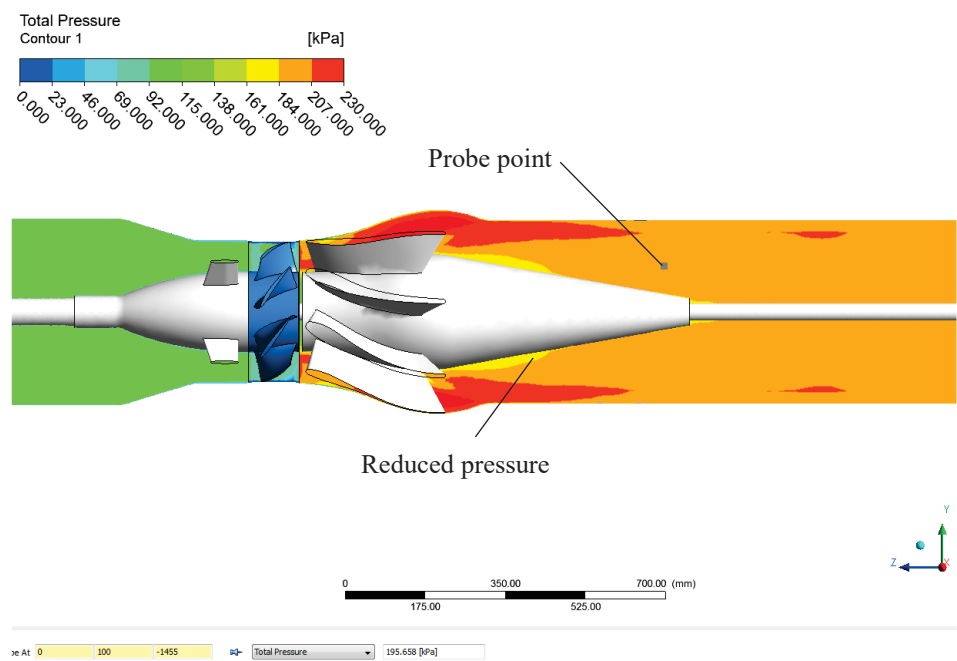


Figure 152 - Predicted outlet pressure for tail piece addition

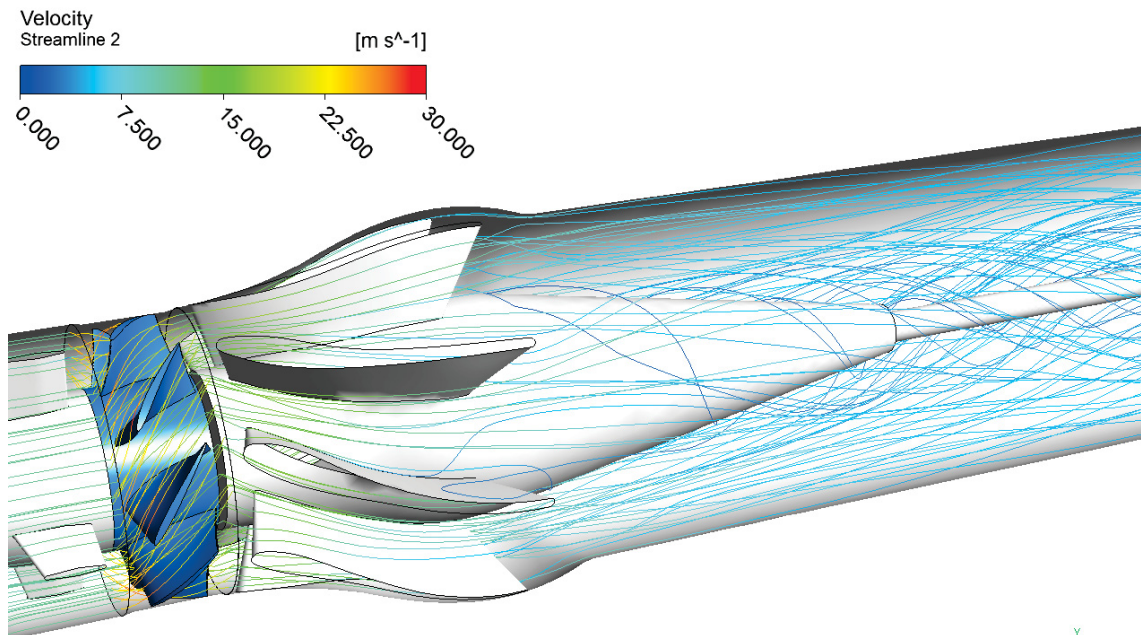
The probe point selected indicated the total discharge pressure gives a reading of 195.7 kPa.

$$H_p = \frac{\Delta p}{\rho g} + z = \frac{195.7 - 100}{9.81 \times 1} + 0 = 9.8 \text{ m}$$

This prediction is 2.8% more than the actual pump test results of 7 m for the flow of 564 L/s (refer to Section 5.2.3.2). There is slight pressure increase to the CFD results for the new diffuser configuration of 2.7% (0.26m). This pressure increase is consistent with the actual laboratory testing where, for the eight vane impeller assembly, the tail piece addition increases the pump performance.

Figure 153 compares the two 3D velocity streamlines of the tail piece addition to the new diffuser by itself. The tail piece addition eliminates the secondary flow by removing the area of sudden enlargement at the back face. The rotational swirl around the centre line of the hub still exists, as the flow direction is determined by the vanes. The higher flow gives the fluid particles high velocity, causing them to travel further into the discharge area before slowing and returning to an axial direction.

This is different to the five vane impeller which has a lower flow with lower velocities therefore creating lower pressures. The fluid particle velocity slows quicker returning the fluid to axial direction. This would mean that the fluid's shear stresses are also smaller resulting with less levels of turbulence than the eight vane impeller with a higher flow.



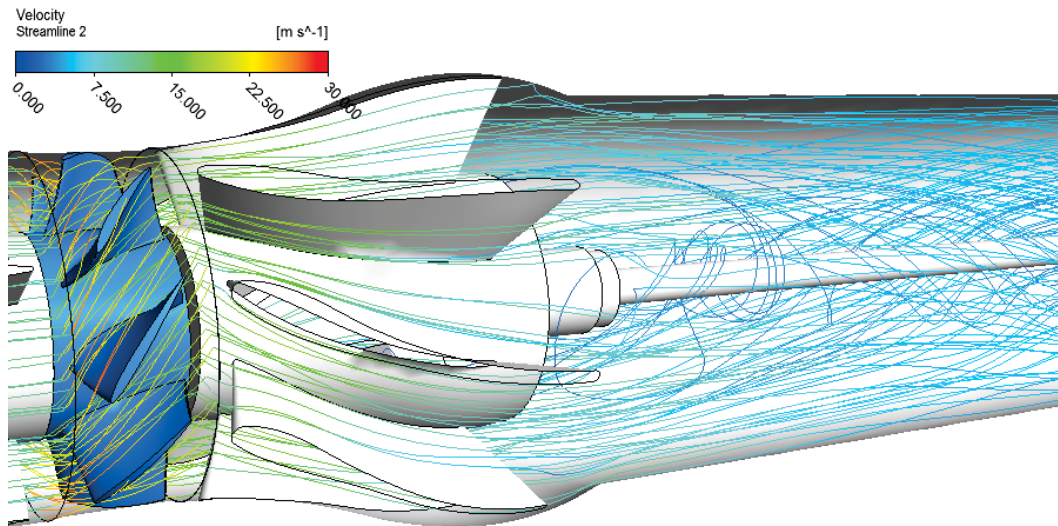


Figure 153 – Comparison of new diffuser and tail piece addition 3D streamline

#### 4.4.2.4 Predicted Pressure Rise

As with the five vane impeller, to assess the total pressure through the two new diffuser configurations, a total pressure plot was taken at a number of equally spaced planes. The results of the area plots are similar to the five vane set-up, (however with greater pressures) with a greater percentage of the sectional areas having an even stable pressure, hence the ability to perform at a lower stall flow.

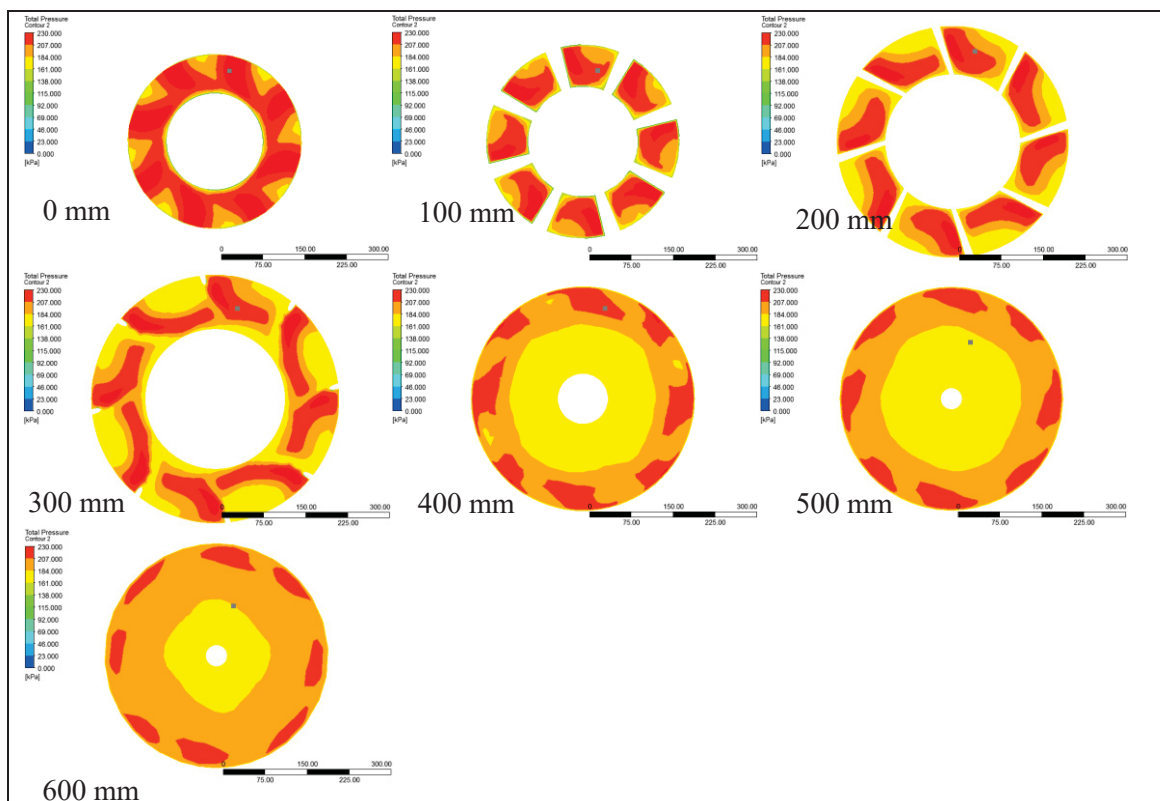


Figure 154 - Predicted pressure rise through new diffuser



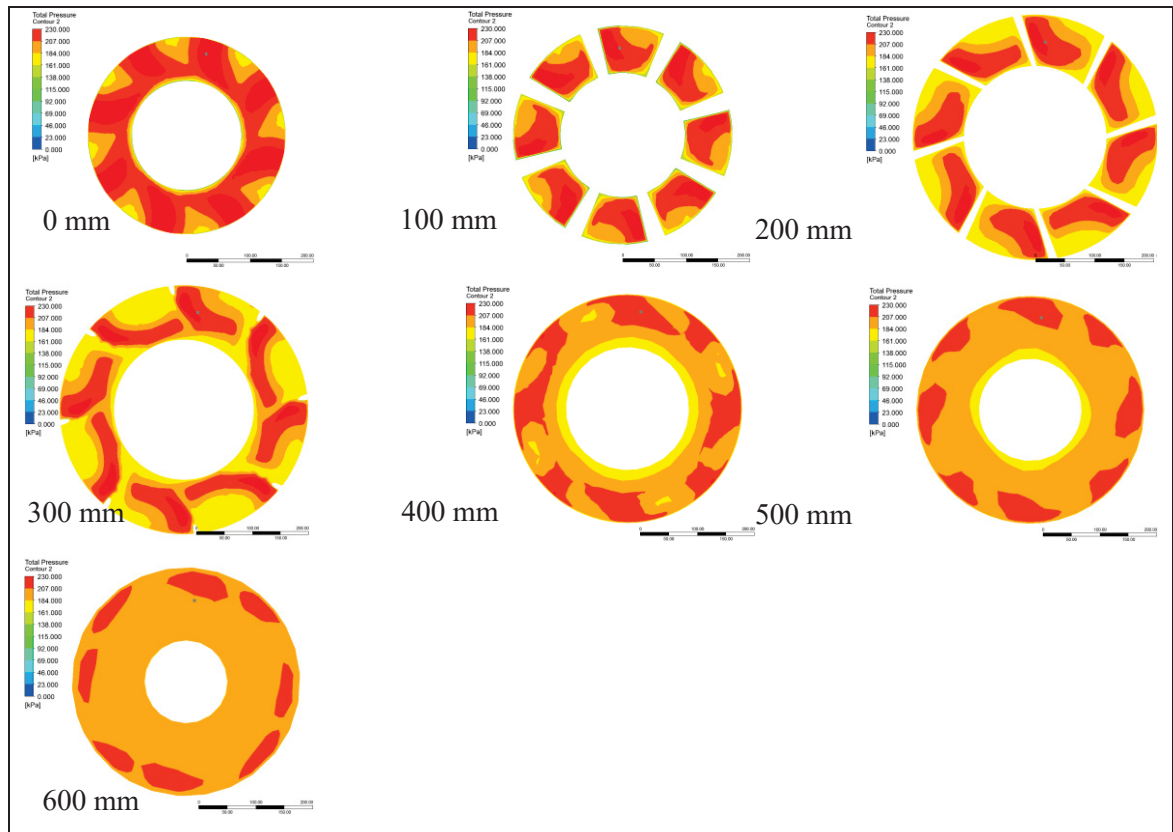


Figure 155 - Predicted pressure rise through new diffuser with tail piece

However when comparing the section plot, the new diffuser has 10% lower pressure at the outlet.

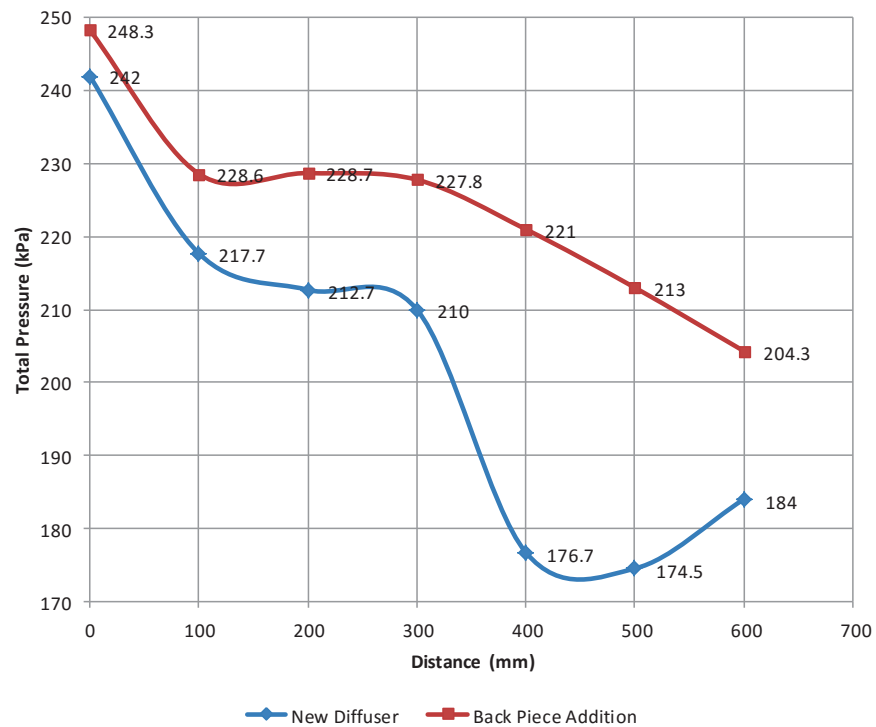


Figure 156 - Predicted pressure through new diffuser with eight vane impeller



### 4.4.3 Analysis at Stall Flow

As a case of interest, CFD analysis was run for both the new diffuser and tail piece pump configurations at the position of the stalled flow rate. The flow rate of 234 L/s was determined from the stall point during the laboratory pump test for the tail piece and the five vane impeller as shown in Section 5.2.3.1.

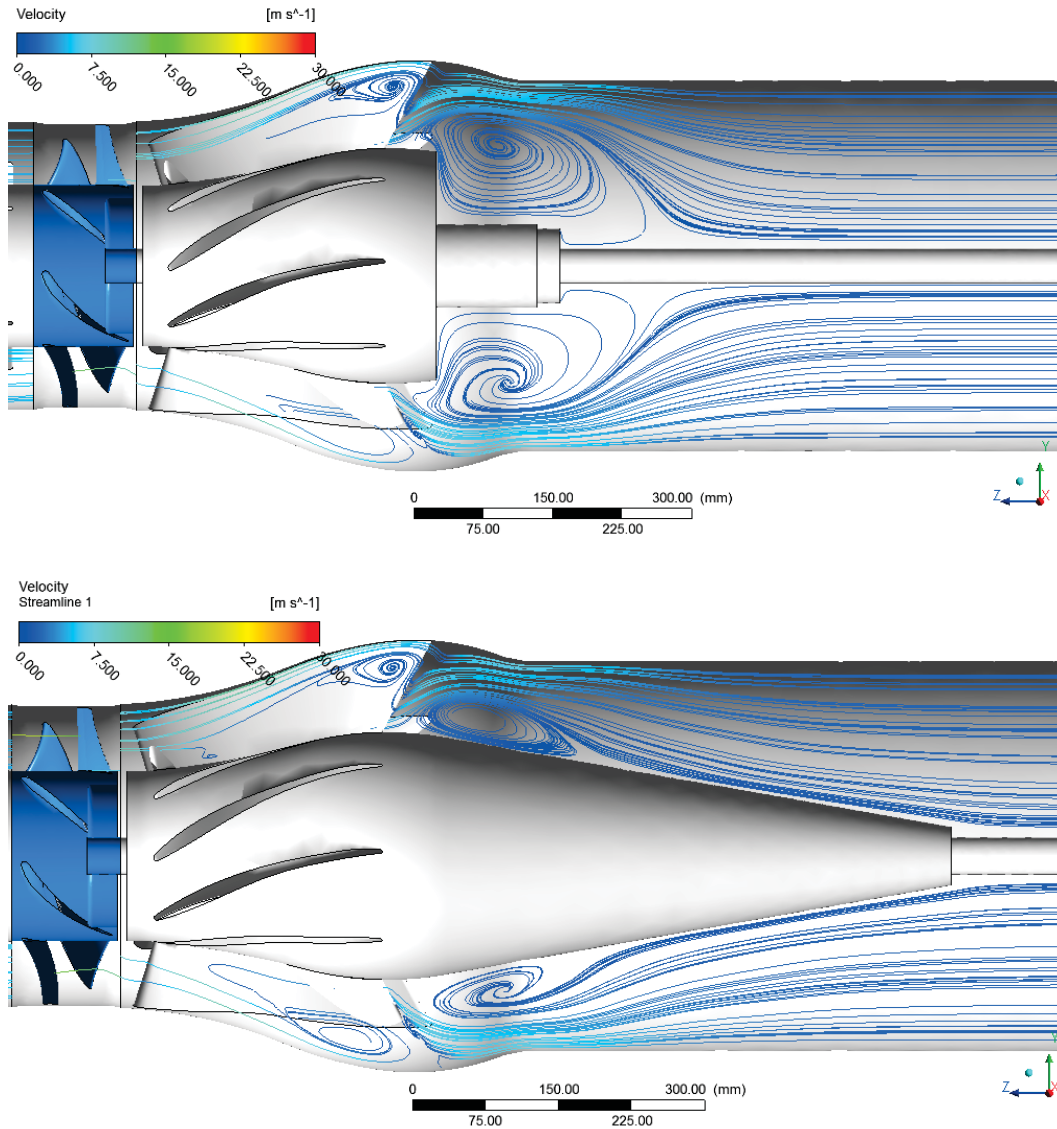


Figure 157 – Test comparison 2D velocity streamlines at 234 L/s

When comparing the two 2D velocity streamline images, the new diffuser by itself shows that the turbulence swirl expands towards the shroud and into the flow passage area therefore decreasing and choking the straight flow area. Where with the tail piece addition, even though the swirl is now present at the vane outlet, it is still not as large as the previous leaving a larger area for the fluid flow to pass, hence the stall is less, therefore increasing the pump's operating range.

The pressure plots in Figure 158 confirm the swirl area by the lower pressures.

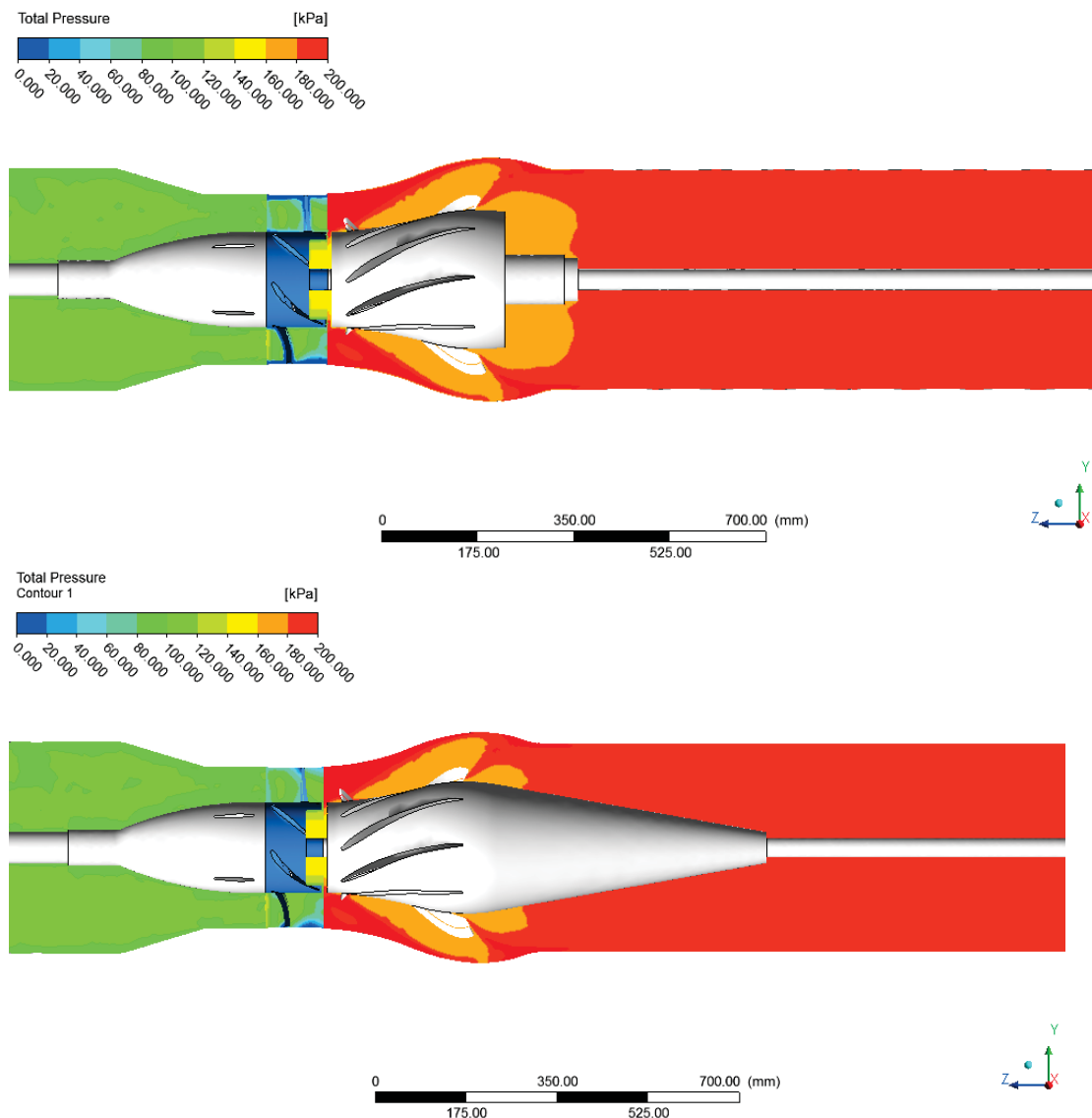


Figure 158 – Test comparison total pressure at 234 L/s

## 4.5 Further Analysis

Further CFD analysis was conducted to determine if a re-design, of the new diffuser shape, could improve its performance. Various modifications to the new diffuser models were made.

### 4.5.1 Inlet Hub Modification

As discussed in Section 4.4.1.2, the impeller hub face was contributing to high velocities at the new diffuser's vane inlet tips. To achieve more appropriate CFD results this face was removed from the model. In this section, the open area, as found on the standard pump impeller has been

incorporated into the model for analysis. The results show that the open area does reduce the high velocity entering the diffuser. A low pressure created in this area, reduces the disk friction between the diffuser and impeller and allows the fluid to recirculate in the area and not force the fluid back into the flow passage.

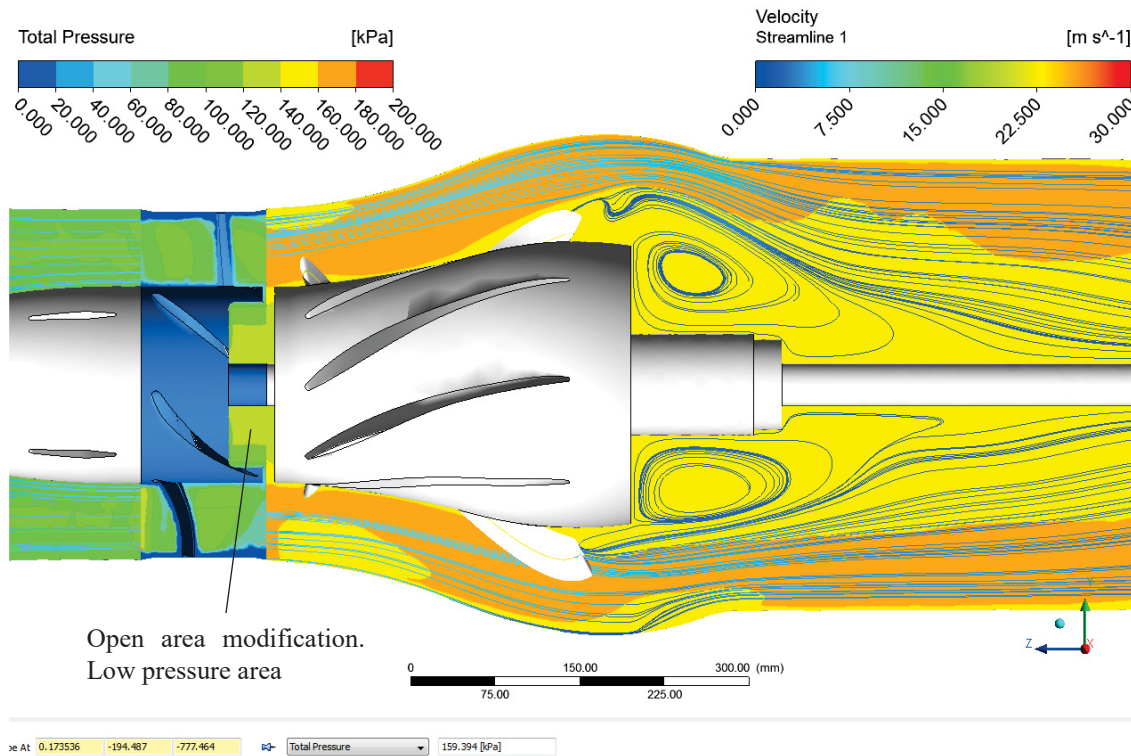


Figure 159 – Impeller hub face open area model modification

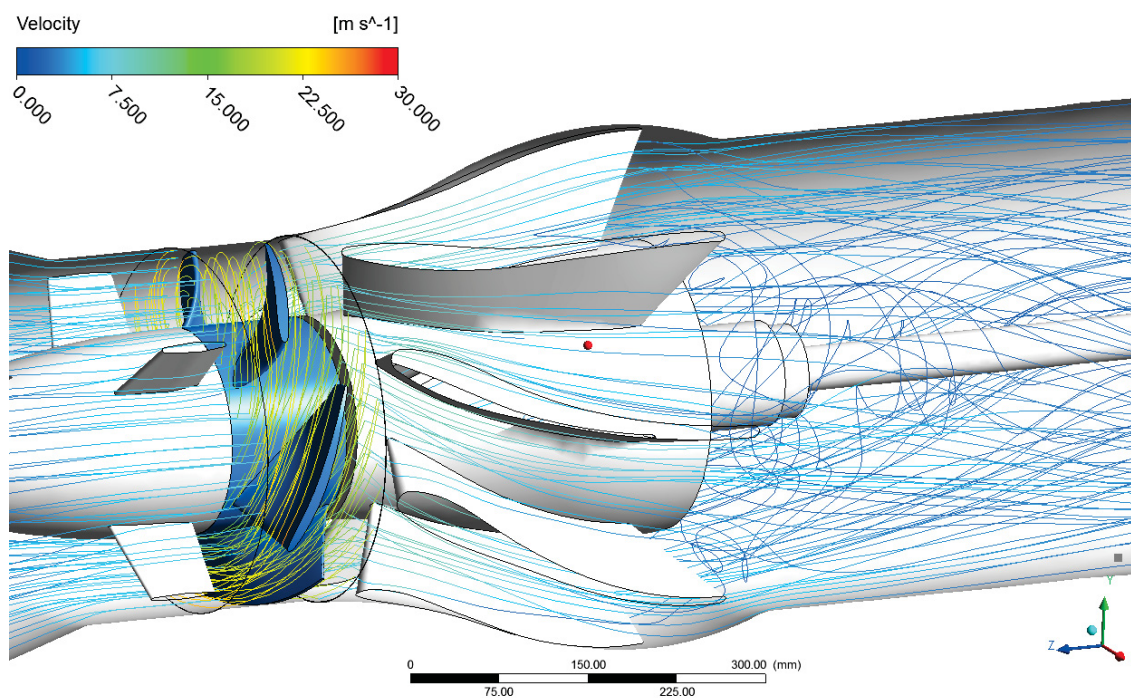


Figure 160 – Impeller hub face open area model modification 3D streamline

## 4.6 Alternative Diffuser Design Analysis

For further interest in the diffuser design process, the theories found in Section 2.3 for a stator-diffuser design were used to re-design the new diffuser concept to suit the five vane impeller configuration. Four different designs were produced and analysed using CFD. The CFD results were compared to each other to determine if one of the designs could be suitable for use with the five vane impeller. Layouts of each are shown in the figures below.

Because the new diffuser vanes did not match the five vane impeller, for the re-design the vane dimensions for the standard Ornel type '5' stator were modified and used to replace the existing new diffuser vanes. It was found during the previous CFD results, that an open surface area at the diffuser's hub face would reduce disk friction between the impeller hub face and diffuser hub face and eliminate high velocities at the diffuser's inlet. For this reason, an open area was added to the re-design. Also the newly designed tail piece was added.

The design process for each design began by using the existing pump constraints of the pump's bowl ring, impeller hub and column pipe dimensions. Once the dimensional constraints were established the shroud and hub outlines are detailed. For designs 1 to 3, the shroud was developed using the design theory recommendation from Section 2.3.1, that the diffuser has a radial angle of a  $4^\circ$  to  $5^\circ$ , to introduce a gradual cross section area with minimum fluid surface separation. To do this, a line with an angle is drawn from the inlet diameter to the outlet with a small section of straight line at the inlet, to smoothly transition into the incline.

For design '1' a slight angle of  $5^\circ$  was added to the hub inlet to allow for a more consistent flow passage section. The shroud was designed with an angle of  $5^\circ$ .

For design number '2' the hub inlet angle was removed to slightly increase the rate of the cross sectional area expansion with a shroud angle of  $5^\circ$ .

For design number '3' the hub dimensions are the same as the design of number '2' but with a change of shroud radial angle to  $4^\circ$  from  $5^\circ$ .

For design number '4' the shroud and hub design are as per the new diffuser. With the existing vanes being replaced with the modified type 5 stator vanes.

To check the gradual expansion of the flow passage section areas, measurements of areas were plotted. The first section measurement was taken where the vane intersects with the hub. Five more section area measurements were recorded at 25mm intervals moving towards the diffuser outlet. The results are shown in Figure 165.

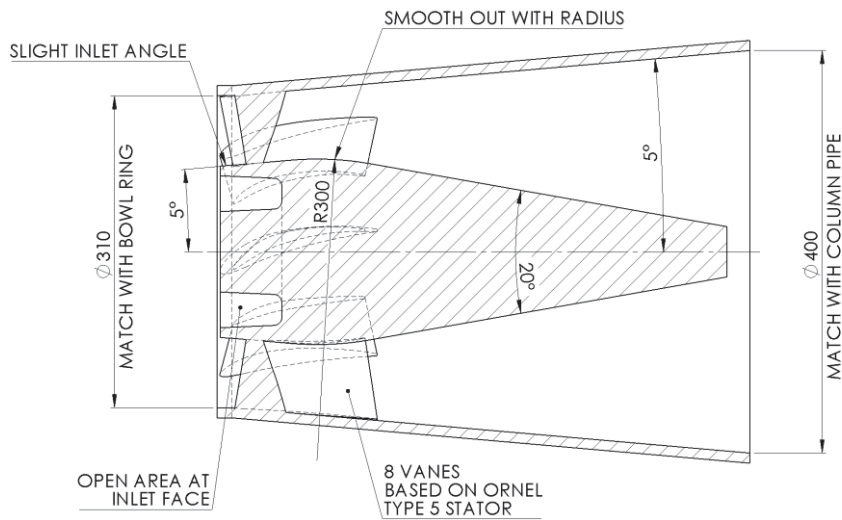


Figure 161 – Layout of diffuser re-design number 1

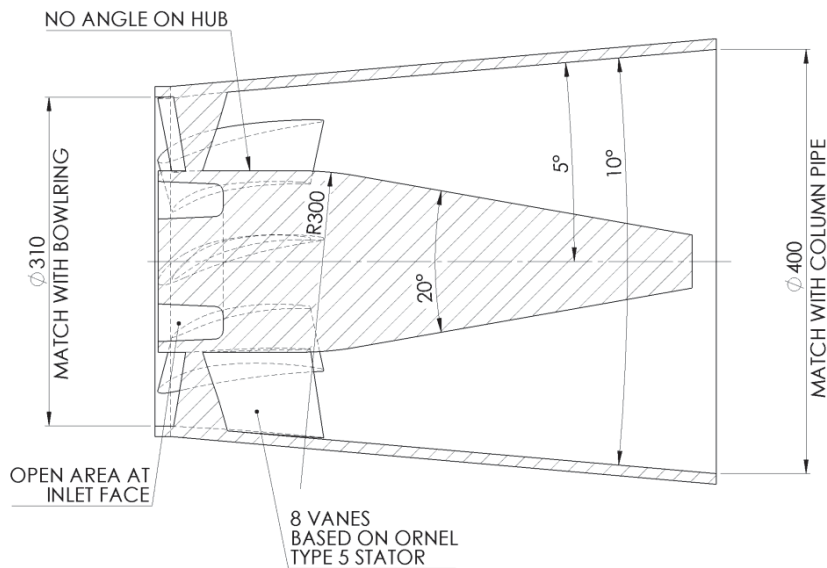


Figure 162 - Layout of diffuser re-design number 2



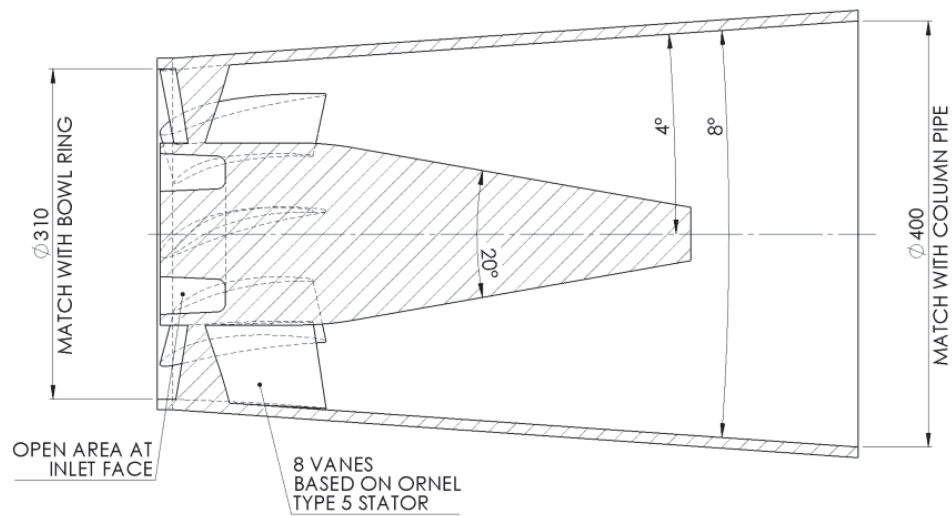


Figure 163 – Layout of diffuser re-design number 3

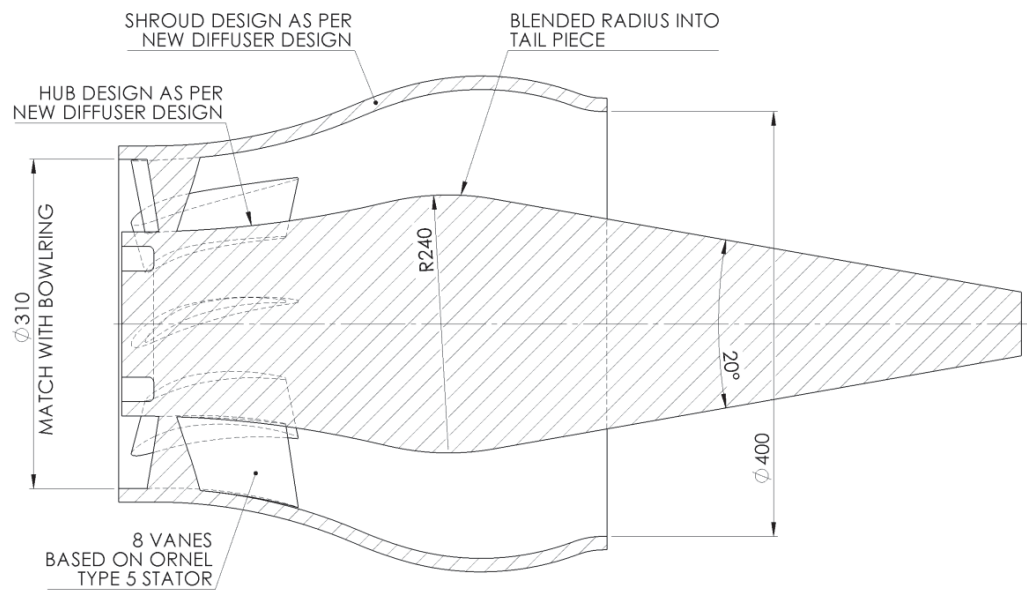


Figure 164 – Layout of diffuser re-design number 4

The graph indicates that the flow passages of the re-designs do expand at a constant rate. The steeper incline of areas expansions are due to the enlarged flow area than the original designs, as a result of the introduced angle of the shroud.



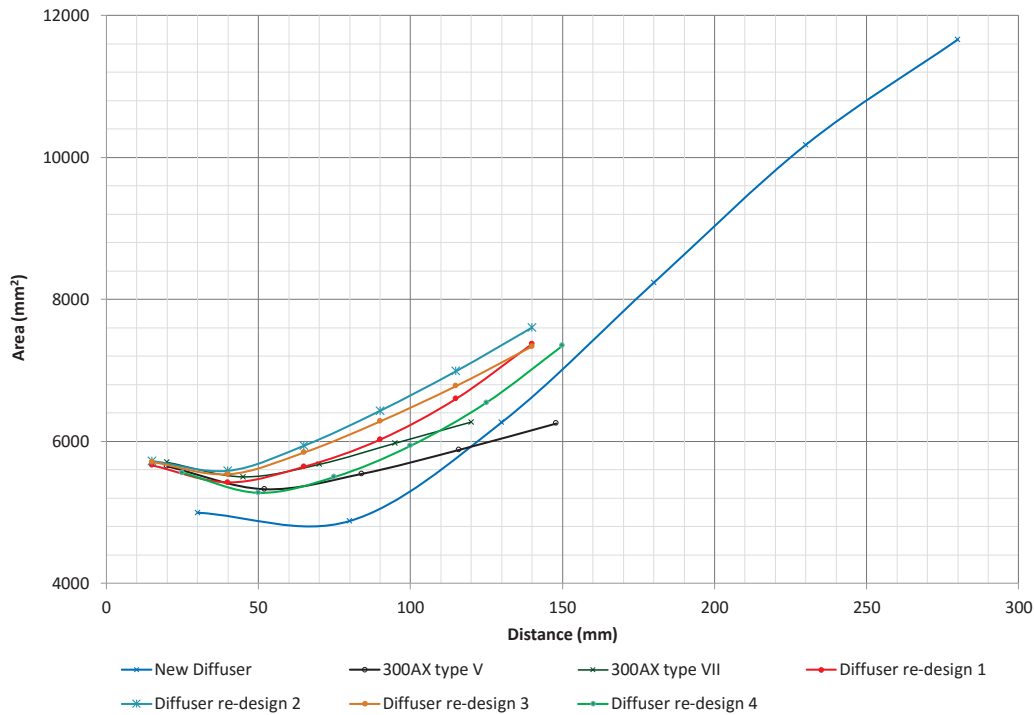


Figure 165 – Flow passage area measurements

Figure 166 compares the 2D velocity streamline of the four diffuser re-designed models. The results indicate that secondary flow is created at the outlet of the diffuser in each of the designs. The secondary flow is found in the low pressure areas as indicated in Figure 167. This shows the predicted total pressure of the four designs. The pressure was recorded at the same point position used in the previous CFD analysis.

Diffuser re-design	Total pressure at probe point
1	164.4 kPa
2	164.6 kPa
3	164.7 kPa
4	161.9 kPa

Table 6 – Re-designed diffuser predicted total pressure

From the results in Table 6, numbers 1 to 3 are similar pressures and number 4 is slightly lower by 2.8 kPa. When compared to the previous CFD results for the tail piece addition of 160.5 kPa, there is only a slight increase in pressure of 4.2 kPa (2.6%), when compared to the best result of 164.7kPa from re-design number 3.

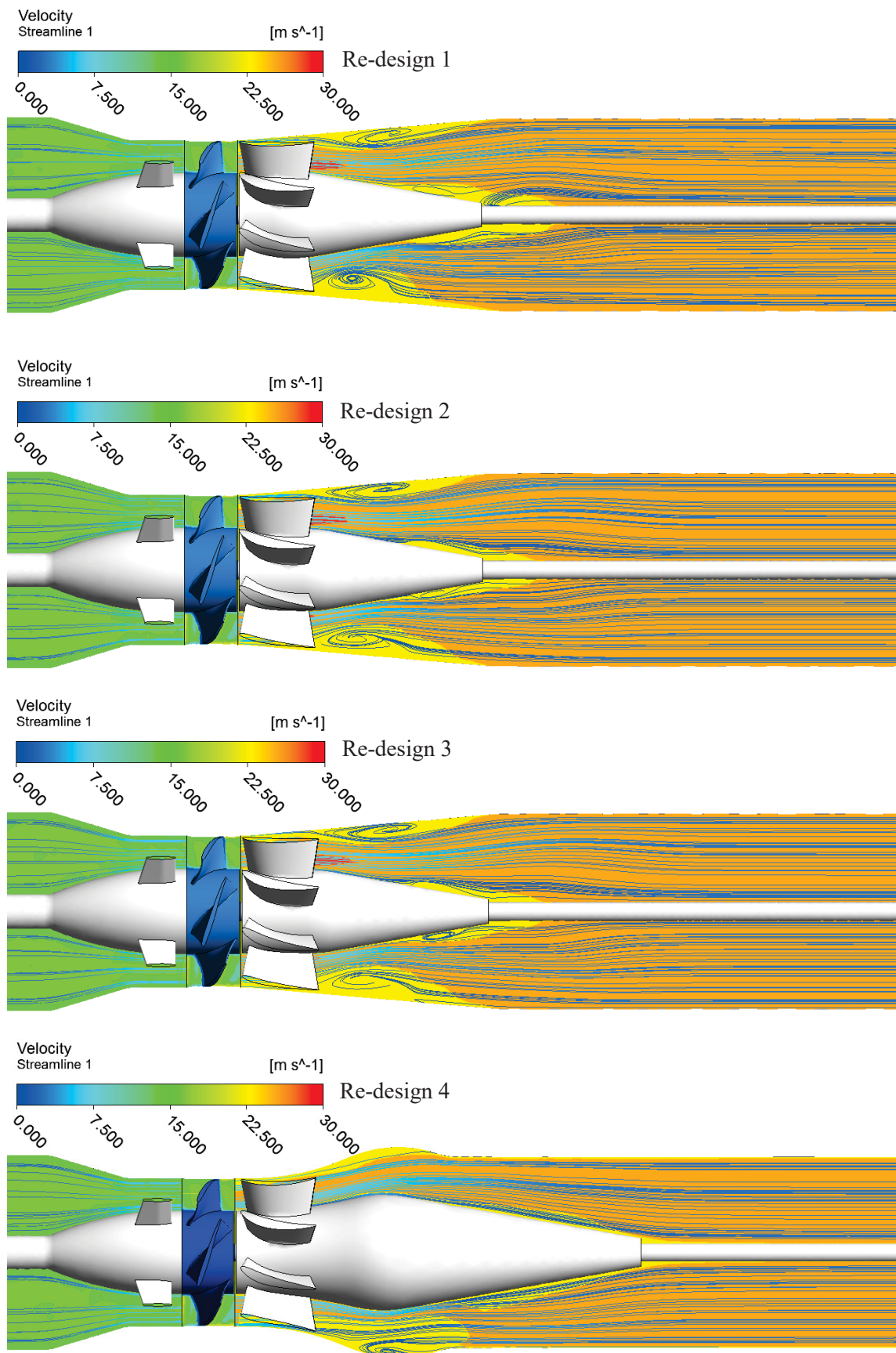


Figure 166 – 2D velocity streamlines of re-designed diffuser

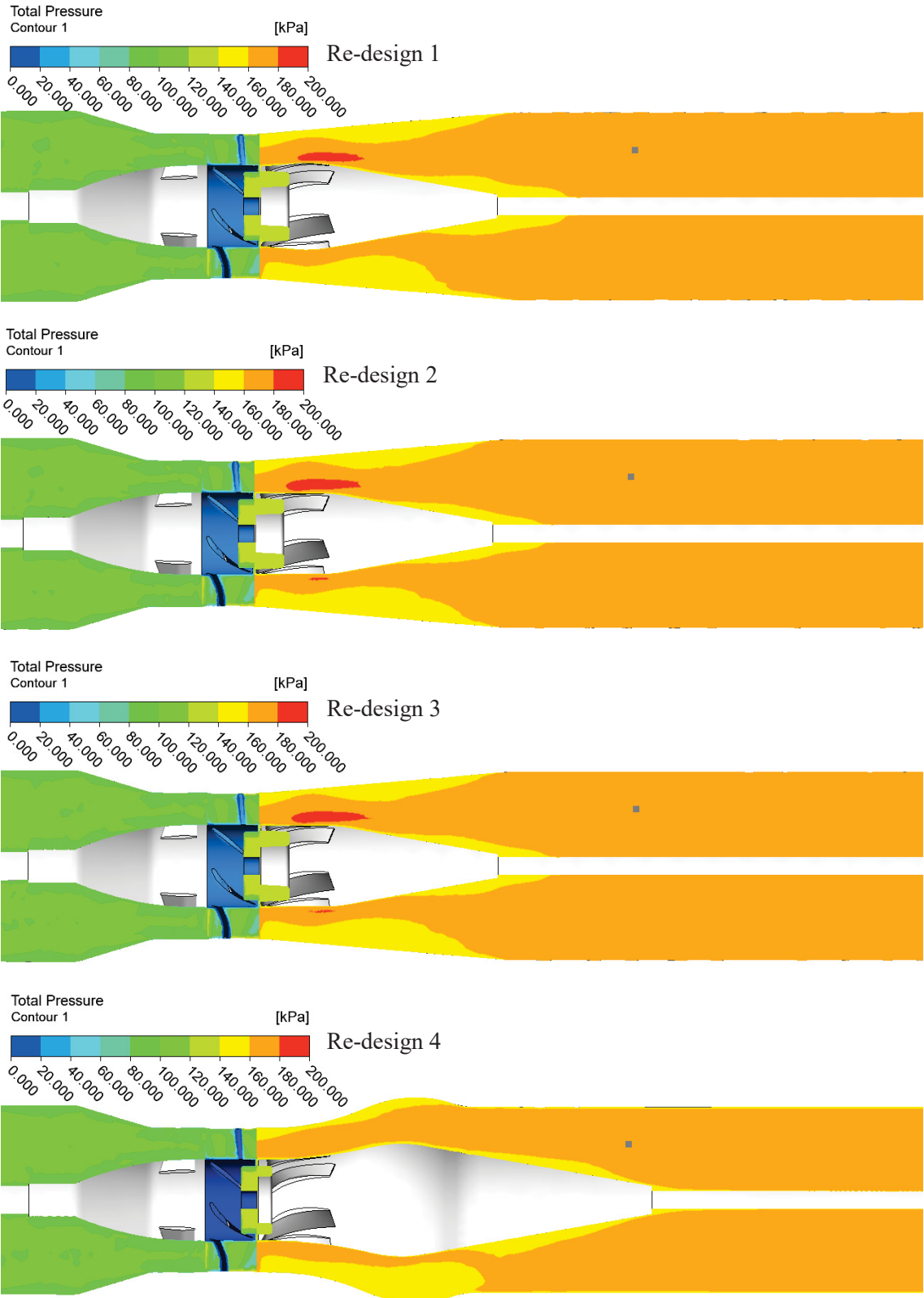


Figure 167 – Total pressure plots for re-designed diffuser

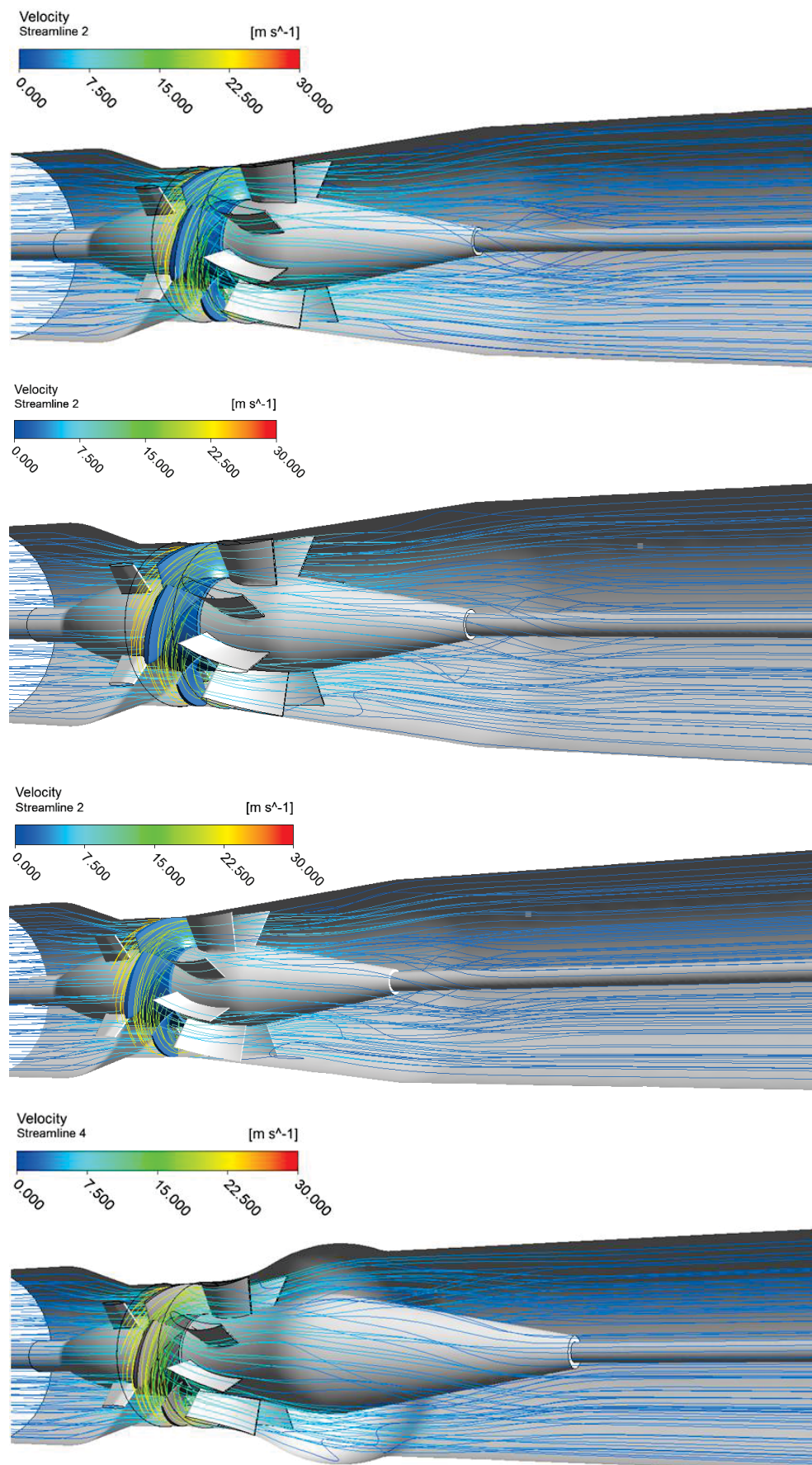


Figure 168 – 3D velocity streamline plots for re-designed diffuser

## 4.7 Chapter Conclusion

During this chapter it was observed that the CFD analysis performed for this thesis had different predicted pressure results than the laboratory testing results. In the case of the five vane impeller, the CFD total pressure results using the BEP flow were 7.5% lower than the laboratory tests, however with the eight vane impeller, CFD total pressure results were 22% higher. The differences may have been due to such circumstances as the CFD model parameter selections or the state of some of the manufactured pump components, (poor surface finish, worn clearances etc).

However, the CFD analysis results did give a better understanding of the fluid flow paths and total pressure predictions within an Axial Flow Pump.

By using CFD analysis with a five vane model the following was observed:

- A tail piece design was determined.
- A reduced surface area at the impeller hub faces decreases the disk friction which was directing high velocity flow perpendicular to the axial flow path. This was introducing blockage in the area and lower downstream pressures in the CFD model.

The CFD models analysed predicted similar flow patterns between the different five and eight vane impeller pump configurations. The similarities found were:

- CFD models using the new diffuser design show the sudden enlargement creates a low pressure region behind the back face which introduces secondary flow, hence a turbulent area as the higher pressure flow path passes in an axial direction.
- The tail piece addition will reduce the secondary flow turbulence.
- The addition of the tail piece introduces a larger amount of the cross sectional area to higher pressure which is sustained for a longer period in the flow passage. This helps to increase the pump's operating range and reduces the wall turbulence.
- The addition of the tail piece will only have a slight pressure rise in the pump.
- The predicted hydraulic grade line within the new diffuser is improved with the tail piece addition.

Additional models were created to determine if a redesign of the new diffuser concept would help to improve the pump performance. The idea was to combine the medium flow stator vanes with (a) the standard diffuser and (b) the new diffuser. The total pressure results in Table 6 from Section 4.6 show that as the shroud and hub angles are reduced, the total pressure slightly increases and the secondary flow turbulence reduces. However, these pressures are still less than the total pressure from the CFD standard pump analysis having 7.4m (172.9 kPa).

Diffuser re-design	Total pressure at probe point
1	164.4 kPa
2	164.6 kPa
3	164.7 kPa
4	161.9 kPa

More investigation would be required in this area to design a diffuser design which could improve the efficiency for the five vane impeller configuration.



# 5 Experimental Investigation

The laboratory test rig layout, pump configurations, testing schedule and testing procedure used to determine the pump performance is detailed in the following section. A number of tests were performed using the Axial Flow Pump assembled in different configurations. The results of the satisfactory tests are analysed in this section, with the results of all performed tests can be found in Appendix D.

## 5.1 Pump Testing

Laboratory testing was used to assess the performance of the standard pump, the new diffuser design and modifications made to the new diffuser. The hydraulics laboratory used for this research is located at the *University of Technology* Sydney.

Pump testing provides the physical proof that design modifications made to the pump components may improve or not improve the pump's performance. Laboratory testing in this controlled environment will produce the most accurate results.

For this research, six different configurations of the Axial Flow Pump were assembled and tested at the recommended speed of 1465rpm as per the OEM pump curves (Figure 15). These results will be compared to each other to analyse the best performance results for the different configurations. The different configurations that were tested for this research are as follows:

Test Pump Configurations				
Configuration No.	Schedule No.	Impeller Vane No.	Stator / Diffuser Configuration	Speed (rpm)
A	1	5	Type standard stator / standard diffuser	1465
B	2	8	Type standard stator / standard diffuser	1465
C	3	5	New diffuser design	1465
D	4	8	New diffuser design	1465
E	5	5	New diffuser design / tail piece	1465
F	6	8	New diffuser design / tail piece	1465

*Table 7 – Pump test configurations*

Previous research for this pump has been conducted using the five and six vane impellers with both the original stator diffuser and the new design of diffuser as per Section 2.4. The results from the previous research using the five vane impeller with the original stator and diffuser was

compared with newly conducted tests to determine any similarity in performance between the different researches. The six vane impeller was not tested during this research, due to both the time restraints and it was believed more beneficial to test the eight vane impeller which, as shown in Section 3.2.2.2, theoretically better matches the inlet vane angle for the new diffuser design. The eight vane impeller was previously unable to be tested due to damage but was repaired to progress with this research as per Section 3.4.

### 5.1.1 Laboratory Test Rig Layout



*Figure 169 – Refurbished hydraulics laboratory pump test rig at UTS*

#### 5.1.1.1 Original Pump Test Rig

The pump test rig was donated to the university in 1982 by Warman (now part of *Weir Minerals*). The test rig is assembled in a closed loop type configuration. In this type of configuration, the pump discharge is fed directly into the pump suction in a closed loop. The pump is installed in a horizontal position. In this type of configuration it is essential that the suction pressure is maintained above the NPSHR to ensure the pump will not cavitate. To enable this, there is a booster pump installed which adds fluid, therefore pressure to the inlet side of the test loop via the tank. The booster pressure is regulated via a valve which, when opened, bypasses the fluid back to the tank and relieving the test loop's pressure.

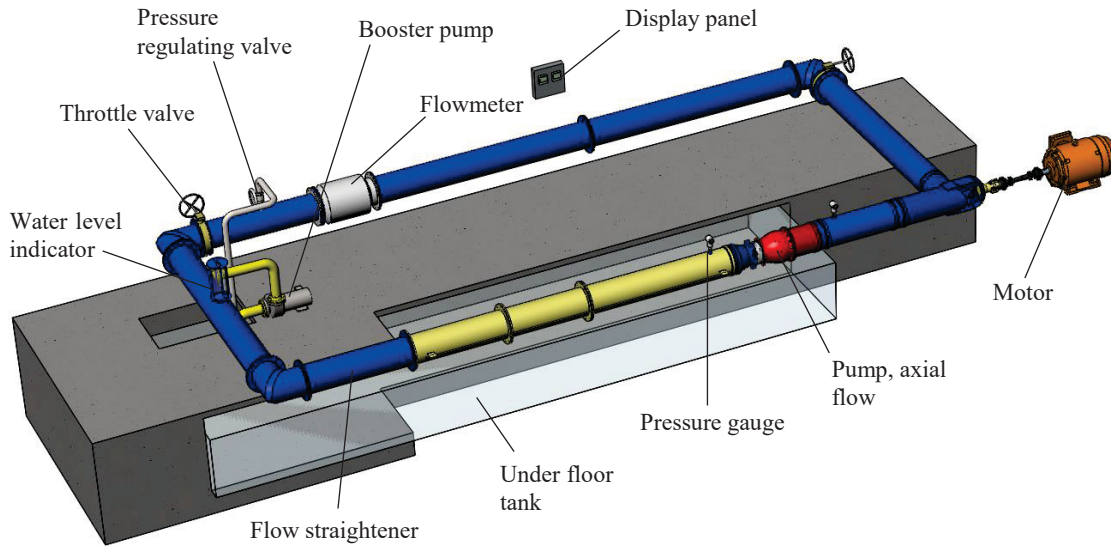


Figure 170 – Test Rig Layout

The closed circuit test rig consists of a number of lengths of 406mm bore fabricated pipes with three fabricated elbows to form the closed loop. Ensuring there is a straight flow into the pump impeller is critical. Flow straighteners are installed in the straight length approaching the pump inlet to reduce any fluid swirl and ensuring the fluid approaches the impeller with a straight flow path. The straightener consists of a number of smaller diameter PVC pipes installed into the test loop pipe. Also each elbow of the loop has guide vanes to ensure that fluid flow is as straight as possible.

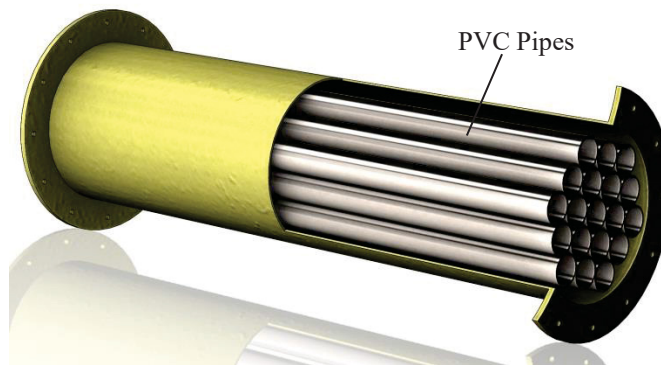
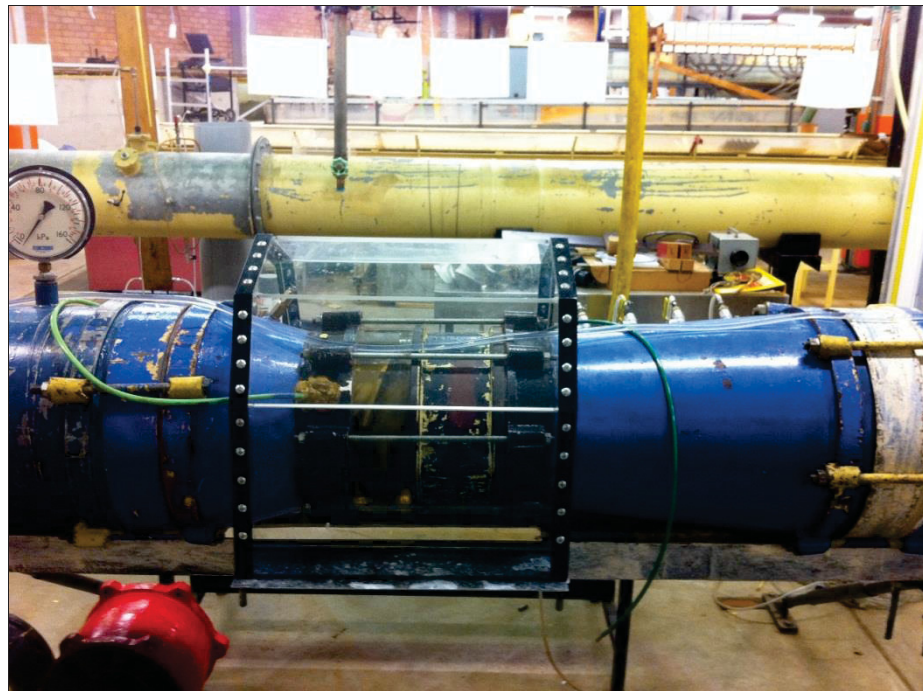


Figure 171 – Straightener pipe section



*Figure 172 – Pipe internals showing straightener section*

The pump is driven by 75 kW *Mather & Platt* electric motor controlled by a variable speed drive (VSD). The loop is filled via the booster pump fed from the tank beneath the floor of the hydraulics laboratory. Air is removed from the system during filling via an air release valve. The valve has a sight chamber to ensure visually the system is free of air (see Figure 174).



*Figure 173 – Pump installation arrangement for Test no.1*





*Figure 174 – Main air release valve chamber*

During testing the pump flow rate and head is controlled by manually opening or closing the throttle valve on the discharge side of the test loop. The throttle valve used is a butterfly type valve controlled by a hand wheel as shown in Figure 175. By closing the valve the pump is pushing the fluid against a blockage in the system. This blockage results in a pressure rise due to the fluid being restricted and causing a drop in fluid flow. The pressure rise resembles the systems head pressure. Extra pressure gauges, which are connected to the suction and discharge pressure gauges, are positioned at the throttle valve to allow for visual indication of the various head pressures to be controlled during the test.



*Figure 175 – Throttle Valve*

### 5.1.1.2 Upgraded Refurbishment of Test Rig

During late 2014 to early 2015 the entire test rig was disassembled and removed from the hydraulics laboratory for refurbishment and upgrade. The following work was carried out:

- Pipe work was cleaned and repainted externally and internally.
- The old redundant magnetic flowmeter was removed and a new magnetic flowmeter was installed.
- The existing mercury manometer was replaced with a new hand held manometer.
- The existing pressure gauges were replaced with new digital pressure gauges, which are linked to a common display panel showing the pressures and flow.
- The following pump components were replaced with new components:
  - Impeller five vane
  - Impeller collet
  - High flow stator (original design)
  - Pump shaft
  - Pump bearings
  - Line shaft
  - Line shaft bearing
- The existing stator was refurbished.
- Thrust bearings were replaced.



The new installed pressure gauges and flowmeter are connected to a single panel for ease of recording accurate data without the need to move from one side of the rig to the other side.

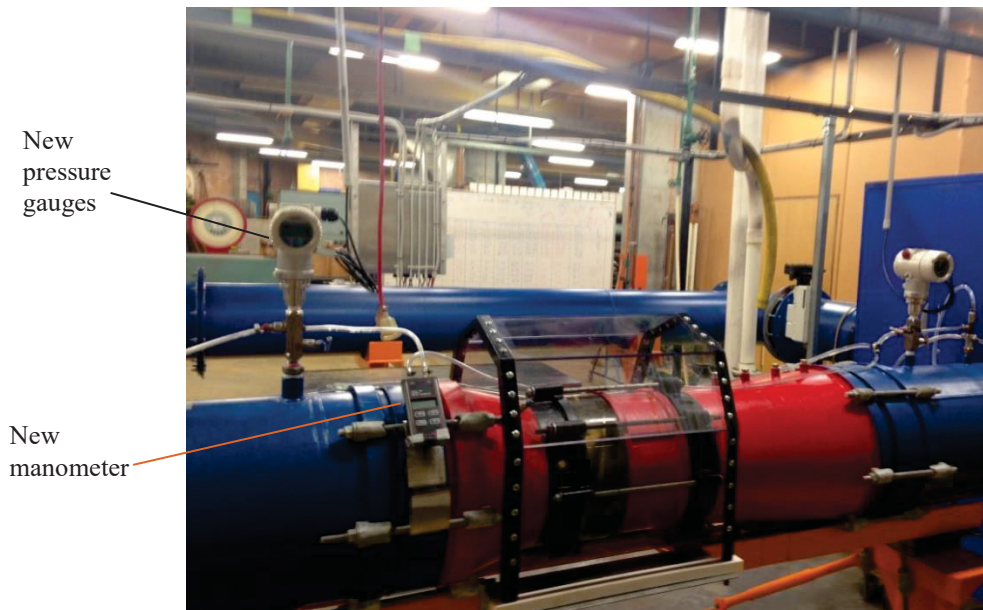


*Figure 176 – Upgraded test rig*



*Figure 177 – New control panel*

## 5.1.2 Pump Test Configurations

The following sections detail the configurations which were tested in the laboratory.

### 5.1.2.1 Configurations A and B

Figure 178 shows Configurations A and B, which is the pump as per its original supply with standard pump components. Configuration A is made up of a five vane impeller followed by the original stator and diffuser, whereas the eight vane impeller is changed over for

configuration B. These are the two configurations used to produce a base set of results as previously mentioned.

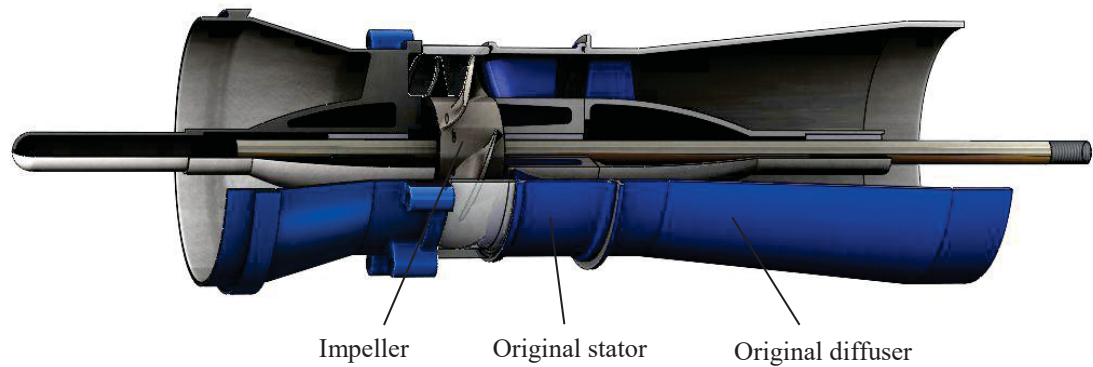


*Figure 178 – Pump assembly configurations A & B*

### 5.1.2.2 Configurations C and D

Configurations C and D are made up of the original five and eight vane impeller combined with the new diffuser design. The new diffuser component has been coated with an epoxy ceramic coating for both protection and smoother surface finish to provide a better efficiency (refer to Section 3.3.2). The results from the previous research will also be compared to Tests 2, and 3 using the new diffuser to investigate if the applied ceramic coating will have an effect on the pump efficiency.

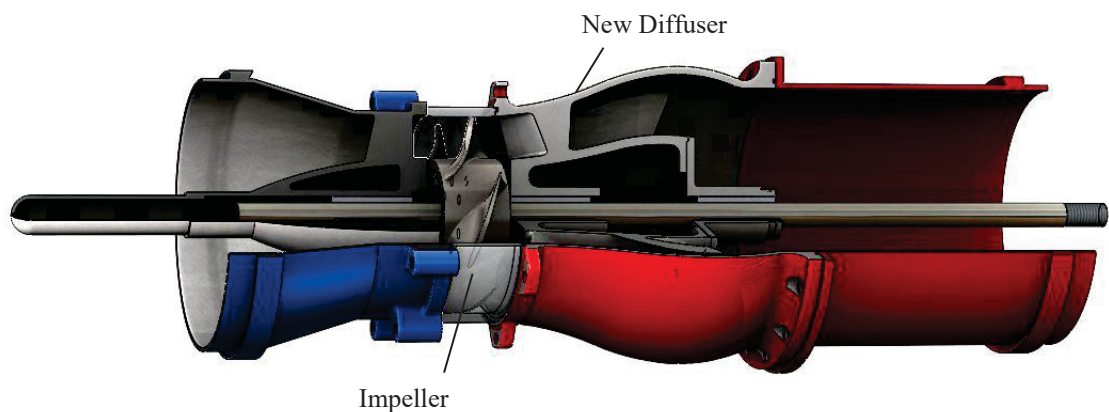


*Figure 179 – Pump assembly configuration C & D*

### 5.1.2.3 Configurations E and F

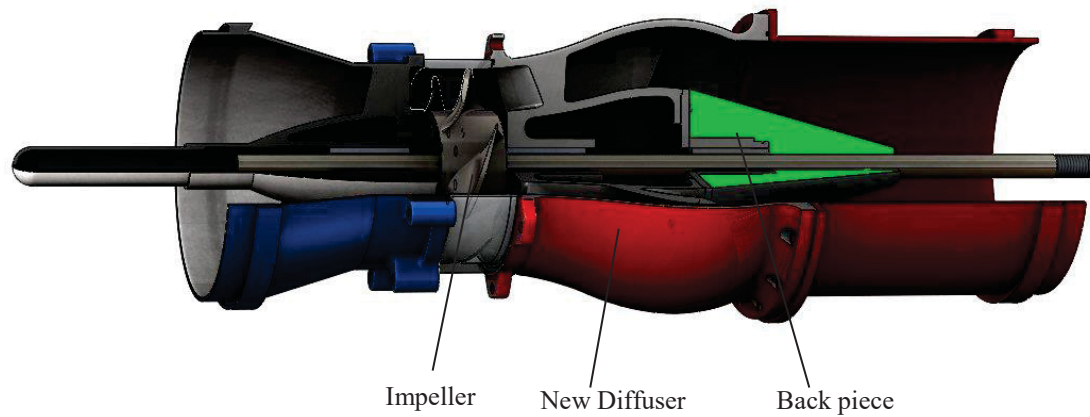


Figure 180 – Pump assembly configuration E & F

The final configuration shown in Figure 180 consists again of the five and eight vane impellers, the new diffuser and the tail piece design bolted to the back face of the diffuser (refer to Section 3.3.3).

### 5.1.3 Test Schedule

To track the testing progress a pump test schedule was created.

Pump Test Schedule - Axial flow pump			
Pump Test No.	Impeller Vane No.	Stator / Diffuser	Complete Date
1.01	5	Std. stator / Std. diffuser	18/07/2014
1.02	5	Std. stator / Std. diffuser	30/07/2014
<b>Refurbished test rig installed</b>			
1.03	5	Std. stator / Std. diffuser	11/05/2015
1.04	5	Std. stator / Std. diffuser	21/05/2015
1.05	5	Std. stator / Std. diffuser	29/05/2015
2.01	8	Std. stator / Std. diffuser	10/02/2016
2.02	8	Std. stator / Std. diffuser	10/02/2016
3.01	5	New diffuser design / no tail piece	31/03/2016
3.02	5	New diffuser design / no tail piece	31/03/2016
4.01	8	New diffuser design / no tail piece	11/05/2016
4.02	8	New diffuser design / no tail piece	11/05/2016
4.03	8	New diffuser design / no tail piece	14/05/2016
4.04	8	New diffuser design / no tail piece	14/05/2016
5.01	5	New diffuser design / tail piece	18/05/2016
5.02	5	New diffuser design / tail piece	18/05/2016
6.01	8	Std. stator / Std. diffuser	23/05/2016
6.02	8	Std. stator / Std. diffuser	23/05/2016
6.03	8	Std. stator / Std. diffuser	23/05/2016

Table 8 – Pump test schedule

A minimum of two tests for each configuration was run. If the tests results had high variances, then a third test would be conducted to produce accurate data for the pump performance assessment. For reference, each set of test results is numbered by the schedule number followed by the test number e.g. 1.01.

Preliminary tests 1.01 and 1.02 were conducted using the same test equipment as per the previous research. It was found a change in the flow measurement equipment was required to achieve more accurate results as referenced in Section 5.1.5.1. However, after pump tests 1.01 and 1.02 were run the pump test rig had a major overhaul resulting in updated measurement equipment being installed. Therefore, testing was required to start again using the results from 1.01 and 1.02 for reference.

### 5.1.4 Test Procedure

The following procedure was performed to test each pump configuration. Each pump test was run for approximately 45minutes. The steps for the test procedure are as follows:

1. Fully open the throttle valve, pressure release valve and the main air release chamber valve. Prime the booster pump and when the water is flowing from the main drain valve, shut the valve, start the booster pump and shut the prime line.
2. Ensure the test loop is filled with water and properly vented and free of air. This is done by having the ball valve on top of the main air release chamber. When the water level in the chamber is midway the valve can be shut.
3. With the booster pump still running, start the main pump and run at a low speed of 200 to 300 rpm to ensure all air is removed from the loop and the pump is running smoothly. Gradually close the pressure regulating valve until the suction pressure gauge reads a minimum pressure of 100 kPa.
4. Gradually increase the speed of the main pump to the test running speed of 1465 rpm. Ensure the suction pressure is maintained at 100 kPa by adjusting the pressure regulating valve.



*Figure 181 – Pressure release valve*

5. When the pump has been operating for approximately five minutes without problems and the flow reading is stable, the first set of data measurements were recorded. The following points were recorded:
  - a. Suction pressure
  - b. Discharge pressure
  - c. Flow
  - d. Torque
  - e. Speed (shaft) – from tachometer
  - f. Motor kW – from VSD
6. Once a set of data is recorded, the throttle valve is closed to one notch indicator on the top of the valve, (once three sets of data have been recorded the valve is shut half a notch).

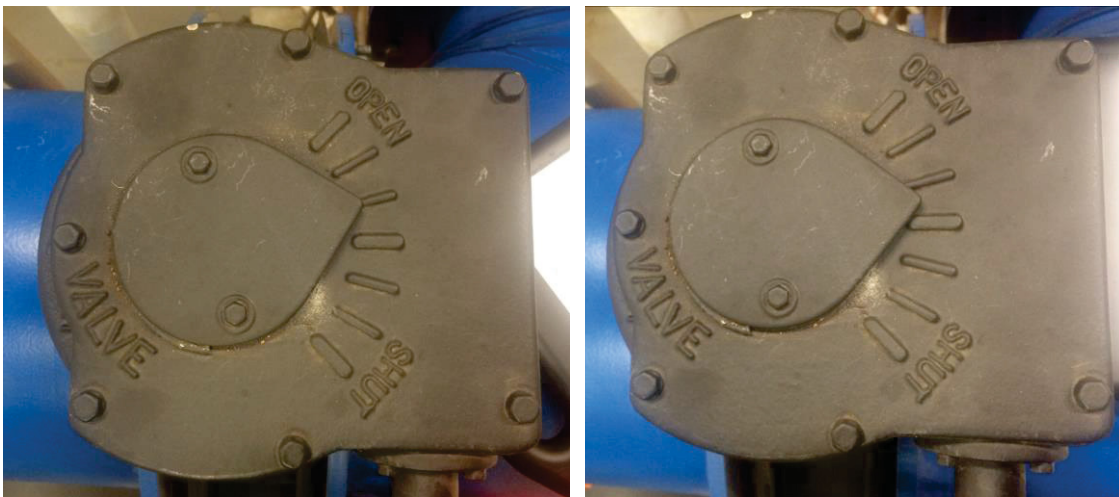


*Figure 182 – Valve notch indicator (a) full notch (b) half notch*

7. When the pump flow is stable again steps 5 and 6 are repeated until the pump starts to stall. One more set of data is recorded and the test is complete. Fully open the pressure regulating valve and fully open the discharge throttle valve.





*Figure 183 – Conducting test 5.01*

### 5.1.5 Test Measurements

To assess the pump performance, measurements are taken during the test for the following conditions:

- Flow (flowmeter)
- Motor torque
- Motor power (from VSD)
- Suction pressure (digital gauge)
- Discharge pressure (digital gauge).
- Head via manometer and pressure gauges
- Pump Speed via tachometer

The above data is recorded on the pump test sheet (see Figure 184) which has been created specifically for this research. The sheet is an excel document which is linked to a number formulas and sheets which will calculate such results as the velocity head coefficient and speed correction results. It will also create the performance curve compared to the original design OEM curve.

Testing was conducted as per AS2417 grade 2. A grade 2 is the industry standard for pump testing, however the test accuracy is lower than that of a grade 1 test and is the industry standard for pump testing. The major difference between the two tests is the duty point percentage.



Two tests for each pump configuration were conducted. Measurements were recorded at several changes of pressure. Data sheets for each test are shown in Appendix H.

<b>PUMP TEST SHEET</b> <small>**** PUMP TESTING CARRIED OUT IN ACCORDANCE WITH AS 2417 Part 2 Class C****</small>																	
Pump Type: <b>Ornel 300AX</b>			Imp vane #: <input style="width: 100px;" type="text"/>			Stator Type: <input style="width: 100px;" type="text"/>			Test No.: <input style="width: 100px;" type="text"/>								
<b>Required Duty Point</b>																	
Test Date		Manometer Fluid p		Flow		Total Head		Pump input power		NPSHR		Pump Efficiency		Pump Speed			
		13.6		318.0 L/s 1144.8 m <sup>3</sup> /hr		8.9 m 87.3 kPa		37 kW		10 m		84 %		1465 rpm			
<b>Test Results</b>																	
Time	Manometer Data (Reference Only)		Suct. Press kPa	Disch. Press kPa	Velocity Head m	Hgt 'Z' m	Total H m	Vol Flow		Speed rpm	Torque force		Motor		Pump Power		Pump Eff %
	Δmm	mH <sub>2</sub> O						L/s	m <sup>3</sup> /s		kg	Nm	V	kW	A	%	
1		0.0			0.000	-0.04	0.0	0.00	0.00		0.0				0.0	0.0	#DW/01
2		0.0			0.000	-0.04	0.0	0.00	0.00		0.0				0.0	0.0	#DW/01
3		0.0			0.000	-0.04	0.0	0.00	0.00		0.0				0.0	0.0	#DW/01
4		0.0			0.000	-0.04	0.0	0.00	0.00		0.0				0.0	0.0	#DW/01
5		0.0			0.000	-0.04	0.0	0.00	0.00		0.0				0.0	0.0	#DW/01
6		0.0			0.000	-0.04	0.0	0.00	0.00		0.0				0.0	0.0	#DW/01
7		0.0			0.000	-0.04	0.0	0.00	0.00		0.0				0.0	0.0	#DW/01
8		0.0			0.000	-0.04	0.0	0.00	0.00		0.0				0.0	0.0	#DW/01
9		0.0			0.000	-0.04	0.0	0.00	0.00		0.0				0.0	0.0	#DW/01
10		0.0			0.000	-0.04	0.0	0.00	0.00		0.0				0.0	0.0	#DW/01
11																	

**Test Conditions**

Suction Dia.: 406 mm  
 Discharge Dia.: 406 mm  
 Vel. Head Conversion Coeff: 0.002-00

$Velocity\ Head\ (m) = Flow^2 \times k_d$   
 where  $k_d$  is the Vel. Head Conversion Coeff.

Datum Elevation: 1000 mm  
 Ambient Temperature: 23 °C  
 S.G. of test fluid: 0.9976  
 Local value of g: 9.7948 m/s<sup>2</sup>  
 Barometric Pressure: - mbar

**Measuring Instrumentation**

Head: Gauge No. \_\_\_\_\_  
 Gauge Height 'Z': \_\_\_\_\_  
 Flow: Ultrasonic Flowmeter  
 Power: VSD  
 Speed: Digital Tachometer No.: \_\_\_\_\_

Discharge: 300 mm  
 Suct 'Zs': 340 mm

**Motor details**

Driver: ELECTRIC  
 Power: 75 kW  
 Voltage: 415 V  
 Load: 125%  
 Efficiency: \_\_\_\_\_

Make: Mather & Platt  
 Speed: 1465 r.p.m.  
 F.L.C.: 12.6 A  
 Phase: 3  
 Ser. No.: \_\_\_\_\_

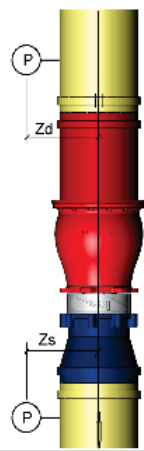


Figure 184 – Blank pump test sheet

### 5.1.5.1 Flow Measurement

Previous research on this pump used a single point pitot tube connected to a mercury manometer to measure the pump flow. The tube is lowered into the pipe directly into the fluid's flow path. To use this device a number of measurements are recorded at various depths of the tube during a set pressure. The results are then added into the formula  $V = \sqrt{2 \cdot g \cdot \Delta h}$  to determine the fluid's velocity. This device was used during a preliminary test but was found to be time consuming and has the possibility to be inaccurate. The latter is due to the vibration of the pitot tube as it is lowered into the pipe resulting in large variations in the manometer readings. Therefore, this device was not used for this research.

An ultrasonic flow meter was then used for measuring the flow of pump tests 1.01 and 1.02. Appendix C gives a full description of the ultrasonic flow meter and how it was used. However, with the test rig refurbishment the new inline magnetic flowmeter was installed and used during the subsequent testing.

### 5.1.5.2 Measurement of Pump Power Input

The pump power input is the power required to drive the pump. This is calculated from measuring the torque and speed of the motor as per Equation 5.

#### 5.1.5.2.1 Torque Measurement

The torque is measured by a gauge used to measure force. An arm is attached to the front of the motor at one end and the force gauge at the other.

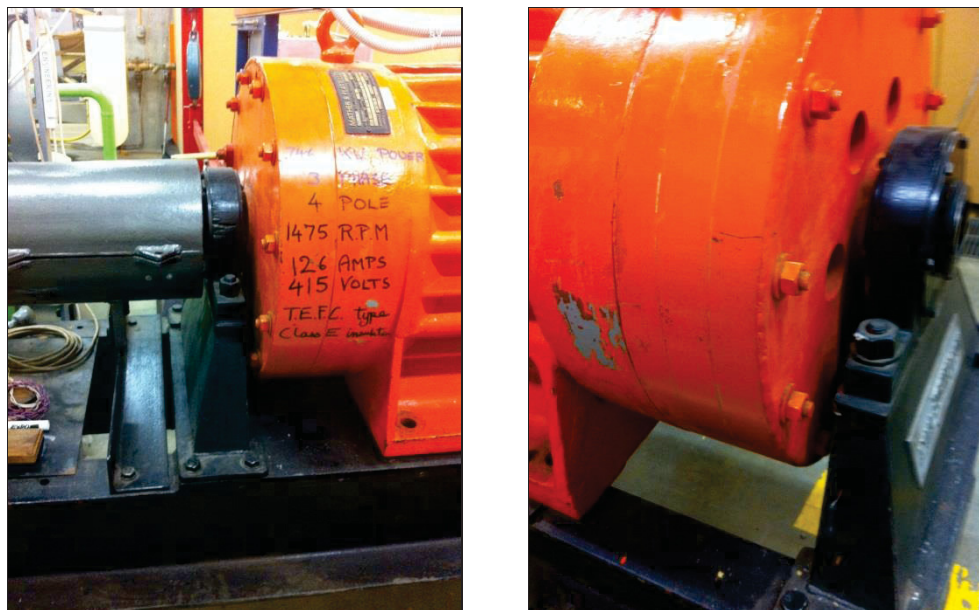


*Figure 185 – Plummer block supports*

The motor is supported at each end by plunger blocks which allow the motor to twist during operation. As the motor twists the arm, so too does the arm. This displacement registers the force on the gauge.

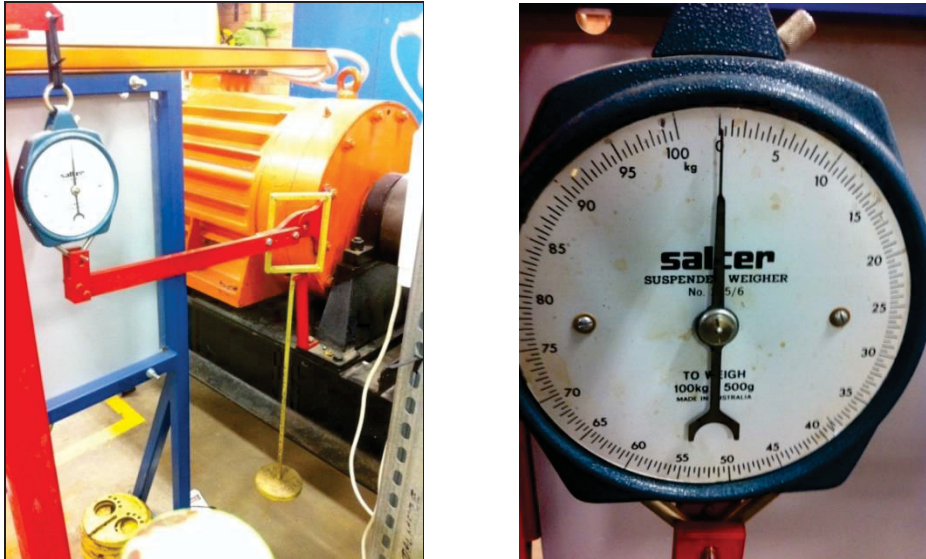


*Figure 186 – Arm and force gauge*

The arm distance is 1 m long, therefore the torque can be calculated by:

$$T = F \times dist$$

*Equation 37*

Due to the motor being run by a VSD, the input power is displayed on the screen. This is used as a check for the power by torque calculation.



*Figure 187 – Test rig VSD*

### 5.1.5.3 Pump Total Head

The pump head for this research is measured by recording the differential pressure between the inlet and the outlet of the pump via pressure gauges. The tapping locations for the measuring equipment are situated at 2 times the pipe diameter away from the suction and discharge of the pump. This is the recommended minimum distance required as per Australian Specification AS2417. By recording readings as close to the pump as possible eliminates any losses from the test loop system (refer to Section 2.1.5.1.1.).

For pump tests 1.01 and 1.02 the pressure at the suction and discharge of the pump is measured using digital pressure gauges. The gauges used are NATA calibrated each year and are on loan from *Weir Minerals Australia*. The pressure difference is converted to metres.

Dimension ‘Z’ is determined by the height difference of the centre of the pressure gauges when measured from the pump centre line. Due to the installed fittings at the time of these two tests the ‘ $\Delta Z$ ’ dimension was 30mm which is taken into account for the final head calculation.

As part of the test rig refurbishment new pressure gauges were installed. The new pressure gauges were installed again at different heights ‘ $\Delta Z$ ’ dimension was 40mm which is taken into account for the final head calculation.

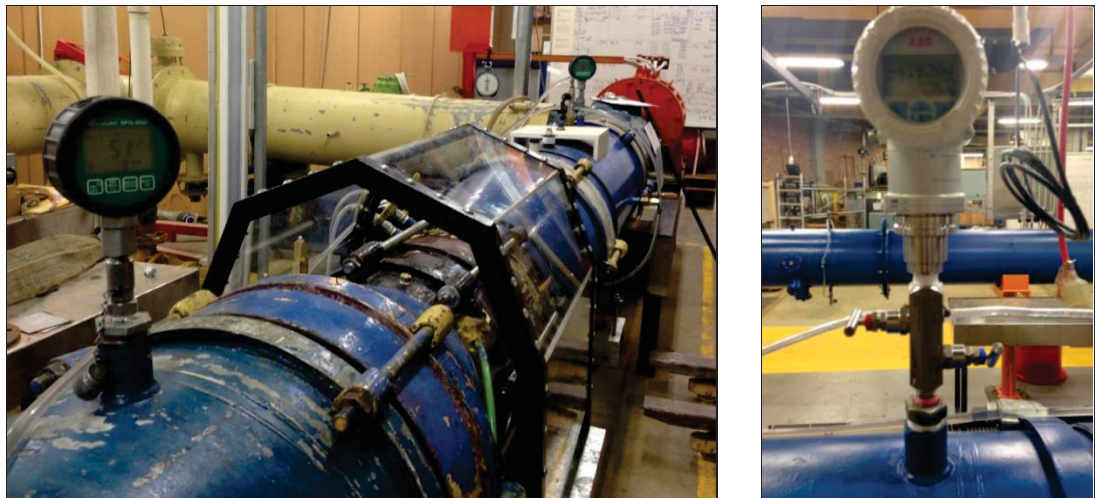


*Figure 188 – Digital pressure gauges*

As a check measurements from a manometer are recorded and compared to the pressure results. The data is measured by using a differential mercury manometer. This device measures the difference in pressure between two positions, in this case the inlet and outlet of the pump. The original manometer used for Test 1.01 and 1.02 is constructed from transparent tube mounted in a ‘U’ shape. All tests completed from 1.03 onwards utilised the new hand held manometer.





Figure 189 – Mercury manometer and replacement hand held manometer

#### 5.1.5.4 Pump Speed

The pump speed was determined from the shaft speed and measured by using a tachometer. The exposed shaft above the thrust bearing was the area measured. See Appendix H. It was found during testing that the speed readings between the VSD and tachometer had an approximate difference of 5 rpm (1%). The tachometer data was used as it is the industry standard.

## 5.2 Test Results

A minimum of two tests were run for each test configuration (see Table 7). The tests are labelled by the test schedule number followed by the number of the test. All recorded test results and test curves are found in Appendix H. For all pump tests the recorded data is speed adjusted to 1465 rpm to determine accurate results against the original pump curve. Therefore, each pump test results table shown in this thesis represents the tests recorded data and the speed adjusted data. The affinity laws, shown below, are used to adjust the flow (Q), head (H), and power (P) to have the correct pump speed of 1465 rpm.

$$\frac{Q_1}{Q_2} = \frac{N_1}{N_2} \quad \text{Therefore} \quad Q_2 = Q_1 \left( \frac{N_2}{N_1} \right) \quad \text{Equation 38}$$

$$\frac{H_1}{H_2} = \frac{N_1^2}{N_2^2} \quad \text{Therefore} \quad H_2 = H_1 \left( \frac{N_2}{N_1} \right)^2 \quad \text{Equation 39}$$

$$\frac{P_1}{P_2} = \frac{N_1^3}{N_2^3} \text{ Therefore } P_2 = P_1 \left( \frac{N_2}{N_1} \right)^3 \quad \text{Equation 40}$$

For all pump tests, the final set of data is recorded when the pump reaches the point of stall.

## 5.2.1 Determine Test Base Results

For this research a base set of results is required to compare all other test configuration results to, for both the five and eight vane impeller pump assemblies.

All of the pump test results for this research were determined using the refurbished test rig.

### 5.2.1.1 Five Vane Impeller Test: Standard Pump

To determine a base set of results for the five vane impeller pump, tests numbers 1.04 or 1.05 were examined to determine which would be the most suitable to be used as the base results.

During the testing there were no major incidents. There was slight cavitation during initial pump running. This was reduced by increasing the suction pressure to above 100kPa. The NPSHR according to the original pump curve is 10m (98.1kPa). Slight leakage was evident between the impeller blade tips and bowl ring<sup>17</sup>. This however is common with every pump test which was run during this research.

As per Table 7 test numbers 1.04 and 1.05 are for a five vane impeller with the standard stator and diffuser fitted. Figure 190 shows a comparison of the pump curve results for these two tests. Both sets of results are almost identical. However, the results for test 1.04 (Table 9) have the closest efficiency readings to the original design curve, therefore making 1.04 the most suitable to be used as the base test results.

The test performance curve (Figure 191) shows that the pump is not performing as per the original design curve with the pump head the same shape as the original, yet shifted left. This results by having the test BEP being at a lower flow rate of 284 L/s but the head at this flow rate is increased to 9.8 m compared to 8.9. The efficiency is the same as the original.

The possible reasons for the difference in the test results, is discussed in Section 5.2.1.2.

---

<sup>17</sup> The pump bowl ring is made of Perspex and by adding a strobe light to the outside of the ring and setting its speed to that of the pump the vanes can be viewed and the cavitation and leakage can be also viewed.



PUMP TEST SHEET (Speed Correction)														
**** PUMP TESTING CARRIED OUT IN ACCORDANCE WITH AS 2417 Part 2 Class C****														
Pump Type Ornel 300AX					Test Number: 1.04					Date: 20-May-15				
Stator Type Std Stator/Diffuser					No. of Impeller Vanes: 5									
DUTY POINT														
VOLUMETRIC FLOW			TOTAL HEAD			PUMP INPUT POWER		PUMP EFFICIENCY		NPSHR		PUMP SPEED		
318.0 L/s			8.90 m			37 kW		84 %		10 m		1465 r.p.m.		
1144.8 m³/hr			87 kPa											

Recorded Data								Speed Corrected Data						
PT.	Flow		Total Head		Pump Power	Pump Eff.	Pump Speed	Flow		Total Head		Pump Power	PUMP EFF. (%)	PUMP SPEED (r.p.m.)
	(L/s)	(m³/hr)	(m)	(kPa)	(kW)	(%)	(r.p.m.)	(L/s)	(m³/hr)	(m)	(kPa)	(kW)		
1	389.50	370.5	2.3	23	19.5	45.7	1460	390.83	1407.0	2.4	23	19.8	45.7	1465
2	388.70	387.5	2.4	23	20.3	44.9	1460	390.03	1404.1	2.4	24	20.5	44.9	1465
3	381.40	367.0	3.0	29	21.0	53.0	1460	382.71	1377.7	3.0	30	21.3	53.0	1465
4	355.60	367.0	5.1	50	25.5	69.1	1460	356.82	1284.5	5.1	50	25.9	69.1	1465
5	315.15	375.5	8.0	78	30.4	80.6	1458	316.66	1140.0	8.0	79	30.9	80.6	1465
6	248.40	376.5	11.1	109	33.8	79.7	1457	249.76	899.2	11.2	110	34.5	79.7	1465
7	207.50	377.5	11.6	113	34.6	67.9	1457	208.64	751.1	11.7	115	35.2	67.9	1465
8														
9														
10														
S.G. 0.9976								Original system curve S.G. 1.0000						

Table 9 – Pump Test Results 1.04

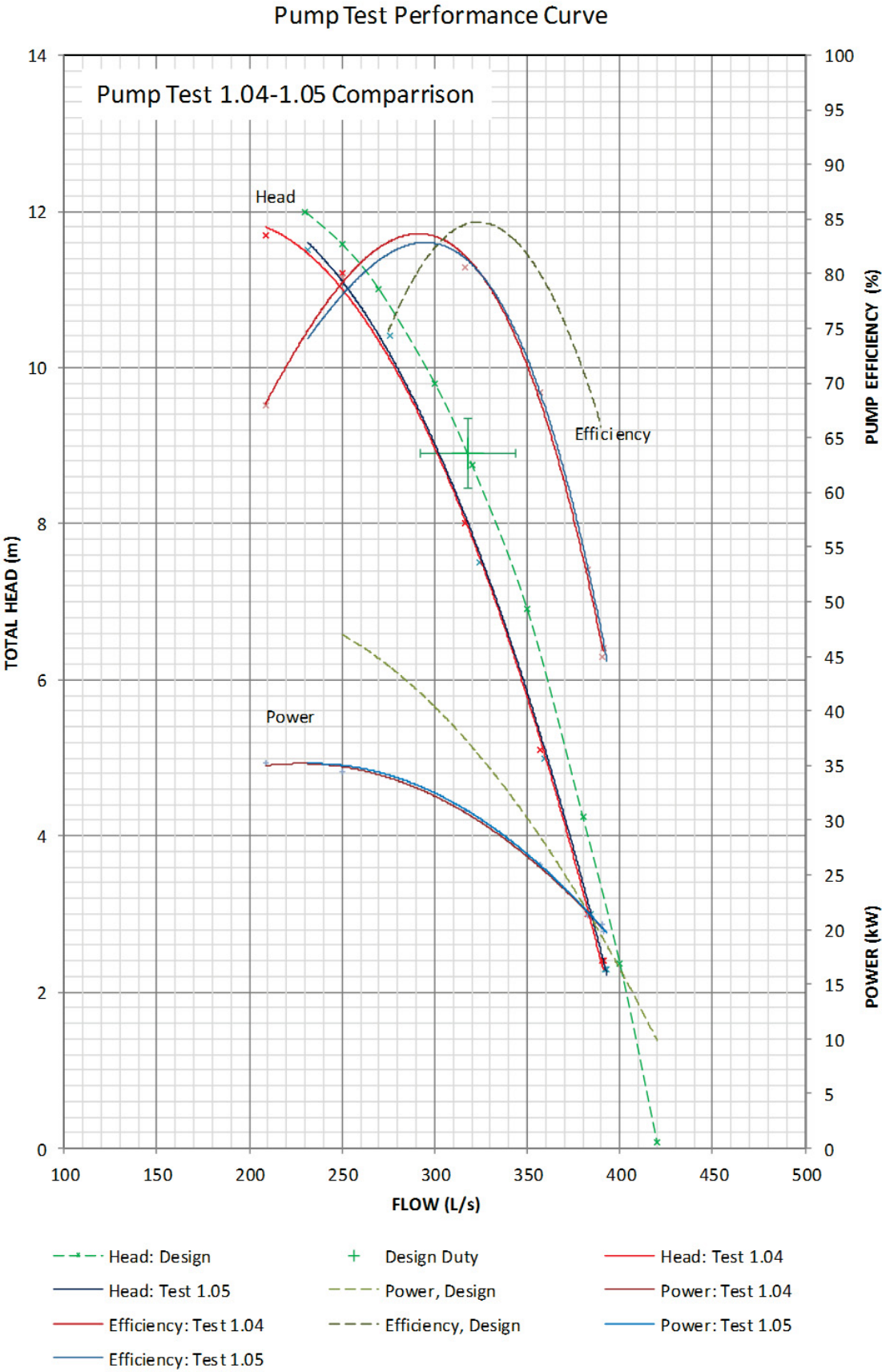


Figure 190 – Comparison of Pump Tests 1.04 and 1.05

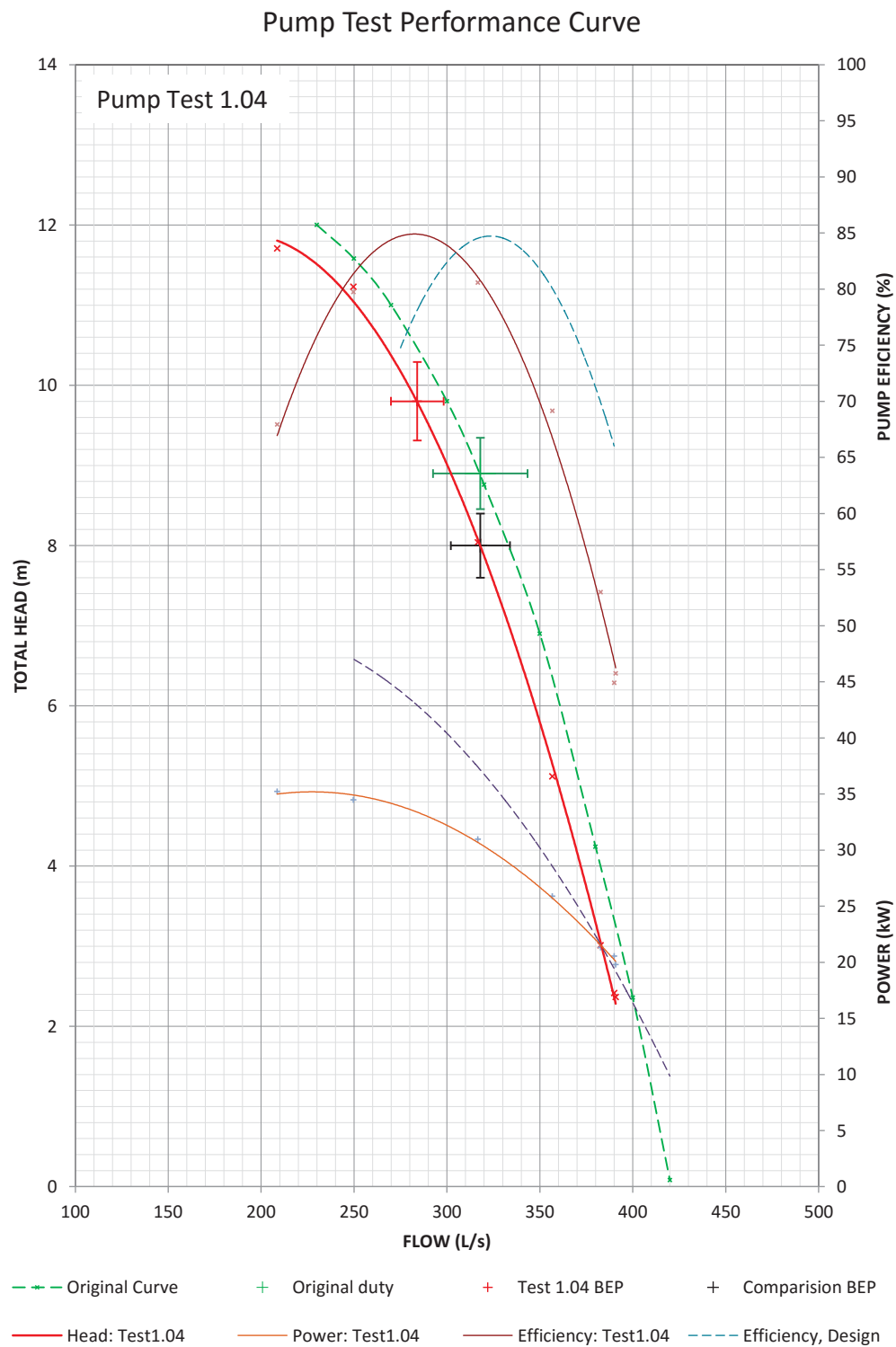


Figure 191 - Test 1.04 Pump Test Performance Curve

### 5.2.1.2 Possible Reasons for Reduced Test Performance Results

Test data recorded for Tests 1.04 and 1.05 and all previous test results, show there is a difference in performance when compared to the original pump curve. This could be due to a number of different reasons such as bowl ring leakage and the impeller vane length as detailed in the following sections.

#### 5.2.1.2.1 Impeller Bowl Ring Leakage

From measurements shown in Section 3.1.2.3, the increased clearance between the impeller and bowl ring is 0.4mm over the design size. When compared to the chart shown in Figure 28, a significant drop in efficiency and head is consistent with the laboratory tests.

#### 5.2.1.2.2 Reduced Impeller Cord Length

As discussed in Section 2.2.8.3 a reduction in the impeller's chord length can also affect the performance of the pump. In Section 3.1.2.2 the new five vane impeller dimensions were determined using the CMM. When compared to the original designed impeller, results show that the vane of the new impeller has a different shape and shorter chord length.

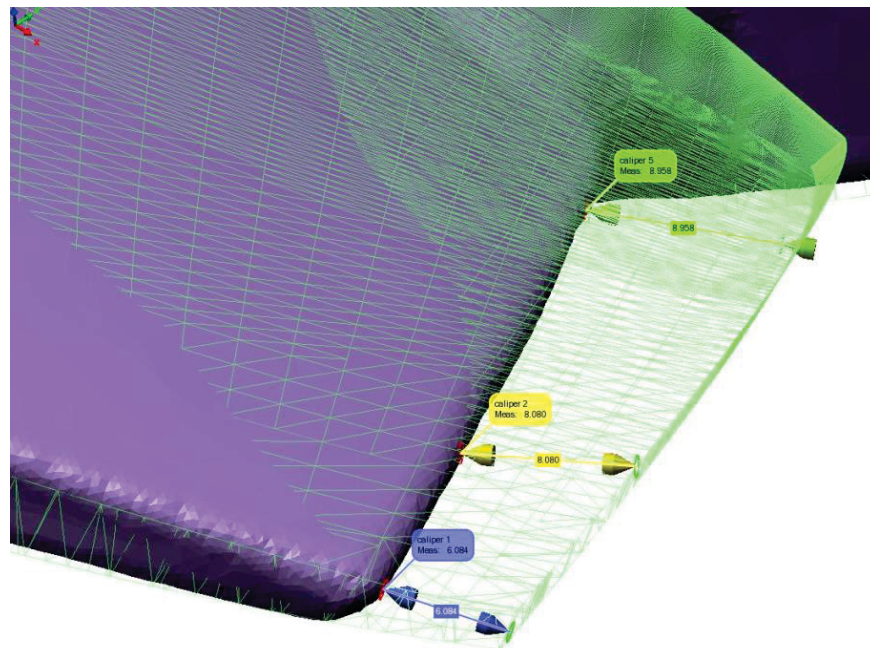
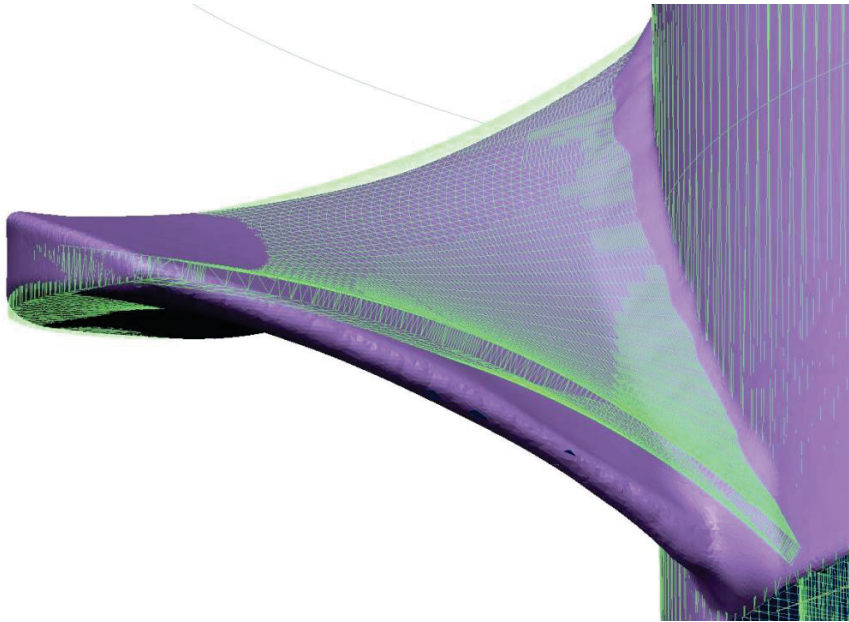


Figure 192 – Difference in impeller chord length



*Figure 193 – Difference in impeller shape*

In Figure 192, the comparison of the two impellers is shown where the new impeller is solid colour and the original impeller is green wireframe. It can be seen that the new impeller's vane outlet tip is up to 9mm shorter than the original. Figure 193 shows the difference in the vane shape of the two impellers.

As with the increased impeller leakage, the reduced chord length will have an effect on the pump's performance.

Therefore, it is concluded that the difference in the performance between the original pump curves and the laboratory test conducted on the standard pump configuration is due to the increased clearances and the reduced chord length and different shape of the impeller's vanes.

### 5.2.1.3 Eight Vane Impeller Test: Standard Pump

When testing the standard pump configuration with the eight vane impeller, the first two tests had a large difference in the efficiency, therefore a third test was required. During the first test 2.01 there was unexpected cavitation with more than the required NPSH of 10m (98.1 kPa). During the final stages of the test, a plastic adaptor holding in an air vent valve failed, therefore the test was abandoned. However enough data had been recorded to plot a curve.

On completion of repairing the damaged fitting with a more suitable replacement, the pump was started, however there was a major failure when the flow straightener tubes had come loose and travelled into the pump suction case, resulting in major repairs being required to the testing rig.

Once the repairs were complete, tests 2.02 and 2.03 for the above pump configuration could be continued. The pump however still had minor cavitation and debris was found on one of the impeller vanes. This was cleared and test 2.03 started.

During test 2.03 the cavitation was still present. When comparing the results between tests 2.02 and 2.03 both the efficiency readings are very low compared to the original curve reaching a high of approximately 74%, which is 13% lower than the original curve of 84%. The pump head again is lower than the original curve, with the power consumption being very close to the original curve.

During testing the motor power reached 76 kW, which is using the motor to its capacity of 75.5 kW rating. This amount of power usage is consistent with the original pump curve shown in Figure 15.

PUMP TEST SHEET (Speed Correction)														
**** PUMP TESTING CARRIED OUT IN ACCORDANCE WITH AS 2417 Part 2 Class C****														
Pump Type Omel 300AX			Test Number: 2.02			Date: 10-Feb-16								
Stator Type Std Stator/Diffuser			No. of Impeller Vanes: 8											
DUTY POINT														
VOLUMETRIC FLOW			TOTAL HEAD			PUMP INPUT POWER		PUMP EFFICIENCY		NPSHR		PUMP SPEED		
565.0 L/s			9.00 m			37 kW		84 %		10 m		1465 r.p.m.		
2034.0 m³/hr			88 kPa											

Recorded Data								Speed Corrected Data						
PT.	Flow		Total Head		Pump Power	Pump Eff.	Pump Speed	Flow		Total Head		Pump Power	Pump Eff.	Pump Speed
	(L/s)	(m³/hr)	(m)	(kPa)	(kW)	(%)	(r.p.m.)	(L/s)	(m³/hr)	(m)	(kPa)	(kW)	(%)	(r.p.m.)
1	599.3	370.5	5.3	52	51.8	60.1	1452	604.7	2176.8	5.4	53	53.4	60.1	1465
2	594.5	387.5	5.3	52	52.6	58.8	1451	600.2	2160.8	5.4	53	54.3	58.8	1465
3	563.9	367.0	7.0	68	55.6	69.0	1451	569.3	2049.4	7.1	70	57.4	69.0	1465
4	524.5	367.0	8.5	83	60.9	71.5	1449	530.2	1908.9	8.7	85	63.0	71.5	1465
5	479.1	375.5	10.3	101	65.4	74.0	1447	485.1	1746.3	10.6	104	68.0	74.0	1465
6	357.7	376.5	11.9	116	64.6	64.2	1448	361.9	1302.8	12.2	119	67.1	64.2	1465
7														
8														
9														
10														

Table 10 - Pump test results 2.02

The poor efficiency results may be due to the poor surface finish of the impeller. But it was decided to use the results from Test number 2.02 which has the highest efficiency of the two set of results. Also as the impeller will be in the same condition during the remaining testing using the eight vane impeller, therefore the results will be conclusive throughout.



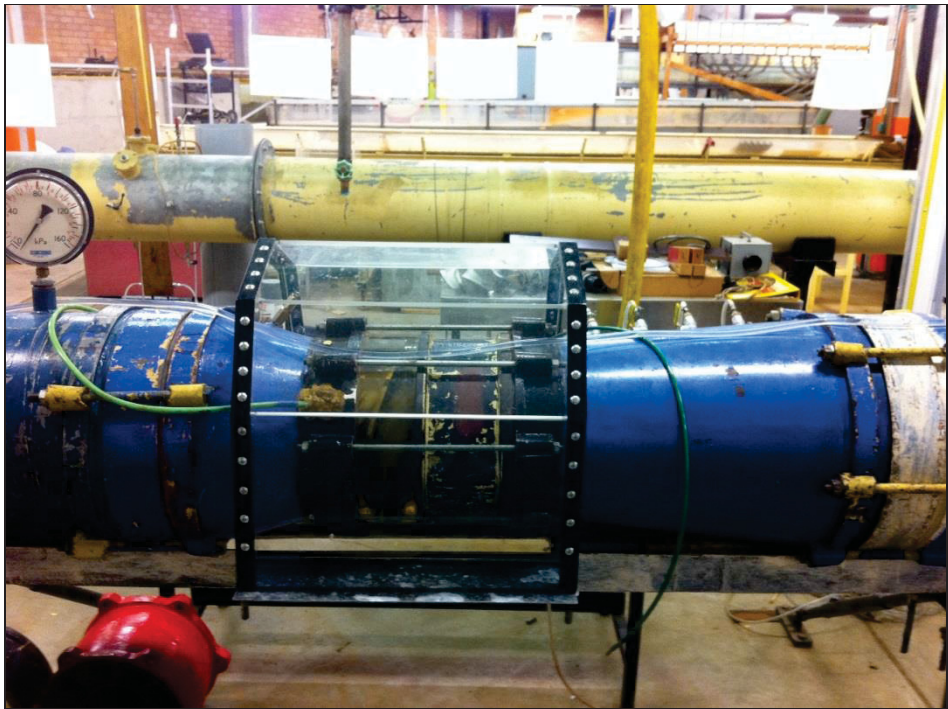


*Figure 194 – Original pump assembly*

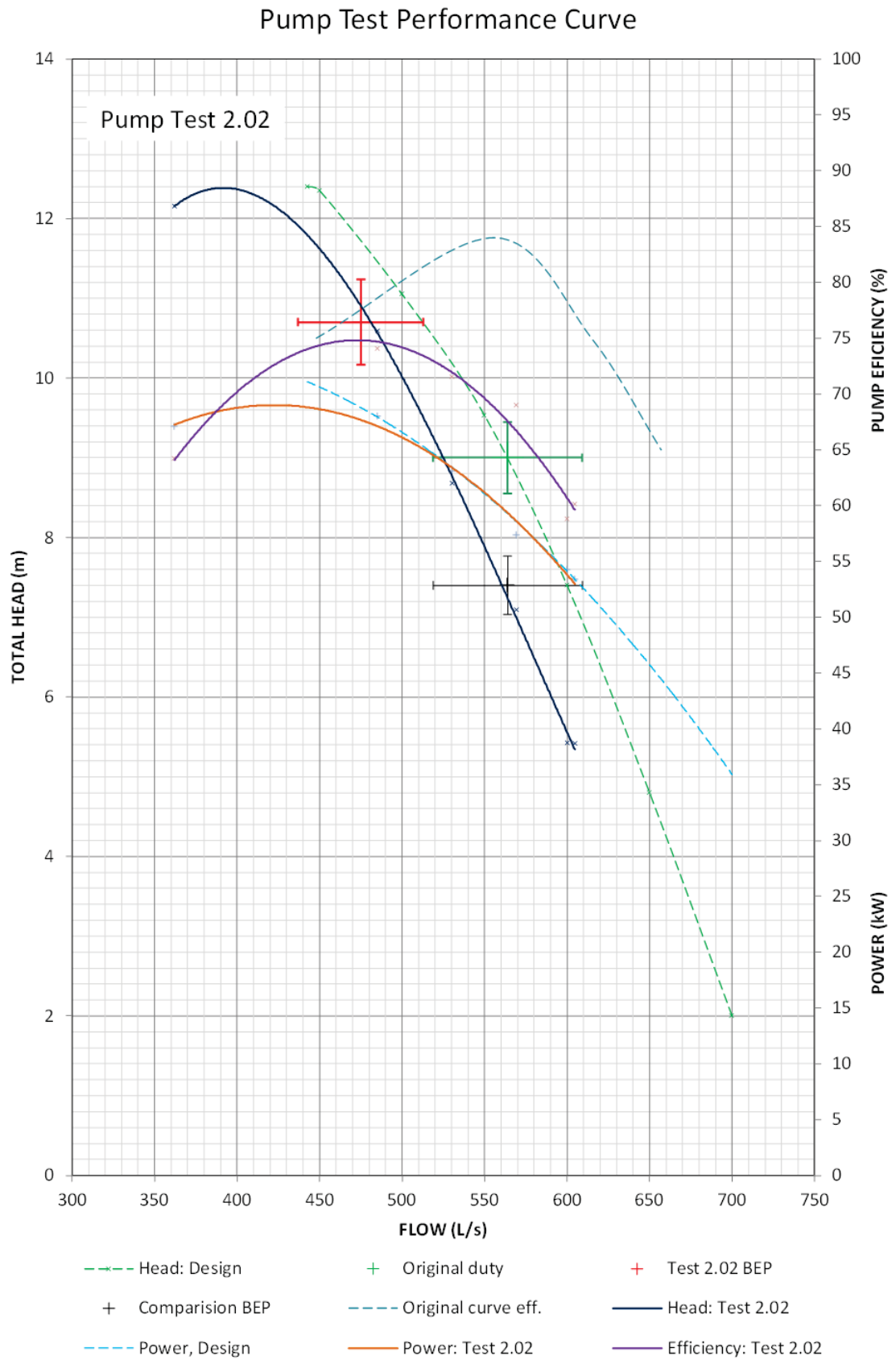


Figure 195 - Test 2.02 pump test performance curve

### 5.2.2 Pump Test with New Diffuser

After the testing the standard pump configurations, the base set of results were complete. The pump assembly was striped and the new diffuser was installed into the test rig.



*Figure 196 – Impeller running gap check, new diffuser installation*

The impeller running gap is set to 5-6mm. The correct way to adjust the running gap is by dropping the impeller to sit on the face of the suction bowl, then to screw the adjusting nut at the top of the thrust block to lift the impeller off the face. However, as this pump is in the horizontal position and not the standard vertical or on a slope, gravity cannot be used to lower the impeller. Therefore, to set the gap a 6mm spacer is placed between the impeller back face and diffuser inlet face. Once the impeller is pushed up against the spacer and tightened into position, the spacer is removed and the suction case can be installed.



*Figure 197 – Installed pump with new diffuser*

### 5.2.2.1 Five Vane Impeller tests

On completion of the two tests 3.01 and 3.02, the H-Q curve results were overlayed and the test results were similar. Test 3.02 produced slightly higher efficiency results, therefore used for analysis.

PUMP TEST SHEET (Speed Correction)														
**** PUMP TESTING CARRIED OUT IN ACCORDANCE WITH AS 2417 Part 2 Class C****														
Pump Type		Ornel 300AX		Test Number:		3.02		Date:		31-Mar-16				
Stator Type		New Diffuser		No. of Impeller Vanes:		5								
DUTY POINT														
VOLUMETRIC FLOW			TOTAL HEAD			PUMP INPUT POWER		PUMP EFFICIENCY		NPSHR		PUMP SPEED		
318.0 L/s			8.90 m			37 kW		84 %		10 m		1465 r.p.m.		
1144.8 m³/hr			87 kPa											
Recorded Data								Speed Corrected Data						
PT.	Flow		Total Head		Pump Power	Pump Eff.	Pump Speed	Flow		Total Head		Pump Power	Pump Eff.	Pump Speed
	(L/s)	(m³/hr)	(m)	(kPa)	(kW)	(%)	(r.p.m.)	(L/s)	(m³/hr)	(m)	(kPa)	(kW)	(%)	(r.p.m.)
1	378.6	370.5	2.3	22	22.2	38.3	1460	379.9	1367.5	2.3	23	22.4	38.3	1465
2	378.3	387.5	2.4	23	22.5	38.8	1460	379.6	1366.7	2.4	23	22.8	38.8	1465
3	371.3	367.0	3.0	29	23.3	46.0	1459	372.8	1342.1	3.0	29	23.6	46.0	1465
4	363.2	367.0	3.7	37	24.8	53.5	1459	364.7	1313.0	3.8	37	25.2	53.5	1465
5	343.5	375.5	5.4	53	27.8	65.2	1458	345.1	1242.5	5.5	54	28.3	65.2	1465
6	311.7	376.5	7.6	74	31.6	73.5	1457	313.4	1128.3	7.7	76	32.2	73.5	1465
7	279.1	377.5	9.5	93	33.8	77.0	1456	280.8	1011.0	9.7	95	34.5	77.0	1465
8														
9														
10														
S.G. 0.9976								Original system curve S.G. 1.0000						

Table 11 - Pump test results 3.02

When comparing the base test results to the new diffuser pump configuration in Figure 198, the head results follow the base curve but are slightly lower. However, the efficiency is 10% lower for the new diffuser with a BEP at 77%. The BEP for test 3.02 is 8.9m @ 295 L/s which is a higher flow but a lower head than the base test results.

The new diffuser design reaches the stall point at a much higher flow therefore reducing the pump's operating range. This was the same in both sets of Tests 3.01 and 3.02.

Overall, the performance of the new diffuser does not improve on the original pump design.

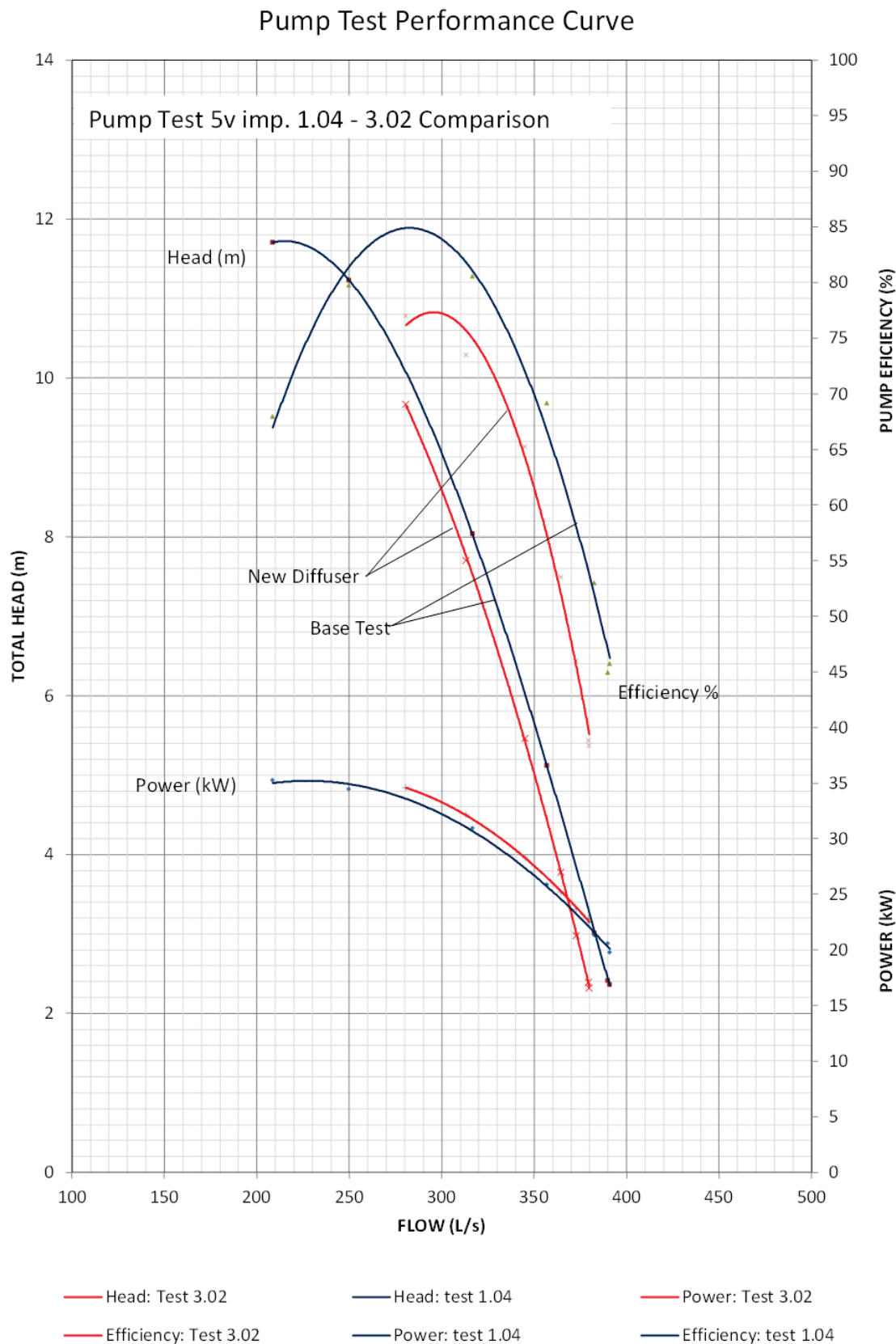


Figure 198 – Five vane impeller base test to new diffuser comparison

### 5.2.2.2 Eight Vane Impeller Tests

The laboratory set-up is the same as with the test using the five vane impeller. During the first pump test 4.01, the running gap was not set and the suction case spacer was not reinstalled. Therefore, this test was inconclusive. After the rebuild, there were high vibrations and again there were unsuitable results.<sup>18</sup>

After all the pump assembly issues were resolved, test number 4.03 and 4.04 had sufficient results. The best result of the two tests was number 4.03 with higher efficiency than 4.04. When compared to the base test results shown in Figure 200, the pump head and power are less, however the efficiency is slightly higher. Also the BEP of test 4.03 is slightly reduced when compared to the base test.

PUMP TEST SHEET (Speed Correction)														
**** PUMP TESTING CARRIED OUT IN ACCORDANCE WITH AS 2417 Part 2 Class C****														
Pump Type		Ornel 300AX		Test Number:		4.03		Date:		11-May-16				
Stator Type		New Diffuser		No.of Impeller Vanes:		8								
DUTY POINT														
VOLUMETRIC FLOW			TOTAL HEAD			PUMP INPUT POWER		PUMP EFFICIENCY		NPSHR		PUMP SPEED		
564.0 L/s			8.90 m			37 kW		84 %		10 m		1465 r.p.m.		
1144.8 m³/hr			87 kPa											

Recorded Data							Speed Corrected Data							
PT.	Flow		Total Head		Pump Power	Pump Eff.	Pump Speed	Flow		Total Head		Pump Power	Pump Eff.	Pump Speed
	(L/s)	(m³/hr)	(m)	(kPa)	(kW)	(%)	(r.p.m.)	(L/s)	(m³/hr)	(m)	(kPa)	(kW)	(%)	(r.p.m.)
1	570.3	2053.2	5.0	49	54.1	51.9	1454	574.6	2068.7	5.1	50	55.5	51.9	1465
2	567.8	2043.9	5.2	51	54.5	52.7	1454	572.0	2059.4	5.3	52	55.9	52.7	1465
3	541.0	1947.6	6.7	66	57.1	62.2	1454	545.1	1962.3	6.8	67	58.5	62.2	1465
4	520.0	1872.0	8.2	81	60.1	69.7	1453	524.3	1887.5	8.4	82	61.8	69.7	1465
5	470.0	1692.0	10.2	100	63.9	73.3	1451	474.5	1708.3	10.4	102	65.9	73.3	1465
6	400.9	1443.2	11.7	115	64.6	71.1	1451	404.8	1457.2	12.0	117	66.7	71.1	1465
7	356.4	1283.0	12.2	120	63.1	67.5	1452	359.6	1294.5	12.5	122	65.0	67.5	1465
8														
9														
10														

Figure 199 - Pump test results 4.03

<sup>18</sup> The pump build issues and repairs are discussed in Appendix B - Section B.5.



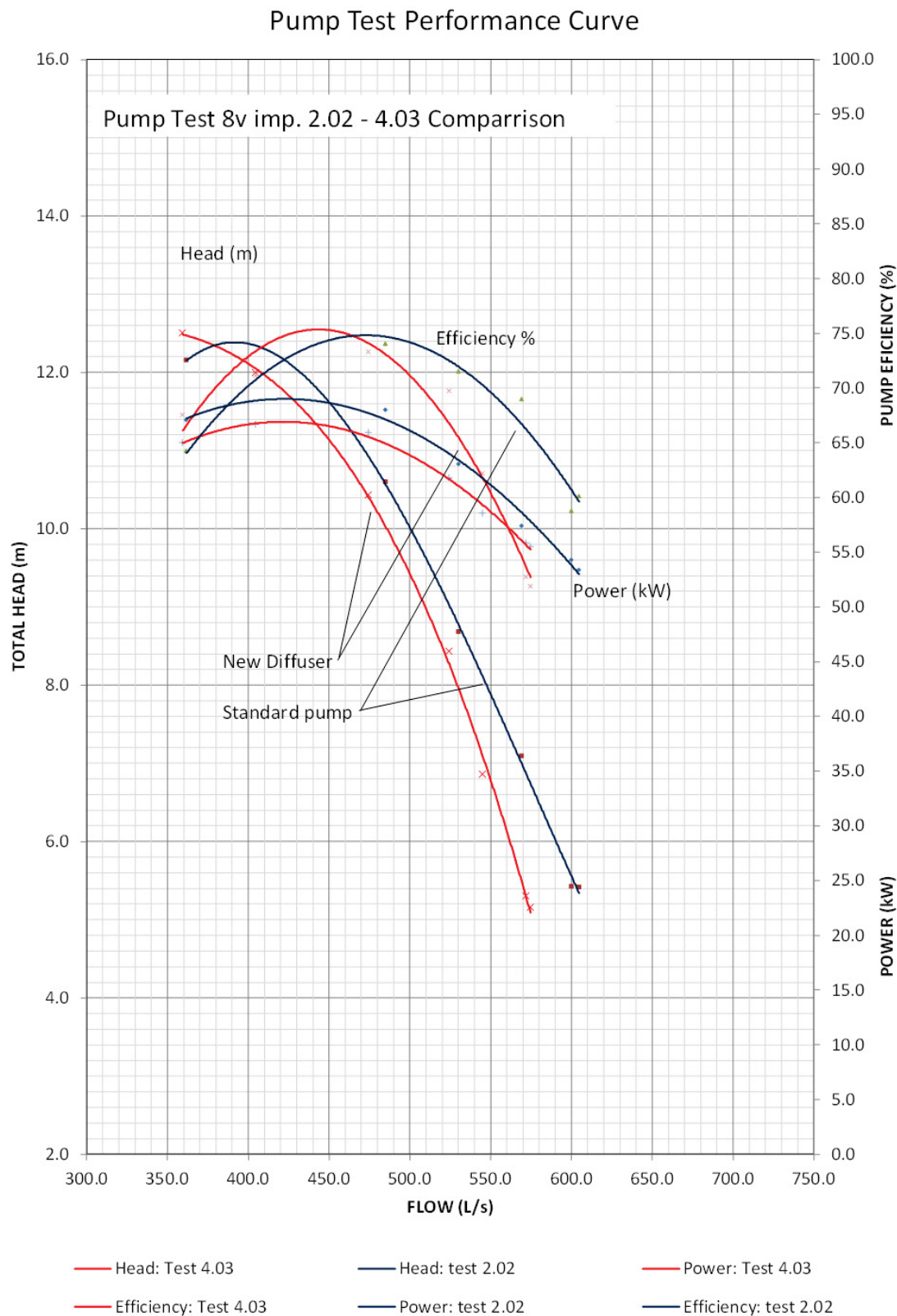
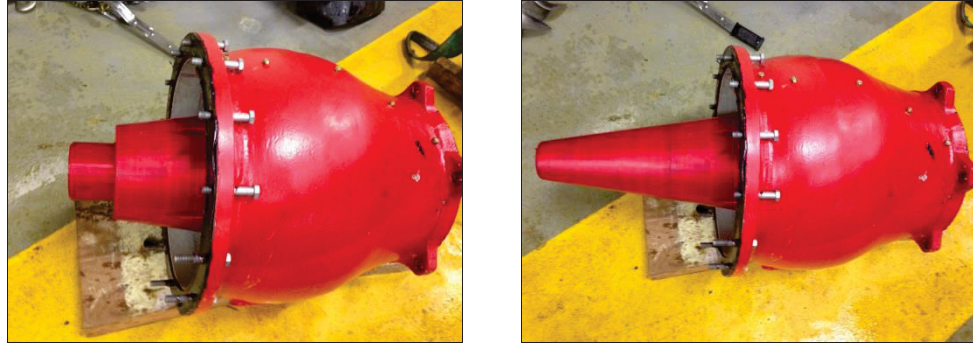


Figure 200 - Eight vane impeller base test to new diffuser comparison

### 5.2.3 Pump Test with Tail piece Addition

The final of the laboratory tests have been run with the addition of the 3D printed tail piece to the new diffuser. As mentioned in previous sections the tail piece is fastened to the new diffuser with socket head cap screws and located with a spigot fit on the outer face of the bearing hub.



*Figure 201 – Preassembly of tail piece, in two steps*



*Figure 202 – Tail piece assembly*

Pre-assembly checks and measurements ensured that the final assembly had no interferences with existing pump components.

The impeller setting running gap for both of the pump configurations, (five and eight vane impeller configuration) were checked prior to reassembly of the suction case to the pump. In each case the setting was the required 5–6 mm.

#### 5.2.3.1 Five Vane Impeller Tests

The two pump tests were run as per the standard requirements and compared with the original pump base test and new diffuser pump tests. The comparison curves between the three final different pump configurations test results can be seen in Figure 205.

When comparing pump test 5.01 and 5.02, test number 5.02 has the better of the results of the two. See Appendix D for the comparison curve.

During the pump testing, it was noticed that the pump ran considerably smoother than previous tests with the new diffuser alone. The pump also ran to a lower flow, (hence higher head) before reaching the pumps stall point when compared to the previous new diffuser pump configuration.

However, the efficiency is slightly lower than the new diffuser but the BEP of 9.3m @ 280 l/s has returned to be more in line with the BEP of the original pump test base results, with an 11% efficiency drop from the base test results.



Figure 203 – Impeller running gap check for five vane impeller

PUMP TEST SHEET (Speed Correction)														
**** PUMP TESTING CARRIED OUT IN ACCORDANCE WITH AS 2417 Part 2 Class C****														
Pump Type Ornel 300AX			Test Number: 5.02			Date: 18-May-16								
Stator Type New Diffuser/back piece			No. of Impeller Vanes: 5											
DUTY POINT														
VOLUMETRIC FLOW			TOTAL HEAD			PUMP INPUT POWER		PUMP EFFICIENCY		NPSHR		PUMP SPEED		
318.0 L/s			8.90 m			37 kW		84 %		10 m		1465 r.p.m.		
1144.8 m³/hr			87 kPa											

Recorded Data								Speed Corrected Data						
PT.	Flow		Total Head		Pump Power	Pump Eff.	Pump Speed	Flow		Total Head		Pump Power	Pump Eff.	Pump Speed
	(L/s)	(m³/hr)	(m)	(kPa)	(kW)	(%)	(r.p.m.)	(L/s)	(m³/hr)	(m)	(kPa)	(kW)	(%)	(r.p.m.)
1	379.9	370.5	2.4	23	21.4	40.8	1462	380.6	1370.3	2.4	23	21.6	40.8	1465
2	380.0	387.5	2.5	24	21.4	42.6	1462	380.7	1370.7	2.5	24	21.6	42.6	1465
3	371.5	367.0	3.2	31	23.3	49.5	1461	372.6	1341.2	3.2	31	23.5	49.5	1465
4	361.5	367.0	3.9	38	24.8	55.4	1461	362.5	1305.0	3.9	38	25.1	55.4	1465
5	339.0	375.5	5.5	54	27.8	65.9	1460	340.2	1224.6	5.6	55	28.2	65.9	1465
6	304.2	376.5	8.0	78	31.9	74.3	1459	305.5	1099.7	8.0	79	32.4	74.3	1465
7	274.4	377.5	9.5	93	34.2	74.6	1459	275.5	991.9	9.6	94	34.7	74.6	1465
8	243.5	378.5	10.3	101	34.9	70.4	1459	244.5	880.0	10.4	102	35.5	70.4	1465
9	233.2	379.5	11.2	109	34.9	72.8	1459	234.2	843.0	11.2	110	35.5	72.8	1465
10														
S.G. 0.9976								Original system curve S.G. 1.0000						

Table 12 - Pump test results 5.02

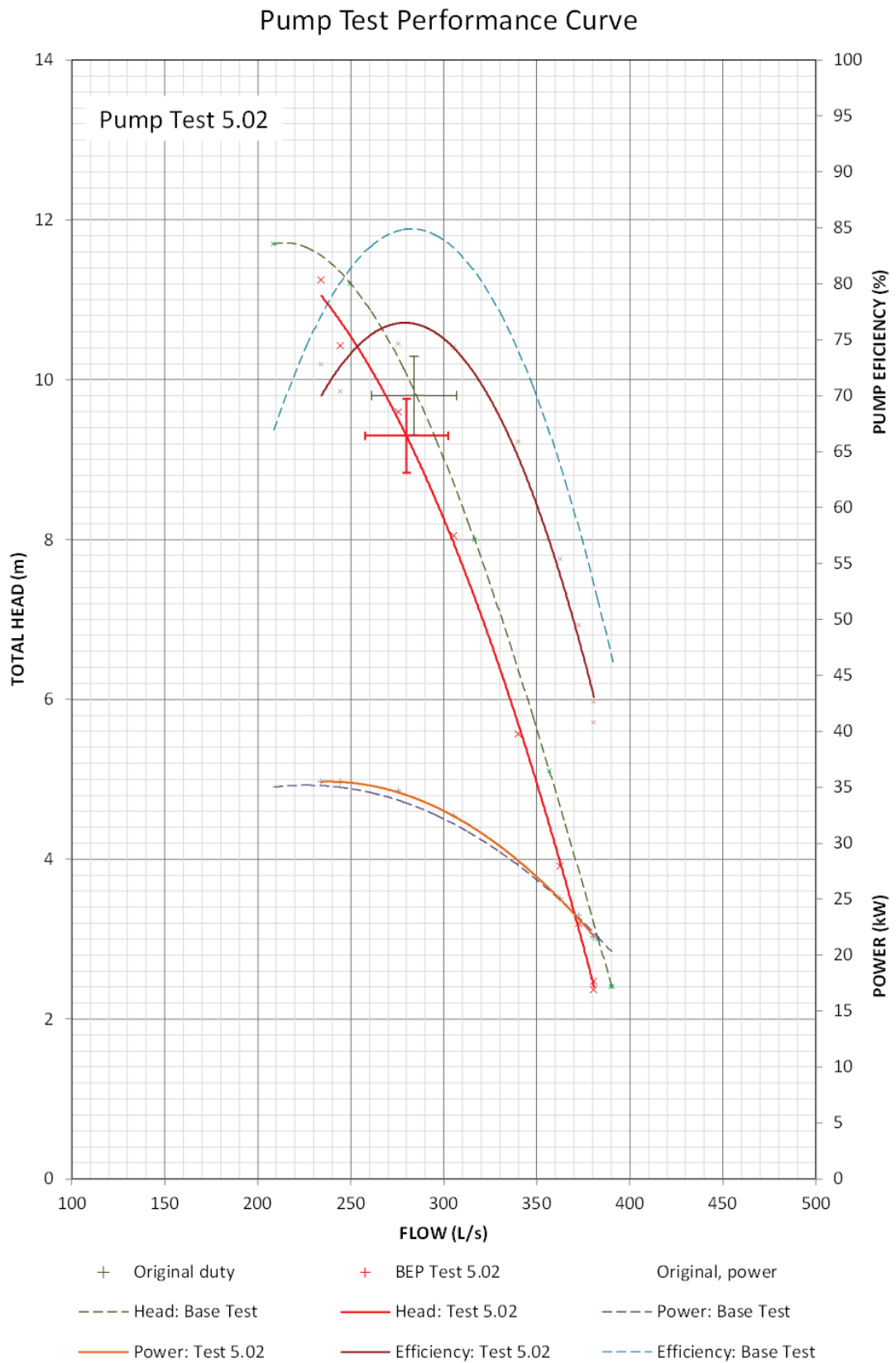


Figure 204 - Test 5.02 performance curve

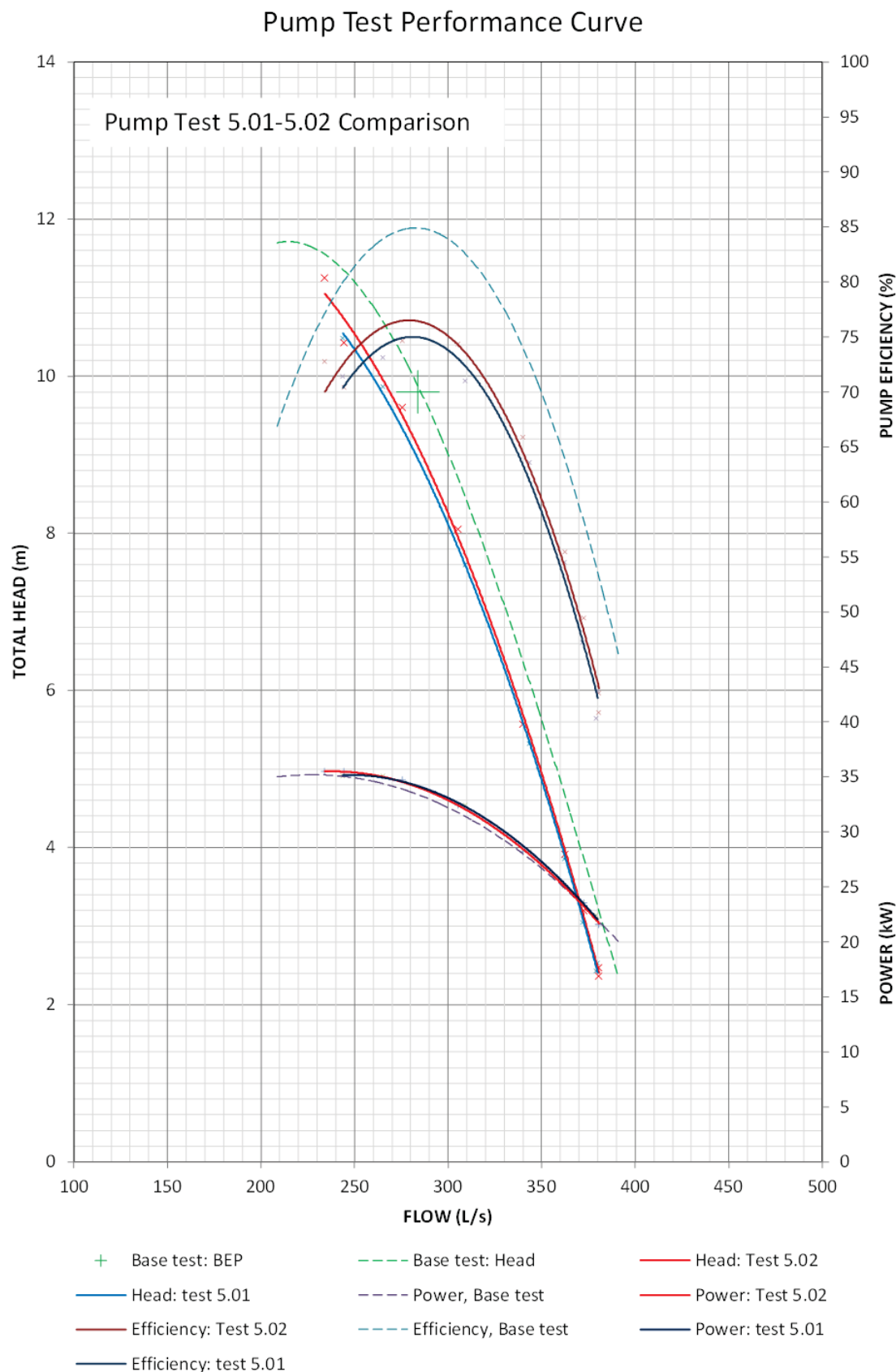


Figure 205 - Five vane impeller, base test to new diffuser and tail piece comparison

### 5.2.3.2 Eight Vane Impeller Tests

The final laboratory pump tests were run with the eight vane impeller and the tail piece added to the new diffuser. Three tests were run with the last of the tests being at a reduced speed so the motor would have reduced load. When speed corrected, the results are similar to the full load tests. The results of all three tests are found in Appendix D with the best of all three being test number 6.01.

PUMP TEST SHEET (Speed Correction)														
**** PUMP TESTING CARRIED OUT IN ACCORDANCE WITH AS 2417 Part 2 Class C****														
Pump Type		Ornel 300AX		Test Number:		6.01		Date:		23-May-16				
Stator Type		New Diffuser/Back piece		No.of Impeller Vanes:		8								
DUTY POINT														
VOLUMETRIC FLOW			TOTAL HEAD			PUMP INPUT POWER		PUMP EFFICIENCY		NPSHR		PUMP SPEED		
564.0 L/s			8.97 m			37 kW		84 %		10 m		1465 r.p.m.		
2030.4 m³/hr			88 kPa											

Recorded Data								Speed Corrected Data						
PT.	Flow		Total Head		Pump Power	Pump Eff.	Pump Speed	Flow		Total Head		Pump Power	Pump Eff.	Pump Speed
	(L/s)	(m³/hr)	(m)	(kPa)	(kW)	(%)	(r.p.m.)	(L/s)	(m³/hr)	(m)	(kPa)	(kW)	(%)	(r.p.m.)
1	582.7	2097.6	5.3	52	53.3	56.4	1454	587.1	2113.5	5.4	53	54.7	56.4	1465
2	580.7	2090.5	5.4	53	54.1	56.5	1454	585.1	2106.3	5.5	54	55.5	56.5	1465
3	550.1	1980.5	6.9	68	57.1	65.1	1454	554.3	1995.5	7.0	69	58.5	65.1	1465
4	522.8	1882.1	8.6	84	60.1	72.7	1452	527.5	1898.9	8.7	86	61.9	72.7	1465
5	487.4	1754.6	10.1	99	63.1	76.2	1451	492.1	1771.6	10.3	101	65.1	76.2	1465
6	436.3	1570.7	11.5	113	65.4	75.2	1451	440.5	1585.8	11.7	115	67.4	75.2	1465
7	400.3	1441.1	12.0	118	64.6	72.9	1451	404.2	1455.0	12.3	120	66.7	72.9	1465
8	364.3	1311.5	12.4	122	63.9	69.4	1451	367.8	1324.1	12.7	125	65.9	69.4	1465
9														
10														

Table 13 - Pump test results 6.01

When comparing the best results from all three different eight vane test configurations, it was found that the addition of the tail piece to the new diffuser increased the pump head to be similar to the base pump tests. However, as with the testing using the five vane impeller the pump ran smoother than previous tests and the pump not only reached stall at a higher head than the new diffuser but also the original pump configuration.

The efficiency was also improved to have an increase of approximately 3.9% higher than the base tests using the original pump.

Overall, it can be concluded that the tail piece addition to the new diffuser, when using the eight vane impeller increases the efficiency of the pump and also can increase the operation range for the pump as previously discussed in Section 4.4.2.4.



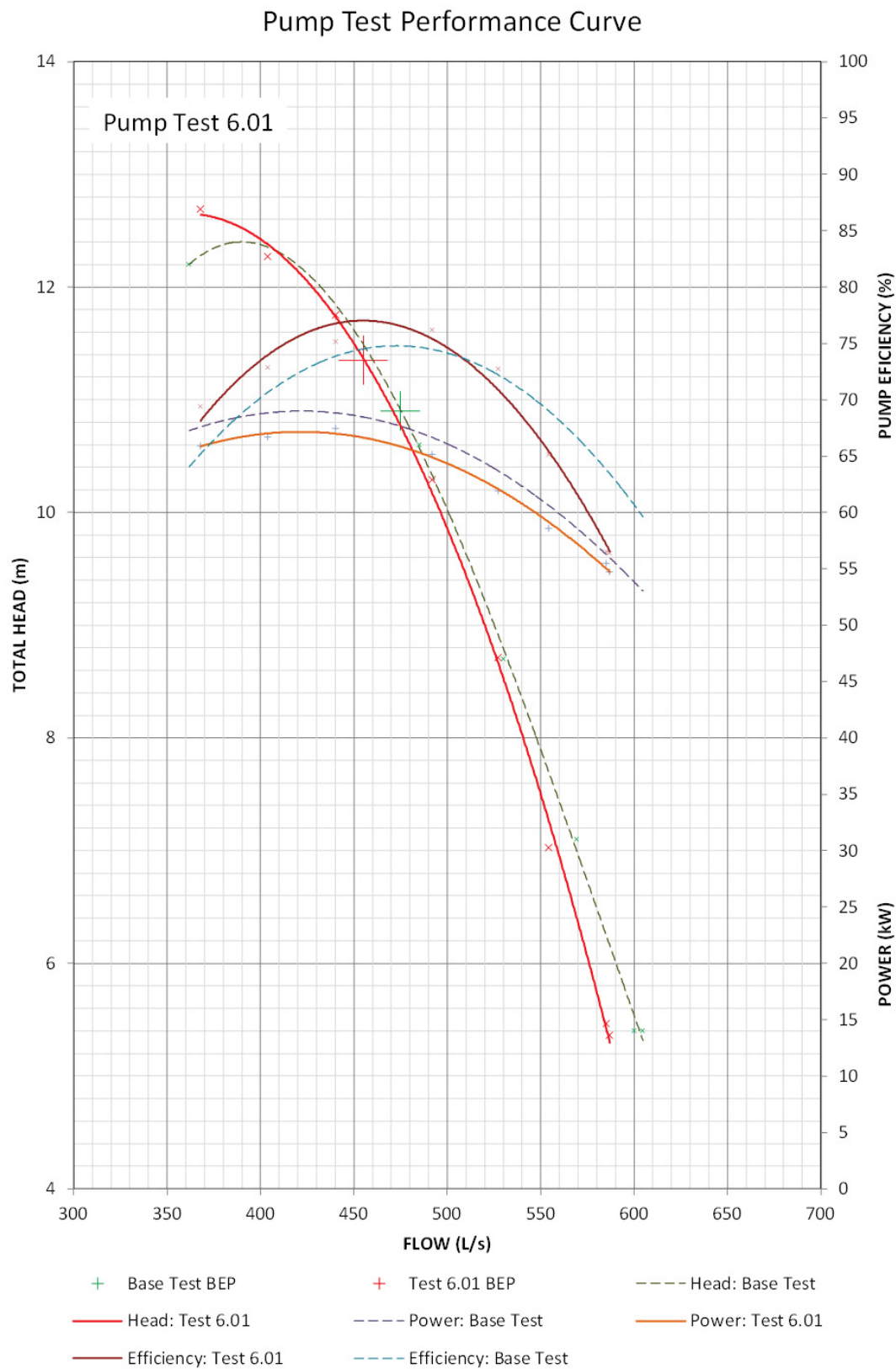


Figure 206 - Test 6.01 performance curve

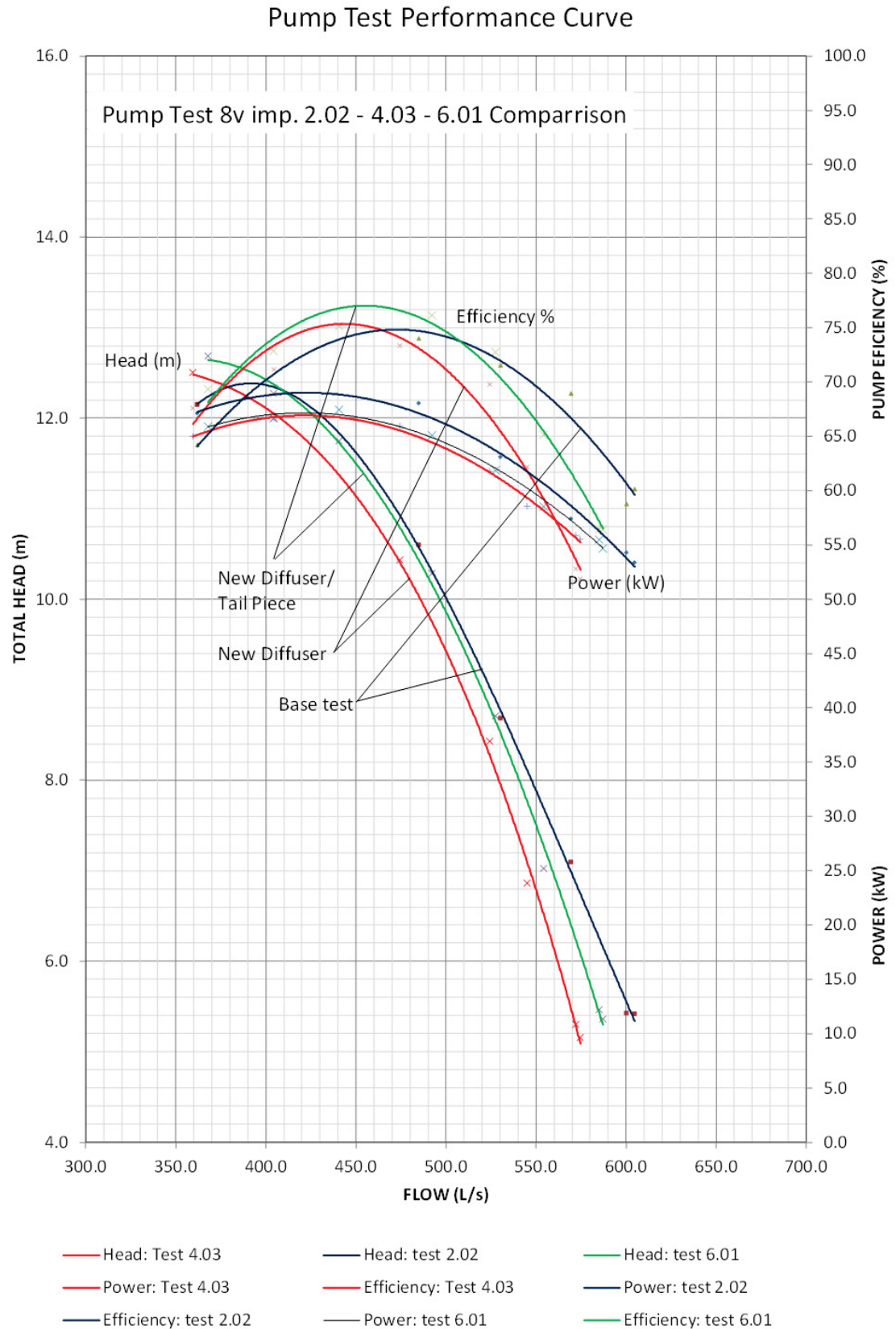


Figure 207 - Eight vane impeller, base test to new diffuser and tail piece comparison

## 5.3 Chapter Conclusion

It was found during laboratory testing that the base test results for both the five and eight vane impeller pump configurations have a lower capacity when compared to the OEM performance curves. This possible drop in capacity was discovered in previous chapters which could be due to vane tip leakage, rough component surface finishes and other mechanical losses within the impeller, with the reduction of the impeller vane chord length being the major factor in this capacity reduction<sup>19</sup>. Therefore, the pump testing proved the theory to be correct.

The laboratory test results for the different five vane impeller pump configurations are found in Table 14. The table compares the test results for the new diffuser plus the tail piece addition to the base test results. The results show that when using a five vane impeller the new diffuser underperformed compared to the base results with a drop in head of 9.2% but an increase in flow of 3.8%. Also with the tail piece addition compared to the new diffuser, the efficiency and pump head were slightly reduced, however the stall line of the pump was improved when compared to the new diffuser but reduced when compared to the base test.

Test Number	Results					
	Head		Flow		Efficiency	
	H (m)	$\Delta H$	Q (L/s)	$\Delta Q$	$\eta$	$\Delta \eta$
Base (1.04)	9.8	-	284	-	85 %	-
New Diff. (3.02)	8.9	- 9.2 %	295	+ 3.8 %	77 %	- 9.5 %
Tail Piece (5.02)	9.3	- 5.2 %	280	- 1.5 %	74.6 %	- 12 %

*Table 14 –Five vane impeller pump test comparison to base test*

Testing using the eight vane impeller gave promising results. The laboratory test results are found in Table 15. The table compares the test results for the new diffuser plus the tail piece addition to the base test results. When comparing the base test to the test using the new diffuser, the efficiency slightly increased but there is a reduction in the pump head. But with the tail piece addition to the new diffuser, the pump head is relatively the same as the base test with a clear increase of efficiency by approximately 3.9%. The pump stall line remains the same.

<sup>19</sup> Trimming the impeller vane tips in all centrifugal pumps is a way of changing a pump's performance capacity.

Test Number	Results					
	Head		Flow		Efficiency	
	H (m)	$\Delta H$	Q (L/s)	$\Delta Q$	$\eta$	$\Delta \eta$
Base (2.02)	10.7	-	475	-	74 %	-
New Diff. (4.03)	11.3	+ 5.4 %	564	+15.8 %	75 %	+ 1.4 %
Tail Piece (6.01)	11.35	+ 5.8 %	455	- 4.3 %	77 %	+ 3.9 %

*Table 15 - Eight vane impeller pump test comparison to base test*

In conclusion, when comparing the pump performance from the two tables of experimental testing results, it is proven that the new diffuser, even with the tail piece modification installed, does not match the five vane impeller nor improves the pump's performance when it is compared to the standard designed pump with separate stator and diffuser configuration. Even though there is an improvement in the pumps operating limit to the new diffuser when the tail piece is added, the original designed pump is proven to be the best performer for medium flow impeller applications.

However, as theoretically predicted in previous chapters, the new diffuser does match an eight vane impeller. The combination of new diffuser and the tail piece greatly improves the efficiency performance of the pump by 3.9%. The efficiency increase would suggest that the new diffuser is designed for high flow impeller applications.

# 6 Summary, Findings and Future Work

## 6.1 Research Summary

The main purpose of this research was to determine the performance of a new diffuser design for an Axial Flow Pump. To do this the existing test rig located in the hydraulics laboratory, at the *University of Technology*, Sydney was used to test a number of different pump configurations using a single stage impeller Axial Flow Pump. Computational fluid dynamics (CFD) along with pump design theory was also used to predict the function of the design, flow patterns and pressures generated within the different pump configurations. The CFD parameters were set to the best efficiency point (BEP) found on the OEM pump performance curves.

To analyse the performance of the new diffuser, the original pump assembly was laboratory tested to establish base results to compare the different pump configurations. In the beginning it was difficult to record the required data for the first laboratory tests performed. Therefore, these tests were deemed insufficient to be used as the base set of results. This was due to the outdated measuring equipment installed, especially the flow measurement pitot tube which was found to be inaccurate due to high vibrations causing high variances in flow determination. To resolve this, the entire test rig was refurbished with new calibrated measurement equipment including magnetic flow meter, digital pressure gauges, data control panel and new pump components as well as blasting and epoxy coating the pipe internals. This ensured the test rig conformed to AS2417 part 2 class ‘C’ an industry standard for pump testing.

Before any analysis could be started, the existing pump components were required to be cleaned, in some cases repairs were required and then dimensionally measured. To determine the dimensions of the pump components, a coordinate measurement machine (CMM) was used. The CMM laser accurately scanned the surfaces of the manufactured impellers and 3D models were created from the scan. The created 3D models of the laboratory components were overlayed onto a 3D model developed from the original design drawings. This was used to determine if the components matched the design. The CMM was also used to measure the new diffuser, as no dimensional information for this component existed. This information was used to compare the found dimensions to design theory to establish an understanding of how the components would perform and if changes would be required.

CFD analysis was performed on the new diffuser design using both the five and eight vane impellers. A final tail piece design was 3D modelled and then 3D printed in two parts from an

ABS material. The printed component was installed into the pump assembly for testing by using the existing fastener locations and spigot location on the bearing support area.

## 6.2 Research Findings

The five vane test impeller was found to be inconsistent with the original impeller design which proved to be the reason for the reduced performance of the pump, when compared to the OEM test curve. However, as the same impeller is used in each laboratory test configuration, the recorded test data was used as the base set of results.

When the refurbished test rig was reinstalled, the pump was retested with conclusive results. However, the pump did not perform as well as the original equipment's manufacturers (OEM) test curve. From the CMM dimensional checks, it was found that the manufactured impeller used for laboratory testing had a shorter vane length than the original impeller design. The dimensional checks also found worn clearances between the impeller vane tips and bowl ring bore. The shorter vane length when combined with the increased vane tip clearance creates increased losses in the pump resulting in a reduction of performance.

The dimensional results from the new diffuser were compared to diffuser design theory and showed that the new diffuser inlet vane tip angle is matched to the eight vane impeller but not suitable for the five or six vane impellers. To further prove the design theory both CFD analysis and experimental pump testing for the five and eight vane impellers were compiled for the different pump configurations<sup>20</sup>.

The CFD results showed there is a large amount of secondary flow past the back face of the diffuser where there is a sharp 90° angle. This is due to the sudden enlargement of the cross sectional flow area from the outlet of the vanes trailing edge to the discharge area. This sudden enlargement creates a low pressure region behind the back face which introduces secondary flow, hence a turbulent area, as the higher pressure flow path passes in an axial direction. The CFD analysis shows this turbulent area is elongated when using the eight vane impeller due to the higher velocity and pressure from the higher pump flow.

To reduce the low pressure region, a tail piece was designed to be added to the outlet of the diffuser. This component will remove the sudden enlargement and introduce a gradual cross section enlargement over a longer distance. CFD results indicated that this gradual enlargement introduced a larger percentage of higher pressure within the flow passage cross sections. This introduces a more steady velocity flow path with the reduction of the lower pressure area, hence

---

<sup>20</sup> Time did not allow for the six vane impeller to be tested, as well as the impeller collet could not be located in the laboratory.



less secondary flow and pump losses. A number of CFD models were analysed with a number of different design parameters for the tail piece. A cone shaped component with an incline angle of  $20^\circ$  was determined to be the most suitable option, as it was predicted to reduce the turbulence to a minimum. The tail piece design parameters were limited, as no physical modifications could be made to the diffuser and the line shaft coupling located downstream of the back face restricted the length available, therefore the tail piece angle was constricted to 20% to prevent interference with the coupling.

From the laboratory pump testing the theoretical assumptions for the five vane impeller performance were proven by:

- The reduced standard pump performance when compared to the OEM performance curve, due to the increased bowling clearances and the reduction in the impeller's vane length.
- The poor performance of the new diffuser installation when the tests results are compared to the base pump tests. The mismatch of the impeller's absolute velocity angle to the diffuser's inlet vane tip angle, the sudden enlargement and a combination of other mechanical losses contribute to the poor performance.
- The addition of the tail piece to the new diffuser, only slightly improves the performance when compared to the new diffuser alone.

Laboratory testing with the eight vane impeller installation proved the theoretical assumptions by:

- The reduced standard pump performance when compared to the OEM performance curve, due to the increased bowling clearances and poor surface finish of the impeller's surfaces.
- The slightly increased efficiency of the new diffuser tests when compared to the base test results shows the matched impeller's absolute velocity angle to the diffuser's inlet vane tip angle has less losses, hence an increase in efficiency.
- The tail piece addition to the new diffuser increases the pump efficiency when compared to the base tests by 3.9%. This shows that the elimination of the sudden enlargement removes the secondary flow losses at the new diffuser outlet.

Overall the research work conducted has proven:

- How combined mechanical losses reduce the capacity within the pump. This has been shown with comparing manufactured components to design theory and proven with laboratory testing.
- The new diffuser design is not a match for low to medium flow applications, (two vanes to six vane impellers) for a 300AX Axial Flow Pump.

- The new diffuser design is a match for high flow applications, (seven to eight vane impellers) for a 300AX Axial Flow Pump.
- The addition of the tail piece to the new diffuser will improve the pump's efficiency, when used with higher flow applications for the 300AX type of pump.

## 6.3 Future Work

Even though the results for this thesis have proven that the design theory and the laboratory testing were conclusive, some future work which could not be accomplished during this thesis would be recommended to further enhance the findings.

- The purchase of new pump components. Specifically an eight vane impeller and a new medium flow stator. The existing items are worn and have poor surface finishes adding mechanical losses to the pump.
- Laboratory testing using a six vane impeller. Separate testing with a medium flow and a high flow stator would be beneficial, as the six vane impeller crosses over from the medium to high flow range.
- Modifications to the new diffuser as shown in Figure 74.
- As CFD was not the main focus of this research, more thorough CFD analysis of the pump models would be beneficial to determine:
  - Pump efficiencies of the various configurations. Unfortunately it was deemed too time consuming to determine full CFD pump curve analysis for this research.
  - Improved diffuser design to improve pump efficiency for the five vane impeller assembly.

# 7 Bibliography

Anon., 2001. *AS2417-2001, Rotodynamic Pumps - hydraulic performance acceptance tests - Grades 1 and 2*. Sydney NSW: Standards Australia International Ltd.

Anon., 2004. *Australian Pump Technical Handbook*. fourth edition ed. Maryborough, Vic: McPherson's Printing Group.

Anon., n.d. <http://www.ultimatecc.com.au/products.htm>. [Online].

ANSYS Inc, 2013. *ANSYS CFX Reference Guide*. 12.1 ed. Canonsburg, PA: ANSYS.

ANSYS Inc, 2013. *ANSYS CFX-Solver Modeling Guide*. 15 ed. Canonsburg,PA: ANSYS.

ANSYS Inc, 2013. *ANSYS CFX-Solver Theory Guide*. 15 ed. Canonsburg, PA: ANSYS.

ANSYS Inc, 2013. *Introduction to ANSYS CFX*. 15 ed. Canonsburg, PA: ANSYS.

ANSYS, 2013. *Introduction to ANSYS CFX*. s.l.:s.n.

ANSYS, I., 2014. *Innovative Turbulence Modeling: SST Model in ANSYS CFX*. Canonsburg, PA : ANSYS.

Brennen, C. E., 1994. *Hydrodynamics of Pumps*. Oxford OX2 6DP, England : Oxford University Press .

Dicmas, J. L., 1987. *Vertical Turbine, Mixed Flow and Propeller Pumps*. New York: McGraw-Hill, Inc..

Erin Koos, Melany L. Hunt and Christopher E. Brennen , 2008. *Shear Stress Measurements of Non-Spherical Particles in High Shear Rate Flows*. Pasadena, California 91125, USA , California Institute of Technology.

Erin Koos, M. L. H. a. C. E. B., 2008. *Erin Koos, Melany L. Hunt and Christopher E. Brennen* , Pasadena, California 91125, USA : California Institute of Technology.

FARO, 2008. *Coordinate measurement technology: An introduction to dealing with microns*, s.l.: FARO Technologies.

Farrell, K., 1989. *An Investigation of End-Wall Vortex Cavitation in a High Reynolds Number Axial-Flow Pump*, Pennsylvania: The Pennsylvania State University.

Hiemenz, J., 2014. *3D Printing With FDM*, s.l.: Stratasys.

Hi-Tech, 2010. *PolyWorks Modeler with NURBS V11.0.12*. Training Workbook ed. Melbourne: Hi-Tech Metrology.

- Institute, H., 1994. *ANSI/HI 2.1-2.5-1994 American National Standard for Vertical Pumps*. Parsippany: Hydraulic Institute.
- Kadyirov, A., 2013. *Numerical Investigation of Swirl Flow in Curved Tube with Various Curvature Ratio*. s.l., Research Center for Power Engineering Problems of the Russia Academy of Sciences .
- Karassik, I. J. M. J. P. C. P. & H. C. C., 2001. *Pump Handbook*. Third ed. s.l.:1986 McGraw-Hill Companies.
- Kinsky, R., 1982. *Applied Fluid Mechanics*. Sydney, NSW: McGraw-Hill Book Company.
- Kovats, A., 1964. *Design and Performance of Centrifugal and Axial Flow Pumps and Compressors*. New York: The Macmillan Company.
- Lazarkiewicz, S. & T. A. T., 1965. *Impeller Pumps*. First ed. London: Pergamon Press Ltd.
- Logan, E., 1993. *Turbomachinery Basic Theory and Applications*. Second ed. New York, U.S.A.: Marcel Dekker.
- Mohammad Taghi Shervani Tabar, Z. P., 2011. An Experimental Study of Tip Vortex Cavitation Inception in an Axial Flow Pump. *International Journal of Mechanical, Aerospace, Industrial, Mechatronic and Manufacturing Engineering* , Vol:5(No:1), pp. 86-89.
- MohammedAhmedEl-Naggar, 2013. *A One-Dimensional Flow Analysis for the Prediction of Centrifugal Pump Performance Characteristics*, Mansoura University, Mansoura 35516, Egypt: Hindawi Publishing Corporation International Journal of Rotating Machinery Volume 2013, Article ID 473512.
- Munson, B. R. O. T. H. H. W. W. & R. A. P., 2013. *Fluid Mechanics*. Seventh ed. Singapore: John Wiley & Sons.
- Nelson, H., n.d. *Ornel Pump Technical Publication TP/OP/1*, Sydney, Australia: Warman International Australia, Ornel Divison.
- Norrie, D. H., 1963. *An Introduction to Incompressible Flow Machines*, London: Edward Arnold.
- O. Toscanelli, V. Colla, 2013. *Numerical Experiments on Deconvolution Applied to LES in The Modeling of Turbulent Flow*. Scuola Superiore S. Anna , s.n.
- Ornel, P. C., 1953. *Thin Blade Impellers, Bowl Vane Impellers*. Australia: Weir Minerals Australia.
- Raghavendra S Muttalli, S. A. H. W., 2014. CFD Simulation of Centrifugal Pump Impeller Using ANSYS-CFX. *International Journal of Innovative Research in Science, Engineering and Technology* , 3(8).

Stepanoff, A., 1957. *Centrifugal and Axial Flow Pumps: Theory, Design and Application*. 2nd ed. New York: John Wiley & Sons.

Strasse, W., 2008. *User Manual UMF601VI-1EN Ultrasonic Flowmeter*. 36, 12681 Berlin Germany: FLEXIM GmbH.

Tu, J. Y. G. L. C., 2008. *Computational Fluid Dynamics*. First ed. Burlington USA: Elsevier.

Weir Engineering Pty Ltd, 1990. *Maintaining 'As New' Efficiency By Coating Pump Internal Surfaces*, s.l.: Weir Engineering Pty Ltd.

Wu Yulin, Liu Shuhong and Shao Jie , 2010. *Numerical Simulation on the Steady and Unsteady Internal Flows of a Centrifugal Pump*. China , Tsinghua University .

## Appendix A. Detailed Calculations

### A.1. Detailed Calculations

The blade profile at each streamline has been detailed to determine the inlet  $\beta_1$  and outlet  $\beta_2$  angles. The streamlines are measured radially at equal sections of the impeller blade.

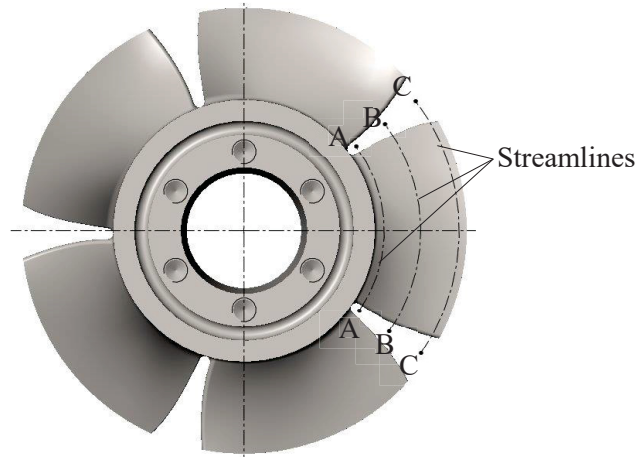


Figure 208 – Impeller streamlines

### A.2. Five Vane Impeller Velocity Calculations

The following calculations are based on the original ‘Ornel’ pump curve no.5V see Figure 15, page 15. Therefore, the best efficiency point (BEP) used for the calculations is 8.8m head and 318 L/s flow running at 1465 rpm.

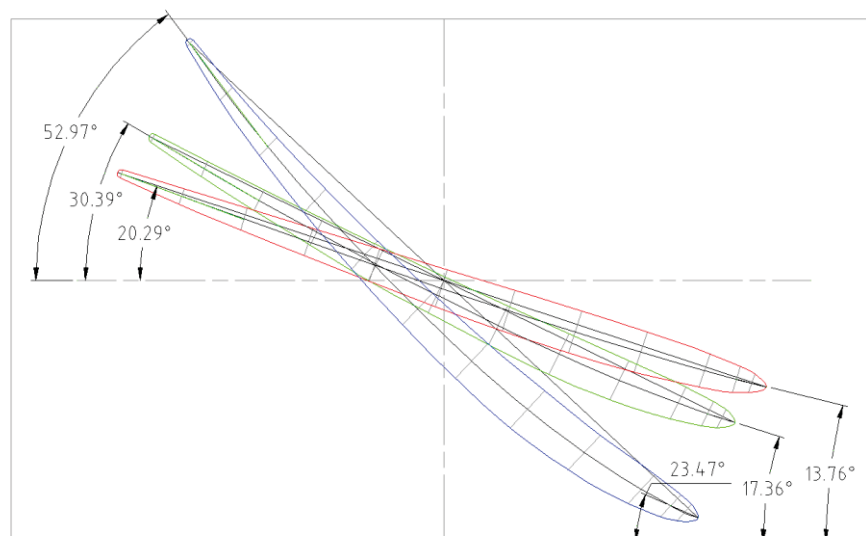


Figure 209 - Overlay of five vane impeller AA, BB & CC streamlines



Figure 209 shows the overlay of the three streamlines as per the original impeller design drawings. Refer to Section Original Impeller 3.1.2.1 which indicates that the scanned measurements of the impeller, within reason, match the blade profiles of the original design drawings. For this reason the original design measurements have been used to determine the inlet  $\beta_1$  and outlet  $\beta_2$  angles.

### A.2.1. Velocity Calculations for Five Vane Impeller

# 5 Vane Impeller

<

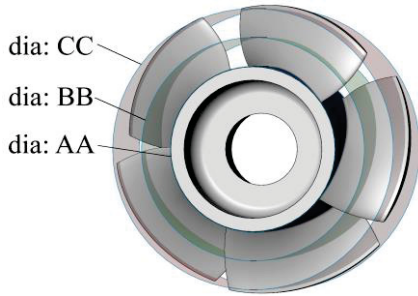


Table 16 – Five vane impeller velocity calculations

## A.2.2. Velocity Triangles for Five Vane Impeller

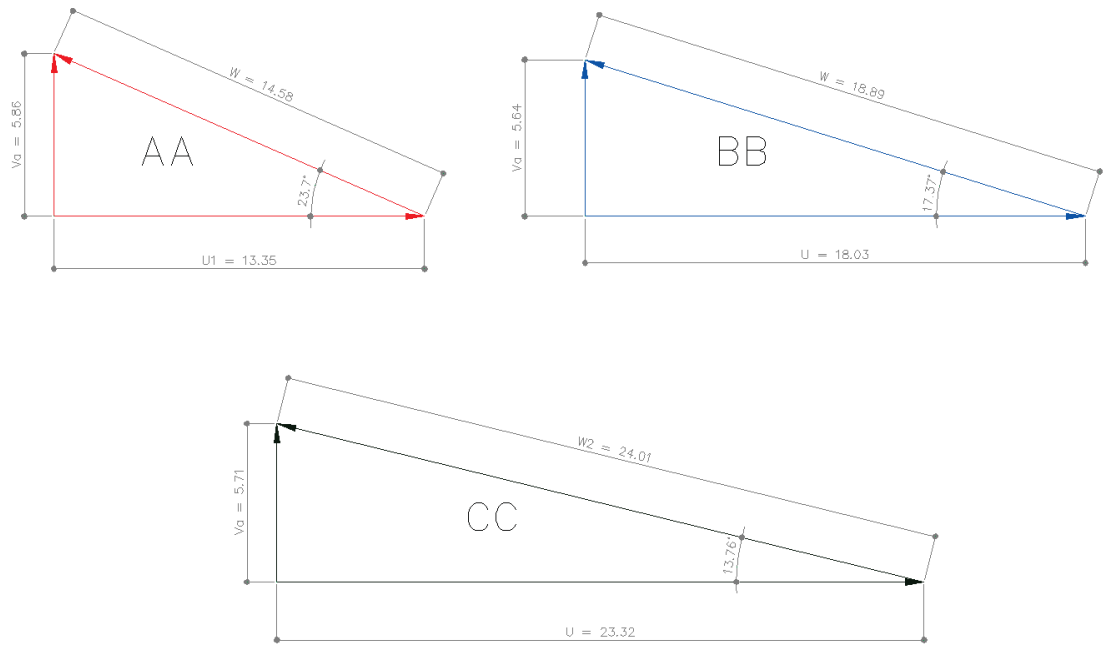


Figure 210 – Velocity Triangle, Streamlines AA, BB & CC, Five Vane Impeller Inlet

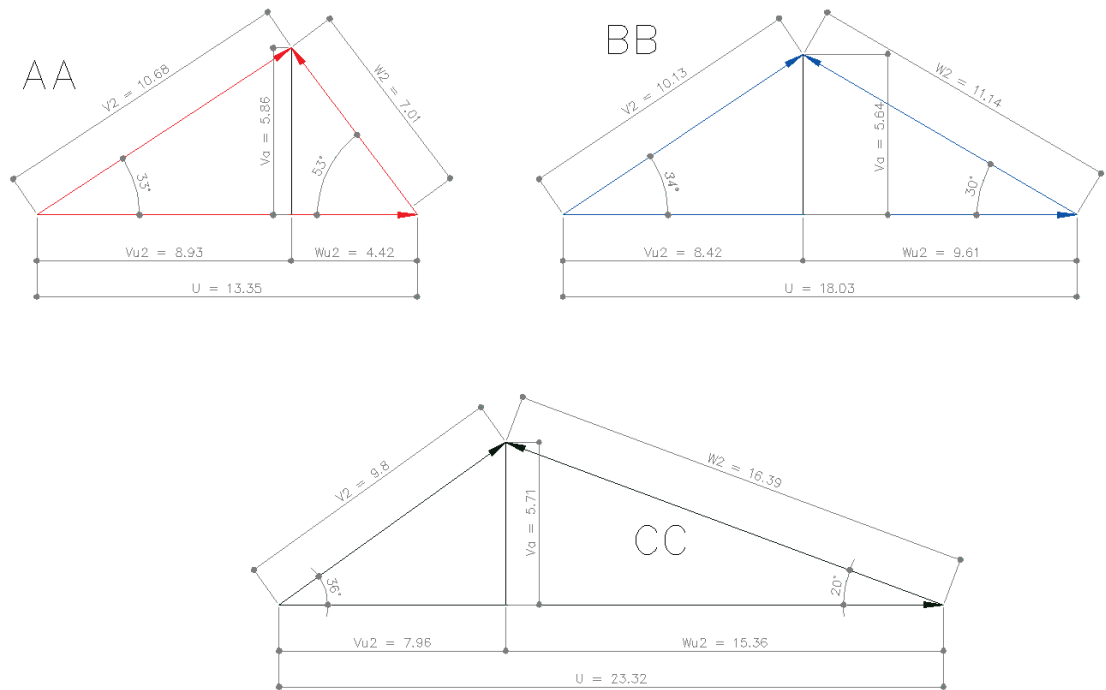


Figure 211- Velocity Triangle, Streamlines AA, BB & CC, Five Vane Impeller Outlet

### A.2.3. Comparisons of Impeller Outlet Angles to New Diffuser Inlet Angles

Comparisons of the impeller outlet angles  $\alpha_2$  and new diffuser angles  $\beta_3$  reveals the difference for streamlines AA, BB and CC are outside the recommended tolerance of  $\pm 5^\circ$ .

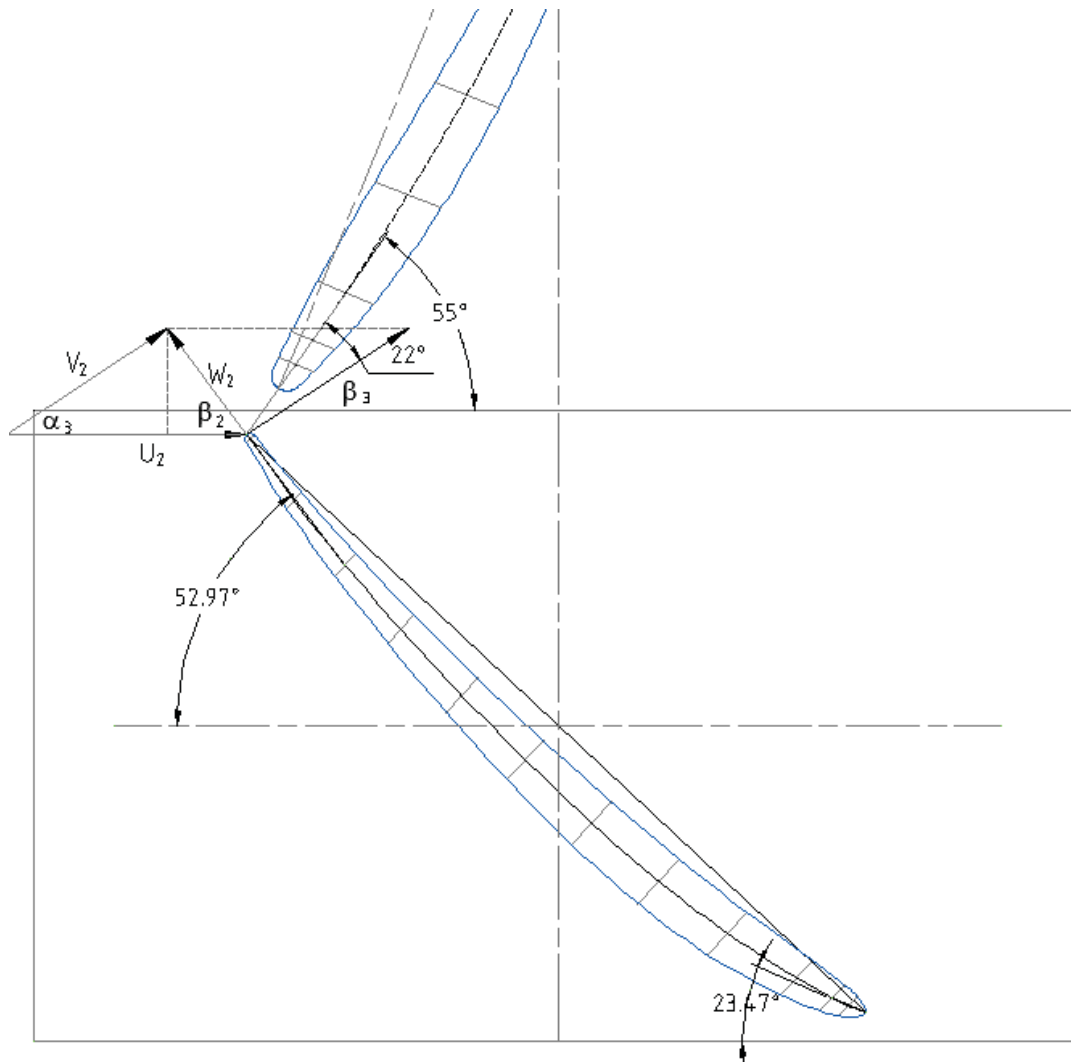


Figure 212 – Streamline AA of five vane impeller and new diffuser inlet

### A.3. Six Vane Impeller Velocity Calculations

The following calculations are based on the original ‘Ornel’ pump curve no.6VI see Figure 15, page 15. Therefore, the best efficiency point (BEP) used for the calculations is 8.8m head and 387 L/s flow running at 1465 rpm.

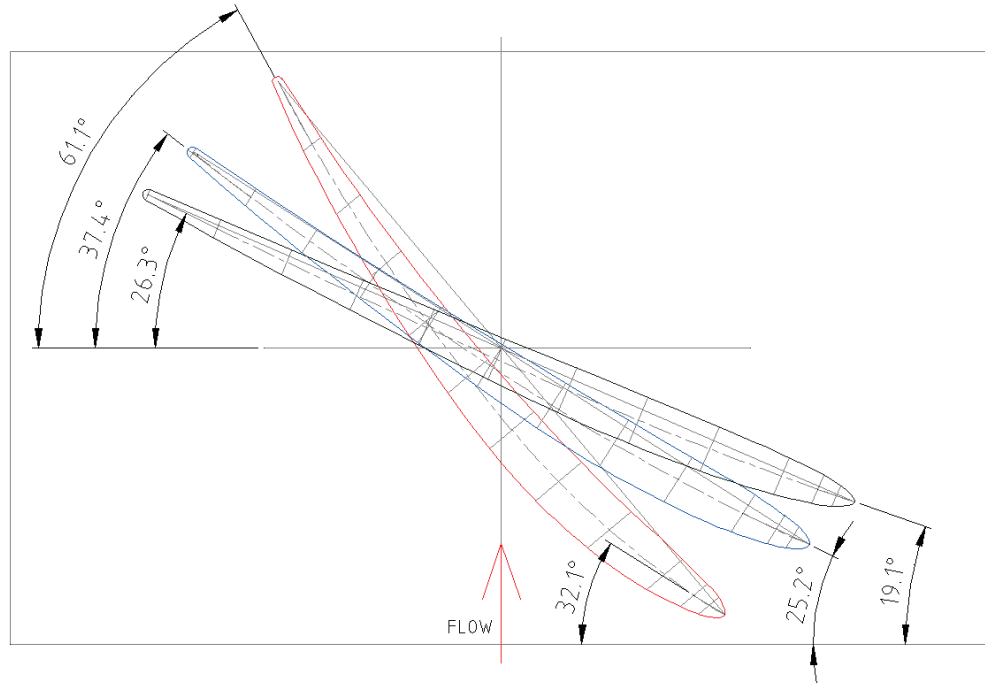


Figure 213 - Overlay of impeller no.6 AA, BB & CC streamlines

Figure 213 shows the overlay of the three streamlines as per the original impeller design drawings. As with the five vane impeller the original design measurements have been used to determine the inlet  $\beta_1$  and outlet  $\beta_2$  angles. This impeller was not scanned.

### A.3.1. Velocity Calculations for Six Vane Impeller

#### 6 Vane Impeller

Velocity Triangles at Pump BEP

Pump Speed and Flow as per Pump Curve at Impeller Outlet			Velocity Calculations at Streamline Sections				
$N$	rpm	1465.00	Equation	Units	Streamline Section		
$Q$	L/s	387.00			AA	BB	CC
$\omega = N \frac{\pi}{30}$	rad/s	153.41	$d$	m	0.174	0.235	0.304
$C_m = Va_{AA} = U \times \tan \beta_{1AA}$	m/s	8.37	$\beta_1$	Deg	32.10	25.20	19.10
$C_m = Va_{BB} = U \times \tan \beta_{1BB}$	m/s	8.48	$\beta_2$	Deg	61.10	37.40	26.30
$C_m = Va_{CC} = U \times \tan \beta_{1CC}$	m/s	8.07	$U = \frac{\omega d}{2}$	m/s	13.35	18.03	23.32
			$W = \sqrt{U^2 + V_a^2}$	m/s	15.76	19.92	24.68
			$W_{u2} = \frac{V_a}{\tan \beta_2}$	m/s	4.62	11.09	16.34
			$C_{u2} = V_{u2} = U - W_{u2}$	m/s	8.73	6.93	6.98
			$W_2 = \sqrt{W_{u2}^2 + V_a^2}$	m/s	9.56	13.97	18.22
			$V_2 = \sqrt{V_{u2}^2 + V_a^2}$	m/s	12.09	10.95	10.67
			$\alpha_2 = \tan^{-1} \frac{V_a}{V_{u2}}$	Deg	44	51	49

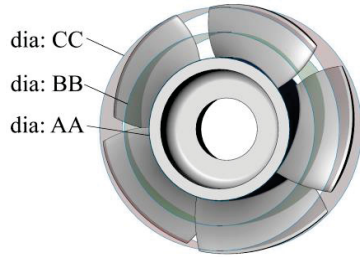


Table 17 – Six Vane Impeller inlet velocity calculations

### A.3.2. Velocity Triangles for Six Vane Impeller

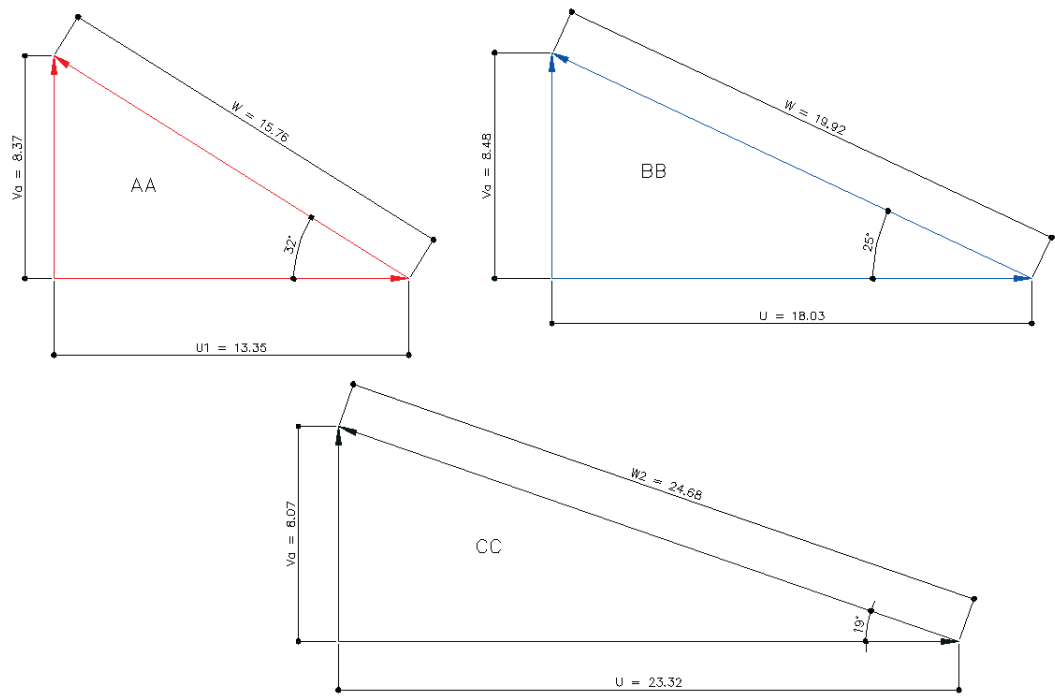


Figure 214 - Velocity Triangle, Streamlines AA, BB & CC, Six Vane Impeller Inlet

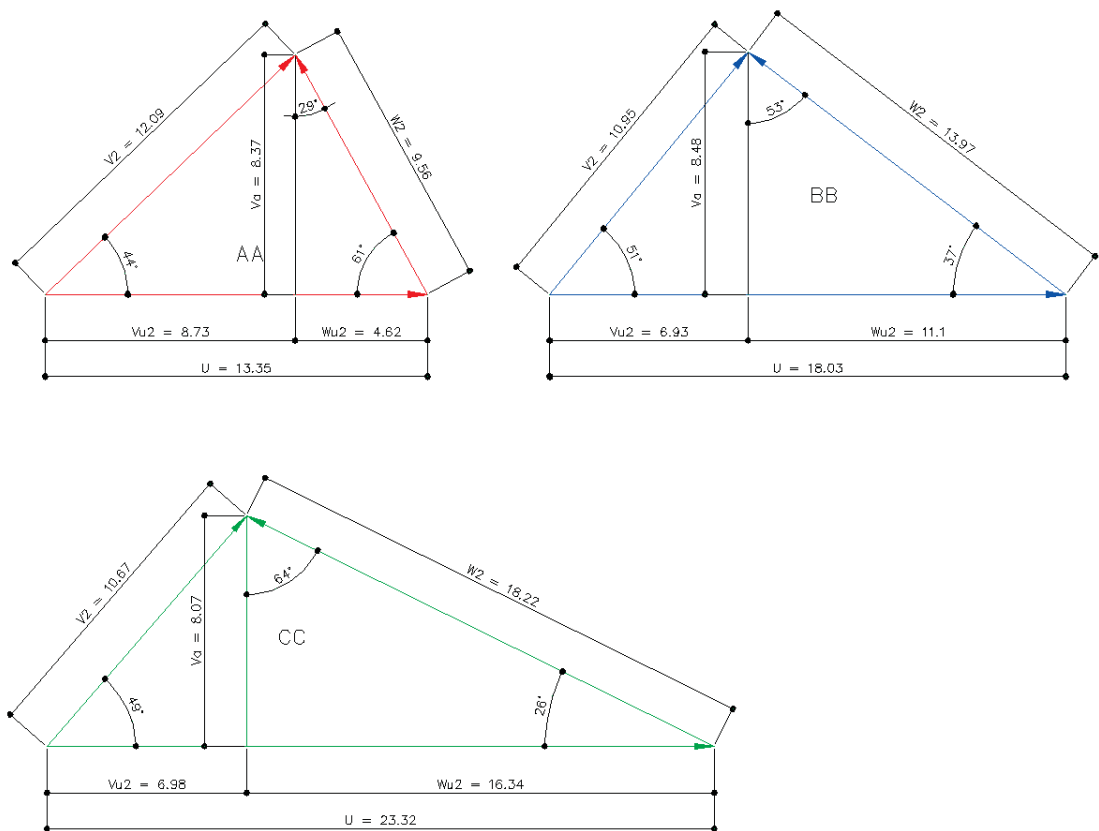


Figure 215 - Velocity Triangle, Streamlines AA, BB & CC, Six Vane Impeller Outlet



### A.3.3. Comparisons of Impeller Outlet Angles to New Diffuser Inlet Angles

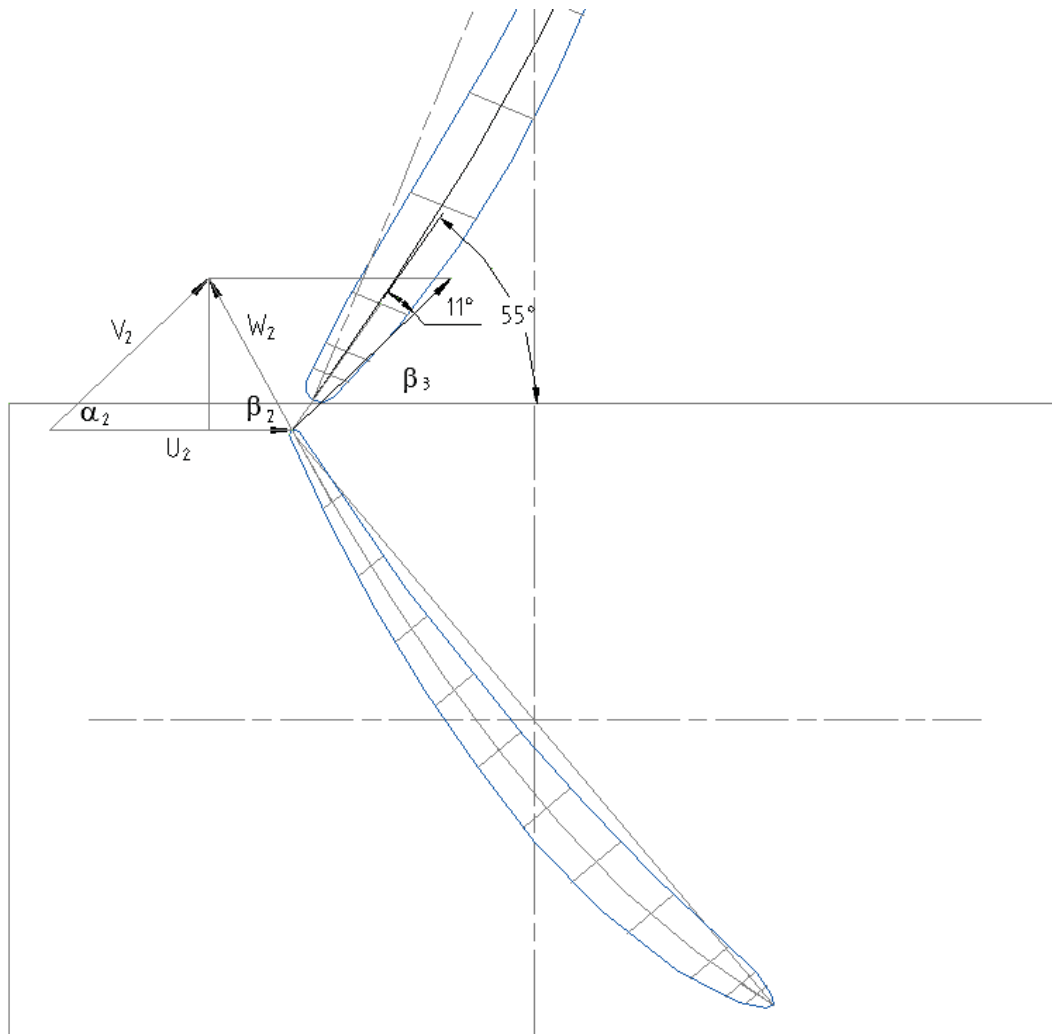
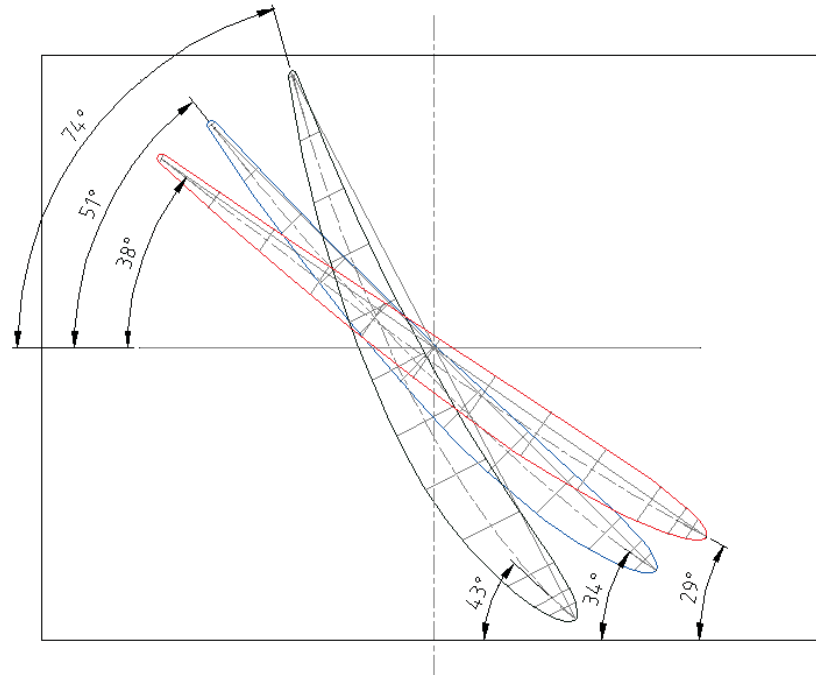


Figure 216 – Streamline AA of Six vane impeller and new diffuser inlet

### A.4. Eight Vane Impeller Velocity Calculations

The following calculations are based on the original ‘Ornel’ pump curve no.8 VIII see Figure 10 page 9. Therefore, the best efficiency point (BEP) used for the calculations is 8.9m head and 564 L/s flow running at 1465 rpm.



*Figure 217 - Overlay of Eight Vane Impeller AA, BB & CC streamlines*

Figure 217 shows the overlay of the three streamlines as per the original impeller design drawings. The original design measurements have been used to determine the inlet  $\beta_1$  and outlet  $\beta_2$  angles. This impeller was not scanned.

## A.4.1. Calculations for Eight Vane Impeller

### 8 Vane Impeller

Velocity Triangles at Pump BEP

Pump Speed and Flow as per Pump Curve at Impeller Outlet			Velocity Calculations at Streamline Sections				
$N$	rpm	1465.00	Equation	Units	Streamline Section		
$Q$	L/s	567.00			AA	BB	CC
$\omega = N \frac{\pi}{30}$	rad/s	153.41	$d$	m	0.174	0.235	0.304
$C_m = Va_{AA} = U \times \tan \beta_{1AA}$	m/s	12.36	$\beta_1$	Deg	42.80	34.20	28.70
$C_m = Va_{BB} = U \times \tan \beta_{1BB}$	m/s	12.25	$\beta_2$	Deg	74.30	51.50	38.30
$C_m = Va_{CC} = U \times \tan \beta_{1CC}$	m/s	12.77	$U = \frac{\omega d}{2}$	m/s	13.35	18.03	23.32
			$W = \sqrt{U^2 + V_a^2}$	m/s	18.19	21.79	26.59
			$W_{u2} = \frac{V_a}{\tan \beta_2}$	m/s	3.47	9.74	16.17
			$C_{u2} = V_{u2} = U - W_{u2}$	m/s	9.87	8.28	7.15
			$W_2 = \sqrt{W_{u2}^2 + V_a^2}$	m/s	12.84	15.65	20.60
			$V_2 = \sqrt{V_{u2}^2 + V_a^2}$	m/s	15.82	14.79	14.63
			$\alpha_2 = \tan^{-1} \frac{V_a}{V_{u2}}$	Deg	51	56	61

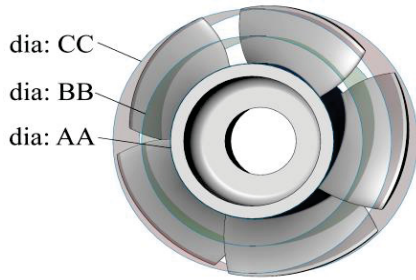


Table 18 – Eight Vane Impeller inlet velocity calculations

## A.4.2. Velocity Triangles for Eight Vane Impeller

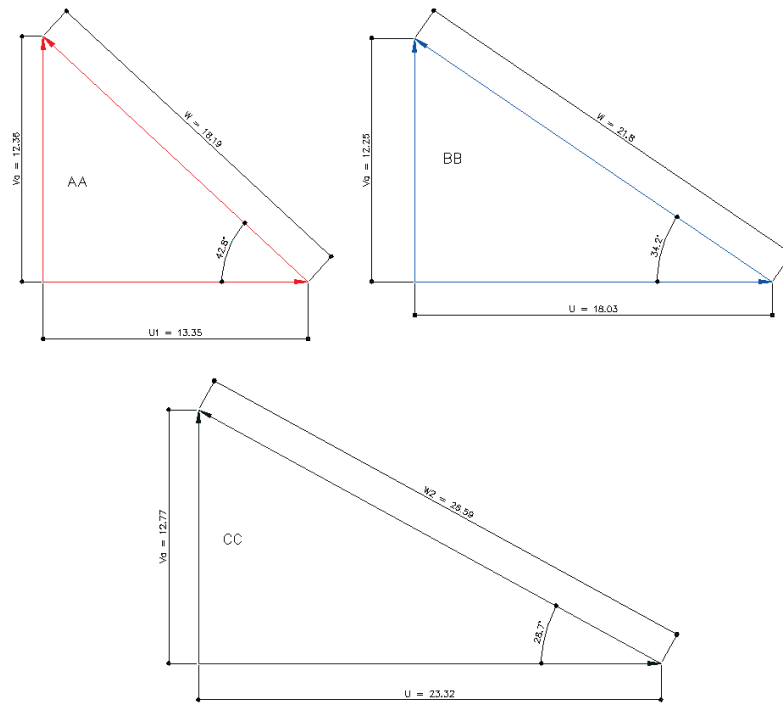


Figure 218 – Velocity Triangle, Streamlines AA, BB & CC, Eight Vane Impeller Inlet

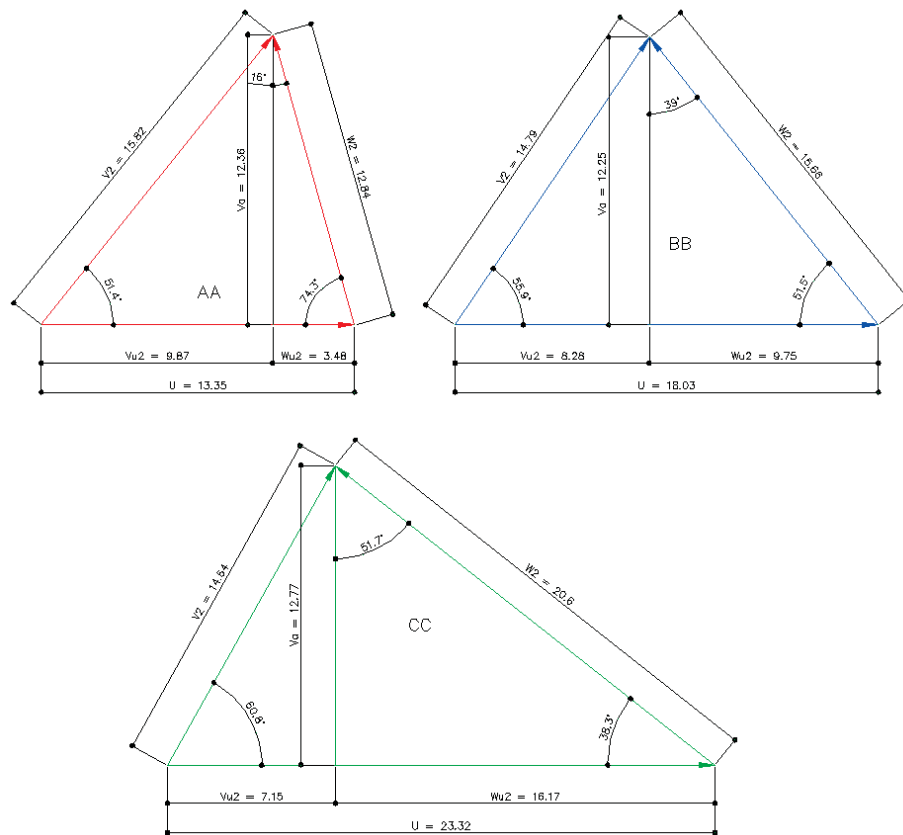


Figure 219 - Velocity Triangle, Streamlines AA, BB & CC, Eight Vane Impeller Outlet

### A.4.3. Comparisons of Eight Vane Impeller Outlet Angles to New Diffuser Inlet Angles

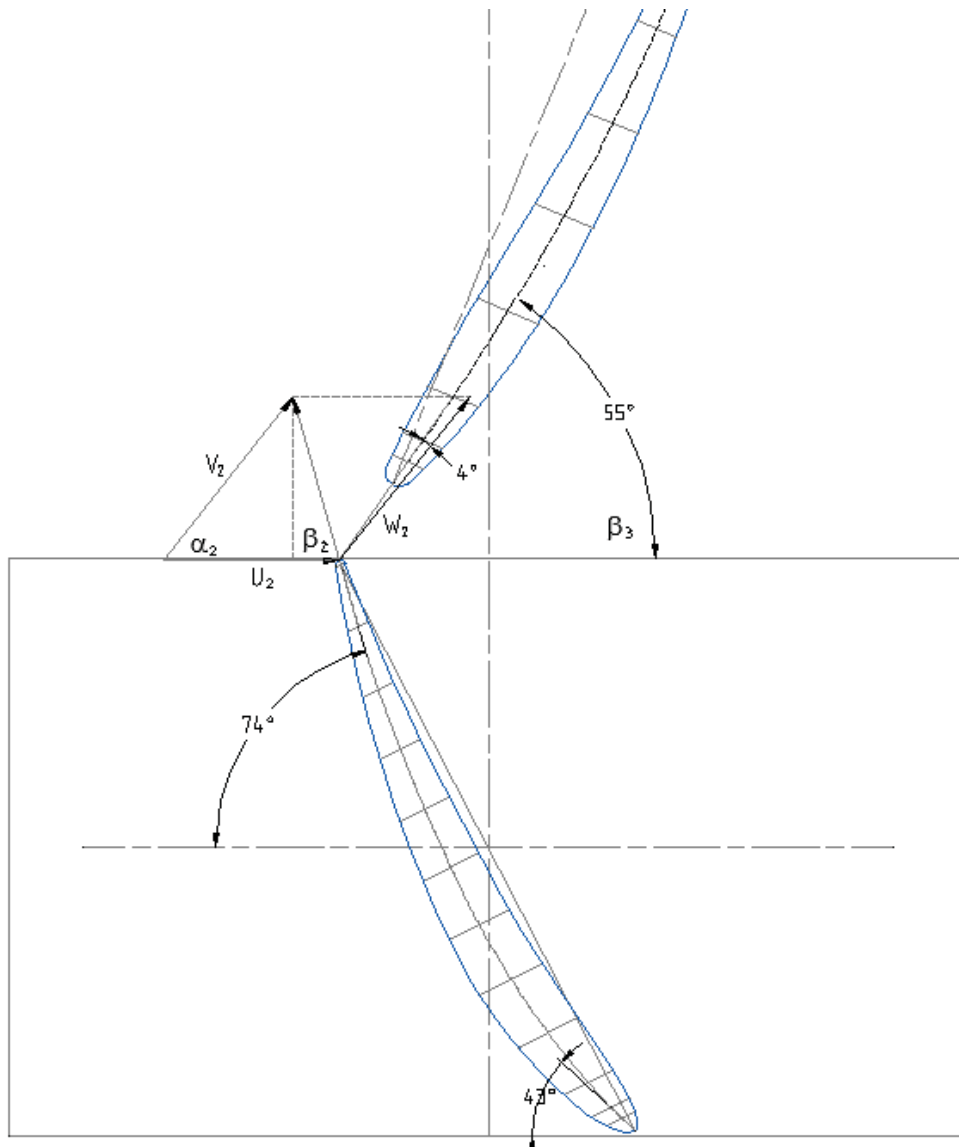


Figure 220 - Streamline AA of eight vane impeller and new diffuser inlet

Angle	Unit	Steamline		
		AA	BB	CC
$\alpha_2$	deg	61	56	51
$\beta_3$	deg	55	59	63
Difference	deg	-6	3	12

Table 19 - Calculations of number eight impeller angles  $\alpha_2$  and  $\beta_3$  at 1465rpm

## A.5. Speed Increase

Due to the mismatch of the  $\alpha_2$  and  $\beta_3$  angles for the no.5 and 6 impellers, calculations have been conducted to investigate the possibility if an increase of speed will change the velocity angles.

Simulation has been used to calculate the new duty points with an increase of speed. A speed increase of 30 rpm has been used for the simulation.

### A.5.1. Results

The results showed an increase of speed, flow and head for the no.5 impeller pump arrangement. An increase in flow meant an increase in velocity. Due to the velocity increase being constant across all of the equations, the angles remained unchanged.

Vane Angle Comparision @ 1465rpm				
Angle	Unit	Streamline AA	Streamline BB	Streamline CC
$\alpha_2$	deg	49	40	26
$\beta_3$	deg	31.5	28.8	25.3
Difference	deg	17	11	1

Vane Angle Comparision @ 1495rpm				
Angle	Unit	Streamline AA	Streamline BB	Streamline CC
$\alpha_2$	deg	49	40	26
$\beta_3$	deg	31.5	28.8	25.3
Difference	deg	17	11	1

Vane Angle Comparision @ 1525rpm				
Angle	Unit	Streamline AA	Streamline BB	Streamline CC
$\alpha_2$	deg	49	40	26
$\beta_3$	deg	31.5	28.8	25.3
Difference	deg	17	11	1

Table 20 – Calculations of angles  $\alpha_2$  and  $\beta_3$  at 1465, 1495 and 1525 rpm





---

188

The speed increase also results in a head increase which means there will be an increase of the power required. An increase in required power, in some cases, will not be a pleasant outcome, due to a larger motor being required and the extra costs in power usage.

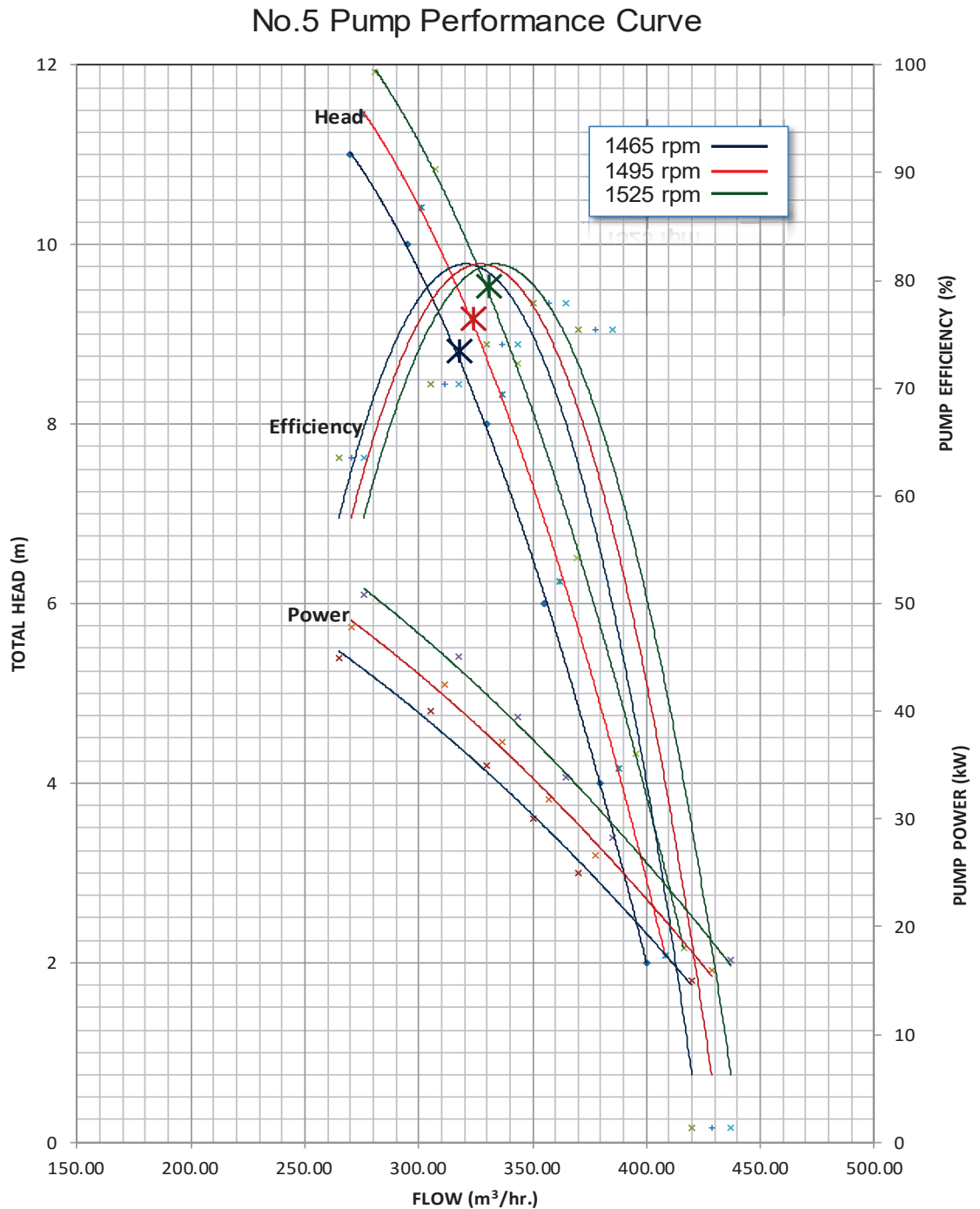


Figure 222 – Performance curve showing speed increase at 1465, 1495 and 1525 rpm

speed: 1465		ORIGINAL CURVE		speed: 1495		SIMULATION CURVE 1	
HEAD		orig duty		HEAD		orig duty	
flow L/S	total head m	flow	head	flow L/S	total head m	flow	head
270.00	11	318	8.8	275.53	11.46	324.51	9.16
295.00	10			301.04	10.41		
330.00	8			336.76	8.33		
355.00	6			362.27	6.25		
380.00	4			387.78	4.17		
400.00	2			408.19	2.08		
		$P_{hyd} = Q \times \rho \times g \times H$				$P_{hyd} = Q \times \rho \times g \times H$	
POWER		HYDRAULIC POWER		POWER		HYDRAULIC POWER	
flow L/S	Power	Head	flow L/S	Power	flow L/S	Power	Head
265.00	45	11	265.00	28.60	270.43	47.82	11.46
305.00	40	9.4	305.00	28.13	311.25	42.51	9.79
330.00	35	8	330.00	25.90	336.76	37.19	8.33
350.00	30	6.8	350.00	23.35	357.17	31.88	7.08
370.00	25	5.2	370.00	18.87	377.58	26.57	5.42
420.00	15	0.05	420.00	0.21	428.60	15.94	0.05
EFFICIENCY		$\eta = \frac{P_{hyd}}{P_{input}}$		EFFICIENCY		$\eta = \frac{P_{hyd}}{P_{input}}$	
flow L/S	efficiency			flow L/S	efficiency		
265.00	63.55			270.43	63.55		
305.00	70.31			311.25	70.31		
330.00	74.00			336.76	74.00		
350.00	77.83			357.17	77.83		
370.00	75.50			377.58	75.50		
420.00	1.37			428.60	1.37		

speed: 1525		SIMULATION CURVE 2		speed: 2000		SIMULATION CURVE 3	
HEAD		orig duty		HEAD		orig duty	
flow L/S	total head m	flow	head	flow L/S	total head m	flow	head
281.06	11.92	331.02	9.54	368.60	20.50	434.13	16.40
307.08	10.84			402.73	18.64		
343.52	8.67			450.51	14.91		
369.54	6.50			484.64	11.18		
395.56	4.33			518.77	7.45		
416.38	2.17			546.08	3.73		
		$P_{hyd} = Q \times \rho \times g \times H$				$P_{hyd} = Q \times \rho \times g \times H$	
POWER		HYDRAULIC POWER		POWER		HYDRAULIC POWER	
flow L/S	Power	Head	flow L/S	Power	flow L/S	Power	Head
275.85	50.76	11.92	275.85	32.26	361.77	114.50	11.92
317.49	45.12	10.19	317.49	31.72	416.38	101.77	10.19
343.52	39.48	8.67	343.52	29.21	450.51	89.05	8.67
364.33	33.84	7.37	364.33	26.34	477.82	76.33	7.37
385.15	28.20	5.63	385.15	21.29	505.12	63.61	5.63
437.20	16.92	0.05	437.20	0.23	573.38	38.17	0.05
EFFICIENCY		$\eta = \frac{P_{hyd}}{P_{input}}$		EFFICIENCY		$\eta = \frac{P_{hyd}}{P_{input}}$	
flow L/S	efficiency			flow L/S	efficiency		
275.85	63.55			361.77	36.95		
317.49	70.31			416.38	40.88		
343.52	74.00			450.51	43.02		
364.33	77.83			477.82	45.25		
385.15	75.50			505.12	43.89		
437.20	1.37			573.38	0.80		

Table 21 – Calculations for an increase in pump speed, for 1465, 1495, 1525 and 2000 rpm

## Appendix B. Test Rig Assembly and Disassembly

The following section gives a description of the physical assembly and disassembly of the laboratory test rig. It outlines the steps required to change out pump components, improvements made to tooling and manual handling to enable safer and quicker component change over times and the difficulties encountered during the test rig.

### B.1. Initial Pump Rig Observations

The removal of the existing test pump set-up was a difficult operation, as many of the tools required to dismantle the pump were unavailable. There is also no crane available a hench, lack of lift height with the available equipment.

Another hindrance during the initial pump strip was that when the previous pump build was assembled, silicon was used to seal the pump and piping joints instead of o’rings and gaskets. According to original design and my previous pump assembly experience, o’rings and gaskets should have been used to ensure ease the removal of equipment.

### B.2. Pump Disassembly Steps

The following steps were developed during many hours and there were problems during disassembling the pump. Two different disassembly procedures were developed, the first for entire pump removal and the second for an impeller change over only.

#### B.2.1. Complete Pump Disassembly

1. Ensure that the loop has been drained from water and that the electric motor has been disabled and tagged out. Open all air vents during draining.
2. Remove fasteners from the clamping flange on the dismantling joint. Remove the outer ring and release the o’ring. Slide the parts along the pipe as far as possible.

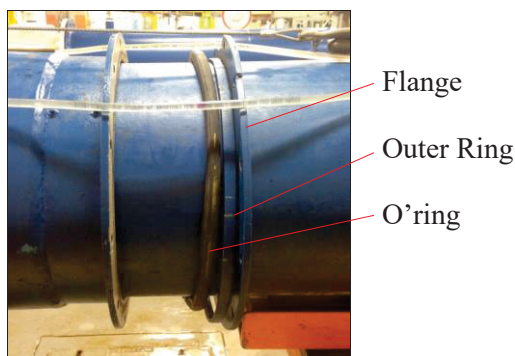


*Figure 223 – Open dismantling joint*

3. Remove the suction case nuts. Leave the threaded rod installed as they are used as guides during pump reassembly.

Dog clamp    Suction case    Bowl ring    Suction case nuts    New diffuser

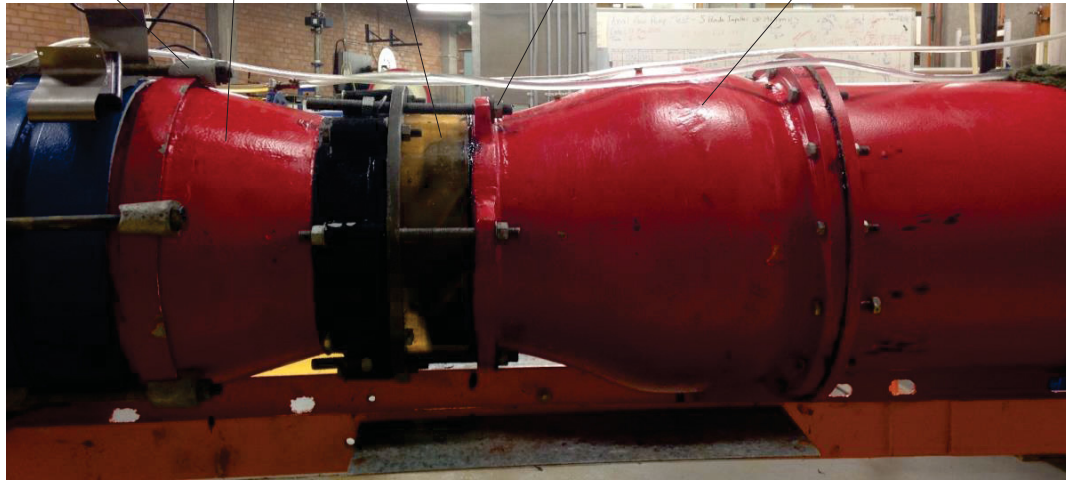


*Figure 224 – Pump assembly*

4. Attach the portable cable winch using lifting straps and D-shackles. Lever in the winch to open the pump between the bowl ring and diffuser. Constantly check after every three levers that the o’ring is away from the pipe gap. The o’ring will continuously be required to be slid towards the pump end to ensure it doesn’t pinch in the gap between pipes.

Cable winch



*Figure 225 – Attachment of cable winch*

5. Ensure that the pump is open enough that the shaft is completely free of the suction case. Remove the dog clamps and bolts from the suction case and lift the case from the assembly.

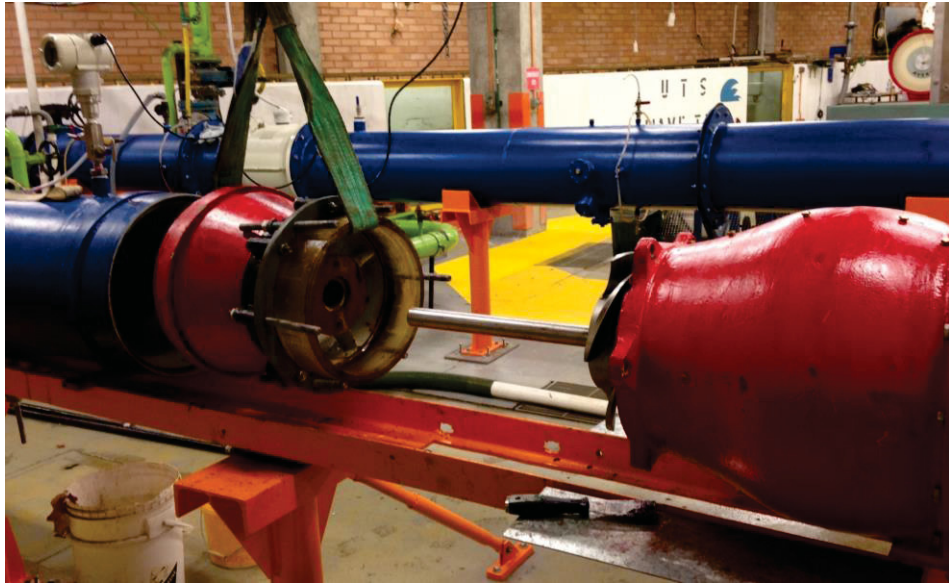


*Figure 226 – Removal of suction case*

6. To remove the impeller from the assembly. Remove the set screws and the collet plate to reveal the collet. Place the backing plate against the hub face of the impeller and force the collet drive against the plate to dislodge the impeller from the collet. To help remove the collet from the shaft, force a wedge into the slots to open the gap and release the collet from the shaft.



*Figure 227 – Impeller Removal*

7. Once the impeller is removed unbolt the diffuser and slide off the shaft and remove from the assembly.

At this stage the pump assembly is fully stripped and no more components are required to be removed.

### B.2.2. Impeller Change Over

For an impeller change over, repeat steps 1, 2, 3, 4 and 6 from Section B.2.1. Step 5 is not required as the suction case can stay assembled during the impeller removal.



## B.3. Pump Assembly Steps

As with the pump disassembly steps, the following assembly steps were developed during many hours and problems during the assembling of the pump. Two different assembly procedures are developed the first for entire pump assembly and the second for an impeller change over only.

### B.3.1. Pump Reassembly Steps

To reassemble the entire pump the following steps are required:

8. Lift the diffuser into position onto the rails. Ensure the centre of the diffuser is aligned to the shaft. If the tail piece is required to be installed, pre-assemble the component onto the shaft.

Support the smaller diameter of the diffuser and slide the component onto the shaft. If the tail piece is being installed, fasten it onto the back face of the diffuser.

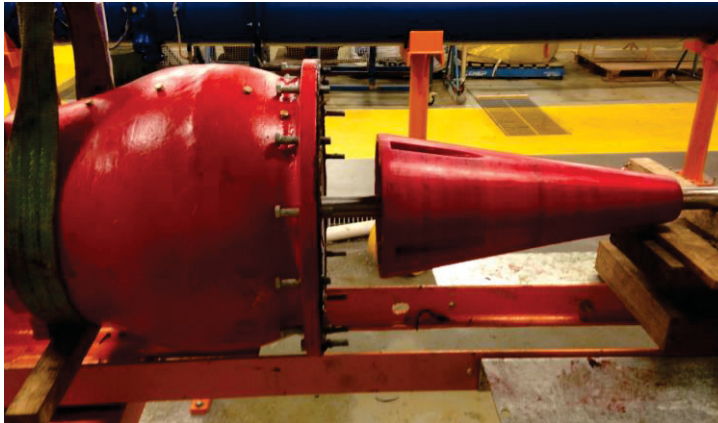


*Figure 228 – Diffuser and tail piece installation*

9. Install o’ring in the groove on the mating flange between the diffuser and pipe adaptor. Also add Loctite gasket eliminator to the flange faces. Slide the diffuser further along the shaft to join the flange faces and bolt the diffuser to the pipe adaptor. When the diffuser is secure the support can be removed.
10. To install the impeller, slide it over the shaft and slide up to the diffuser face. Slide the collet onto shaft and up to the impeller. Push the collet into the impeller bore and ensure the impeller is sitting perpendicular to the shaft. When the impeller is secure on the collet, insert a 6mm spacer between the impeller hub face and the diffuser hub front face.  
  
Force the collet drive against the collet face to drive the collet into the impeller and secure into position.
11. Remove the spacer and check the impeller running gap is approximately 6mm. If the gap is acceptable, install the locking plate and fasteners.



Figure 229 – Impeller installation

12. Lift the suction case onto the pump support structure and align the bearing bore centre to the pump shaft. Using the dog bolts, fasten the suction case to the pump coupling. Ensure the o’ring is installed and Loctite gasket eliminator has been used on the mating faces.

*Note: For the new diffuser assembly a 13mm thick spacer is required to be installed on the face of the suction spacer, to make up for the large gap between the impeller hub and new diffuser hub face. For a standard pump setup with the original pump stator, this spacer is required to be removed.*

13. When the suction case is in position, install an o’ring in the groove of the diffuser flange. Coat the flange face and the mating face of the bowl ring.
14. Attach the portable cable winch to the discharge head and the spigots of the dismantling joint. Lever in the winch to close the pump between the bowl ring and diffuser. Constantly check after every three levers that the o’ring is close to the pipe gap. The o’ring will continuously be required to be slid towards the gap to ensure it doesn’t pinch in the gap between the pipe and support structure. Use the threaded rod in the suction case for alignment to the diffuser. When mating faces are connected, fasten the two components together.



Figure 230 – Lever to close pump assembly

15. When the pump is fully closed, push the dismantling joint o’ring against the gap between the sliding pipes. Push the steel ring over the o’ring and clamp the assembly together using the loose flange. Start fastening the flange loosely from the top hole position and gradually fasten down evenly each side of the flange to finish at the bottom hole. This will ensure even pressure is applied to the steel ring to seal the o’ring. When the flange is fully fastened, finish tightening the fasteners to seal the pipe.



*Figure 231 – Assembled dismantling joint*

16. Fill the test loop to check for leaks.

### B.3.2. Installation of Impeller only

To install an impeller only, follow assembly steps 3, 6, 7, 8 and 9.

## B.4. Test Rig Tool Improvements

During working on the test rig, it was found that some of the existing tooling used for the assembly and disassembly was sometimes a hindrance and required to be modified to improve the time taken and safety of the tool usage. In some cases, it was found that a new approach to the procedure was required.

### B.4.1. Opening and Closing the Pump

When disassembling the pump for the first time to exchange components, the procedure to open the pump was to disassemble the dismantling joint and open the pump by using threaded rods on either side of the pipe and screwing nuts against a spigot. Once this was open approximately 200mm, a turnbuckle and chain was used. When using the turnbuckle, after every 200mm of travel the chains were required to be removed, the turnbuckle screwed open, the chains

reconnected and then start again. This procedure could take approximately 2.5 hours to open the pump. To close the pump this procedure was reversed.

The introduction of the portable cable winch reduced this time to approximately 20 minutes and a much safer process.

## B.4.2. Impeller Installation and Removal

The original procedure to remove and install the impeller is again a time consuming process. Due to the pump being in a horizontal position, gravity cannot be used for setting the impeller as per the original pump design. Also as the pump is built from the top down not the bottom up, as per the original pump design, the impeller installation is not as the original procedure therefore over the years different methods have been adapted.

### B.4.2.1. Backing Plate Modification

During the original disassembly of the impeller, it required a backing plate to be slid over the shaft and pushed against the hub face of the impeller. Studs were then inserted into the tapped holes in the collet. Nuts are screwed onto the studs against the backing plate. When the nuts are tightened the collet is pulled from the impeller. The nuts are required to be turned at the same time for the collet to be removed evenly.



*Figure 232 – Stud and nut collet removal*

To make the back plate installation simpler, the plate was modified by having a slot machined for it to fit over the shaft and not requiring to be slid from the end.

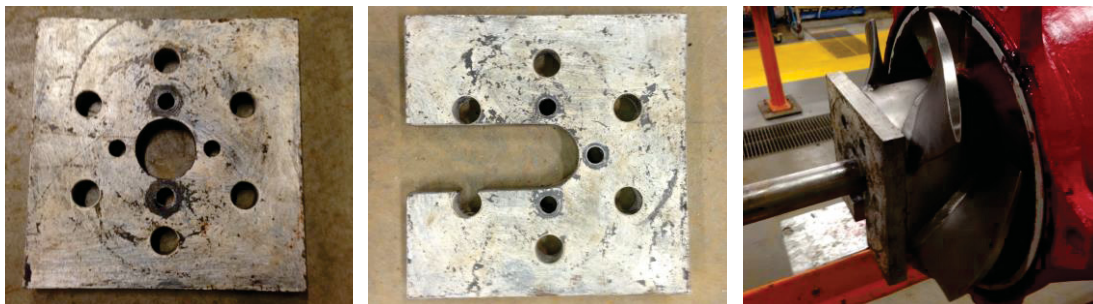


*Figure 233 – Backing plate modification*



#### B.4.2.2. Collet Drive

Originally a collet drive would be used during the impeller installation, to drive the collet into position. As the author has access to this tool, this was used to push against the backing plate during impeller removal and to drive the collet into position during assembly see Sections B.3.1 step 3 and B.2.1 step 6 for details. By using the collet drive the stud and nut method was not required which reduced the install and removal time.



*Figure 234 – Collet drive*

#### B.4.2.3. Setting Running Gap

As previously discussed, due to the pump installation being installed in a horizontal position, gravity could not be used to adjust the pumps running gap as required. Normally, with the pump in a vertical position, the adjusting nut, located above the thrust bearing, is loosened to allow the impeller to sit on the hub of the suction case. The nut is then tightened to lift the impeller 6mm off the suction case which sets the required running gap.

To compensate for the lack of gravity to lower the impeller, a 6mm spacer is placed between the impeller hub and diffuser or stator's hub. The spacer is left in place until the collet has been locked in place with the retaining plate and two fasteners. When the spacer is removed and the gap is measured and if correct, the remaining fasteners are installed.

By using the spacer there is also no need to remove the adjusting nut or uncouple the motor. This again saves a great amount of time.

### B.5. Pump Laboratory Issues

Over the course of the laboratory testing, issues during the assembly, disassembly and pump testing postponed and added some major delays to the testing process. A majority of the issues could be responded to and resolved quickly, however some of the more serious problems prevented testing for a couple of months. The following paragraphs outline some of the above mentioned issues and their resolutions.

### B.5.1. Rubber Gaskets and Debris

On a number of occasions pump testing had to be halted due to debris finding its way into the testing loop and being lodged on the impeller inlet vanes or between the vane tip and bowl ring clearance. This could be resolved sometimes by stopping the pump and the item would dislodge itself. But on two occasions the pump was required to be stripped and the item removed and then the pump was to be rebuilt, which could take up to 4.5 hours (including draining and refilling the loop). The majority of the time the debris was rubber gasket material. With the refurbishment of the test rig this problem was mostly resolved.

### B.5.2. Pump Sealing and Leaking

On a number of pump tests, sealing the pump was an issue. During the initial tests, the pump was heavily sealed with silicon which posed an issue during disassembly with breaking apart sealing faces and cleaning mating faces. This was resolved with the introduction of o'rings and Loctite gasket eliminator. However, a leak could not be found until the test rig was full of water and under pressure, therefore the pump was required to be resealed once or twice. This was found mainly on components, which over the years had been damaged on the sealing face making them difficult to seal.

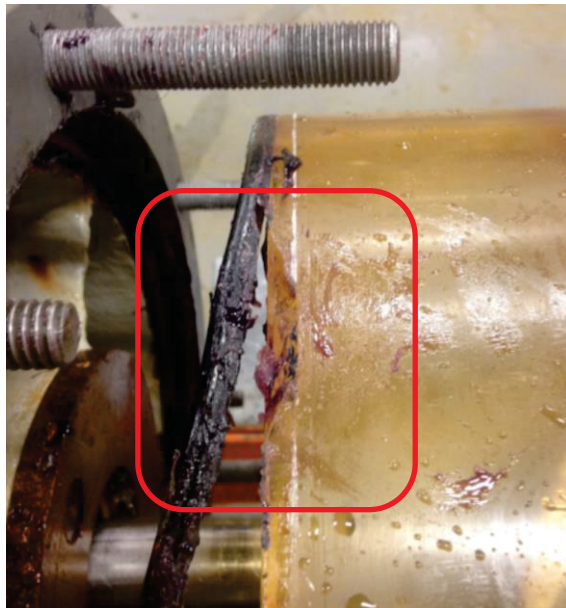


*Figure 235 – Damaged sealing face of bowl ring*

The dismantling joint is another area which will leak if the fasteners are not properly tightened. If leaking is found, it can be resolved by tightening the fasteners.

One major leak occurred after the refurbishment at the discharge spool piece of the flowmeter. After investigation, it was found that the flange holes of the joining faces were two different diameters. Due to the fastener being matched to the smaller hole, there was not enough surface



contact on the larger hole size to sufficiently clamp the faces together. To resolve this problem, a thicker oversize washer was installed under the fastener head to add sufficient surface area.

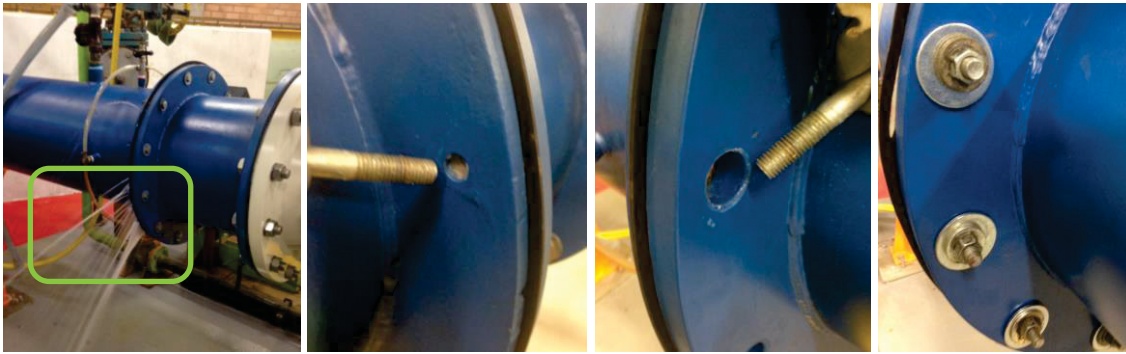


*Figure 236 – Leakage and repair at spool piece*

### B.5.3. Test Rig Straightening Tubes

One of the major issues as mentioned in Section 5.2.1.3 during tests being completed by another student the flow straightener tubes came loose and broke free finding its way into the pump's suction case. To repair the flow straightener, the component was required to be removed and all of the PVC piping was required to be replaced. The removal, repair and reinstallation took two months to resolve before testing could be resumed.

### B.5.4. Pump Assembly

On a number of the pump assemblies, the build was undertaken by an outside party. Without supervision, some of the details of the assembly were overlooked which in some cases resulted in a large amount of testing downtime to resolve the issues.

On initial inspection of the assembly for pump test 3.01 it could be seen (through the Perspex bowl ring) that the installed impeller was not the correct impeller. The original five vane impeller which had been coated, (which was bright blue) was installed with the new impeller which was used in all the testing was on the bench. As the loop had been filled it was decided to run the test with the coated impeller to have another set of results. On disassembly of the pump to install the correct five vane impeller, the suction spacer that was required for the new diffuser assembly had not been installed therefore this set of results were unusable. This in total was a downtime of 5 hours.

During running the pump test 4.01, a rubbing noise was present within the pump. As the pump speed was increased, so did the noise and the diffuser was heating up. The pump test was terminated immediately and the pump was stripped.

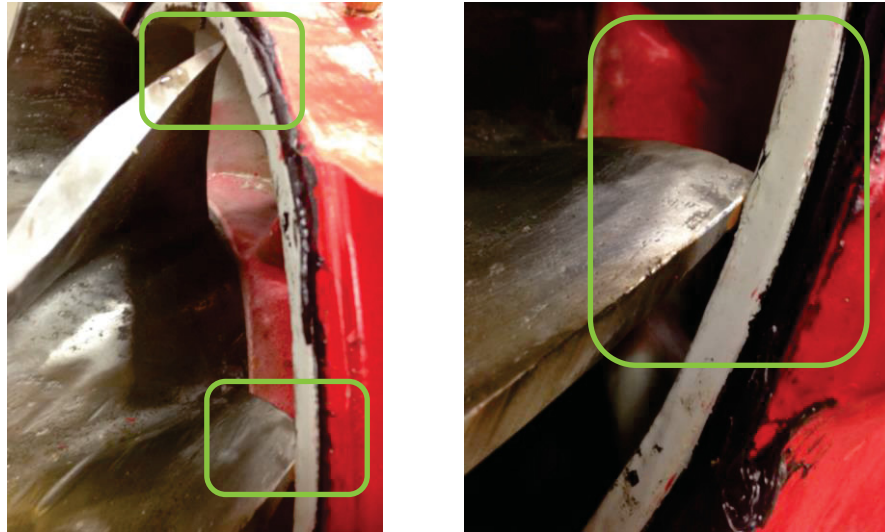


*Figure 237 – Impeller installation with no running gap*

Upon initial visual inspection, it was clear there was no running gap between the impeller and diffuser hubs which is shown in Figure 237. The impeller vane tips were interfering with the inlet shroud face of the diffuser. As the impeller was being reset it was difficult to lock the component onto the shaft. Closer inspection of the assembly found that the collet and fasteners used were for the five vane impeller which was not suitable for the eight vane impeller. With the correct collet and fasteners installed and the running gap set, the pump was rebuilt and the test was run with no issues.

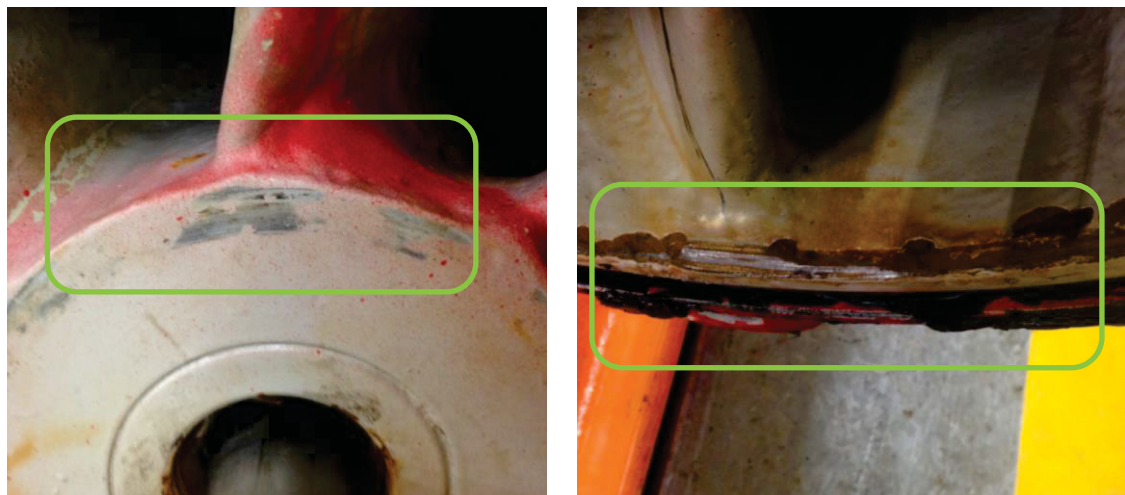


*Figure 238 – Damage to new diffuser*

The above figure shows the rub marks on the diffuser hub and the damage to the internal coating by the impeller tips. Testing down time was, 7 hours.

## Appendix C. Ultrasonic Flow Meter

The flowmeter is NATA calibrated and on loan from *Weir Minerals Australia*. The author has had several years using this flowmeter in the field for pump testing and pumps system analysis.

This type of flowmeter works by using ultrasonic signals to measure the transit time difference between two transducers. The transducers are positioned a set distance apart on one side of the pipe and on the discharge side of the pump. The first transducer emits signals which reflect off the inner wall of the pipe to the second transducer. The signals are also emitted alternatively in and against the flow direction.

The transit time of the signals directed against the flow is shorter than the signals directed with the flow. The transit time difference is measured to determine the average flow velocity of the path of the ultrasonic signals. A flow profile correction is then performed to obtain the area average of the flow velocity, which is proportional to the volume flow.

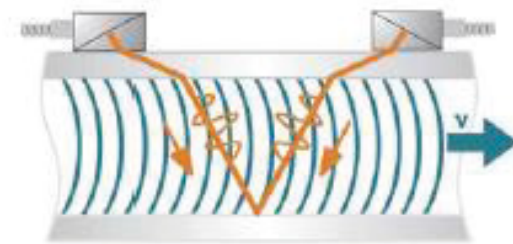


Figure 239 – Path of Ultrasonic Signal (User Manual UMF601V1-1EN Ultrasonic Flowmeter, 2008)

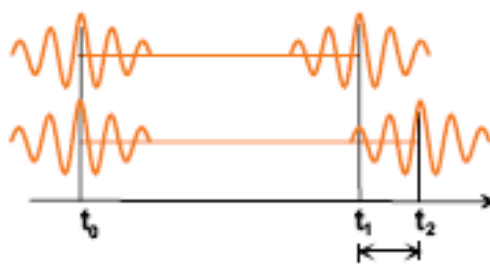
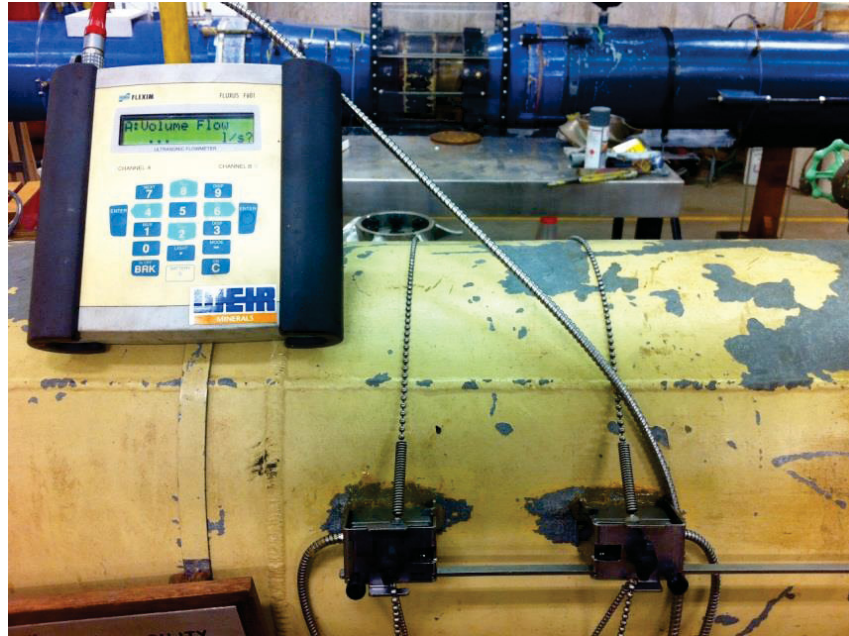


Figure 240 – Transit time difference (User Manual UMF601V1-1EN Ultrasonic Flowmeter, 2008)



*Figure 241 – Ultrasonic flowmeter installation*

To achieve reliable and accurate results, the selection of the measuring position is crucial. The ultrasound measuring position must be positioned on the pipe where there is high amplitude, the pipe is fully filled and the flow is fully developed. The flow must also be free of solids and bubbles. The pipe in the test loop is assembled in the horizontal position, therefore the transducers must be mounted on the side of the pipe, (see Figure 241) to eliminate the possibility of air bubbles on the top of the pipe or solid on the bottom of the pipe interfering with the ultrasonic signals. It is important that the measuring position is at a sufficient distance from any disturbance sources such as bends, valves etc. For this research the position selected is after a bend and before the existing flowmeter<sup>21</sup>. The recommended straight line distance from the bend is 10 times the diameter of the pipe which is 4.18 m and 2.10 m before the flowmeter. However, measuring results can be obtained even if the recommended distance to disturbance sources cannot be observed for practical reasons. Due to experience, using this flowmeter in the field and founding in many cases there is no difference in results by changing the measuring position during testing.

The following pipe and medium parameters are required to be entered into the flowmeter for the selected measuring position. For this research the parameters in green were input:

- Outer Diameter                      418.0 mm
- Wall Thickness                        5.2 mm
- Roughness                             0.1 mm
- Pipe Material                         Carbon Steel

---

<sup>21</sup> The loop has an existing magnetic particle flowmeter, which no longer works but has not been removed for the test loop.

• Lining	Without lining
• Medium	Water
• Medium Temperature.	24 C
• Fluid pressure	1.00 bar
• Transducer Type	CDM1EZ714273
• Sound Path	2 NU

## C.1. Sound Path

The sound path is the number of ultrasonic waves which are transmitted through the medium. An increased number of waves will increase the accuracy of results but is also dependant on the 'A' distance between the transducers.

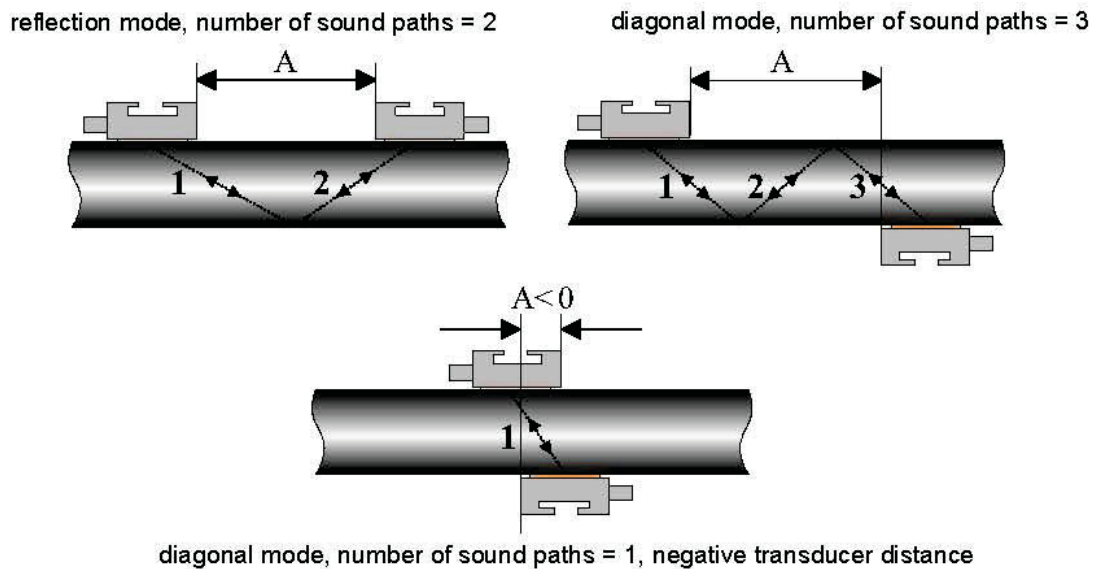
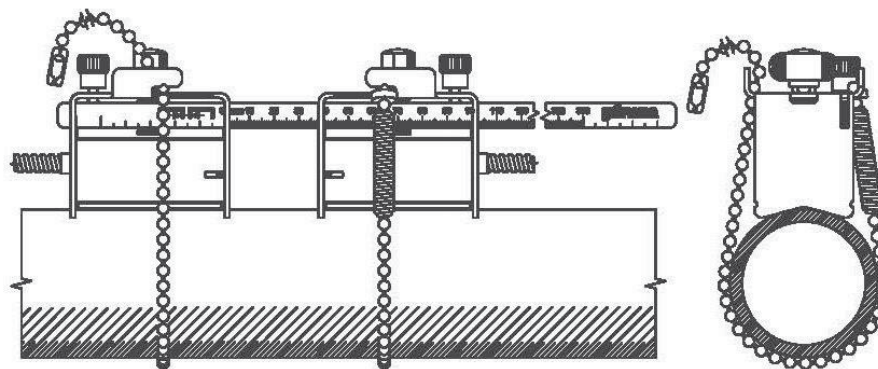


Figure 242 – Flowmeter transducer sound path

The 'A' distance is determined by the pipe parameters and calculated automatically by the flowmeter. For this research a distance of 265.9 mm is calculated using a sound path of 2. A sound path of 2 was selected due to the distance restriction and the difficulty of aligning the transducers on large pipes for an odd number. A ruler and mounting shoes are used for the alignment, (see Figure 243) then chains attach the assembly to the pipe.

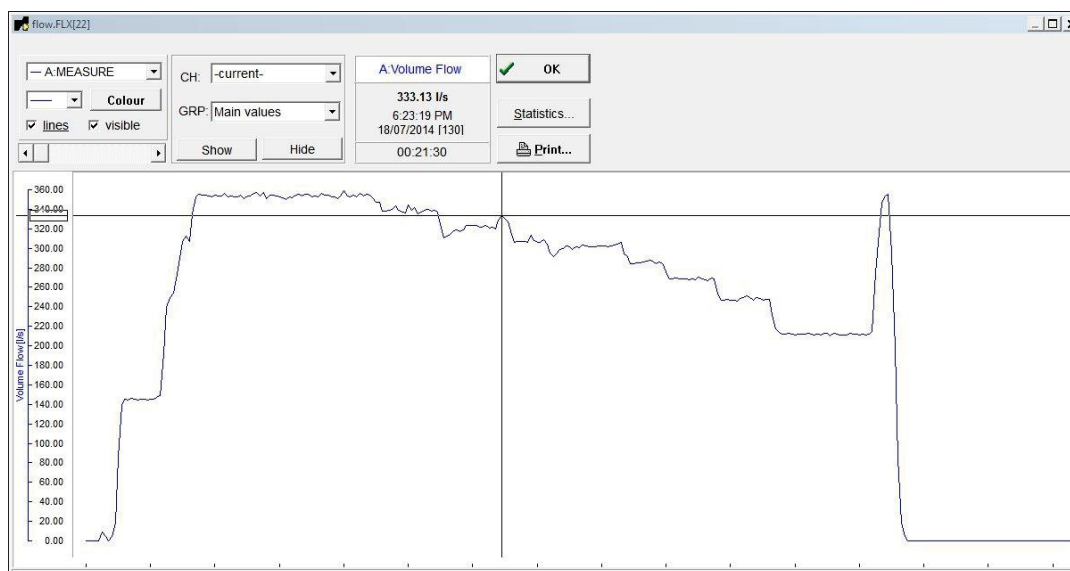
When mounting the transducers, contact on the pipe diameter is important, as elements such as paint and rust will absorb the sound signal. Paint was removed from pipe's OD at the required area to form adequate contact. A lubricant gel is applied to the transducer to ensure there are no air pockets during contact.



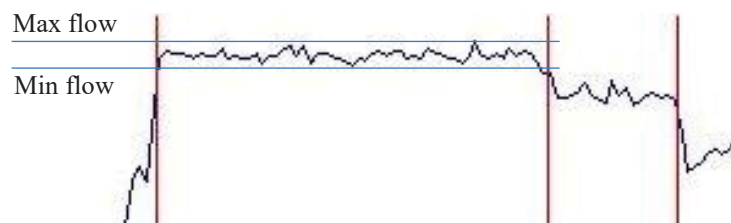
*Figure 243 – Mounting of transducer*

## C.2. Flow Measurement Recording

The flowmeter records and stores the flow data. A time space of 10 seconds was selected for the reading of each data point. The recorded results are transferred to a computer using *FluxData* software. The data recorded for test 1-01 is shown below.

*Figure 244 – Flow data for test 1-01.*

The average between the maximum and minimum flow at each test point is used in the final test results.

*Figure 245 – Test point 1, test 1-01*



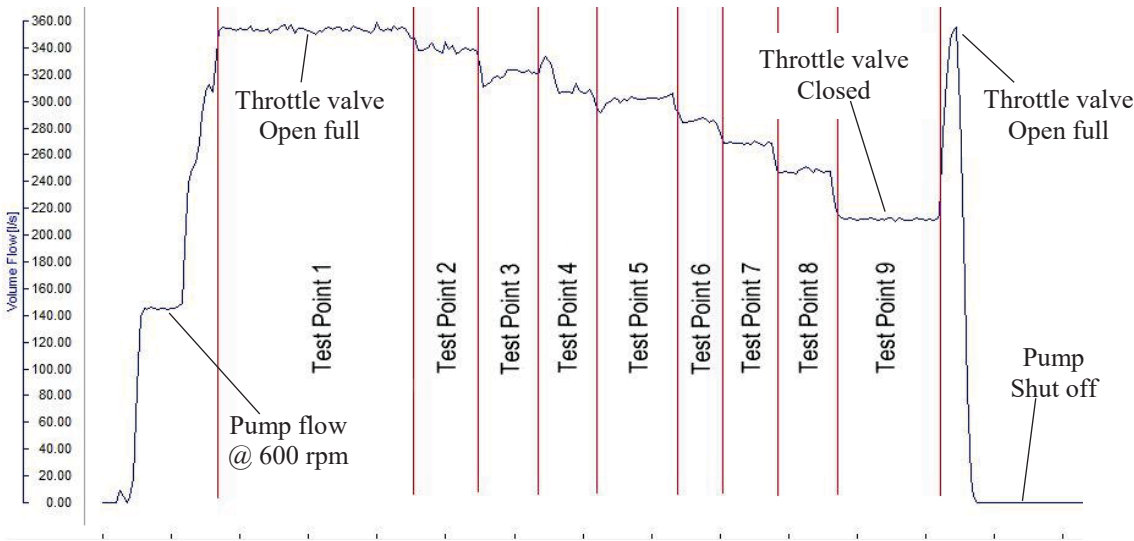


Figure 246 – Flow results test points for test 1-01

# Appendix D. Laboratory Test Data

## D.1. Pump Tests 1

### D.1.1. Tests 1.01 and 1.02

Pump tests 1.01 and 1.02 were performed on the standard pump design with a five vane impeller using the original laboratory test rig with the ultrasonic flow meter (see Appendix C). Due to the test loop being refurbished with updated measurement equipment fitted these test were not used in the final research analysis.

PUMP TEST SHEET (Speed Correction)																	
**** PUMP TESTING CARRIED OUT IN ACCORDANCE WITH AS 2417 Part 2 Class C****																	
PUMP TYPE/SIZE: APPLICATION:			Ornel 300AX 0			PUMP SERIAL No:			DATE: 18-Jul-14								
DUTY POINT																	
VOLUMETRIC FLOW			TOTAL HEAD			PUMP INPUT POWER			PUMP EFFICIENCY			NPSHR			PUMP SPEED		
318.0 L/s 1144.8 m³/hr			8.60 m 84 kPa			37 kW			84 %			10 m			1465 r.p.m.		
Recorded Data									Speed Corrected Data								
PT.	VOL. FLOW (L/s)	VOL. FLOW (m³/hr)	TOTAL HEAD (m)	TOTAL HEAD (kPa)	PUMP POWER INPUT (kW)	PUMP POWER INPUT (hp)	PUMP EFF. (%)	PUMP SPEED (r.p.m.)	VOL. FLOW (L/s)	VOL. FLOW (m³/hr)	TOTAL HEAD (m)	TOTAL HEAD (kPa)	PUMP POWER INPUT (kW)	PUMP POWER INPUT (hp)	PUMP EFF. (%)	PUMP SPEED (r.p.m.)	
1	359.20	1293.1	3.7	36	22.5	30.2	57.8	1465	359.20	1293.1	3.7	36	22.5	30.2	57.8	1465	
2	344.40	1239.8	4.9	48	25.5	34.3	65.1	1465	344.40	1239.8	4.9	48	25.5	34.3	65.1	1465	
3	323.90	1166.0	6.0	58	27.8	37.3	67.9	1465	323.90	1166.0	6.0	58	27.8	37.3	67.9	1465	
4	313.60	1129.0	7.1	69	30.1	40.3	72.3	1465	313.60	1129.0	7.1	69	30.1	40.3	72.3	1465	
5	306.30	1102.7	7.4	72	30.8	41.3	71.9	1465	306.30	1102.7	7.4	72	30.8	41.3	71.9	1465	
6	287.90	1036.4	8.4	82	32.3	43.3	73.3	1465	287.90	1036.4	8.4	82	32.3	43.3	73.3	1465	
7	270.60	974.2	9.5	93	33.8	45.3	74.7	1465	270.60	974.2	9.5	93	33.8	45.3	74.7	1465	
8	251.40	905.0	10.3	101	35.3	47.4	72.1	1465	251.40	905.0	10.3	101	35.3	47.4	72.1	1465	
9	213.10	767.2	10.5	103	35.3	47.4	62.3	1465	213.10	767.2	10.5	103	35.3	47.4	62.3	1465	
10																	
11																	
S.G. 1.0000									Original system curve S.G. 1.0000								

Table 22 – Pump test 1.01

PUMP TEST SHEET (Speed Correction)																			
**** PUMP TESTING CARRIED OUT IN ACCORDANCE WITH AS 2417 Part 2 Class C****																			
PUMP TYPE/SIZE: APPLICATION:				Ornel 300AX 0				PUMP SERIAL No: 1.02				DATE: 30-Jul-14							
DUTY POINT																			
VOLUMETRIC FLOW				TOTAL HEAD				PUMP INPUT POWER				PUMP EFFICIENCY				NPSHR		PUMP SPEED	
318.0 L/s 1144.8 m³/hr				8.60 m 84 kPa				37 kW				84 %				10 m		1465 r.p.m.	
Recorded Data									Speed Corrected Data										
PT.		(m³/hr)	TOTAL HEAD (m)	TOTAL HEAD (kPa)	PUMP POWER INPUT (kW)	PUMP POWER INPUT (hp)	PUMP EFF. (%)	PUMP SPEED (r.p.m.)	VOL. FLOW (L/s)	VOL. FLOW (m³/hr)	TOTAL HEAD (m)	TOTAL HEAD (kPa)	PUMP POWER INPUT (kW)	PUMP POWER INPUT (hp)	PUMP EFF. (%)	PUMP SPEED (r.p.m.)			
1	351.50	370.5	3.2	31	22.5	30.2	48.8	1465	351.50	1265.4	3.2	31	22.6	30.3	48.8	1465			
2	331.70	387.5	3.5	34	24.0	32.2	47.3	1465	331.70	1194.1	3.5	34	24.1	32.3	47.3	1465			
3	321.90	367.0	4.9	48	26.3	35.3	59.1	1465	321.90	1158.8	4.9	49	26.4	35.3	59.1	1465			
4	305.60	367.0	5.7	55	27.8	37.3	60.8	1465	305.60	1100.2	5.7	56	27.9	37.4	60.8	1465			
5	302.70	375.5	6.9	67	30.1	40.3	67.8	1465	302.70	1089.7	6.9	68	30.1	40.4	67.8	1465			
6	291.70	1050.1	7.7	75	31.6	42.3	69.6	1465	291.70	1050.1	7.7	76	31.6	42.4	69.6	1465			
7	271.90	978.8	8.7	85	33.1	44.3	70.2	1465	271.90	978.8	8.7	86	33.1	44.4	70.2	1465			
8	249.60	898.6	9.8	95	34.6	46.3	68.8	1465	249.60	898.6	9.8	96	34.6	46.5	68.8	1465			
9	213.90	770.0	10.2	99	36.1	48.4	58.9	1465	213.90	770.0	10.2	100	36.2	48.5	58.9	1465			
10																			
11																			
S.G. 0.9976									Original system curve S.G. 1.0000										

Table 23 – Pump test 1.02

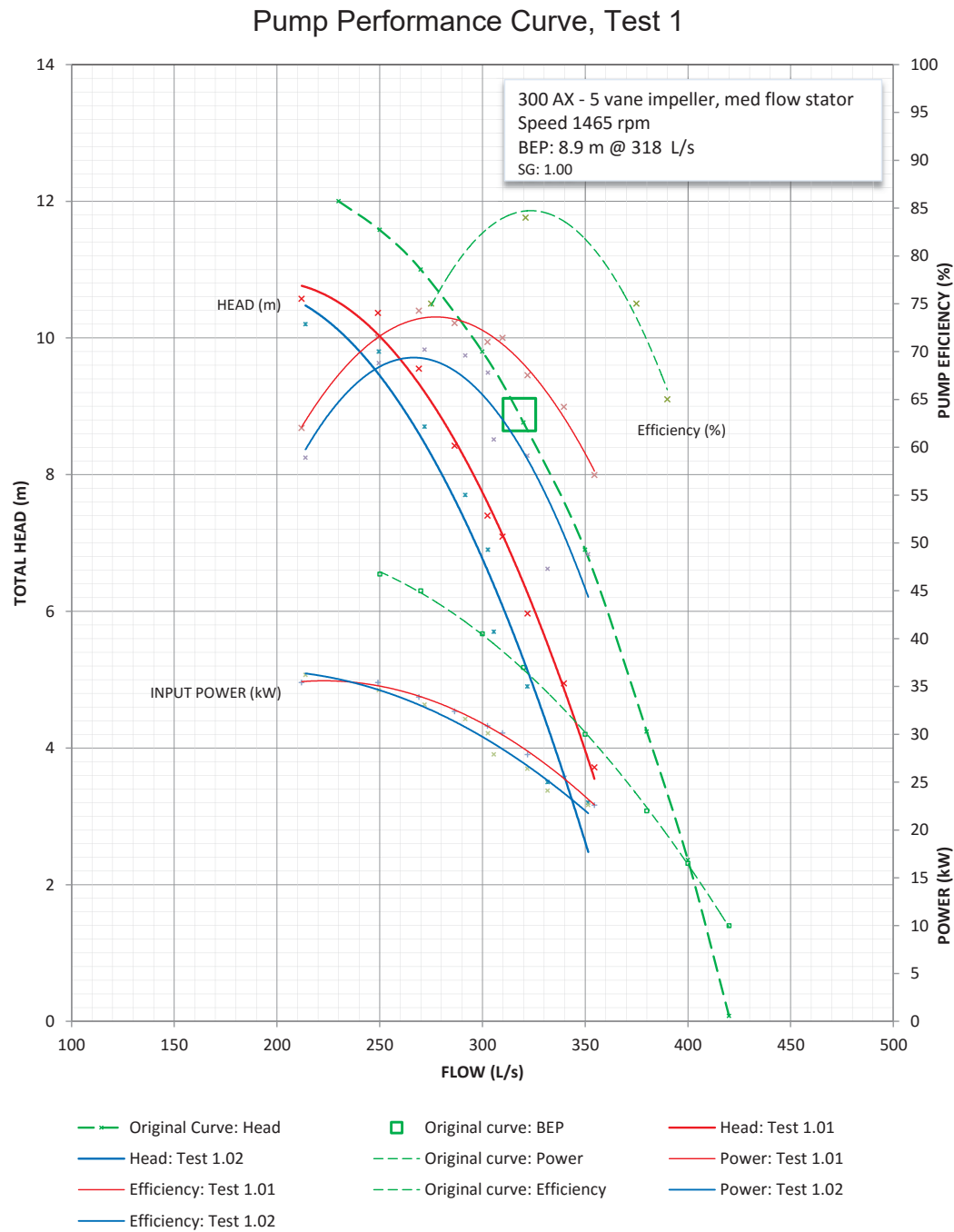


Figure 247 – Test curve, Tests 1-01 and 1-02

### D.1.2. Test 1.03

Pump test number 1.03 was conducted on completion of the refurbishment of the test rig. This was the first full pump test run using the new equipment. This test was performed as part of a laboratory lesson for undergraduate students. The data recorded during the testing was performed by the students, therefore was used only as a comparison for the following laboratory tests. The results were similar to test numbers 1.04 and 1.05.

## Appendix D – Laboratory Test Data

PUMP TEST SHEET (Speed Correction)																	
**** PUMP TESTING CARRIED OUT IN ACCORDANCE WITH AS 2417 Part 2 Class C****																	
Pump Type / Size		Ornel 300AX		Impeller #		5		DATE: 11-May-15									
Stator Type		Med Flow				1.03											
DUTY POINT																	
VOLUMETRIC FLOW				TOTAL HEAD				PUMP INPUT POWER				PUMP EFFICIENCY		NPSHR		PUMP SPEED	
318.0 L/s				8.90 m				37 kW				84 %		10 m		1465 r.p.m.	
1144.8 m³/hr				87 kPa													
Recorded Data									Speed Corrected Data								
PT.	VOL. FLOW (L/s)	VOL. FLOW (m³/hr)	TOTAL HEAD (m)	TOTAL HEAD (kPa)	PUMP POWER INPUT (kW)	PUMP POWER INPUT (hp)	PUMP EFF. (%)	PUMP SPEED (r.p.m.)	VOL. FLOW (L/s)	VOL. FLOW (m³/hr)	TOTAL HEAD (m)	TOTAL HEAD (kPa)	PUMP POWER INPUT (kW)	PUMP POWER INPUT (hp)	PUMP EFF. (%)	PUMP SPEED (r.p.m.)	
1	386.70	0.39	2.3	22	20.7	27.7	42.0	1460	388.02	1396.9	2.3	23	20.9	28.1	42.0	1465	
2	381.20	0.38	2.9	28	21.9	29.4	48.6	1460	382.51	1377.0	2.9	28	22.2	29.8	48.6	1465	
3	374.80	0.37	3.5	34	23.3	31.2	54.8	1459	376.34	1354.8	3.5	35	23.6	31.7	54.8	1465	
4	362.69	0.36	5.5	53	27.0	36.3	71.7	1458	364.43	1312.0	5.5	54	27.5	36.9	71.7	1465	
5	322.86	0.32	7.4	72	30.8	41.3	76.0	1458	324.41	1167.9	7.5	74	31.3	42.0	76.0	1465	
6	249.70	0.25	10.9	106	36.1	48.4	73.5	1456	251.24	904.5	11.0	108	36.8	49.4	73.5	1465	
7																	
8																	
9																	
10																	
11																	
S.G. 0.9976									Original system curve S.G. 1.0000								

Table 24 – Pump test 1.03

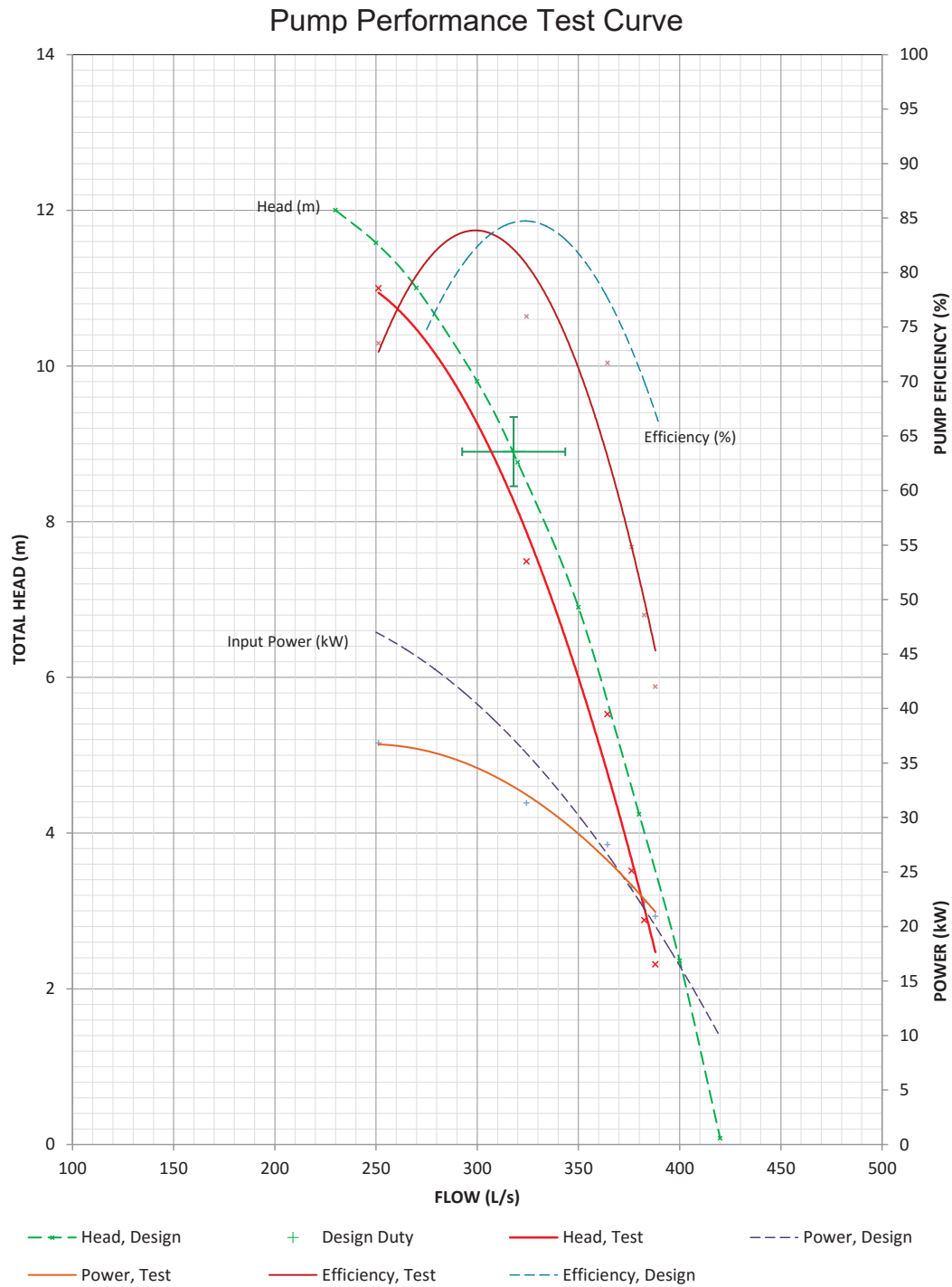


Figure 248 – Pump test curve 1.03

### D.1.3. Tests 1.04 and 1.05

Pump tests numbers 1.04 and 1.05 were used as the first two tests, to be used as base tests. Detailed test result analysis can be found in Section 5.2.1.1.

PUMP TEST SHEET (Speed Correction)														
**** PUMP TESTING CARRIED OUT IN ACCORDANCE WITH AS 2417 Part 2 Class C****														
Pump Type Ornel 300AX			Test Number: 1.04			Date: 20-May-15								
Stator Type Std Stator/Diffuser			No. of Impeller Vanes: 5											
DUTY POINT														
VOLUMETRIC FLOW			TOTAL HEAD			PUMP INPUT POWER		PUMP EFFICIENCY		NPSHR		PUMP SPEED		
318.0 L/s			8.90 m			37 kW		84 %		10 m		1465 r.p.m.		
1144.8 m³/hr			87 kPa											
Recorded Data								Speed Corrected Data						
PT.	Flow		Total Head		Pump Power	Pump Eff.	Pump Speed	Flow		Total Head		Pump Power	PUMP EFF. (%)	PUMP SPEED (r.p.m.)
	(L/s)	(m³/hr)	(m)	(kPa)	(kW)	(%)	(r.p.m.)	(L/s)	(m³/hr)	(m)	(kPa)	(kW)		
1	389.50	370.5	2.3	23	19.5	45.7	1460	390.83	1407.0	2.4	23	19.8	45.7	1465
2	388.70	387.5	2.4	23	20.3	44.9	1460	390.03	1404.1	2.4	24	20.5	44.9	1465
3	381.40	367.0	3.0	29	21.0	53.0	1460	382.71	1377.7	3.0	30	21.3	53.0	1465
4	355.60	367.0	5.1	50	25.5	69.1	1460	356.82	1284.5	5.1	50	25.9	69.1	1465
5	315.15	375.5	8.0	78	30.4	80.6	1458	316.66	1140.0	8.0	79	30.9	80.6	1465
6	248.40	376.5	11.1	109	33.8	79.7	1457	249.76	899.2	11.2	110	34.5	79.7	1465
7	207.50	377.5	11.6	113	34.6	67.9	1457	208.64	751.1	11.7	115	35.2	67.9	1465
8														
9														
10														
S.G. 0.9976								Original system curve S.G. 1.0000						

Table 25 – Pump test results 1.04

PUMP TEST SHEET (Speed Correction)														
**** PUMP TESTING CARRIED OUT IN ACCORDANCE WITH AS 2417 Part 2 Class C****														
Pump Type Ornel 300AX					Test Number: 1.05					Date: 29-May-15				
Stator Type Std Stator/Diffuser					No. of Impeller Vanes: 5									
DUTY POINT														
VOLUMETRIC FLOW			TOTAL HEAD			PUMP INPUT POWER		PUMP EFFICIENCY		NPSHR		PUMP SPEED		
318.0 L/s			8.90 m			37 kW		84 %		10 m		1465 r.p.m.		
1144.8 m³/hr			87 kPa											

Recorded Data								Speed Corrected Data						
PT.	Flow		Total Head		Pump Power	Pump Eff.	Pump Speed	Flow		Total Head		Pump Power	Pump Eff.	Pump Speed
	(L/s)	(m³/hr)	(m)	(kPa)	(kW)	(%)	(r.p.m.)	(L/s)	(m³/hr)	(m)	(kPa)	(kW)	(%)	(r.p.m.)
1	391.7	370.5	2.3	22	19.2	45.1	1460	393.1	1415.0	2.3	22	19.4	45.1	1465
2	391.2	387.5	2.3	22	19.9	43.5	1461	392.3	1412.2	2.3	22	20.1	43.5	1465
3	383.2	367.0	3.0	29	21.0	53.1	1460	384.5	1384.2	3.0	29	21.3	53.1	1465
4	357.8	367.0	4.9	48	25.2	68.6	1460	359.0	1292.5	5.0	49	25.5	68.6	1465
5	323.0	375.5	7.4	72	29.7	78.9	1458	324.6	1168.4	7.5	74	30.2	78.9	1465
6	274.5	376.5	10.3	101	33.4	82.6	1457	276.0	993.7	10.4	102	34.1	82.6	1465
7	230.1	377.5	11.4	111	34.6	73.9	1457	231.4	832.9	11.5	113	35.2	73.9	1465
8														
9														
10														
S.G. 0.9976								Original system curve S.G. 1.0000						

Table 26 – Pump test results 1.05



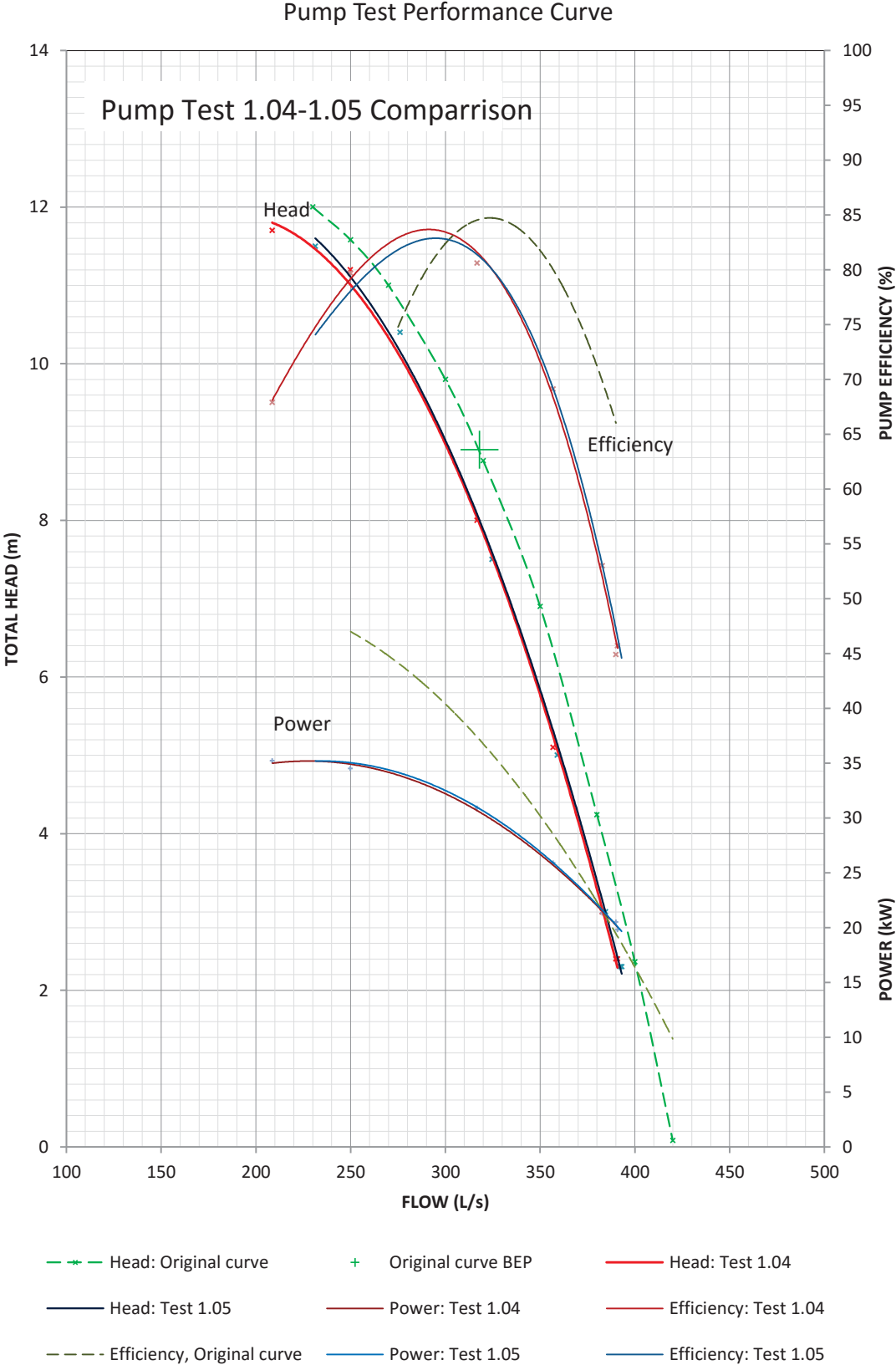


Figure 249 - Comparison of pump tests 1.04 and 1.05

## D.1.4. Tests 2.02 and 2.03

Pump test numbers 2.02 and 2.03 are to determine the base set of results for the eight vane impeller pump configuration.

PUMP TEST SHEET (Speed Correction)													
**** PUMP TESTING CARRIED OUT IN ACCORDANCE WITH AS 2417 Part 2 Class C****													
Pump Type		Ornel 300AX		Test Number:		2.02		Date:		10-Feb-16			
Stator Type		Std Stator/Diffuser		No. of Impeller Vanes:		8							
DUTY POINT													
VOLUMETRIC FLOW			TOTAL HEAD			PUMP INPUT POWER		PUMP EFFICIENCY		NPSHR		PUMP SPEED	
565.0 L/s			9.00 m			37 kW		84 %		10 m		1465 r.p.m.	
2034.0 m³/hr			88 kPa										

Recorded Data								Speed Corrected Data						
PT.	Flow		Total Head		Pump Power	Pump Eff.	Pump Speed	Flow		Total Head		Pump Power	Pump Eff.	Pump Speed
	(L/s)	(m³/hr)	(m)	(kPa)	(kW)	(%)	(r.p.m.)	(L/s)	(m³/hr)	(m)	(kPa)	(kW)	(%)	(r.p.m.)
1	599.3	2157.5	5.3	52	51.8	60.1	1452	604.7	2176.8	5.4	53	53.4	60.1	1465
2	594.5	2140.2	5.3	52	52.6	58.8	1451	600.2	2160.8	5.4	53	54.3	58.8	1465
3	563.9	2029.9	7.0	68	55.6	69.0	1451	569.3	2049.4	7.1	70	57.4	69.0	1465
4	524.5	1888.0	8.5	83	60.9	71.5	1449	530.2	1908.9	8.7	85	63.0	71.5	1465
5	479.1	1724.9	10.3	101	65.4	74.0	1447	485.1	1746.3	10.6	104	68.0	74.0	1465
6	357.7	1287.7	11.9	116	64.6	64.2	1448	361.9	1302.8	12.2	119	67.1	64.2	1465
7														
8														
9														
10														
S.G. 0.9976								Original system curve S.G. 1.0000						

Table 27 - Pump test results 2.02

PUMP TEST SHEET (Speed Correction)														
**** PUMP TESTING CARRIED OUT IN ACCORDANCE WITH AS 2417 Part 2 Class C****														
Pump Type		Ornel 300AX		Test Number:		2.03		Date:		10-Feb-16				
Stator Type		Std Stator/Diffuser		No. of Impeller Vanes:		8								
DUTY POINT														
VOLUMETRIC FLOW			TOTAL HEAD			PUMP INPUT POWER		PUMP EFFICIENCY		NPSHR		PUMP SPEED		
565.0 L/s			9.00 m			37 kW		84 %		10 m		1465 r.p.m.		
2034.0 m³/hr			88 kPa											
Recorded Data								Speed Corrected Data						
PT.	Flow		Total Head		Pump Power	Pump Eff.	Pump Speed	Flow		Total Head		Pump Power	Pump Eff.	Pump Speed
	(L/s)	(m³/hr)	(m)	(kPa)	(kW)	(%)	(r.p.m.)	(L/s)	(m³/hr)	(m)	(kPa)	(kW)	(%)	(r.p.m.)
1	599.4	370.5	5.3	52	51.8	60.1	1453	604.4	2175.7	5.4	53	53.3	60.1	1465
2	597.8	387.5	5.4	53	52.6	60.2	1458	600.7	2162.4	5.5	54	53.5	60.2	1465
3	566.0	367.0	6.8	66	56.4	66.3	1451	571.5	2057.3	6.9	68	58.1	66.3	1465
4	521.4	367.0	8.5	83	61.6	70.2	1450	526.8	1896.5	8.7	85	63.7	70.2	1465
5	468.5	375.5	10.3	101	64.6	73.2	1447	474.3	1707.4	10.6	104	67.2	73.2	1465
6	358.3	376.5	11.2	109	63.9	61.2	1448	362.5	1305.0	11.4	112	66.3	61.2	1465
7														
8														
9														
10														
S.G. 0.9976								Original system curve S.G. 1.0000						

Table 28 - Pump test results 2.03

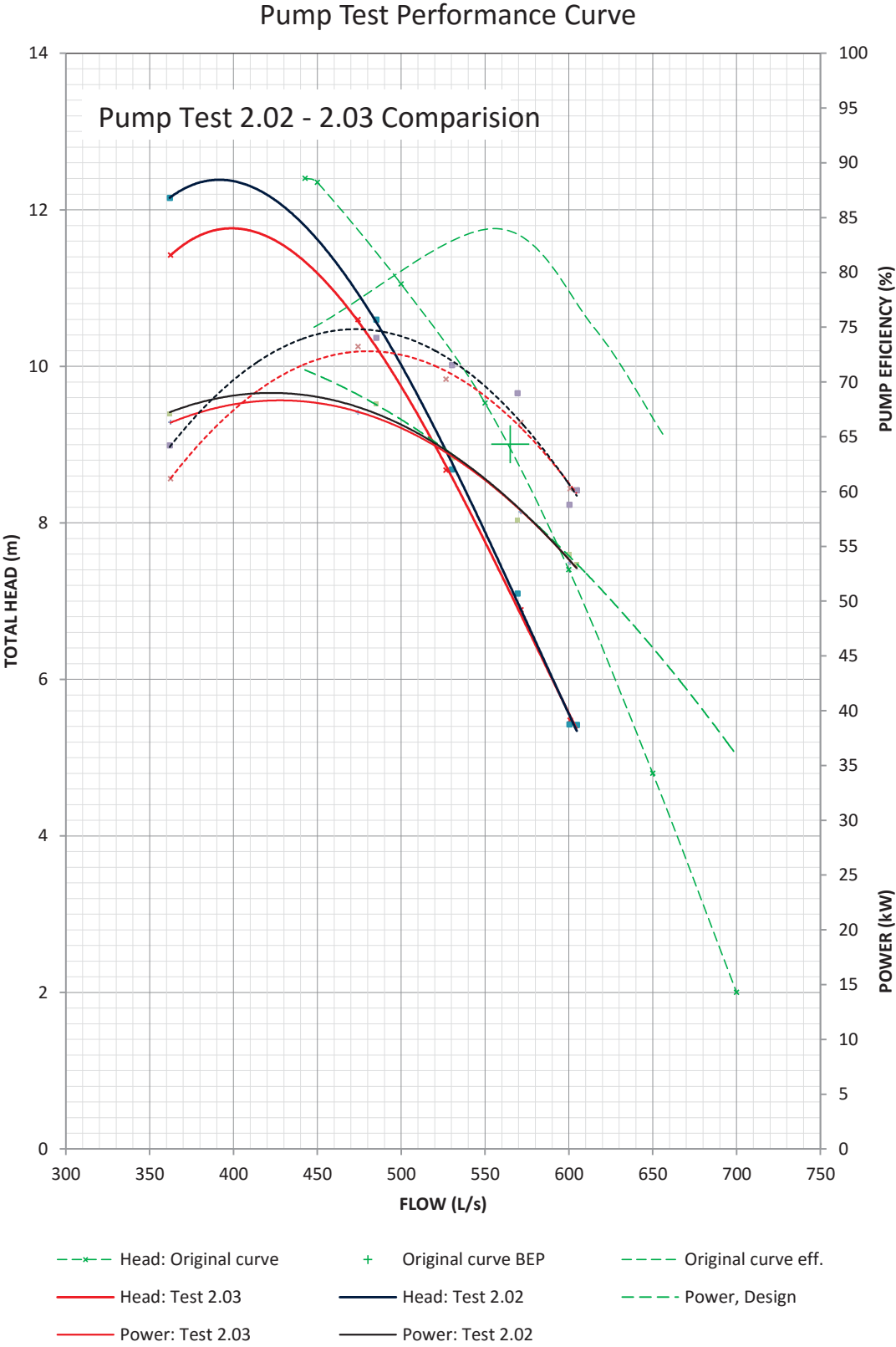


Figure 250 - Comparison of pump tests 2.02 and 2.03

The above test curve is the comparison tests of 2.02, 2.03 and the OEM pump curve. From the two tests, number 2.02 has the best set of results.

## D.1.5. Tests 3.01 and 3.02

The five vane impeller tests results with the new diffuser are shown below. The pump curve test number 3.02 had the best results, with both test results being very close.

PUMP TEST SHEET (Speed Correction)														
**** PUMP TESTING CARRIED OUT IN ACCORDANCE WITH AS 2417 Part 2 Class C****														
Pump Type		Ornel 300AX		Test Number:		3.01		Date:		31-Mar-16				
Stator Type		New Diffuser		No. of Impeller Vanes:		5								
DUTY POINT														
VOLUMETRIC FLOW			TOTAL HEAD			PUMP INPUT POWER		PUMP EFFICIENCY		NPSHR		PUMP SPEED		
318.0 L/s			8.90 m			37 kW		84 %		10 m		1465 r.p.m.		
1144.8 m³/hr			87 kPa											
Recorded Data								Speed Corrected Data						
PT.	Flow		Total Head		Pump Power	Pump Eff.	Pump Speed	Flow		Total Head		Pump Power	Pump Eff.	Pump Speed
	(L/s)	(m³/hr)	(m)	(kPa)	(kW)	(%)	(r.p.m.)	(L/s)	(m³/hr)	(m)	(kPa)	(kW)	(%)	(r.p.m.)
1	383.3	1379.7	2.4	23	21.8	40.9	1460	384.6	1384.4	2.4	24	22.1	40.9	1465
2	382.7	1377.6	2.4	24	21.8	42.0	1460	384.0	1382.3	2.5	24	22.1	42.0	1465
3	377.2	1357.7	3.0	29	22.5	48.9	1459	378.7	1363.3	3.0	30	22.9	48.9	1465
4	361.3	1300.6	3.8	37	24.8	53.5	1459	362.8	1306.0	3.8	37	25.2	53.5	1465
5	341.4	1229.0	5.4	53	27.8	65.2	1458	343.0	1234.9	5.5	54	28.3	65.2	1465
6	309.8	1115.1	7.6	74	31.6	73.0	1458	311.2	1120.5	7.7	75	32.1	73.0	1465
7	282.5	1017.0	9.3	91	33.8	75.9	1457	284.1	1022.6	9.4	92	34.5	75.9	1465
8														
9														
10														
S.G. 0.9976								Original system curve S.G. 1.0000						

Table 29 - Pump test results 3.01

PUMP TEST SHEET (Speed Correction)														
**** PUMP TESTING CARRIED OUT IN ACCORDANCE WITH AS 2417 Part 2 Class C****														
Pump Type		Ornel 300AX		Test Number:		3.02		Date:		31-Mar-16				
Stator Type		New Diffuser		No. of Impeller Vanes:		5								
DUTY POINT														
VOLUMETRIC FLOW			TOTAL HEAD			PUMP INPUT POWER		PUMP EFFICIENCY		NPSHR		PUMP SPEED		
318.0 L/s			8.90 m			37 kW		84 %		10 m		1465 r.p.m.		
1144.8 m³/hr			87 kPa											
Recorded Data							Speed Corrected Data							
PT.	Flow		Total Head		Pump Power	Pump Eff.	Pump Speed	Flow		Total Head		Pump Power	Pump Eff.	Pump Speed
	(L/s)	(m³/hr)	(m)	(kPa)	(kW)	(%)	(r.p.m.)	(L/s)	(m³/hr)	(m)	(kPa)	(kW)	(%)	(r.p.m.)
1	378.6	1362.9	2.3	22	22.2	38.3	1460	379.9	1367.5	2.3	23	22.4	38.3	1465
2	378.3	1362.0	2.4	23	22.5	38.8	1460	379.6	1366.7	2.4	23	22.8	38.8	1465
3	371.3	1336.6	3.0	29	23.3	46.0	1459	372.8	1342.1	3.0	29	23.6	46.0	1465
4	363.2	1307.7	3.7	37	24.8	53.5	1459	364.7	1313.0	3.8	37	25.2	53.5	1465
5	343.5	1236.6	5.4	53	27.8	65.2	1458	345.1	1242.5	5.5	54	28.3	65.2	1465
6	311.7	1122.2	7.6	74	31.6	73.5	1457	313.4	1128.3	7.7	76	32.2	73.5	1465
7	279.1	1004.8	9.5	93	33.8	77.0	1456	280.8	1011.0	9.7	95	34.5	77.0	1465
8														
9														
10														
S.G. 0.9976							Original system curve S.G. 1.0000							

Table 30 - Pump test results 3.02

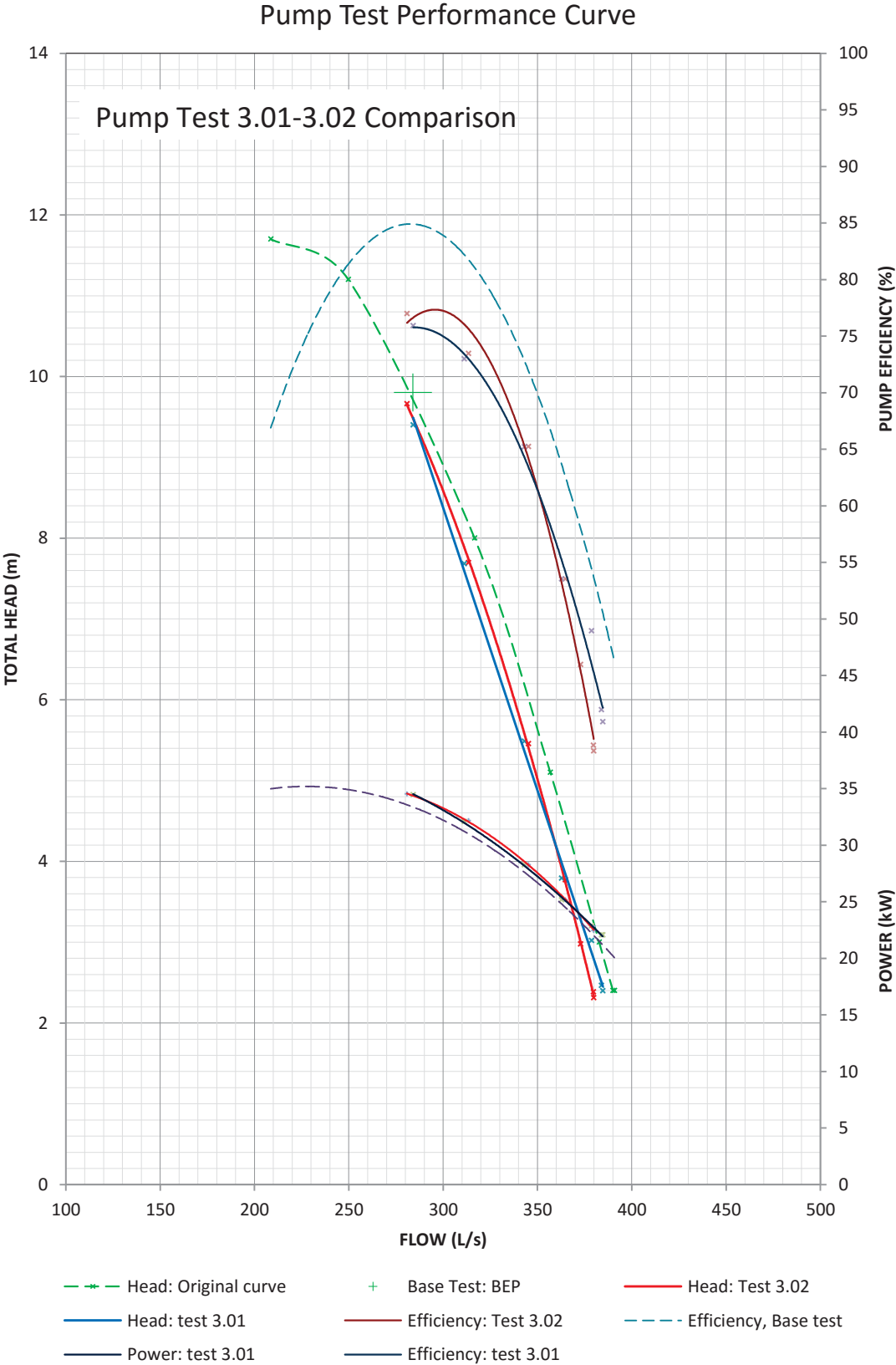


Figure 251 - Comparison of pump tests 3.01 and 3.02

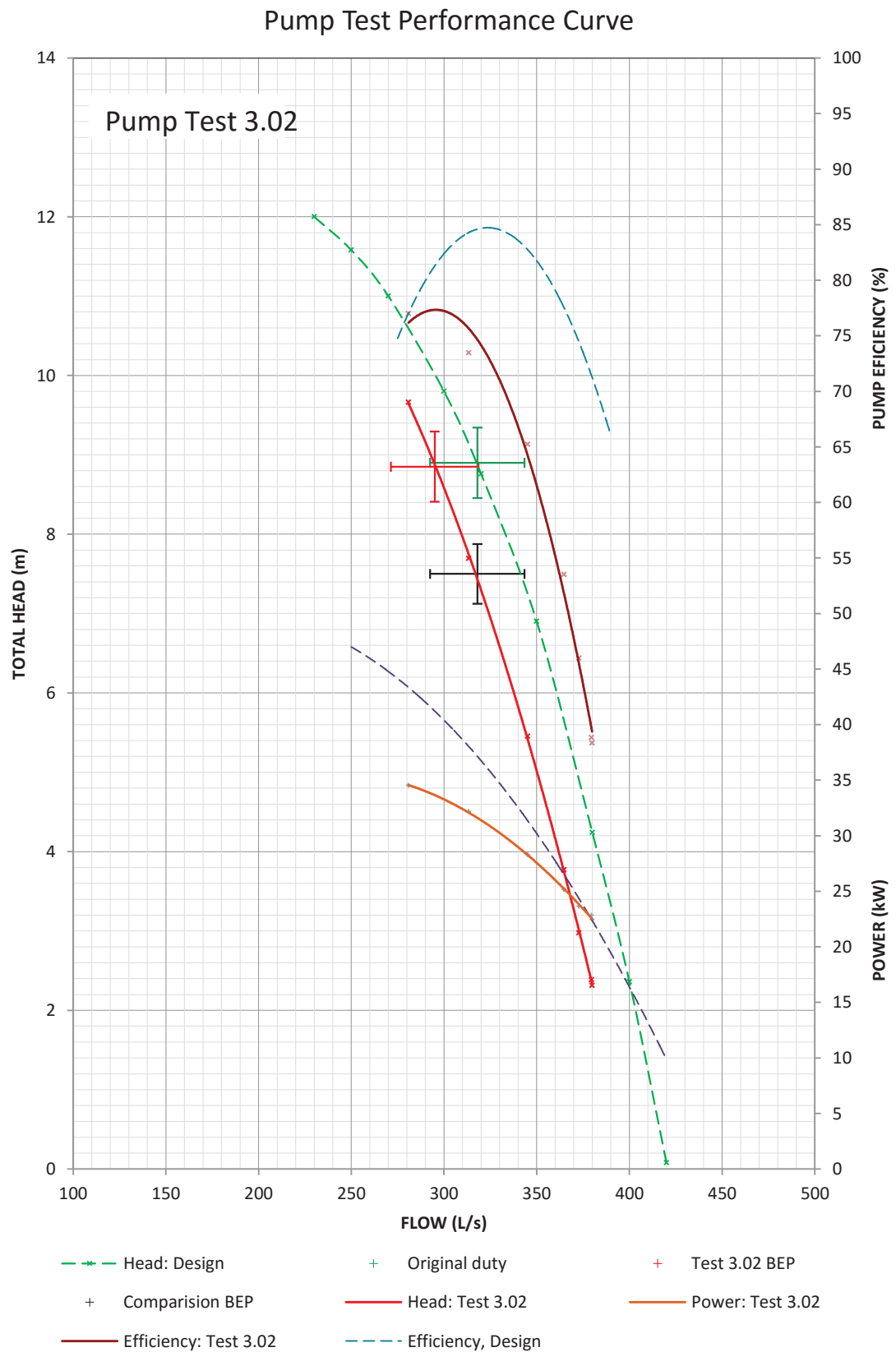


Figure 252 - Test 3.02 performance curve compare to original design.



## D.1.6. Tests 4.01 and 4.02

PUMP TEST SHEET (Speed Correction)														
**** PUMP TESTING CARRIED OUT IN ACCORDANCE WITH AS 2417 Part 2 Class C****														
Pump Type		Ornel 300AX		Test Number:		4.01		Date:		11-May-16				
Stator Type		New Diffuser		No. of Impeller Vanes:		8								
DUTY POINT														
VOLUMETRIC FLOW			TOTAL HEAD			PUMP INPUT POWER		PUMP EFFICIENCY		NPSHR		PUMP SPEED		
318.0 L/s			8.90 m			37 kW		84 %		10 m		1465 r.p.m.		
1144.8 m³/hr			87 kPa											

Recorded Data								Speed Corrected Data						
PT.	Flow		Total Head		Pump Power	Pump Eff.	Pump Speed	Flow		Total Head		Pump Power	Pump Eff.	Pump Speed
	(L/s)	(m³/hr)	(m)	(kPa)	(kW)	(%)	(r.p.m.)	(L/s)	(m³/hr)	(m)	(kPa)	(kW)	(%)	(r.p.m.)
1	580.7	2090.5	5.2	51	54.1	54.6	1455	584.7	2104.9	5.3	52	55.4	54.6	1465
2	576.7	2076.0	5.3	52	54.5	55.0	1455	580.6	2090.3	5.4	53	55.7	55.0	1465
3	550.1	1980.5	6.7	65	56.4	63.8	1453	554.7	1996.9	6.8	67	57.9	63.8	1465
4	509.5	1834.2	7.7	75	62.4	61.3	1452	514.1	1850.7	7.8	77	64.2	61.3	1465
5	467.0	1681.1	9.6	94	65.4	67.3	1451	471.5	1697.3	9.8	96	67.4	67.3	1465
6	374.5	1348.3	11.5	112	61.6	68.2	1451	378.1	1361.3	11.7	115	63.6	68.2	1465
7	319.9	1151.6	10.7	105	58.6	57.2	1454	322.3	1160.4	10.9	107	60.1	57.2	1465
8														
9														
10														
S.G. 0.9976								Original system curve S.G. 1.0000						

Table 31 - Pump test results 4.01

PUMP TEST SHEET (Speed Correction)														
**** PUMP TESTING CARRIED OUT IN ACCORDANCE WITH AS 2417 Part 2 Class C****														
Pump Type		Ornel 300AX		Test Number:		4.02		Date:		11-May-16				
Stator Type		New Diffuser		No. of Impeller Vanes:		8								
DUTY POINT														
VOLUMETRIC FLOW			TOTAL HEAD			PUMP INPUT POWER		PUMP EFFICIENCY		NPSHR		PUMP SPEED		
318.0 L/s			8.90 m			37 kW		84 %		10 m		1465 r.p.m.		
1144.8 m³/hr			87 kPa											
Recorded Data								Speed Corrected Data						
PT.	Flow		Total Head		Pump Power	Pump Eff.	Pump Speed	Flow		Total Head		Pump Power	Pump Eff.	Pump Speed
	(L/s)	(m³/hr)	(m)	(kPa)	(kW)	(%)	(r.p.m.)	(L/s)	(m³/hr)	(m)	(kPa)	(kW)	(%)	(r.p.m.)
1	579.3	2085.4	5.2	51	54.1	54.8	1455	583.3	2099.8	5.3	52	55.4	54.8	1465
2	573.0	2062.9	5.3	52	54.8	54.3	1454	577.4	2078.5	5.4	53	56.2	54.3	1465
3	544.0	1958.5	6.9	68	58.6	62.7	1453	548.5	1974.7	7.0	69	60.2	62.7	1465
4	519.0	1868.3	8.3	81	60.9	69.3	1452	523.6	1885.1	8.5	83	62.7	69.3	1465
5	472.6	1701.4	10.2	100	63.9	74.1	1451	477.2	1717.8	10.4	103	65.9	74.1	1465
6	385.3	1387.1	11.8	115	64.6	68.6	1450	389.3	1401.4	12.0	118	66.8	68.6	1465
7	322.5	1161.0	11.0	108	58.6	59.4	1453	325.2	1170.6	11.2	110	60.2	59.4	1465
8														
9														
10														
S.G. 0.9976								Original system curve S.G. 1.0000						

Table 32 - Pump test results 4.02

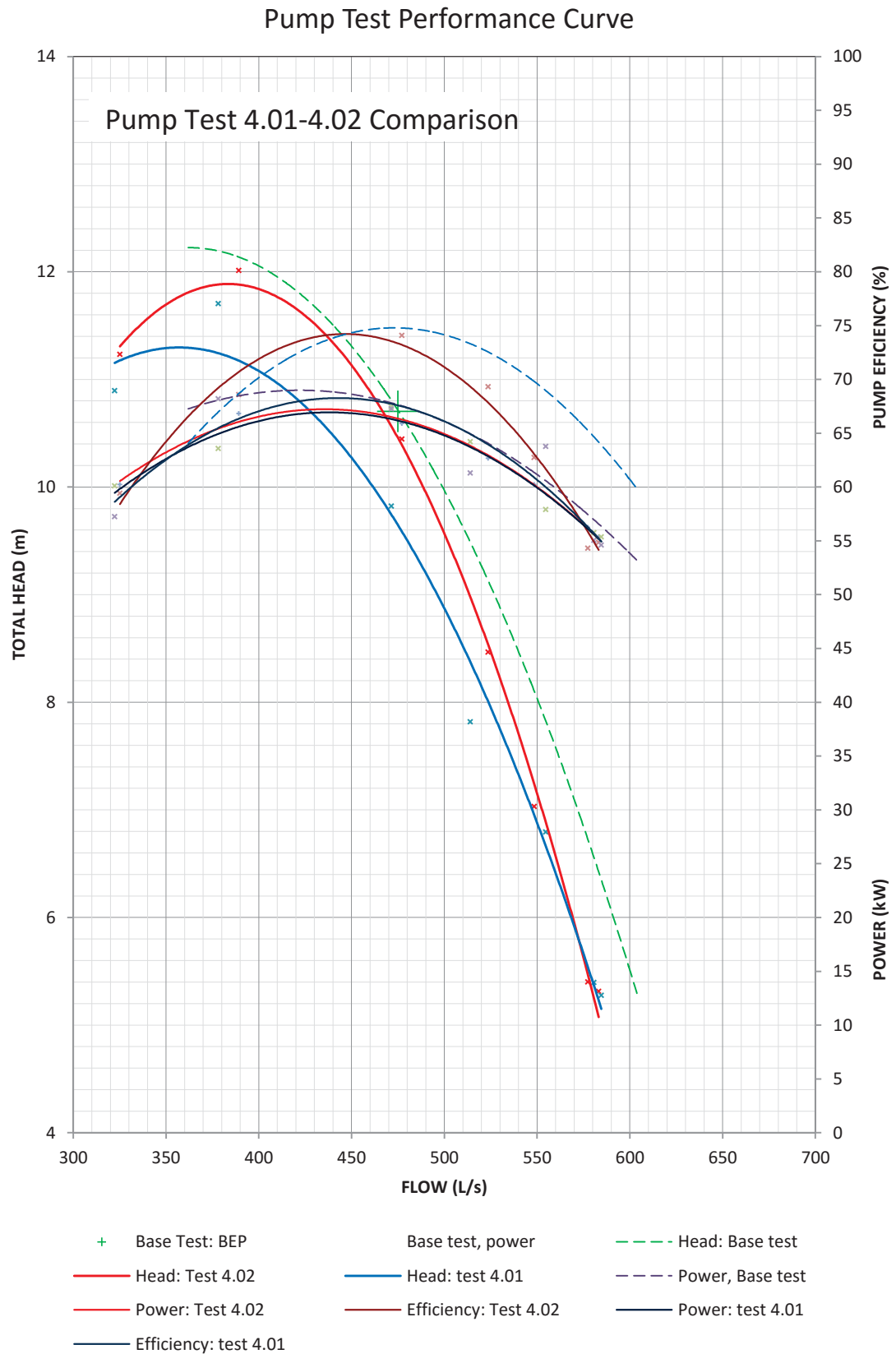


Figure 253 - Comparison of pump tests 4.01 and 4.02

## D.1.7. Tests 4.03 and 4.04

PUMP TEST SHEET (Speed Correction)														
**** PUMP TESTING CARRIED OUT IN ACCORDANCE WITH AS 2417 Part 2 Class C****														
Pump Type		Ornel 300AX			Test Number:		4.03		Date:		11-May-16			
Stator Type		New Diffuser			No. of Impeller Vanes:		8							
DUTY POINT														
VOLUMETRIC FLOW			TOTAL HEAD			PUMP INPUT POWER		PUMP EFFICIENCY		NPSHR		PUMP SPEED		
564.0 L/s			8.90 m			37 kW		84 %		10 m		1465 r.p.m.		
1144.8 m³/hr			87 kPa											

Recorded Data								Speed Corrected Data						
PT.	Flow		Total Head		Pump Power	Pump Eff.	Pump Speed	Flow		Total Head		Pump Power	Pump Eff.	Pump Speed
	(L/s)	(m³/hr)	(m)	(kPa)	(kW)	(%)	(r.p.m.)	(L/s)	(m³/hr)	(m)	(kPa)	(kW)	(%)	(r.p.m.)
1	570.3	2053.2	5.0	49	54.1	51.9	1454	574.6	2068.7	5.1	50	55.5	51.9	1465
2	567.8	2043.9	5.2	51	54.5	52.7	1454	572.0	2059.4	5.3	52	55.9	52.7	1465
3	541.0	1947.6	6.7	66	57.1	62.2	1454	545.1	1962.3	6.8	67	58.5	62.2	1465
4	520.0	1872.0	8.2	81	60.1	69.7	1453	524.3	1887.5	8.4	82	61.8	69.7	1465
5	470.0	1692.0	10.2	100	63.9	73.3	1451	474.5	1708.3	10.4	102	65.9	73.3	1465
6	400.9	1443.2	11.7	115	64.6	71.1	1451	404.8	1457.2	12.0	117	66.7	71.1	1465
7	356.4	1283.0	12.2	120	63.1	67.5	1452	359.6	1294.5	12.5	122	65.0	67.5	1465
8														
9														
10														
S.G. 0.9976								Original system curve S.G. 1.0000						

Table 33 - Pump test results 4.03

PUMP TEST SHEET (Speed Correction)														
**** PUMP TESTING CARRIED OUT IN ACCORDANCE WITH AS 2417 Part 2 Class C****														
Pump Type		Ornel 300AX			Test Number:		4.04		Date:		11-May-16			
Stator Type		New Diffuser			No. of Impeller Vanes:		8							
DUTY POINT														
VOLUMETRIC FLOW			TOTAL HEAD			PUMP INPUT POWER		PUMP EFFICIENCY		NPSHR		PUMP SPEED		
318.0 L/s			8.90 m			37 kW		84 %		10 m		1465 r.p.m.		
1144.8 m³/hr			87 kPa											

Recorded Data								Speed Corrected Data						
PT.	Flow		Total Head		Pump Power	Pump Eff.	Pump Speed	Flow		Total Head		Pump Power	Pump Eff.	Pump Speed
	(L/s)	(m³/hr)	(m)	(kPa)	(kW)	(%)	(r.p.m.)	(L/s)	(m³/hr)	(m)	(kPa)	(kW)	(%)	(r.p.m.)
1	579.0	2084.4	5.3	52	53.3	56.0	1455	583.0	2098.7	5.4	53	54.6	56.0	1465
2	577.4	2078.6	5.3	52	54.1	55.1	1454	581.8	2094.4	5.4	53	55.5	55.1	1465
3	550.2	1980.7	6.7	66	57.1	63.2	1454	554.4	1995.7	6.8	67	58.5	63.2	1465
4	512.7	1845.7	8.7	85	60.9	71.3	1452	517.3	1862.2	8.8	87	62.7	71.3	1465
5	471.4	1697.0	10.5	103	63.1	76.6	1452	475.6	1712.2	10.7	105	65.0	76.6	1465
6	418.1	1505.3	11.8	116	72.9	66.3	1451	422.2	1519.8	12.1	118	75.2	66.3	1465
7	348.9	1256.0	12.3	121	63.1	66.7	1452	352.0	1267.3	12.6	123	65.0	66.7	1465
8														
9														
10														

Table 34 - Pump test results 4.04

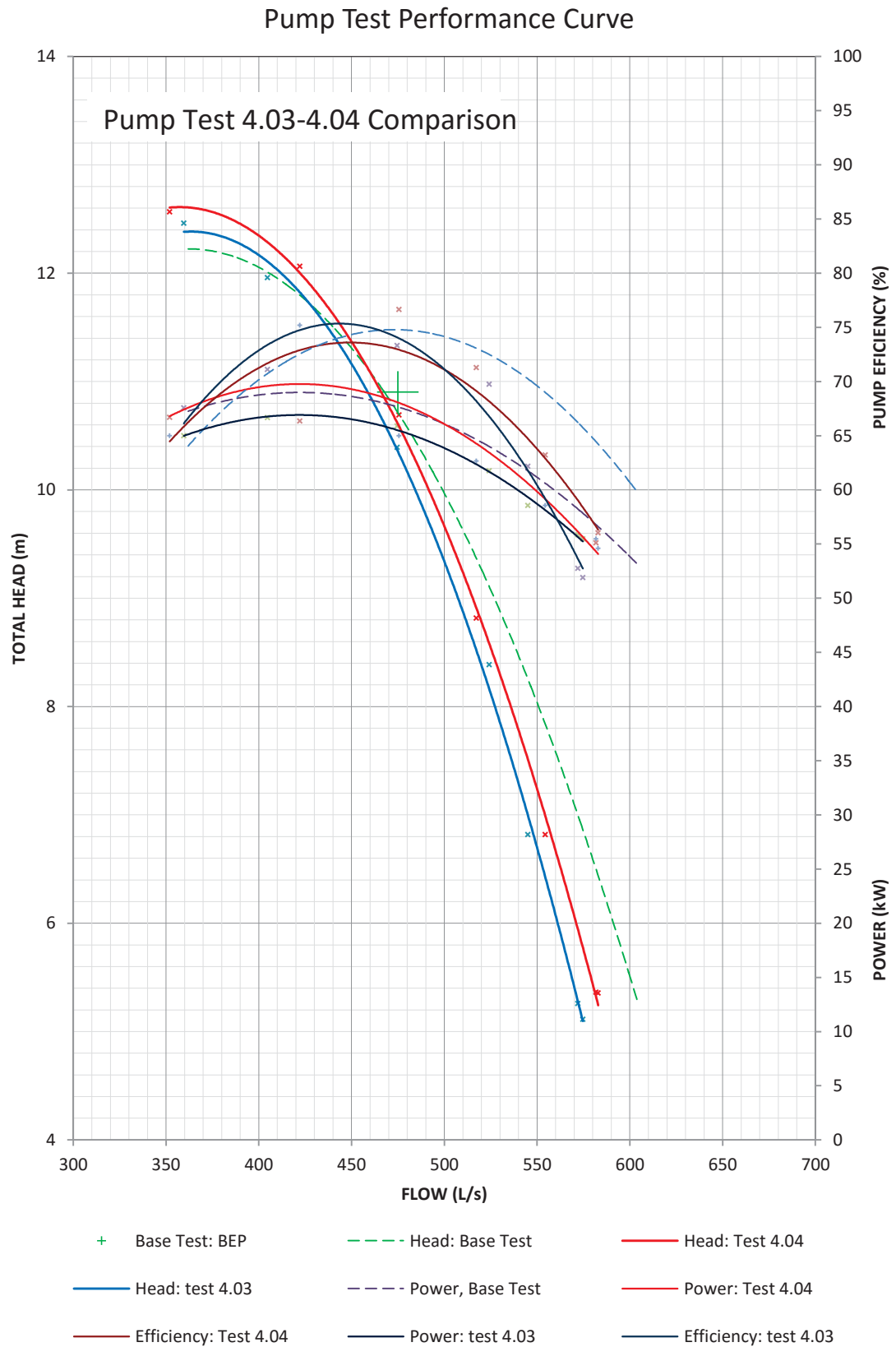


Figure 254 - Comparison of pump tests 4.03 and 4.04

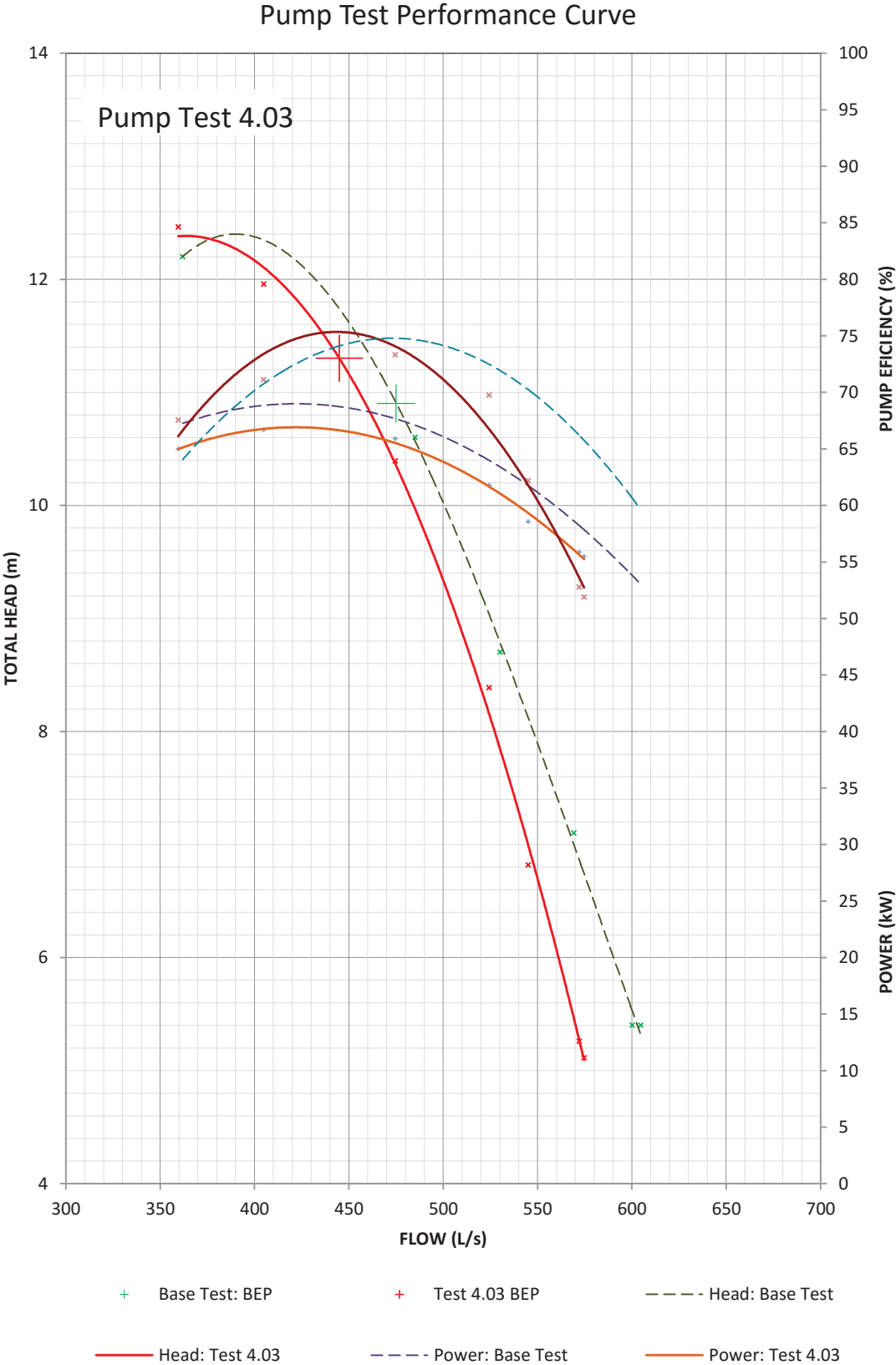


Figure 255 - Test 4.03 performance curve compared to original design curve

## D.1.8. Tests 5.01 and 5.02

PUMP TEST SHEET (Speed Correction)															
**** PUMP TESTING CARRIED OUT IN ACCORDANCE WITH AS 2417 Part 2 Class C****															
Pump Type		Ornel 300AX			Test Number:			5.01		Date:			31-Mar-16		
Stator Type		New Diffuser			No. of Impeller Vanes:			5							
DUTY POINT															
VOLUMETRIC FLOW			TOTAL HEAD			PUMP INPUT POWER		PUMP EFFICIENCY		NPSHR		PUMP SPEED			
318.0 L/s			8.90 m			37 kW		84 %		10 m		1465 r.p.m.			
1144.8 m³/hr			87 kPa												
Recorded Data								Speed Corrected Data							
PT.	Flow		Total Head		Pump Power	Pump Eff.	Pump Speed	Flow		Total Head		Pump Power	Pump Eff.	Pump Speed	
	(L/s)	(m³/hr)	(m)	(kPa)	(kW)	(%)	(r.p.m.)	(L/s)	(m³/hr)	(m)	(kPa)	(kW)	(%)	(r.p.m.)	
1	379.3	1365.3	2.5	25	21.8	42.8	1462	380.0	1368.1	2.5	25	22.0	42.8	1465	
2	378.3	1361.9	2.4	24	22.2	40.3	1461	379.3	1365.6	2.4	24	22.4	40.3	1465	
3	371.1	1336.0	3.0	30	23.3	47.2	1461	372.1	1339.7	3.0	30	23.5	47.2	1465	
4	361.2	1300.3	3.8	37	24.8	54.5	1461	362.2	1303.8	3.8	38	25.1	54.5	1465	
5	342.4	1232.6	5.3	52	27.8	63.6	1460	343.6	1236.9	5.3	52	28.2	63.6	1465	
6	307.9	1108.4	7.5	74	31.9	71.0	1459	309.2	1113.0	7.6	75	32.4	71.0	1465	
7	264.2	951.1	9.8	96	34.6	73.1	1459	265.3	955.0	9.9	97	35.1	73.1	1465	
8	242.8	874.0	10.4	102	34.6	71.4	1459	243.8	877.6	10.5	103	35.1	71.4	1465	
9															
10															
S.G. 0.9976								Original system curve S.G. 1.0000							

Table 35 - Pump test results 5.01

PUMP TEST SHEET (Speed Correction)														
**** PUMP TESTING CARRIED OUT IN ACCORDANCE WITH AS 2417 Part 2 Class C****														
Pump Type Ornel 300AX			Test Number: 5.02			Date: 31-Mar-16								
Stator Type cw Diffuser/back pic			No. of Impeller Vanes: 5											
DUTY POINT														
VOLUMETRIC FLOW			TOTAL HEAD			PUMP INPUT POWER		PUMP EFFICIENCY		NPSHR		PUMP SPEED		
318.0 L/s			8.90 m			37 kW		84 %		10 m		1465 r.p.m.		
1144.8 m³/hr			87 kPa											
Recorded Data								Speed Corrected Data						
PT.	Flow		Total Head		Pump Power	Pump Eff.	Pump Speed	Flow		Total Head		Pump Power	Pump Eff.	Pump Speed
	(L/s)	(m³/hr)	(m)	(kPa)	(kW)	(%)	(r.p.m.)	(L/s)	(m³/hr)	(m)	(kPa)	(kW)	(%)	(r.p.m.)
1	379.9	1367.5	2.4	23	21.4	40.8	1462	380.6	1370.3	2.4	23	21.6	40.8	1465
2	380.0	1367.9	2.5	24	21.4	42.6	1462	380.7	1370.7	2.5	24	21.6	42.6	1465
3	371.5	1337.5	3.2	31	23.3	49.5	1461	372.6	1341.2	3.2	31	23.5	49.5	1465
4	361.5	1301.4	3.9	38	24.8	55.4	1461	362.5	1305.0	3.9	38	25.1	55.4	1465
5	339.0	1220.4	5.5	54	27.8	65.9	1460	340.2	1224.6	5.6	55	28.2	65.9	1465
6	304.2	1095.2	8.0	78	31.9	74.3	1459	305.5	1099.7	8.0	79	32.4	74.3	1465
7	274.4	987.8	9.5	93	34.2	74.6	1459	275.5	991.9	9.6	94	34.7	74.6	1465
8	243.5	876.4	10.3	101	34.9	70.4	1459	244.5	880.0	10.4	102	35.5	70.4	1465
9	233.2	839.6	11.2	109	34.9	72.8	1459	234.2	843.0	11.2	110	35.5	72.8	1465
10														
S.G. 0.9976								Original system curve S.G. 1.0000						

Table 36 - Pump test results 5.02



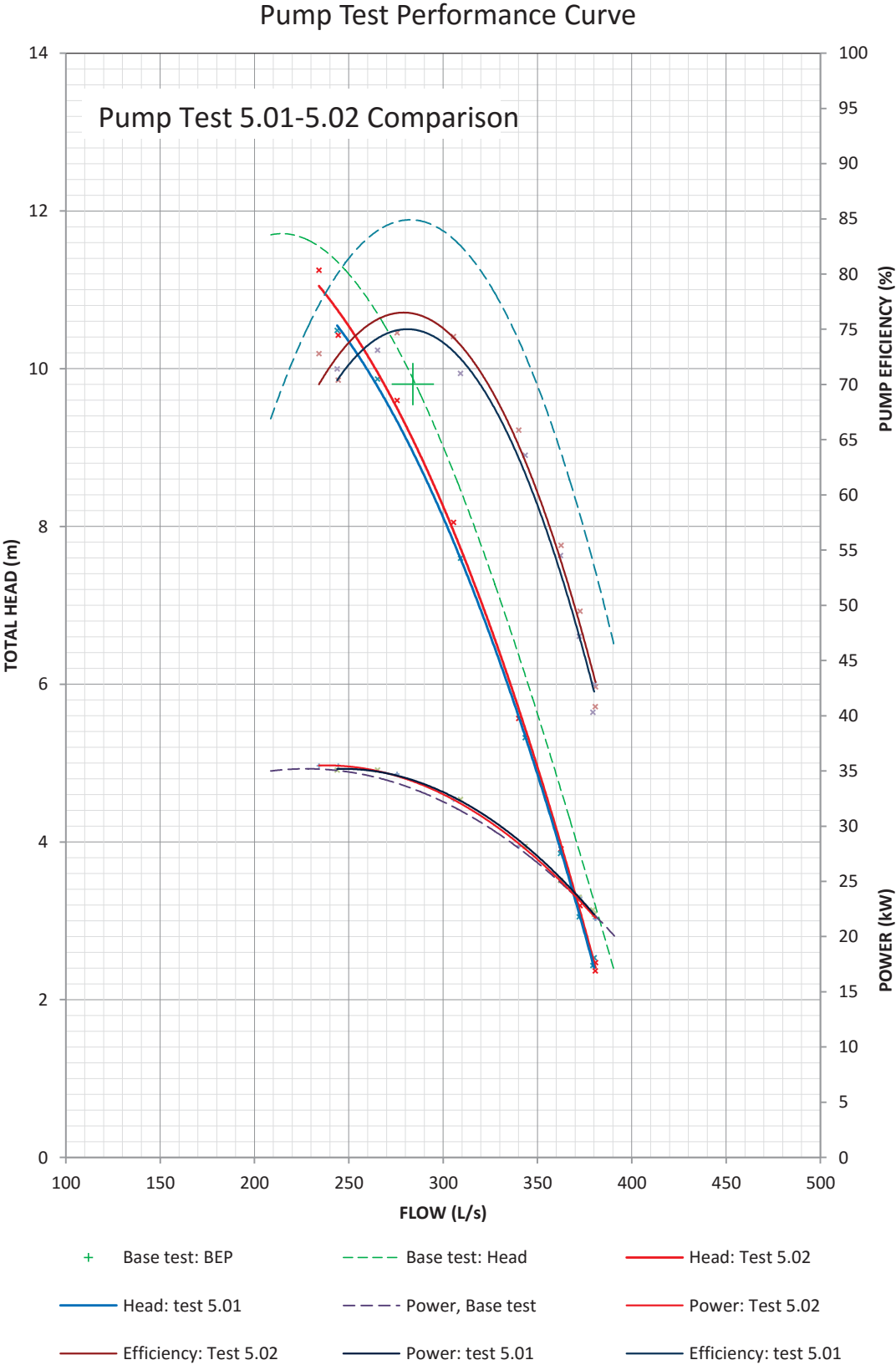


Figure 256 – Comparison of pump tests 5.01 and 5.02

## D.1.9. Tests 6.01, 6.02 and 6.03

PUMP TEST SHEET (Speed Correction)														
**** PUMP TESTING CARRIED OUT IN ACCORDANCE WITH AS 2417 Part 2 Class C****														
Pump Type Ornel 300AX			Test Number: 6.01			Date: 23-May-16								
Stator Type New Diffuser/Back piece			No.of Impeller Vanes: 8											
DUTY POINT														
VOLUMETRIC FLOW			TOTAL HEAD			PUMP INPUT POWER		PUMP EFFICIENCY		NPSHR		PUMP SPEED		
564.0 L/s			8.97 m			37 kW		84 %		10 m		1465 r.p.m.		
2030.4 m³/hr			88 kPa											

Recorded Data								Speed Corrected Data						
PT.	Flow		Total Head		Pump Power	Pump Eff.	Pump Speed	Flow		Total Head		Pump Power	Pump Eff.	Pump Speed
	(L/s)	(m³/hr)	(m)	(kPa)	(kW)	(%)	(r.p.m.)	(L/s)	(m³/hr)	(m)	(kPa)	(kW)	(%)	(r.p.m.)
1	582.7	2097.6	5.3	52	53.3	56.4	1454	587.1	2113.5	5.4	53	54.7	56.4	1465
2	580.7	2090.5	5.4	53	54.1	56.5	1454	585.1	2106.3	5.5	54	55.5	56.5	1465
3	550.1	1980.5	6.9	68	57.1	65.1	1454	554.3	1995.5	7.0	69	58.5	65.1	1465
4	522.8	1882.1	8.6	84	60.1	72.7	1452	527.5	1898.9	8.7	86	61.9	72.7	1465
5	487.4	1754.6	10.1	99	63.1	76.2	1451	492.1	1771.6	10.3	101	65.1	76.2	1465
6	436.3	1570.7	11.5	113	65.4	75.2	1451	440.5	1585.8	11.7	115	67.4	75.2	1465
7	400.3	1441.1	12.0	118	64.6	72.9	1451	404.2	1455.0	12.3	120	66.7	72.9	1465
8	364.3	1311.5	12.4	122	63.9	69.4	1451	367.8	1324.1	12.7	125	65.9	69.4	1465
9														
10														
S.G. 0.9976								Original system curve S.G. 1.0000						

Table 37 - Pump test results 6.01

PUMP TEST SHEET (Speed Correction)														
**** PUMP TESTING CARRIED OUT IN ACCORDANCE WITH AS 2417 Part 2 Class C****														
Pump Type		Ornel 300AX			Test Number:		6.02		Date:		23-May-16			
Stator Type		New Diffuser/Back piece			No. of Impeller Vanes:		8							
DUTY POINT														
VOLUMETRIC FLOW			TOTAL HEAD			PUMP INPUT POWER		PUMP EFFICIENCY		NPSHR		PUMP SPEED		
564.0 L/s			9.00 m			37 kW		84 %		10 m		1465 r.p.m.		
1144.8 m³/hr			88 kPa											

Recorded Data								Speed Corrected Data						
PT.	Flow		Total Head		Pump Power	Pump Eff.	Pump Speed	Flow		Total Head		Pump Power	Pump Eff.	Pump Speed
	(L/s)	(m³/hr)	(m)	(kPa)	(kW)	(%)	(r.p.m.)	(L/s)	(m³/hr)	(m)	(kPa)	(kW)	(%)	(r.p.m.)
1	585.5	2107.8	5.4	53	52.6	58.6	1454	589.9	2123.7	5.5	54	53.9	58.6	1465
2	583.1	2099.3	5.5	54	53.3	58.6	1454	587.5	2115.1	5.6	55	54.7	58.6	1465
3	555.9	2001.2	6.8	67	56.4	65.7	1453	560.5	2017.8	6.9	68	57.9	65.7	1465
4	527.6	1899.4	8.4	82	59.4	72.5	1452	532.3	1916.4	8.5	83	61.1	72.5	1465
5	494.3	1779.5	9.5	93	62.4	73.4	1451	499.1	1796.6	9.7	95	64.3	73.4	1465
6	451.9	1626.8	10.9	107	64.6	74.6	1451	456.3	1642.5	11.1	109	66.7	74.6	1465
7	422.0	1519.2	11.4	112	64.6	72.9	1451	426.1	1533.9	11.6	114	66.7	72.9	1465
8														
9														
10														
S.G. 0.9976								Original system curve S.G. 1.0000						

Table 38 - Pump test results 6.02

PUMP TEST SHEET (Speed Correction)														
**** PUMP TESTING CARRIED OUT IN ACCORDANCE WITH AS 2417 Part 2 Class C****														
Pump Type Ornel 300AX Stator Type New Diffuser/Back piece					Test Number: 6.03 No. of Impeller Vanes: 8					Date: 23-May-16				
DUTY POINT														
VOLUMETRIC FLOW 318.0 L/s 1144.8 m³/hr			TOTAL HEAD 8.90 m 87 kPa			PUMP INPUT POWER 37 kW		PUMP EFFICIENCY 84 %		NPSHR 10 m		PUMP SPEED 1465 r.p.m.		
Recorded Data								Speed Corrected Data						
PT.	Flow		Total Head		Pump Power	Pump Eff.	Pump Speed	Flow		Total Head		Pump Power	Pump Eff.	Pump Speed
	(L/s)	(m³/hr)	(m)	(kPa)	(kW)	(%)	(r.p.m.)	(L/s)	(m³/hr)	(m)	(kPa)	(kW)	(%)	(r.p.m.)
1	520.2	1872.6	4.4	43	42.1	52.7	1292	589.8	2123.3	5.6	55	61.5	52.7	1465
2	518.6	1867.0	4.4	43	42.1	52.5	1292	588.0	2116.9	5.6	55	61.5	52.5	1465
3	492.6	1773.4	5.5	54	45.1	58.6	1292	558.6	2010.8	7.1	69	65.9	58.6	1465
4	463.5	1668.6	6.7	66	47.3	64.2	1291	526.0	1893.5	8.6	85	69.3	64.2	1465
5	425.5	1531.8	8.2	81	49.6	69.2	1291	482.8	1738.3	10.6	104	72.6	69.2	1465
6	375.2	1350.7	9.6	94	51.1	68.7	1291	425.8	1532.8	12.3	121	74.8	68.7	1465
7	301.9	1086.8	9.5	93	46.6	60.0	1291	342.6	1233.3	12.2	120	68.2	60.0	1465
8														
9														
10														
S.G. 0.9976								Original system curve S.G. 1.0000						

Table 39 - Pump test results 6.03

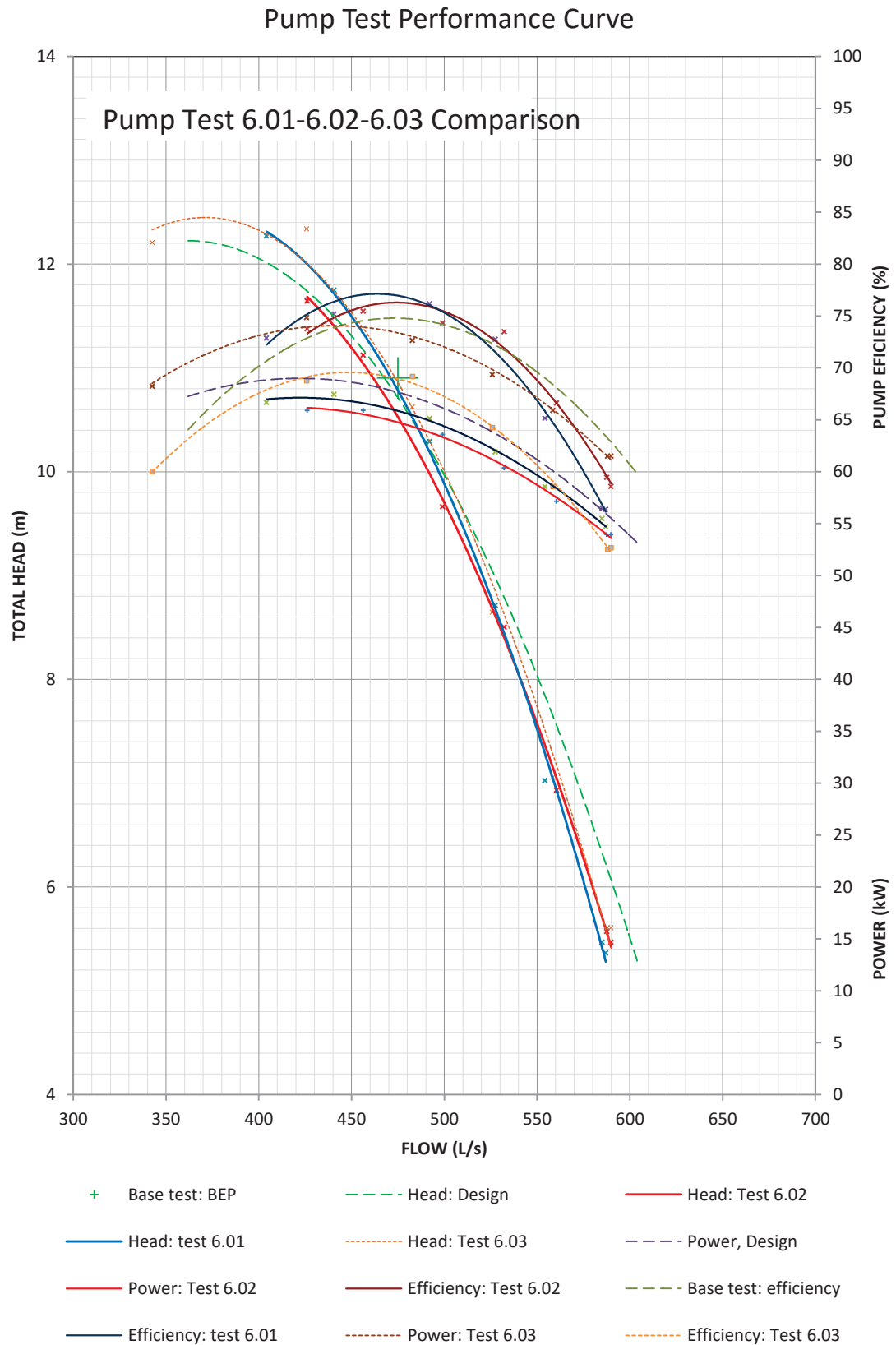


Figure 257 - Comparison of pump tests 6.01, 6.02 and 6.03

## Appendix E. CFD Models

In this section, images of all the models analysed are shown. To keep this section brief, only the 2D velocity streamlines and the total pressure plots of each analysis are shown.

### E.1. Standard Pump Initial CFD Analysis

As discussed in Section 4.3, to determine the most suitable set of parameters to apply to each CFD model, a number of models with different settings were run and analysed. The standard pump configuration is the model which was used in each case. The following figures show the results for each of these CFD models. The parameters used and the inlet and outlet total pressure point readings are listed in the figure descriptions.

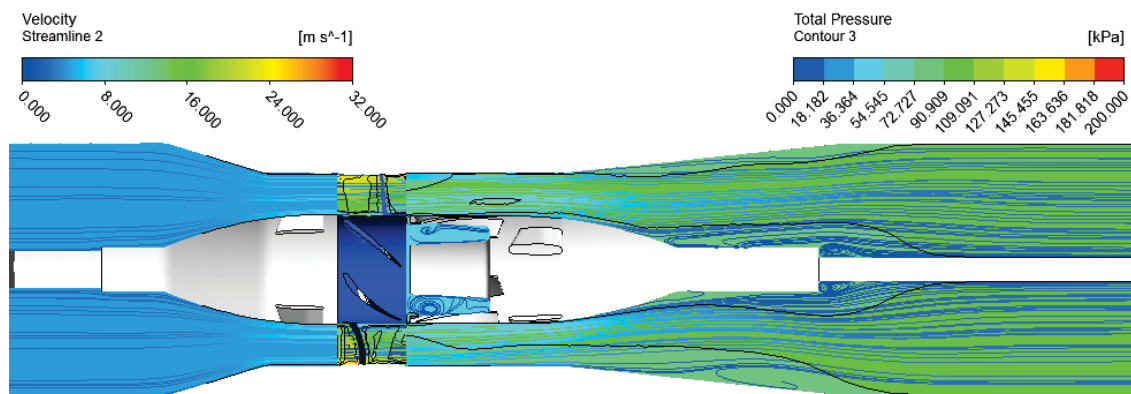


Figure 258 – STT analysis, fine mesh, inlet: mass flow rate, outlet: 90 kPa, probe pressure point suction: 23.6 kPa, discharge: 94.1 kPa

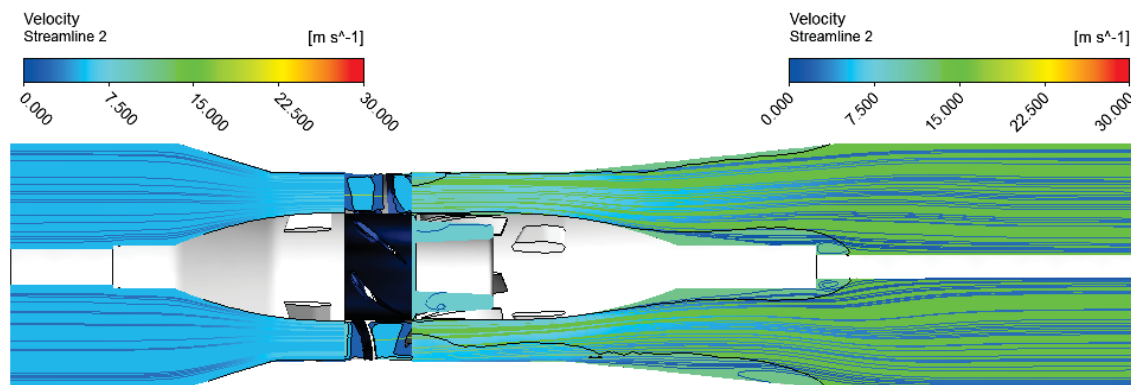


Figure 259 –  $k$ - $\epsilon$  analysis, medium mesh, inlet: mass flow rate, outlet: 90 kPa, point probe point suction: 27 kPa, discharge: 93 kPa

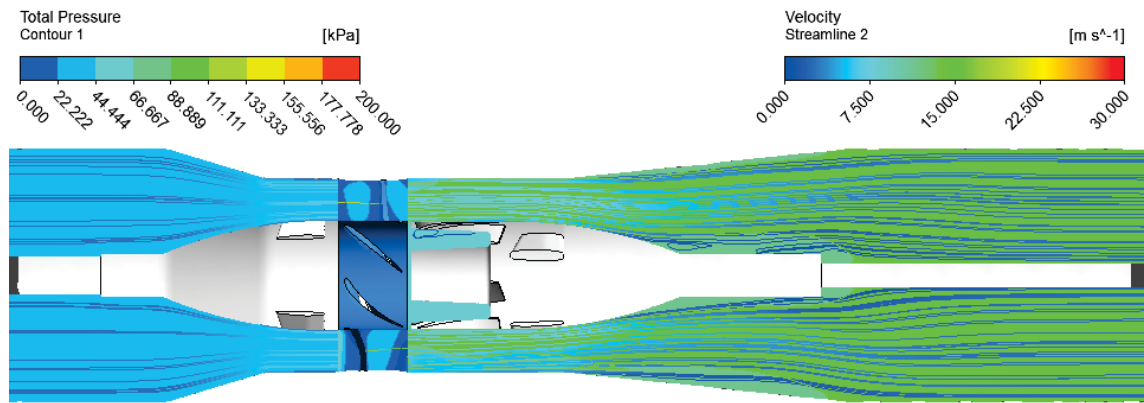


Figure 260 - *k-e* analysis, coarse mesh, inlet: mass flow rate, outlet: 90 kPa, point probe point suction: 27.5 kPa, discharge: 93.5 kPa

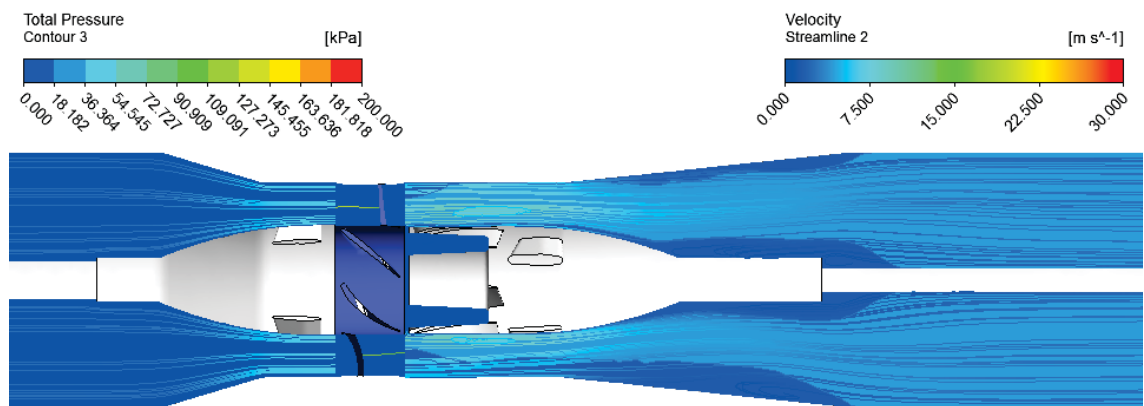


Figure 261 - *SST* analysis, fine mesh, inlet: mass flow rate, outlet: mass flow rate, point probe point suction: -48.5 kPa, discharge: 22.6 kPa

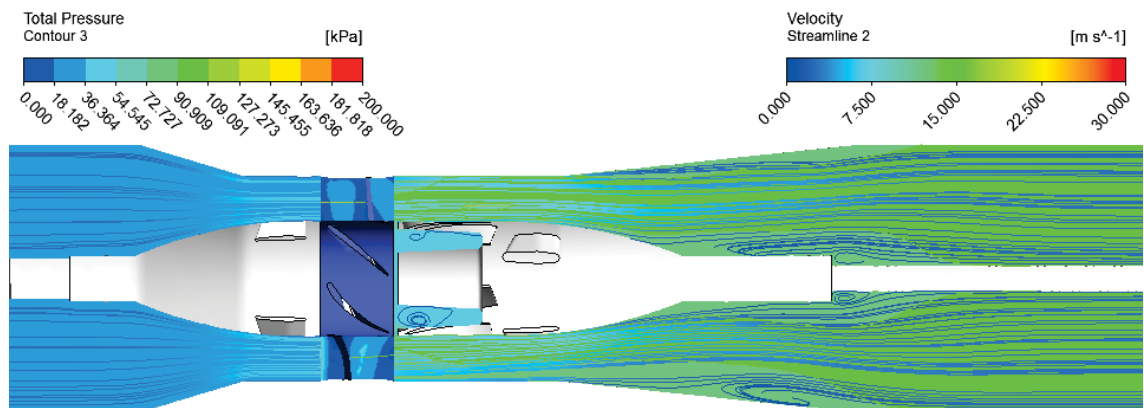


Figure 262 - *SST* analysis, fine mesh, inlet: mass flow rate, outlet: 90 kPa, point probe point suction: 23.6 kPa, discharge: 94.14 kPa



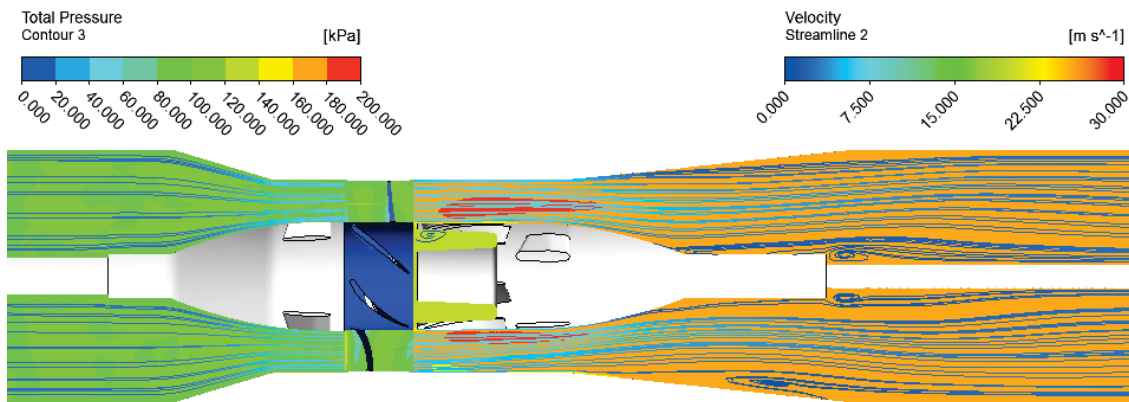


Figure 263 - SST analysis, fine mesh, inlet: 100 kPa, outlet: mass flow rate, point probe point suction: 100 kPa, discharge: 172.1 kPa

Figure 263 was the model which had the closest results to the pump performance curves. The model above was using a fine mesh, which was found to be similar results to the medium mesh, which was used in the CFD analysis found in Section 4.4.

## E.2. New Diffuser with Elongated Tail piece

The model shown below was not featured in Section 4.4.1.3, as the analysis showed the predicted secondary flow was too extreme to consider for the tail piece design. The idea was to elongate the diffuser hub with a 30° taper at the discharge. From the 2D velocity and total pressure plots' it can be seen that the high velocity creating large secondary flow in the diffuser inlet is creating an increase in the suction pressure to almost stall-like conditions. The elongated section is also creating a blockage at the shroud bell area.

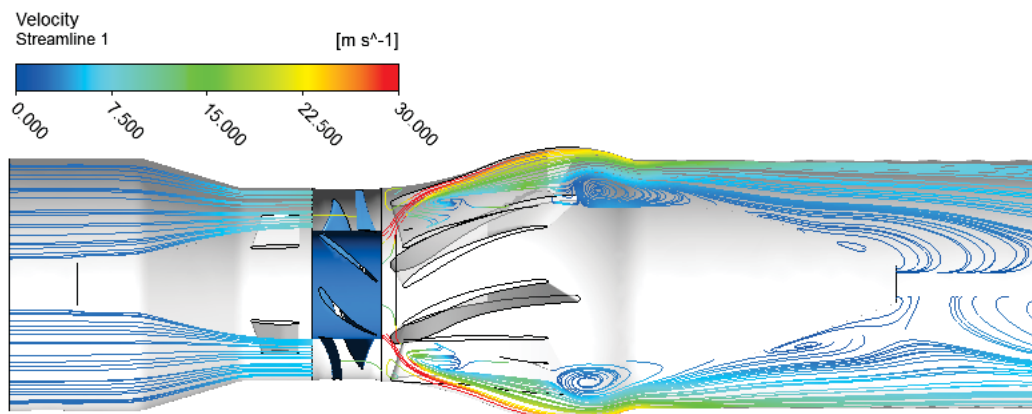


Figure 264 – Elongated tail piece 2D velocity streamlines

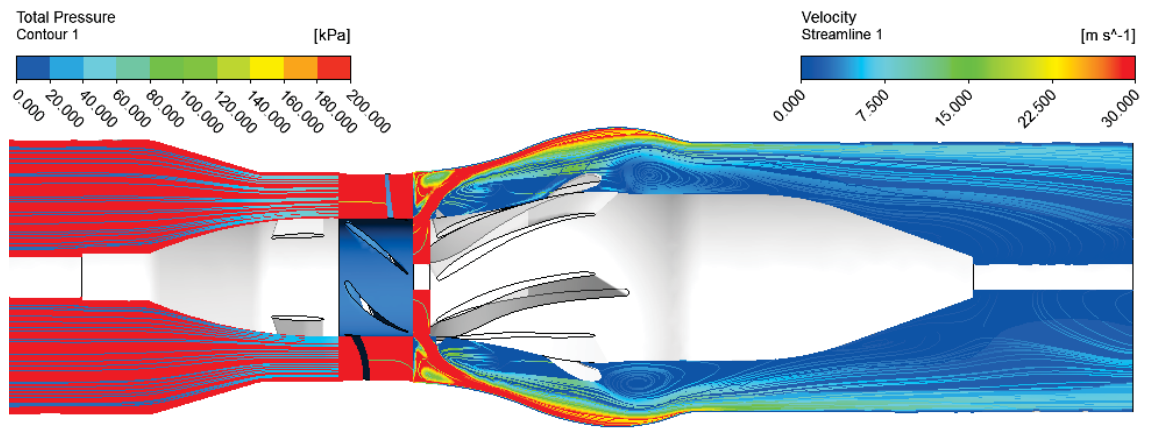


Figure 265 –Elongated tail piece total pressure and 2D velocity streamlines

### E.3. Complete Diffuser Design

It was hoped that a complete redesign of the diffuser using the relative diffuser design theories, would result in a working design for the five vane impeller assembly. However the CFD results were not as promising as hoped, with more work required. The 2D velocity streamlines indicate there is a large secondary flow created in the outlet area with high pressure at the vane inlet.

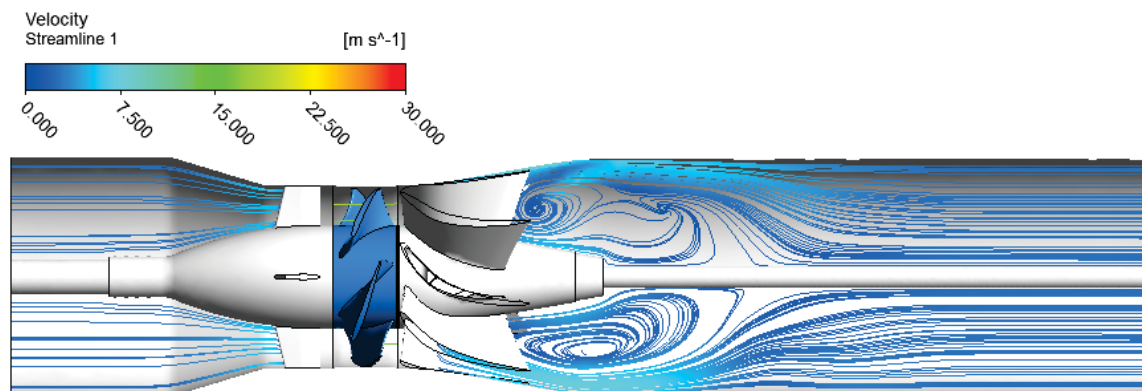


Figure 266 – 2D velocity streamline plot for new design number 1

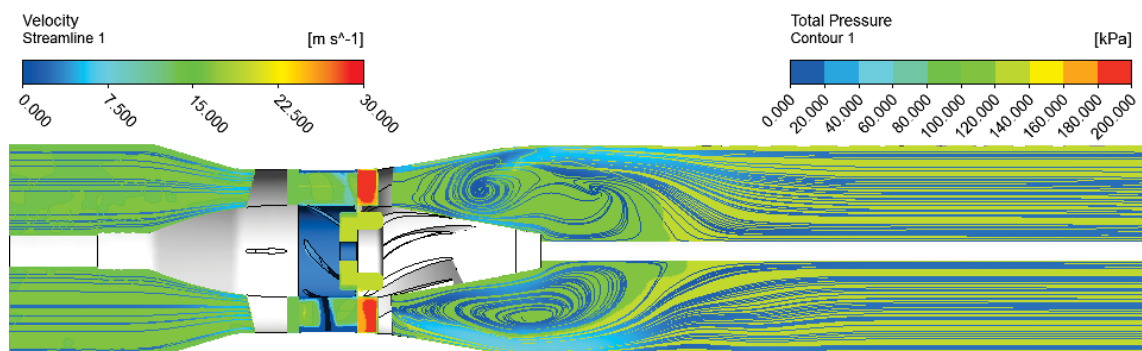


Figure 267 – Total pressure plot for new design number 1

For this design it was assumed that instead of using a similar bell shape to the new diffuser, that a standard diffuser shape combined with the blades would keep the fluid flow in an axial direction. Figure 268 shows the selected hub and shroud dimensions, where Figure 269 details the new designed vane profiles.

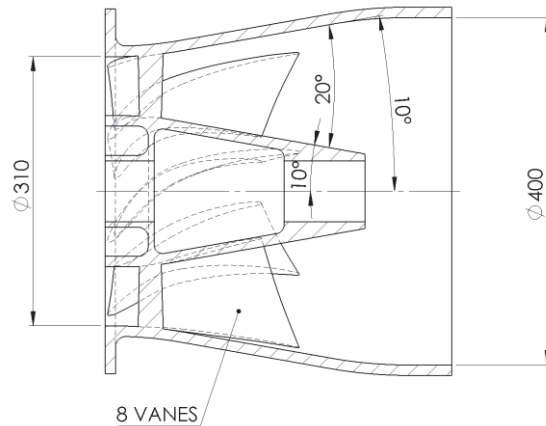


Figure 268 – New design number 1, shroud and hub outline

The inlet angle for the vanes was made to match the absolute velocity of the impeller vane outlet. This angle was tangent to a curve which blended to a zero degree outlet angle. The blades were aligned as per Figure 270, at the 30% point along the mean line. This gives a slight angle of the blade at the outlet. It was thought that this would counter some of the vortex rotation created between the vanes. The vane length was made longer than the standard stator, yet shorter than the new diffuser design.

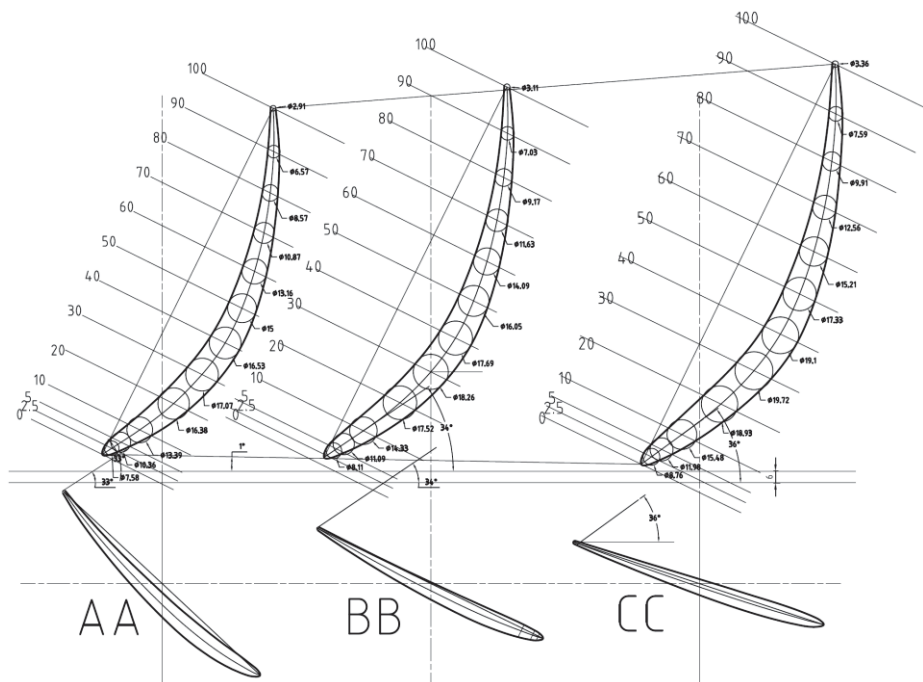


Figure 269 – Vane profile for new design number 1

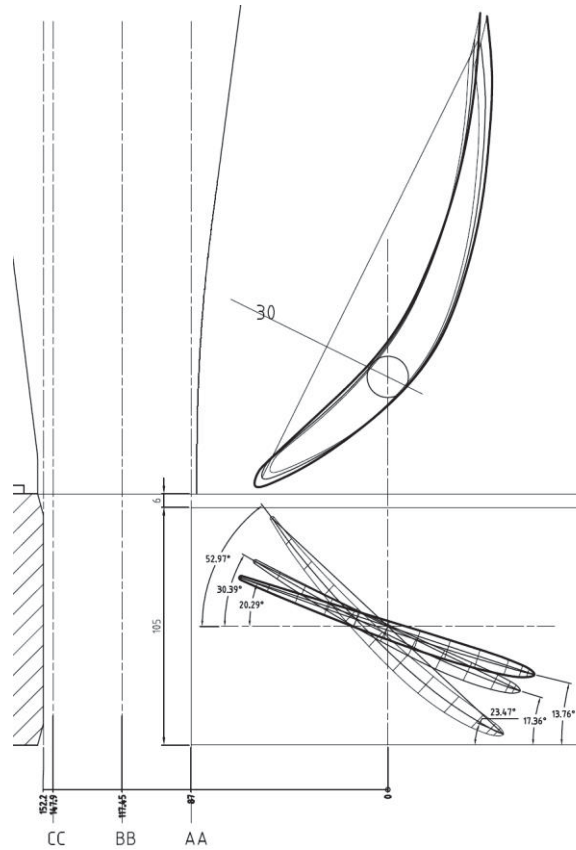


Figure 270 – Vane profile alignment design number 1

However, from the total pressure plot it can be seen that there is a high pressure area at the inlet tip area, as well as large amount of secondary flow due to fluid separation from the shroud and hub radial angles of  $10^\circ$ . To try to reduce the fluid separation, a second design was created with a smaller radial shroud angle of  $4^\circ$ , as shown in Figure 271. The CFD analysis results show there is only a slight reduction in secondary flow, which is now concentrated to the hub area' which would indicate the hub angle of  $10^\circ$  is required to be reduced. The high pressure has also moved position to midway through the vane flow passage. The measured total pressure at the probe point position is 132.7 kPa, (total pump pressure of 32.7 kPa or 3m head) which is very low when compared to CFD analysis shown in Section 4.4.1.

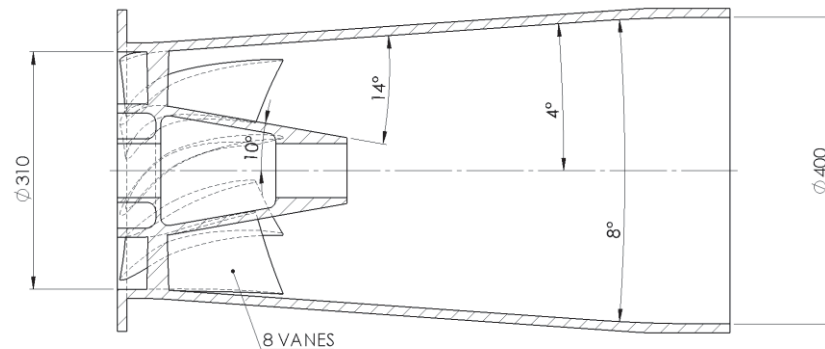


Figure 271 - New design number 2, shroud and hub outline

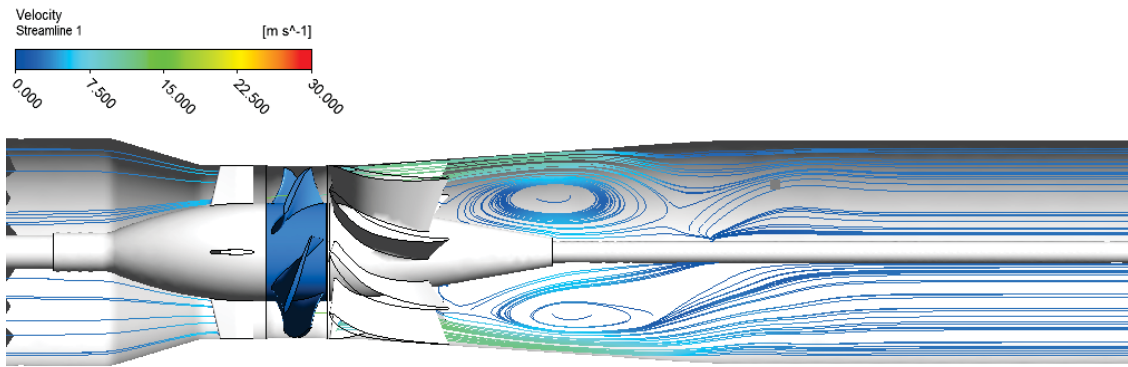


Figure 272 - 2D velocity streamline plot for new design number 2

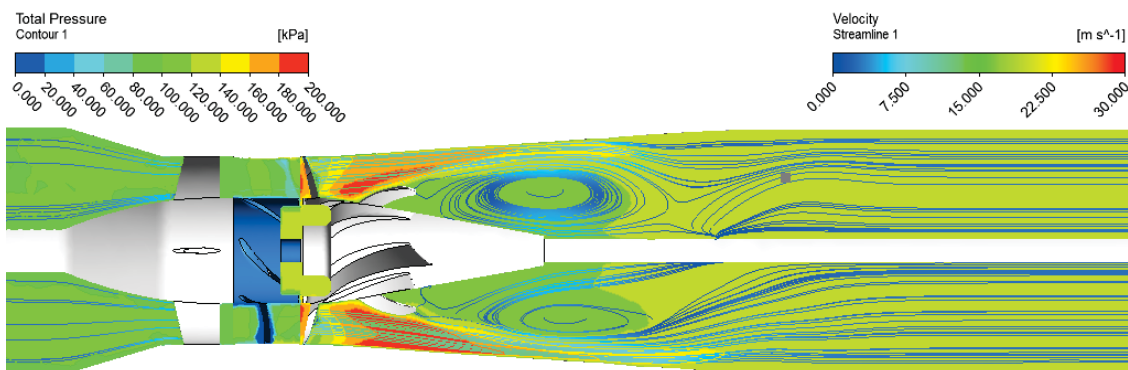


Figure 273 – Total pressure plot for new design number 2

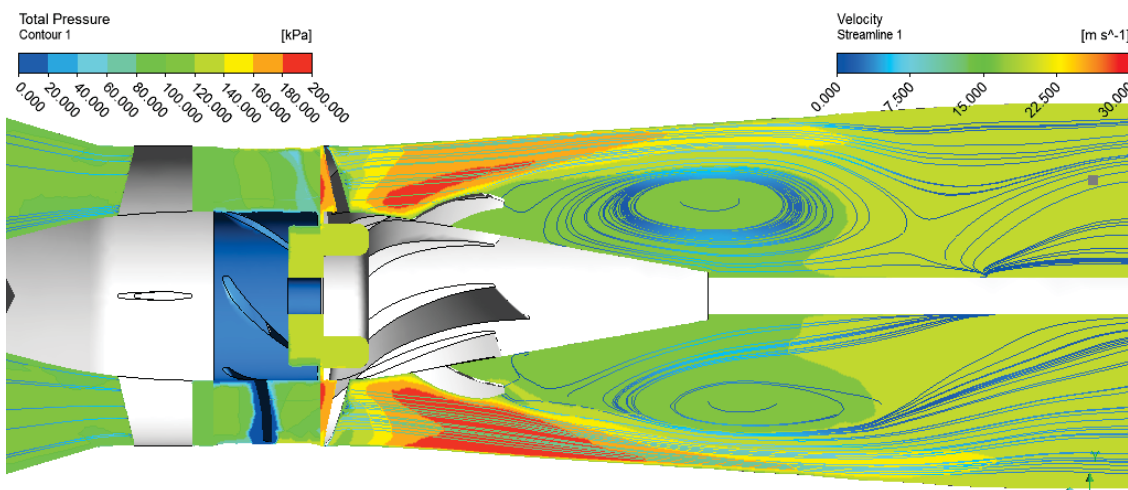


Figure 274 – Zoom view of Figure 273

A final modification was made to the new design with the inlet vane angle modified and the vane profile positioning also modified. The vane inlet angle was modified to reduce the angle, to try to reduce the high pressure at the inlet. An angle of  $+5^\circ$ , (maximum limit of the recommended tolerance) was used. The vane profile alignment was also modified to have the

outlet tips in a straight line perpendicular to the hub. The hub radial angle was also modified to  $4^\circ$ , to reduce the fluid separation.

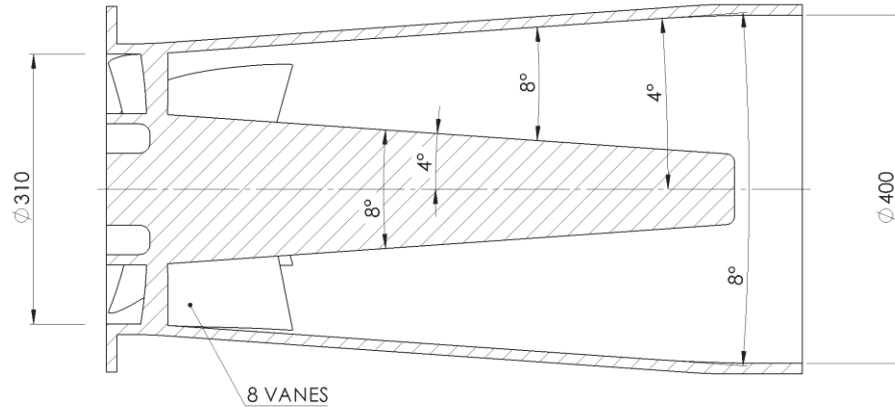


Figure 275 - New design number 3, shroud and hub outline

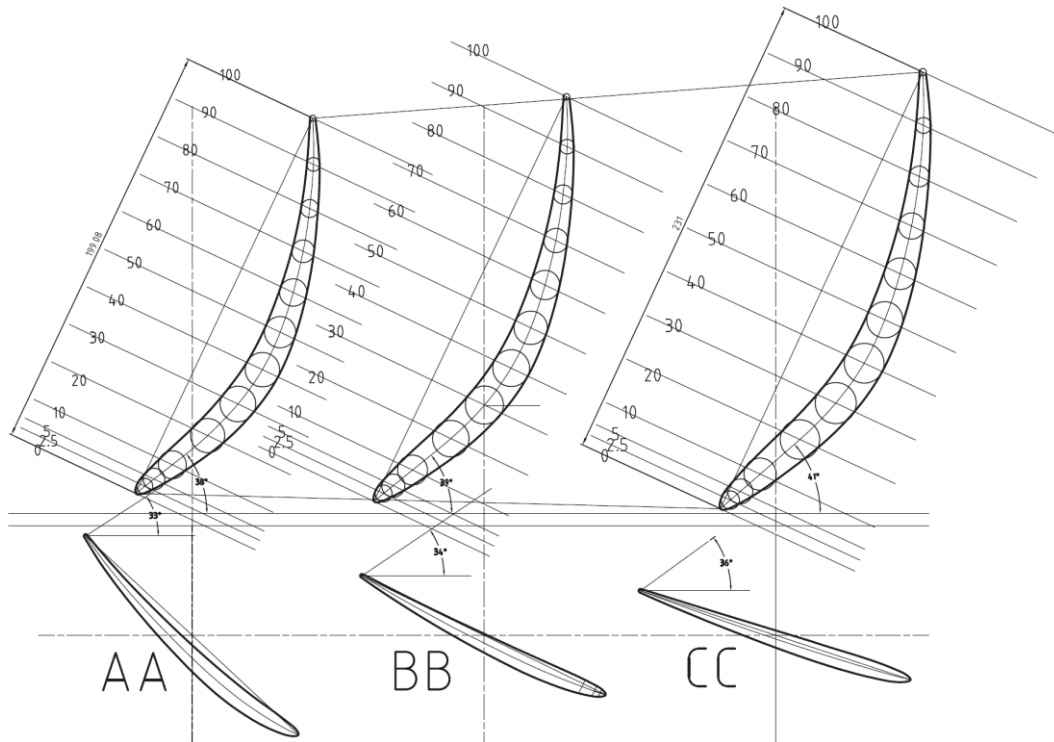


Figure 276 - Vane profile for new design number 3

The CFD results showed an improvement in reducing the secondary flow at the hub area but the high pressure in the vane flow area is still present. The pump outlet total pressure was measured to be 153.7 kPa, (5.5m head) which is a 3.2m increase when compared to design number 2. However, this is 2m less than the CFD results for the standard pump of 7.4m, (see Section 4.4.1.1).

Overall the CFD results indicate that the original stator design is still the most appropriate configuration to use with the five vane impeller. With some more modifications or another



redesign of the diffuser vanes, it may be possible to improve the pumps performance however, this exercise would be more appropriate for future research.

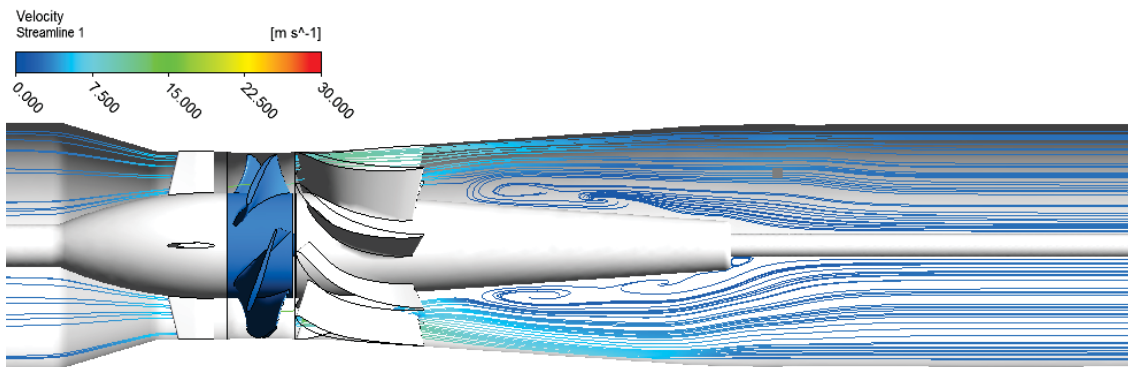


Figure 277 - 2D velocity streamline plot for new design number 3

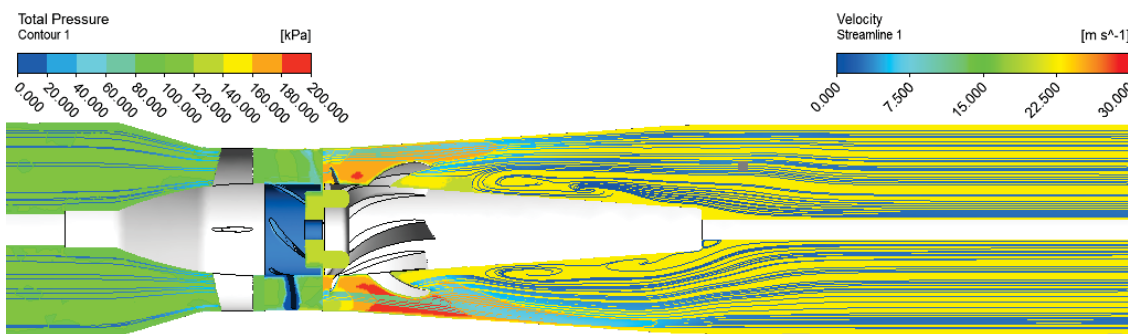


Figure 278 – Total pressure plot for new design number 3

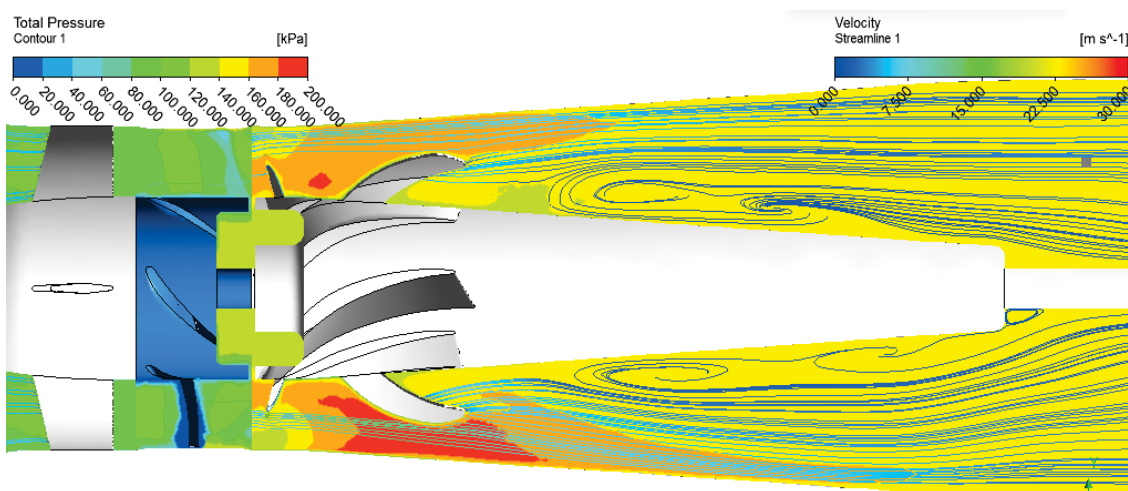


Figure 279 - Zoom view of Figure 278

# Appendix F. Coordinate Measurement Machine

www.faroasia.com **FARO**

## FaroArm® Platinum



### Temperature & Overload Sensors

Located in each joint, they allow the Arm to "feel" and react to thermal variations and improper handling for maximum accuracy

### NEW – Bluetooth® Cable-Free Operation

Inspect and digitize wirelessly up to 30ft. (10m) away

### Optional 7-Axis Availability

Provides an additional Axis of Rotation for non-contact Laser Line Probes or curved probes

### Internal Counterbalancing

Internal counter balancing provides comfortable stress-free usage

### Multi-Probe Capability

Including various Ball Diameters, Touch-Sensitive, Curved and Extensions

### Extended-Use Battery

Integrated extended-use battery Provides true "measure anywhere" capability

### NEW – Auto Sleep Mode

Automatically turn off unit to save energy and extend component life

### The Best-Selling Portable CMM!

The **FaroArm Platinum**'s high accuracy renders traditional CMMs, hand tools and other portable inspection equipment obsolete. Anyone, anywhere can now inspect, reverse engineer or perform CAD-to-Part-analysis on parts, fixtures and assemblies with previously unheard of precision. When you partner that accuracy with its adaptable 3D measurement technology, it is ideal for forming, molding, fabricating, casting and assembly facilities needing basic 3D measurements or advanced GD&T and SPC output.

### Most Common Applications

**Aerospace:** Alignment, Tooling & Mold Certification, Part Inspection

**Automotive:** Tool Building & Certification, Alignment, Part Inspection

**Metal Fabrication:** OMI, First article inspection, Periodic Part Inspection

**Molding/Tool & Die:** Mold and Die Inspection, Prototype Part Scanning

### Features

- ▶ Up to +/- 0.020mm precision
- ▶ 7-Axis Availability
- ▶ 6-Degrees-of-Freedom Probe
- ▶ Adaptable 3D Measurement Technology
- ▶ Composite Material Construction

www.faroasia.com/FaroArm



## FaroArm Platinum



### Performance Specifications

Model (Measuring Range)	Single Point Articulation Performance Test (Max-Min)/2		Volumetric Maximum Deviation		FaroArm Weight	
	axis	6	7	6	7	6
Platinum 6 ft. (1.8 m)	.0008 in. (.020 mm)	.0010 in. (.026 mm)	±.0011 in. (±.029 mm)	±.0015 in. (±.037 mm)	20.5 lbs. (9.3 kg)	21 lbs. (9.5 kg)
Platinum 8 ft. (2.4 m)	.0010 in. (.025 mm)	.0012 in. (.030 mm)	±.0014 in. (±.036 mm)	±.0017 in. (±.043 mm)	21 lbs. (9.5 kg)	21.5 lbs. (9.75 kg)
Platinum 10 ft. (3.0 m)	.0017 in. (.043 mm)	.0020 in. (.052 mm)	±.0024 in. (±.061 mm)	±.0029 in. (±.073 mm)	21.5 lbs. (9.75 kg)	22 lbs. (9.98 kg)
Platinum 12 ft. (3.7 m)	.0024 in. (.061 mm)	.0029 in. (.073 mm)	±.0034 in. (±.086 mm)	±.0041 in. (±.103 mm)	22 lbs. (9.98 kg)	22.5 lbs. (10.21 kg)

**FaroArm Test Methods** - (Test methods are a subset of those given in the B89.4.22 standard.)

**Single Point Articulation Performance Test (Max-Min)/2:**

The probe of the FaroArm is placed within a conical socket, and individual points are measured from multiple approach directions. Each individual point measurement is analyzed as a range of deviations in X, Y, Z. This test is a method for determining articulating measurement machine repeatability.

**Volumetric Maximum Deviation:**

Determined by using traceable length artifacts, which are measured at various locations and orientations throughout the working volume of the FaroArm. This test is a method for determining articulating measurement machine accuracy.

### Hardware Specifications

**Operating Temp range:** 10°C to 40°C (50°F to 104°F)

**Operating Humidity Range:** 0-95%, noncondensing

**Temperature Rate:** 3°C/5min. (5.4°F/5min. Max)

**Power Supply:** Universal worldwide voltage  
85-245VAC,  
50/60 Hz

**Certifications:** MET (UL, CSA Certified) • CE Compliance • Directive 93/68/EEC, (CE Marking) • Directive 89/336/EEC, (EMC) • FDA CDRH, Subchapter J of 21 CFR 1040.10  
Electrical Equipment for Measurement, Control & Lab Use  
**EN 61010-1:2001, IEC 60825-1, EN 61326**  
Electromagnetic Compatibility (EMC)  
**EN 55011, EN 61000-3-2, EN 61000-3-3, EN 61000-4-4, EN 61000-4-5, EN 61000-4-6, EN 61000-4-8, EN 61000-4-11**



**To learn more, visit [www.faroasia.com/FaroArm](http://www.faroasia.com/FaroArm)**

**FARO Singapore Pte Ltd (Asia Pacific Headquarter)**

China • India • Japan • Malaysia • Thailand • Vietnam • Indonesia • Philippines • South Korea • Australia

3 Changi South Street 2, Xilin Districentre Tower B, Singapore 486548

Tel: +65 6511 1350 Fax: +65 6543 0111

Email: [salesap@faro.com](mailto:salesap@faro.com)

**FARO Business Technologies India Pvt Ltd**

E-12, B-1 Extension, Mohan Cooperative Industrial Estate, Mathura Road,  
New Delhi-110044, India

Tel: +91 11 4646 5656 Fax: +91 11 4646 5660

Email: [enquiry-india@faro.com](mailto:enquiry-india@faro.com)

Global Head Quarters: USA - Lake Mary, Florida 32746

Europe Head Quarters: Germany - Lingwiesenstr. 11/2 - 70825 Kornal-Münchingen

Revised: December 2010  
© 2010 FARO Technologies, Inc.

04REF101-004.pdf

# Appendix G. Coating Data Sheet



## TECHNICAL DATA SHEET

TX11/0302

### CERAMI-TECH C.R.

#### Two Component Epoxy Ceramic Coating



**Thortex Cerami-Tech C.R.** is a high performance solvent free coating designed for use as a resurfacing and lining system to improve the efficiency in fluid flow environments.

**Thortex Cerami-Tech C.R.** is based on a specifically selected blend of epoxy resins and non toxic polyamino curing agents reinforced with carbide and inert flow enhancing pigments which produces a system with optimum physical and mechanical strengths and excellent resistance to erosion and corrosion.

**Thortex Cerami-Tech C.R.** is simple, safe and easy to use and its excellent low friction surface improves flow rates in pumps and pipelines which makes it an ideal choice for the protection of waterboxes, tube sheets, pumps, impellers, valves and heat exchangers.

**Thortex Cerami-Tech C.R.** is approved for contact with potable water:

**Before proceeding, please read the following information carefully to ensure that the correct application procedure is fully understood.**

#### SURFACE PREPARATION

Heavy contamination due to oil or grease must be removed using with **Thortex Universal Cleaner**.

Surfaces to be coated should then be abrasive blast cleaned to a minimum Sa2½ BS7079 Part A1 : 1989/ISO 8501-1: 1988 to give medium blast profile as defined by BS 7079: Part C3 1989/ISO 85031 1988.

Equipment which has become salt impregnated due to service conditions should first be wet blasted then dry abrasive blasted and checked for presence of salts, this process should be repeated until the salts are removed.

Alternatively the surface should be sweated using a blow torch or heat gun to remove the impregnated salts, prior to re-blasting.

This procedure should be repeated until no further impregnated salts are present.

Care should be taken on pitted surfaces to ensure that all contamination is removed from the bottom.

#### MIXING

**Thortex Cerami-Tech C.R.** is a two component product supplied as a base component and an activator component which must be mixed together immediately prior to use.

Stir the contents of the base component, continue stirring and gradually add the total contents of the activator container, stir the combined mix until completely homogeneous.

The mixed material must be used within 45 minutes of mixing at 20°C (68°F). This time will be reduced at higher temperatures and extended at lower temperatures.

#### APPLICATION

Application should not be carried out when air and substrate temperatures are below 7°C nor when relative humidity exceeds 85% or when the surface to be coated is less than 3°C above the dew point.

**Thortex Cerami-Tech C.R.** can be applied by brush or roller, with brush application being preferred for the first coat of a two coat application. Good quality brushes or short to medium pile roller should be used.

**Thortex Cerami-Tech C.R.** should be worked into the surface to ensure complete wetting of the surface. On deeply pitted surfaces, care should be taken to avoid air entrapment in the pitted areas.



TX11/0302

Best application results are obtained with a minimum substrate temperature of 15°C with 20°C being the ideal temperature.

All equipment must be cleaned IMMEDIATELY after use with **Thortex Universal Cleaner**.

**Theoretical Coverage Rate**

2.7m<sup>2</sup>/kilo at 250 microns dft (29 ft<sup>2</sup>/kilo at 10 mils dft)

**Recommended Film Thickness**

Wet 250 microns (10 mils)

Dry 250 microns (10 mils)

Detailed working recommendations are available from the Technical Centre on request.

**PHYSICAL CONSTANTS**

Mixing Ratio	Base	Activator	
	2	1	By volume
	4	1	By weight

Appearance	Base	Thixotropic Coloured Liquid
	Activator	Clear Liquid

**Drying & Cure times**

at 20°C (68°F)	Usable Life	45 minutes
	Touch Dry	6 hours
	Minimum Overcoating	6 hours
	Maximum Overcoating	48 Hours
	Full Cure	7 days

**Volume Solids** 100%

**V.O.C.** Nil

**Shelf Life** Use within 5 years of purchase. Store in original sealed containers at temperatures between 5°C (40°F) and 30°C (86°F).

FOR FURTHER INFORMATION PLEASE CONTACT



**Food Contact** Meets USDA requirements for incidental food contact. Meets FDA requirements CFR 21.175.300 for food contact.

**Potable Water** DWI and BS6920 approved for cold water service.

**PHYSICAL PROPERTIES**

<b>Abrasion Resistance</b>	0.08 ml loss per 1000 cycles
ASTM D4060	
<b>Shore D Hardness</b>	85
<b>Tensile Shear Adhesion</b>	175 kg per cm <sup>2</sup> (2500 psi)
ASTM D1002	(Grit Blasted Steel)
<b>Corrosion Resistance</b>	Excellent, unaffected after 10,000 hours exposure
ASTM B117	
<b>Flexural Strength</b>	570 kg/cm <sup>2</sup> (8100 psi)
ASTM D790	
<b>Compressive Strength</b>	700 kg/cm <sup>2</sup> (10000 psi)
ASTM D695	
<b>Impact Resistance</b>	40 Joules (355 in lbs)
ASTM D256	

**HEALTH AND SAFETY**

As long as normal good practice is observed **Thortex Cerami-Tech C.R.** can be safely used.

Protective gloves should be worn during use.

A fully detailed **Material Safety Data Sheet** is either included with the material or is available on request.

**PACKAGING**

Supplied in 1 and 3 kg packs.

The information provided in this Product Data Sheet is intended as a general guide only and should not be used for specification purposes. The information is given in good faith but we assume no responsibility for the use made of the product or this information because this is outside the control of the company. Users should determine the suitability of the product for their own particular purposes by their own tests.



**Thortex Division of E. Wood Ltd.**  
 Standard Way, Northallerton, N. Yorks. U.K. DL6 2XA  
 Tel: 01609 780170 Fax: 01609 780438 & 777905  
 E Mail: [grant@ewood.co.uk](mailto:grant@ewood.co.uk)  
 URL: <http://www.thortex.co.uk>

Figure 280 – Coating data sheet

## Appendix H. Tachometer Technical Sheet

Pinpoint accuracy combined with measurement versatility

### SKF Tachometer TKRT 20

The SKF TKRT 20 is a user-friendly and accurate tachometer utilising laser or contact for measuring rotational and linear speed. Equipped with a laser and contact adaptor, it offers excellent speed measurement versatility in five different modes.

- The user can select the following to measure:
  - $r/min$  and  $r/s$ , metres, yards, feet, per min and per sec,
  - length or revolution counting, or
  - time interval
- Wide speed range and the various measurement modes make the SKF TKRT 20 suitable for measuring speed in many applications.
- Large angular range of  $\pm 80^\circ$  to target facilitates easy measuring in areas where straight-line access is difficult.
- The laser optical system allows easy and quick measurements at a safe distance from rotating machinery.
- The large inverting LCD display facilitates easy reading, even when pointing the unit down into the machinery.
- The SKF TKRT 20 can also be equipped with a remote laser sensor, which is optionally available.







#### Technical data

Designation	TMRT 20
Display	Inverting vertical 5 digit LCD
Memory	Last reading held for 1 minute
Measurement	
Optical modes	r/min and r/s (also count and time interval)
Contact modes	r/min and r/s, metres, yards, feet, per min and per sec
Count modes	total revs, metres, feet, yards
Sampling time	0.8 seconds on time between pulses 0.1 seconds auto-selection in max or min capture mode
Linear speed	0.3 to 1 500 metres/min (4 500 ft/min) or equivalent in seconds
Optical measurement	
Rotational speed range	3 to 99 999 r/min
Accuracy	±0.00% of reading ±1 digit
Measuring distance	50 to 2 000 mm (1.9 to 78.7 in.)
Angle of operation	±80°
Laser sensor	1 x built-in class 2 laser
Remote laser sensor	Optional TMRT1-56

Contact measurement	
Rotational speed range	Max. 50 000 r/min for 10 sec
Accuracy	±3% of reading ±1 digit
Contact adaptors	Included with r/min in cone and non-able metric wheel assembly
Battery	4 x AAA alkaline type IEC LR03
Operation time	24 hours continuous use
Product dimensions	213 x 40 x 29 mm (8.3 x 1.5 x 1.1 in.)
Product weight	170 g (0.37 lb)
Case dimensions	260 x 85 x 180 mm (10.2 x 3.4 x 7.0 in.)
Case weight	432 g (0.9 lb)
Operating temperature	0 to 40 °C (32 to 104 °F)
Storage temperature	-10 to +50 °C (14 to 122 °F)
Relative humidity	10 to 90% RH non-condensing
IP rating	IP 40



The laser optical system allows easy and quick measurements at a safe distance from rotating machinery.

© SKF is a registered trademark of the SKF Group.

© SKF Group 2014

The contents of this publication are the copyright of the publisher and may not be reproduced (even verbatim) without prior written permission. Every care has been taken to ensure the accuracy of the information contained in this publication but the publisher cannot be held responsible for any loss or damage whether direct, indirect or consequential arising out of the use of the information contained therein.

PUB-MF/P-1323-Y1-EN - October 2014



[www.mapro.skf.com](http://www.mapro.skf.com) • [skf.com/mount](http://skf.com/mount) • [skf.com/lubrication](http://skf.com/lubrication)

## Appendix I. 3D Printer Data Sheet

# FORTUS 400mc™



**Flexible, fast, predictable, and simple to operate. Manufacture Real Parts™ in a wide range of thermoplastics.**

The Fortus 400mc™ allows you to manufacture Real Parts™ in-house with multiple production-grade thermoplastics, such as ABS-M30, PC, PPSF, ULTEM® 9085, PC-ABS blend and more. Fortus 400mc is a user configurable high-performance workhorse, ideal for creating Real Parts for conceptual models, functional prototypes, manufacturing tools, and end-use parts.

The Fortus 400mc coupled with Insight™ front-end processing software lets you quickly manufacture parts that match your mechanical, thermal, aesthetic and resolution needs. With the Fortus 400mc, you can accurately manufacture Real Parts with complex geometries, that are strong enough not only for functional testing, but end use as well.

**Learn more about the Fortus 400mc at [stratasys.com](http://stratasys.com)**

 **Stratasys** | Production Series

# FORTUS 400mc™



## System Specifications

BASE SYSTEM CONFIGURATION	
Build Envelope (XYZ)	14 x 10 x 10 inches (355 x 254 x 254 mm)
Material Delivery	One (1) Build material canister 92 in <sup>3</sup> (1508 cc) One (1) Support material canister 92 in <sup>3</sup> (1508 cc)
UPGRADE CONFIGURATION	
Build Envelope (XYZ)	16 x 14 x 16 inches (406 x 355 x 406 mm)
Material Delivery	Two (2) Build material canisters 92 in <sup>3</sup> (1508 cc) Two (2) Support material canisters 92 in <sup>3</sup> (1508 cc) Auto changeover between canisters
MATERIAL OPTIONS	
Layer Thickness:	ABS: ABS-M30 ABS-M30 PC-ABS PC-190 PC ULTEMP 9085 PPSF
0.013 inch (0.330 mm)	X X X X X X X X X
0.010 inch (0.254 mm)	X X X X X X X X X
0.007 inch (0.178 mm)	X X X X X X X X X
0.005 inch (0.127 mm)	X X X X X X X X X
Support Structure:	Soluble Soluble Soluble Soluble Soluble BABS BABS BABS BABS
Available Colors:	<div> <input type="checkbox"/> Natural  <input type="checkbox"/> Black  <input type="checkbox"/> White  <input type="checkbox"/> Red  <input type="checkbox"/> Blue  <input type="checkbox"/> Dark Grey  <input type="checkbox"/> Light Grey  <input type="checkbox"/> Yellow  <input type="checkbox"/> Green  <input type="checkbox"/> Orange  <input type="checkbox"/> Purple  <input type="checkbox"/> Brown  <input type="checkbox"/> Silver  <input type="checkbox"/> Gold  <input type="checkbox"/> Bronze  <input type="checkbox"/> Copper  <input type="checkbox"/> Nickel  <input type="checkbox"/> Zinc  <input type="checkbox"/> Aluminum  <input type="checkbox"/> Steel  <input type="checkbox"/> Titanium  <input type="checkbox"/> Inconel  <input type="checkbox"/> Hastelloy  <input type="checkbox"/> Monel  <input type="checkbox"/> Nickel  <input type="checkbox"/> Cobalt  <input type="checkbox"/> Chromium  <input type="checkbox"/> Manganese  <input type="checkbox"/> Silicon  <input type="checkbox"/> Boron  <input type="checkbox"/> Nitrogen  <input type="checkbox"/> Oxygen  <input type="checkbox"/> Hydrogen  <input type="checkbox"/> Helium  <input type="checkbox"/> Neon  <input type="checkbox"/> Argon  <input type="checkbox"/> Krypton  <input type="checkbox"/> Xenon  <input type="checkbox"/> Radon  <input type="checkbox"/> Francium  <input type="checkbox"/> Radium  <input type="checkbox"/> Actinium  <input type="checkbox"/> Thorium  <input type="checkbox"/> Protactinium  <input type="checkbox"/> Uranium  <input type="checkbox"/> Neptunium  <input type="checkbox"/> Plutonium  <input type="checkbox"/> Americium  <input type="checkbox"/> Curium  <input type="checkbox"/> Berkelium  <input type="checkbox"/> Californium  <input type="checkbox"/> Einsteinium  <input type="checkbox"/> Fermium  <input type="checkbox"/> Mendelevium  <input type="checkbox"/> Nobelium  <input type="checkbox"/> Lawrencium  <input type="checkbox"/> Rutherfordium  <input type="checkbox"/> Dubnium  <input type="checkbox"/> Seaborgium  <input type="checkbox"/> Bohrium  <input type="checkbox"/> Hassium  <input type="checkbox"/> Meitnerium  <input type="checkbox"/> Darmstadtium  <input type="checkbox"/> Roentgenium  <input type="checkbox"/> Copernicium  <input type="checkbox"/> Nihonium  <input type="checkbox"/> Flerovium  <input type="checkbox"/> Tennessine  <input type="checkbox"/> Oganesson </div>
OTHER SPECIFICATIONS	
System Size/Weight	50.45 x 35.25 x 77.25 inches (1281 x 895.35 x 1962 mm) With crate: 1511 lbs. (687 kg) Without crate: 1309 lbs. (593 kg)
Achievable Accuracy	Parts are produced within an accuracy of +/- .005 inch or +/- .0015 inch per inch whichever is greater (or +/- .127 mm or +/- .0038 mm per mm whichever is greater) *Note: Accuracy is geometry dependent. Achievable accuracy specification derived from statistical data at 95% dimensional yield. See Fortus 400mc/500mc accuracy white paper for more information.
Network Communication	10/100 base T connection. Ethernet protocol.
Operator Attendance	Limited attendance for job start and stop required.
Operating Environment	Maximum room temperature of 85°F (29.4°C). Maximum room dew point of 78°F (25.6°C).
Power Requirements	230 VAC, 50/60 Hz, 3 phase, 16A/phase (20 amp dedicated circuit required)
Regulatory Compliance	CE
Software	All Fortus systems include Insight™ and Control Center™ job processing and management software.

\*PC can attain 0.005 inch (0.127mm) layer thickness when used with SP-100 soluble support.

Stratasys | [www.stratasys.com](http://www.stratasys.com) | [info@stratasys.com](mailto:info@stratasys.com)

7665 Commerce Way  
Eden Prairie, MN 55344  
+1 888 480-3548 (US Toll Free)  
+1 952 937-3000 (Intl)  
+1 952 937-0070 (Fax)

2 Holzman St.,  
Science Park, PO Box 2495  
Rehovot 76124, Israel  
+972 74 745-4000  
+972 74 745-5000 (Fax)

Local Street Address  
City, State, Zip  
Phone #  
Fax #

©2013 Stratasys Inc. All rights reserved. Stratasys, FDM and Fortus are registered trademarks and Fused Deposition Modeling, FDM Technology, Fortus 250mc, Fortus 300mc, Fortus 400mc, Fortus 900mc, Insight and Control Center are trademarks of Stratasys Inc., registered in the United States and other countries. \*ULTEM 9085 is a trademark of SABIC Innovative Plastics IP BV. All other trademarks are the property of their respective owners. Product specifications subject to change without notice. Fortus400mcSheet-US-1013

### At the core:

#### Advanced FDM Technology™

Fortus systems are based on Stratasys FDM — Fused Deposition Modeling™ — technology. FDM is the industry's leading additive manufacturing technology, and the only one that uses production grade thermoplastics, enabling the most durable parts.

Fortus systems use a wide range of thermoplastics with advanced mechanical properties so your parts can endure high heat, caustic chemicals, sterilization, and high impact applications.

#### No special facilities needed

You can install a Fortus 3D Production System just about anywhere. No special venting is required because Fortus systems don't produce noxious fumes, chemicals, or waste.

#### No special skills needed

Fortus 3D Production Systems are easy to operate and maintain compared to other additive fabrication systems because there are no messy powders or resins to handle and contain. They're so simple, an operator can be trained to operate a Fortus system in less than 30 minutes.

#### Get your benchmark on the future of manufacturing

Fine details. Smooth surface finishes. Accuracy. Strength. The best way to see the advantages of a Fortus 3D Production System is to have your own part built on a Fortus system. Get your free part at: [stratasys.com](http://stratasys.com)



**Stratasys** | Production Series

## Appendix J. Drawings

C163 – Impellers all Sizes, General Blade Forms

C168 – Thin Blade Impellers Section Dimensions

C269 – No. 8 impeller Blade Section Dimensions

C277 – Bowl Vane Dimensions type 3-4-5-6

C400 – Bowl Vane 6-7-8

UTS0001 – Exit Profile Addition

UTS0002 – Adaptor

UTS0003 – Assembly Cone Piece

UTS0004 – Proposed Modification (New Diffuser)

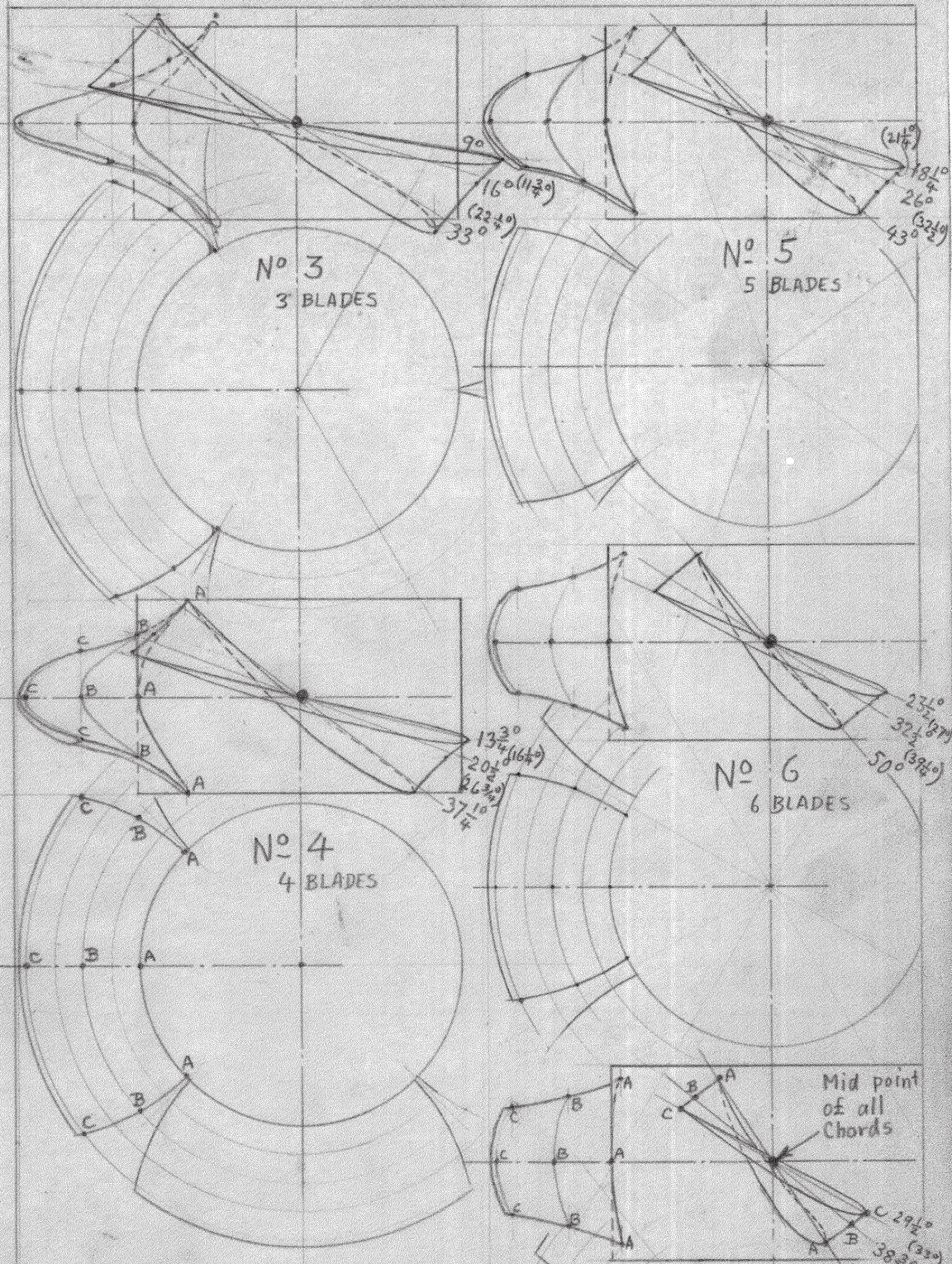
UTS0005 – Collet Drive

UTS0006 – Tail Piece, Base

UTS0007 – Tail Piece, Top

UTS0008 – Tail Piece Assembly





6  
 $4\frac{1}{4}d$   
 $3\frac{3}{8}d$   
 $2\frac{1}{2}d$   
 Max. blade  
 12.75  
 10.12  
 $7\frac{1}{2}$   
 $2.4 \text{ in } 60^\circ$   
 17.45  
 13.275  
 10.25

No 8  
 INCREASE  
 No 7 BLADE  
 $5\frac{3}{4}^\circ$

Mk II

**ORNEL TUBEWELL PUMPS ALL SIZES**

**IMPELLERS: "THIN BLADE" Types 3, 4, 5, 6, 7**

Drawn approx. to scale as follows:-

FOUR INCH 1:52:1    SIX INCH 1:1  
 FIVE INCH 1:25:1    EIGHT INCH 1:73:1

For dimensions see DR. No C. 160  
 For blade sections see separate tables.  
 Each Blade section is based upon a straight line "chord" at the angle given drawn upon the developed cylindrical surface (AAA, BBB & CCC)

SCALE	α	ORNEL TUBEWELL PUMPS
DRAWN	HBN	IMPELLERS ALL SIZES
		GENERAL BLADE FORMS.



# ORNEL SIX INCH TUBEWELL PUMP "THIN BLADE" IMPELLERS

BLADING DIMENSIONS Reference DR. NO C.163

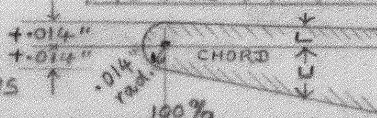
Sections are on cylindrical surfaces as follows

Outside Diameter:  $4\frac{3}{8} = .030$  " (OUTSIDE RADIUS =  $2.1750/2.1725$ )

(A=AAA at 1.250" rad.  
(AB) at 1.469" "  
B=BBB at 1.6875" "  
(BC) at 1.906" "  
C=CCC at 2.125" "

#	IMP	SECTION	CHORD			POSITION AS % OF CHORD FROM LEADING EDGE																																																																																																																																																																																																																																																																																																																																																																																																																																																																																																																				
			LEN GTH	ANGLE		90	80	70	60	50	40	30	20	10	5	2.5																																																																																																																																																																																																																																																																																																																																																																																																																																																																																																										
3	A	3.10	33°	L		-.026	-.059	-.083	-.097	-.103	-.101	-.087	-.058	-.017	+.003	+.011																																																																																																																																																																																																																																																																																																																																																																																																																																																																																																										
					U		.082	.138	.182	.217	.240	.251	.243	.207	.140	.090	.059																																																																																																																																																																																																																																																																																																																																																																																																																																																																																																									
	B	3.38	16°	L			+.006	-.001	-.004	-.005	-.002	+.002	+.008	+.017	+.025	+.025	+.022																																																																																																																																																																																																																																																																																																																																																																																																																																																																																																									
					U		.045	.070	.092	.109	.122	.129	.128	.113	.082	.056	.039																																																																																																																																																																																																																																																																																																																																																																																																																																																																																																									
	C	3.64	9°	L			+.017	+.019	+.022	+.026	+.031	+.035	+.039	+.042	+.039	+.032	+.025																																																																																																																																																																																																																																																																																																																																																																																																																																																																																																									
					U		.033	.048	.062	.073	.082	.088	.089	.081	.062	.045	.032																																																																																																																																																																																																																																																																																																																																																																																																																																																																																																									
4	A	2.46	37½°	L			-.017	-.043	-.060	-.071	-.075	-.072	-.061	-.037	-.005	+.009	+.013																																																																																																																																																																																																																																																																																																																																																																																																																																																																																																									
					U		.071	.118	.155	.185	.205	.215	.208	.179	.122	.080	.052																																																																																																																																																																																																																																																																																																																																																																																																																																																																																																									
	B	2.64	20½°	L			+.008	+.003	+.001	+.001	+.004	+.008	+.014	+.022	+.028	+.026	+.022																																																																																																																																																																																																																																																																																																																																																																																																																																																																																																									
					U		.042	.066	.085	.101	.113	.120	.119	.106	.077	.054	.037																																																																																																																																																																																																																																																																																																																																																																																																																																																																																																									
	C	2.82	13¾°	L			+.017	+.019	+.023	+.027	+.032	+.036	+.040	+.043	+.039	+.032	+.025																																																																																																																																																																																																																																																																																																																																																																																																																																																																																																									
					U		.032	.047	.060	.071	.080	.086	.087	.080	.061	.044	.032																																																																																																																																																																																																																																																																																																																																																																																																																																																																																																									
5	A	2.07	43°	L			-.011	-.031	-.045	-.052	-.054	-.051	-.038	-.020	+.006	+.015	+.016																																																																																																																																																																																																																																																																																																																																																																																																																																																																																																									
					U		.067	.110	.145	.172	.191	.201	.196	.169	.118	.078	.053																																																																																																																																																																																																																																																																																																																																																																																																																																																																																																									
	B	2.17	26°	L			+.010	+.007	+.006	+.007	+.011	+.015	+.021	+.028	+.032	+.029	+.024																																																																																																																																																																																																																																																																																																																																																																																																																																																																																																									
					U		.042	.066	.086	.102	.114	.121	.121	.108	.079	.056	.039																																																																																																																																																																																																																																																																																																																																																																																																																																																																																																									
	C	2.30	18½°	L			+.018	+.021	+.025	+.030	+.035	+.040	+.044	+.046	+.043	+.035	+.027																																																																																																																																																																																																																																																																																																																																																																																																																																																																																																									
					U		.034	.050	.065	.077	.087	.093	.094	.086	.067	.048	.034																																																																																																																																																																																																																																																																																																																																																																																																																																																																																																									
6	A	1.76	50°	L			-.007	-.025	-.036	-.043	-.044	-.040	-.030	-.013	+.009	+.016	+.017																																																																																																																																																																																																																																																																																																																																																																																																																																																																																																									
					U		.062	.101	.133	.158	.176	.185	.181	.157	.110	.073	.050																																																																																																																																																																																																																																																																																																																																																																																																																																																																																																									
	B	1.85	32½°	L			+.010	+.006	+.005	+.007	+.010	+.015	+.020	+.027	+.032	+.028	+.023																																																																																																																																																																																																																																																																																																																																																																																																																																																																																																									
					U		.042	.065	.084	.100	.112	.120	.119	.106	.079	.055	.039																																																																																																																																																																																																																																																																																																																																																																																																																																																																																																									
	C	1.95	23½°	L			+.015	+.016	+.018	+.022	+.026	+.031	+.035	+.038	+.037	+.031	+.024																																																																																																																																																																																																																																																																																																																																																																																																																																																																																																									
					U		.034	.050	.064	.076	.086	.092	.092	.084	.064	.046	.033																																																																																																																																																																																																																																																																																																																																																																																																																																																																																																									
7	A	1.53	56¾°	L			-.004	-.020	-.029	-.034	-.034	-.030	-.021	-.005	+.013	+.019	+.018																																																																																																																																																																																																																																																																																																																																																																																																																																																																																																									
					U		.060	.097	.127	.152	.169	.178	.174	.152	.107	.073	.050																																																																																																																																																																																																																																																																																																																																																																																																																																																																																																									
	B	1.58	38¾°	L			+.010	+.006	+.005	+.006	+.009	+.013	+.019	+.025	+.030	+.027	+.022																																																																																																																																																																																																																																																																																																																																																																																																																																																																																																									
					U		.041	.064	.083	.098	.110	.117	.116	.104	.076	.054	.038																																																																																																																																																																																																																																																																																																																																																																																																																																																																																																									
	C	1.66	29½°	L			+.014	+.014	+.015	+.018	+.022	+.027	+.031	+.034	+.034	+.029	+.022																																																																																																																																																																																																																																																																																																																																																																																																																																																																																																									
					U		.035	.051	.066	.078	.088	.094	.094	.086	.065	.046	.033																																																																																																																																																																																																																																																																																																																																																																																																																																																																																																									

TRAILING EDGE ALL SECTIONS



6 INCH ORNEL TUBEWELL PUMP  
"THIN BLADE" IMPELLERS  
SECTION DIMENSIONS

ORNEL PUMP COMPANY PTY/LTD.

DATE FEB 53. DR. NO 7-9C.168

Mk II



8 INCH PUMP NO 8 IMPELLER SEE ALSO DR. NO C. 169.

8	A	1.84	62 $\frac{1}{2}$ <sup>°</sup>	L	+.005	+.021	+.031	+.034	+.033	+.028	+.016	+.002	+.022	+.028	+.025
	(AB)	1.86	52 $\frac{1}{2}$ <sup>°</sup>	U	+.072	+.120	+.158	+.189	+.211	+.223	+.218	+.191	+.136	+.094	+.064
	B	1.89	45 <sup>°</sup>	L	+.008	+.003	+.002	+.003	+.007	+.013	+.020	+.029	+.036	+.033	+.027
	(BC)	1.93	39 <sup>°</sup>	U	+.051	+.081	+.107	+.128	+.143	+.152	+.150	+.134	+.099	+.069	+.048
	C	1.99	34 $\frac{3}{4}$ <sup>°</sup>	L	+.016	+.018	+.021	+.025	+.031	+.037	+.042	+.046	+.045	+.037	+.029
				U	+.041	+.062	+.080	+.097	+.109	+.116	+.117	+.106	+.081	+.058	+.041
		Length	Angle		90	80	70	60	50	40	30	20	10	5	2.5
		CHORD			POSITION AS % OF CHORD FROM LEADING EDGE										

Mk II

These dimensions for No 8 Impellers to be considered as additions to the dimension sheets for #3,4,5,6&7 Impellers for each pump size (ie. DR. NO C. 169 for 8" Pump)

Applicable to DR. No C. 160	ORNEL TUBEWELL PUMPS
" " C. 163	No 8 IMPELLERS - THIN BLADE
	SECTION DIMENSIONS
ORNEL PUMP COMPANY Pty. Ltd.	MAR. 53.   DR. No C. 269



C.L.  
Entry Exit

# SECTION DIMENSIONS: INCHES.

54° 5½° 4408

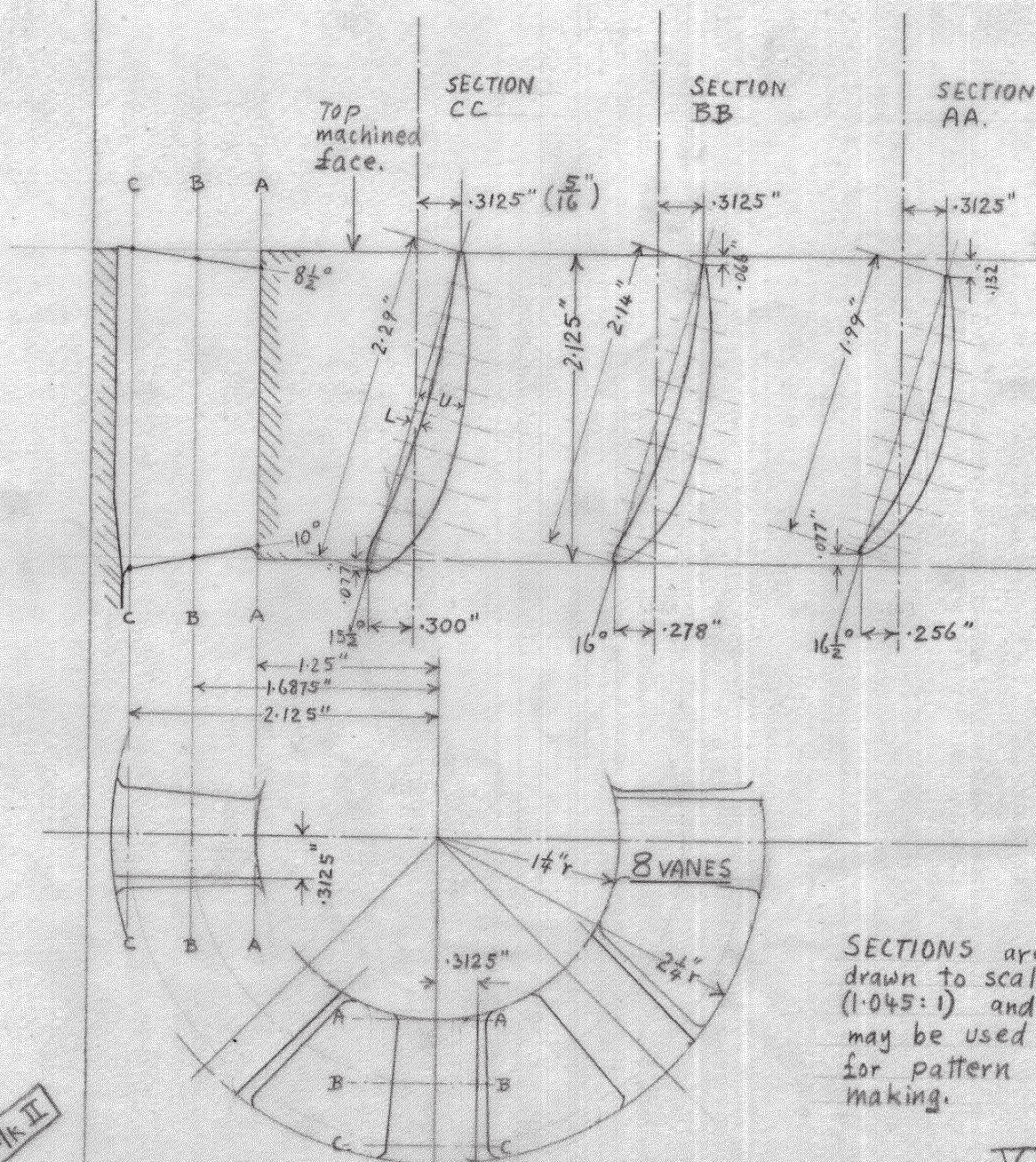
46° 1½° 4411

41° -1° 4413

		PER CENT OF CHORD FROM LEADING (LOWER) EDGE.											
		CHORD	2.5	5	10	20	30	40	50	60	70	80	90
A	1.99" 16½°	U	.066	.104	.164	.249	.295	.307	.294	.266	.224	.171	.102
		L	.001	.013	.044	.103	.143	.161	.160	.149	.126	.090	.041
B	2.14" 16°	U	.082	.123	.185	.267	.310	.319	.305	.274	.230	.174	.104
		L	.020	.015	.006	.047	.080	.097	.102	.097	.084	.059	.024
C	2.29" 15½°	U	.098	.142	.207	.292	.334	.340	.324	.291	.243	.183	.110
		L	.034	.037	.027	.007	.037	.054	.062	.063	.055	.038	.013

NOTE Sections are on flat surfaces as shown.

Trailing (top) edge, all sections  
U = .019" L = .019"



MARK II

V

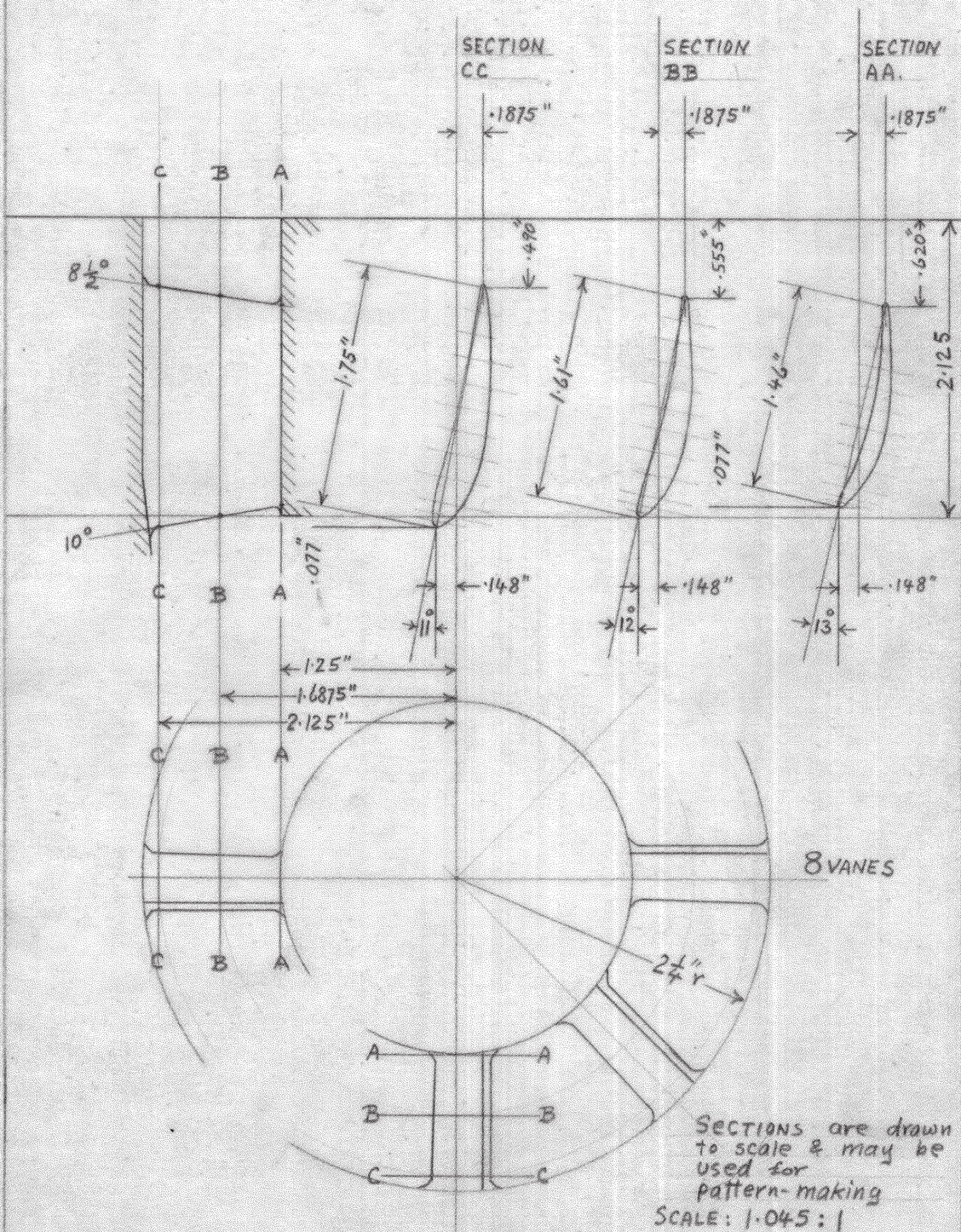
SCALE 1.045:1	ORNEL GINCH TUBEWELL PUMP
DRAWN HBM	BOWL VANE DIMENSIONS
	TYPE (3)-4-5-(6)
ORNEL PUMP COMPANY Pty. Ltd.	DATE MAR. 53
	DR. NO C. 277.



SECTION DIMENSIONS — INCHES													
			PER CENT OF CHORD FROM LEADING EDGE										
	CHORD		2.5	5	10	20	30	40	50	60	70	80	90
A	1.46	U	.050	.069	.117	.172	.203	.210	.200	.181	.152	.116	.073
		L	.007	.002	.008	.047	.071	.075	.076	.072	.068	.047	.017
B	1.61	U	.066	.095	.137	.189	.215	.218	.207	.185	.155	.118	.074
		L	.027	.031	.028	.012	.006	.017	.022	.026	.023	.014	.001
C	1.75	U	.078	.110	.154	.207	.231	.233	.218	.196	.162	.123	.077
		L	.037	.048	.054	.046	.033	.022	.014	.007	.003	.004	.011

NOTE: Sections are on flat surfaces as shown.

TRAILING EDGE: All sections  
U = .019" L = .019"

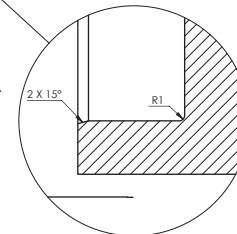
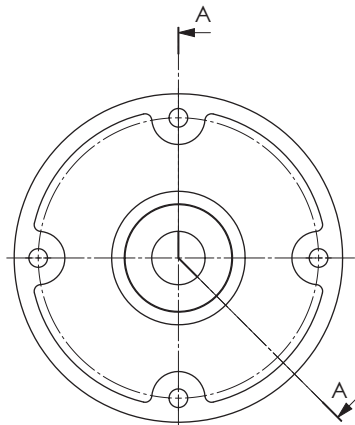
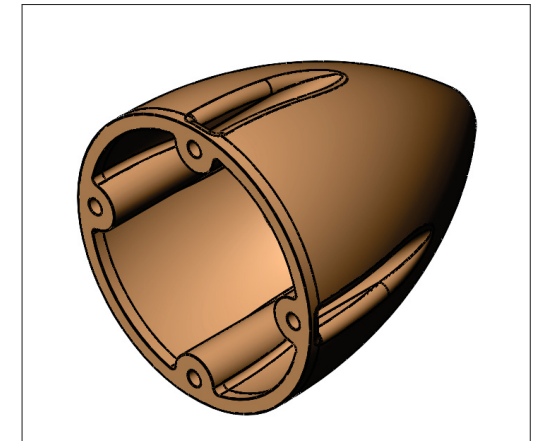



VII

SCALE 1.045:1	ORNEL 6" PUMP
H. H. H. H.	BOWL VANE 6-7-8
ORNEL PUMP COMPANY PRY. LTD.	OCT. 56.
	DR. NO C 400

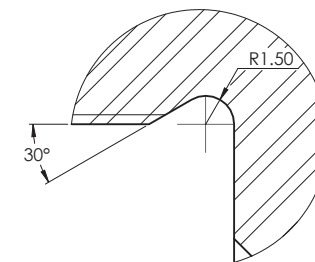
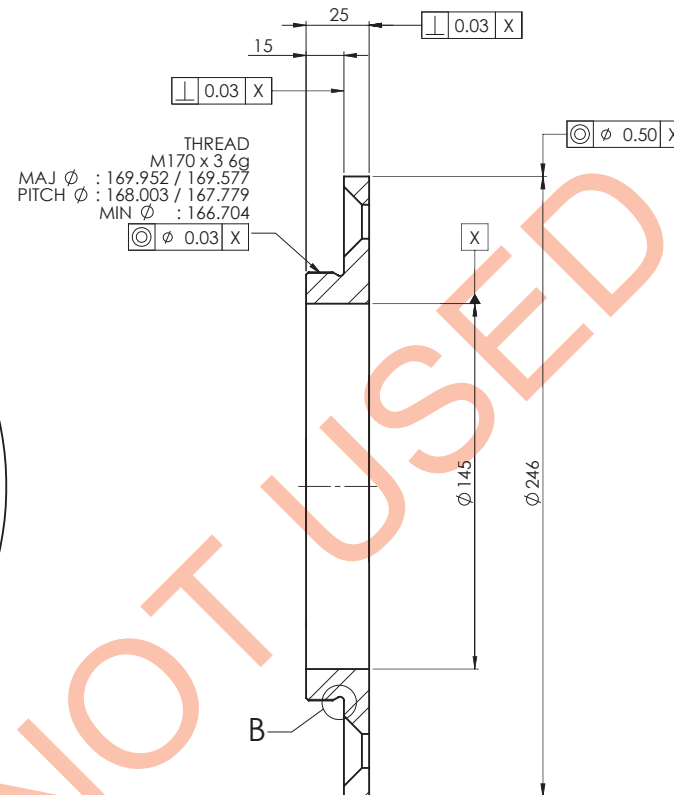
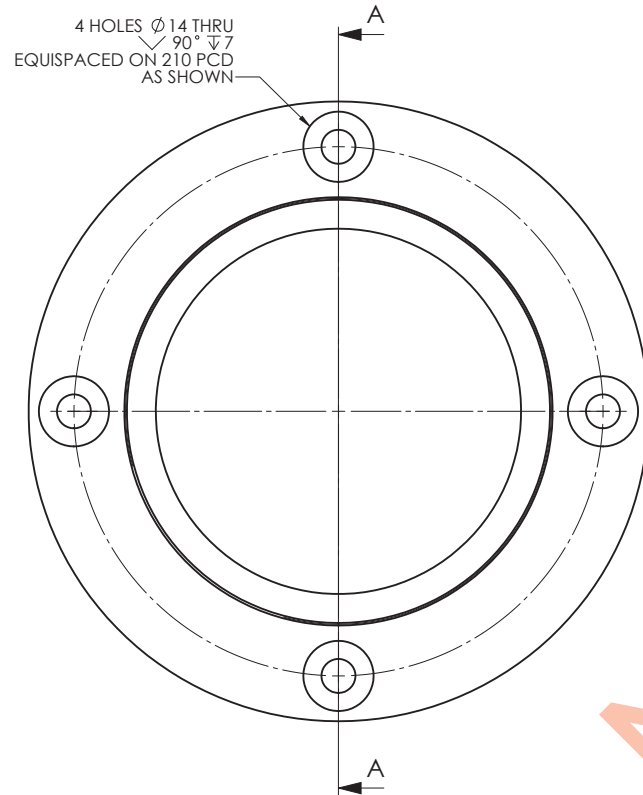


2. ALL MACHINED SURFACES TO BE  $\sqrt{3.2}$  UNLESS OTHERWISE STATED.



TITLE:			
<h1>EXIT PROFILE ADDITION</h1> <h2>MODIFIED DIFFUSER DESIGN</h2> <h3>RESEARCH - 11149580</h3>			
 <b>UTS</b> Faculty of Engineering & Information Technology	DWG NO.	UTS0001	REV 0


1. REMOVE ALL BURRS AND SHARP EDGES.
2. ALL MACHINED SURFACES TO BE  $\frac{3.2}{\sqrt{ }}$  UNLESS OTHERWISE STATED.
3. MATERIAL: AS3678-250 (MILD STEEL)



DETAIL B  
SCALE 5 : 1

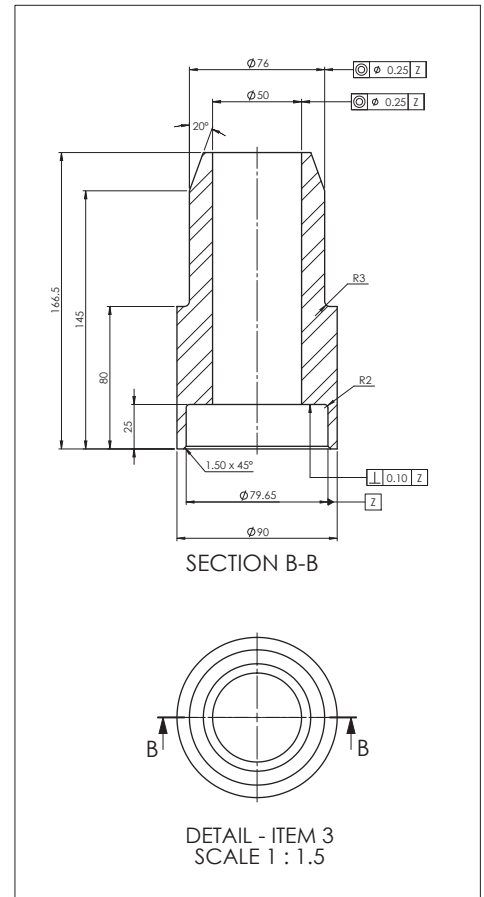
SECTION A-A

- THE FOLLOWING CONDITION APPLY UNLESS OTHERWISE SPECIFIED:
1. DIMENSIONS ARE IN MILLIMETERS
  2. SURFACE TEXTURE VALUES IN  $\mu\text{m Ra}$  (BASED ON AS1100.201)
  3. MACHINED SURFACES INDICATED AS THUS
  4. UNTOLERANCED MACHINED DIMENSIONS TO BE:  
 $\pm 0.05$  UP TO 500       $\pm 0.075$  OVER 500 TO 1000       $\pm 0.8$  OVER 1000 TO 2000  
 $\pm 1.3$  OVER 2000 TO 3000,     $\pm 2.0$  OVER 3000,    ANGULAR  $\pm 0.30^\circ$
  5. CHAMFER M/CD SHARP EDGES 1.2 TO 1.0 AT  $45^\circ$ .
  6. INTERNAL M/CD CORNER RADII 1.0 TO 0.7.
  7. DRAWING SYMBOLS BASED ON AS1100.201
  8. WELDING SYMBOLS BASED ON AS1100.3

WGT	3 kg	TITLE:	ADAPTOR 300AX STATOR MODIFICATION RESEARCH - 11149580	REV
APP'VD				
CHK'D				
DRAWN	RR			
DATE	14/02/2014	 UTS Faculty of Engineering & Information Technology	DWG NO.	
SCALE:1:1.5			UTS0002	0

- NOTES:
1. REMOVE ALL BURRS AND SHARP EDGES.
  2. ALL MACHINED SURFACES TO BE  $\sqrt{32}$  UNLESS OTHERWISE STATED
  3. ALL WELDING TO BE 3mm CONTINUOUS FILLET WELDING UNLESS SHOWN OTHERWISE, WELDS TO CONFORM TO AS1554.1 SP
  4. MACHINE THREAD AND FRONT AFTER WELDING ASSEMBLY
  5. ITEM TO BE PAINTED AS PER:

Item	Desc	Paint Manufacturer	Product Name	Min DFT (microns)
Surface Preparation	Abrasive Blast to AS1627.4 Class 2 1/2			
Primer	Epoxy Zinc Phosphate	Jotun	Penguard Special	100
Finish Coat	Alkyd Enamel	Jotun	Jotacote QD	50



BOM Table				
WGT	ITEM NO.	QTY.	DESCRIPTION	Material
2.5	1	1	RND BAR HOLLOW: 246 OD x 165 ID x 14 LD (FMS)	AS3678-250
3	2	1	SHEET: 3mm THK CUT TO SUIT	AS3678-250
4	3	1	RND BAR HOLLOW: 90 OD x 50 ID x 167 LG (FMS)	AS3678-250

APPROV'D

CHK'D

DRAWN

DATE

SCALE:1:2

14/02/2014

RR

UTS

Faculty of Engineering & Information Technology

ASSEMBLY CONE PIECE

300AX STATOR MODIFICATION

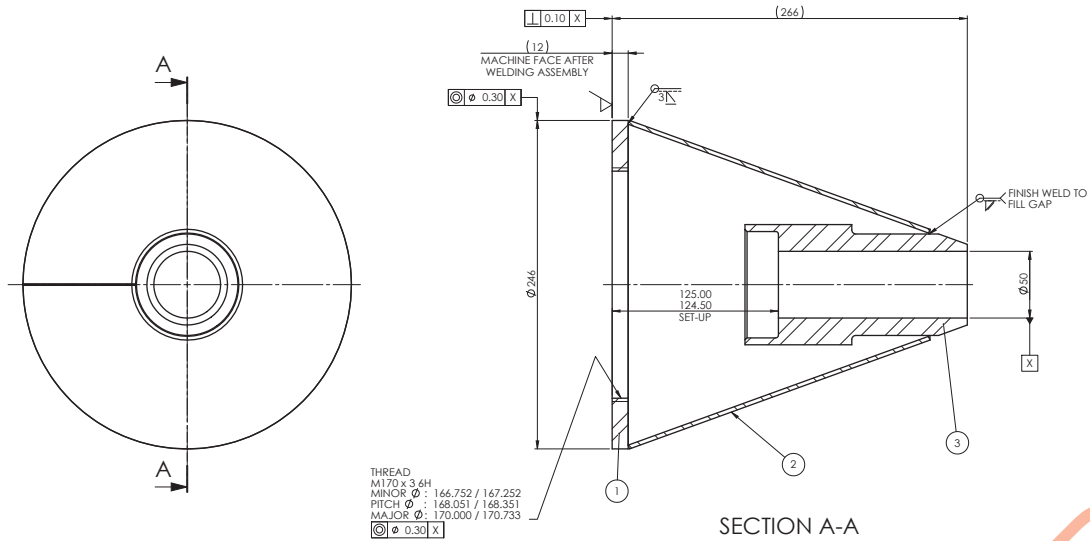
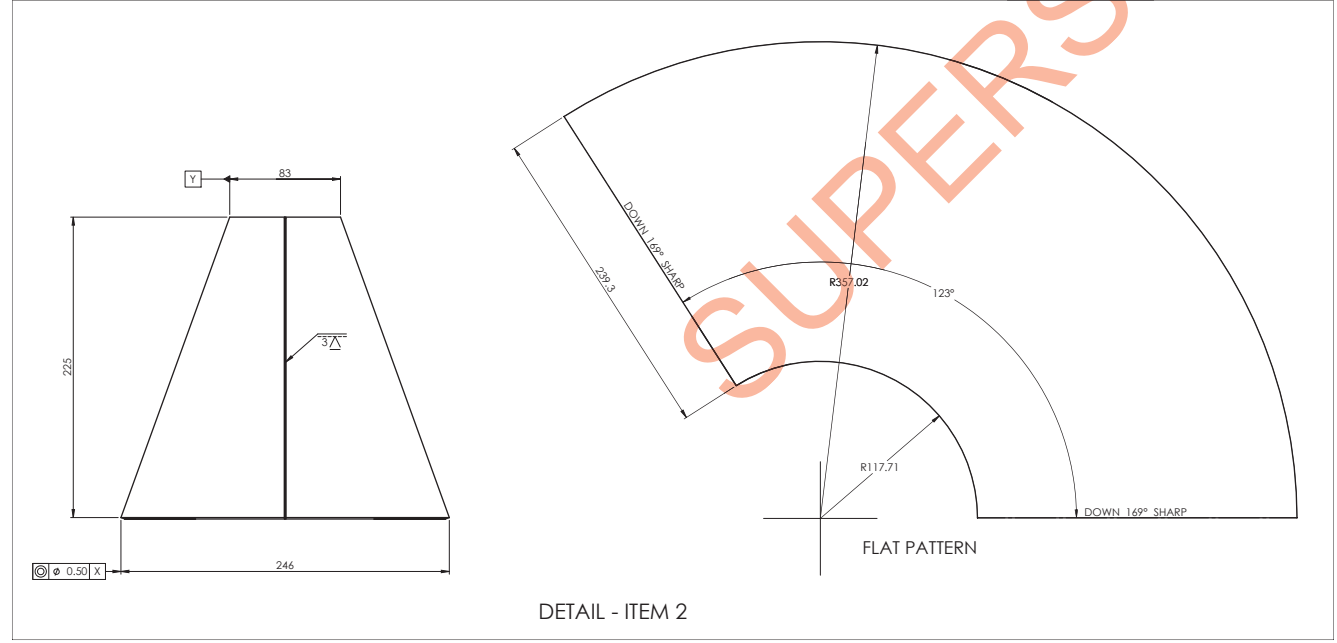
RESEARCH - 11149580

DWG NO.

UTS0003

REV

0

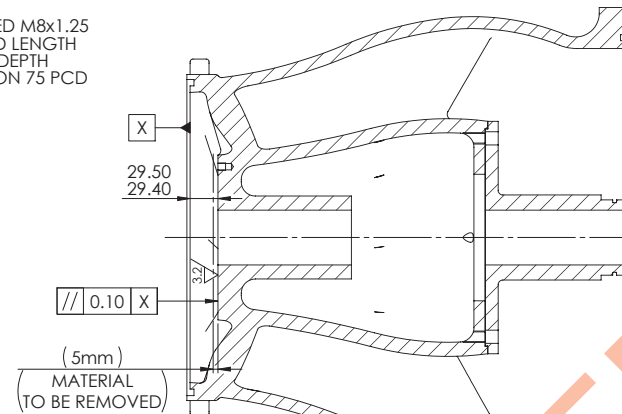
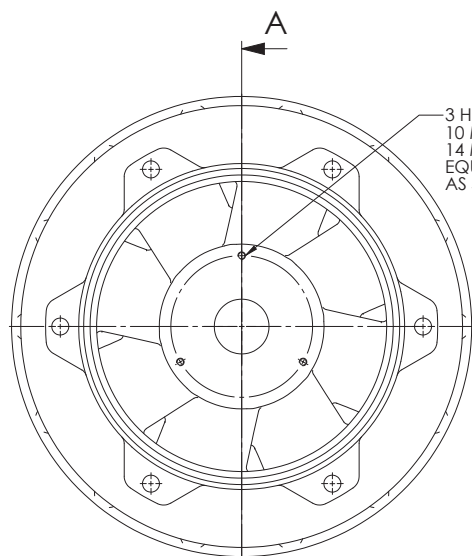


REV.	ECH No.	ECH By	DATE
1	1	RR	14/02/2014

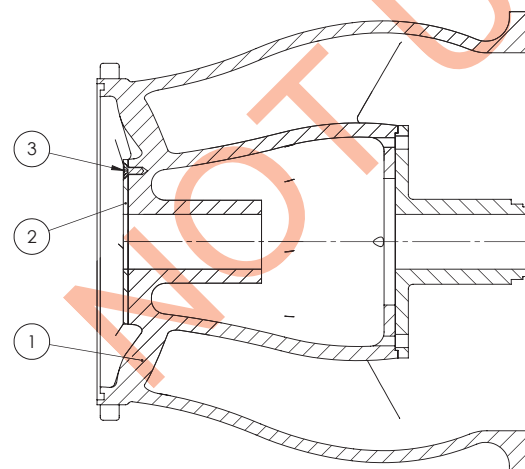
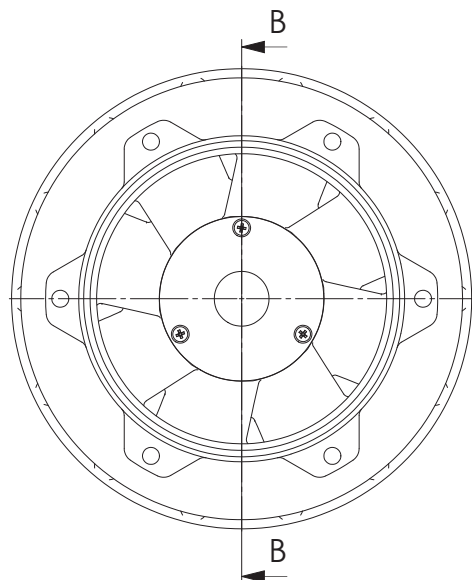
THE FOLLOWING CONDITIONS APPLY UNLESS OTHERWISE SPECIFIED:  
1. DIMENSIONS ARE IN MILLIMETRES  
2. SURFACE TEXTURE VALUES IN  $\mu m Ra$  (BASED ON AS1100.201)  
3. MACHINED SURFACES INDICATED AS THUS  
4. UNTOLERANCED MACHINED DIMENSIONS TO BE:  
 $\pm 0.25$  UP TO 500,  $\pm 0.5$  OVER 500 TO 1000,  $\pm 0.8$  OVER 1000 TO 2000  
 $\pm 1.3$  OVER 2000 TO 3000,  $\pm 2.0$  OVER 3000. ANGULAR  $\pm 0.5^\circ$   
5. CHAMFER M/C/D SHARP EDGES 1.2 TO 1.0 AT 45°  
6. INTERNAL M/C/D CORNER RADI 1.0 TO 0.7  
7. DRAWING SYMBOLS BASED ON AS1100.201  
8. WELDING SYMBOLS BASED ON AS1100.3



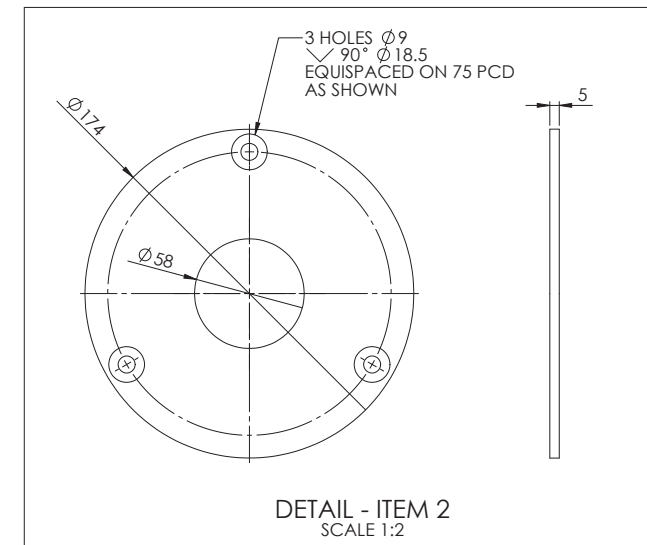
- NOTES:
1. REMOVE ALL BURRS AND SHARPE EDGES.
  2. ALL MACHINED SURFACES TO BE  $\sqrt{3.2}$  UNLESS OTHERWISE STATED.



SECTION A-A



SECTION B-B



BOM Table				
WGT	ITEM NO.	QTY.	DESCRIPTION	Material
0	1	1	NEW DIFFUSER	
0.8	2	1	PLATE: 175 OD x 75 ID x 5 THK	AS2837-316
0	3	3	COUNTER SUNK HEAD SCREW: M8 x 10 LG	

- THE FOLLOWING CONDITIOND APPLY UNLESS OTHERWISE SPECIFIED:
1. DIMENSIONS ARE IN MILLIMETERS
  2. SURFACE TEXTURE VALUES IN  $\mu m Ra$  (BASED ON AS1100.201)
  3. MACHINED SURFACES INDICATED AS THUS
  4. UNTOLERANCED MACHINED DIMENSIONS TO BE:-  
 $\pm 0.25$  UP TO 500,  $\pm 0.5$  OVER 500 TO 1000,  $\pm 0.8$  OVER 1000 TO 2000  
 $\pm 1.3$  OVER 2000 TO 3000,  $\pm 2.0$  OVER 3000, ANGULAR  $\pm 0^{\circ}30'$
  5. CHAMFER M/CD SHARP EDGES 1.2 TO 1.0 AT 45°.
  6. INTERNAL M/CD CORNER RADII 1.0 TO 0.7.
  7. DRAWING SYMBOLS BASED ON AS1100.201
  8. WELDING SYMBOLS BASED ON AS1100.3

APPV'D

CHK'D

DRAWN RR

DATE 03/05/2015

SCALE:1:4

TITLE:  
PROPOSED MODIFICATION  
NEW DIFFUSER - 300AX ORNEL PUMP  
RESEARCH - 11149580

Faculty of Engineering & Information Technology

DWG NO.  
UTS0004

REV  
0

IF IN DOUBT  
ASK

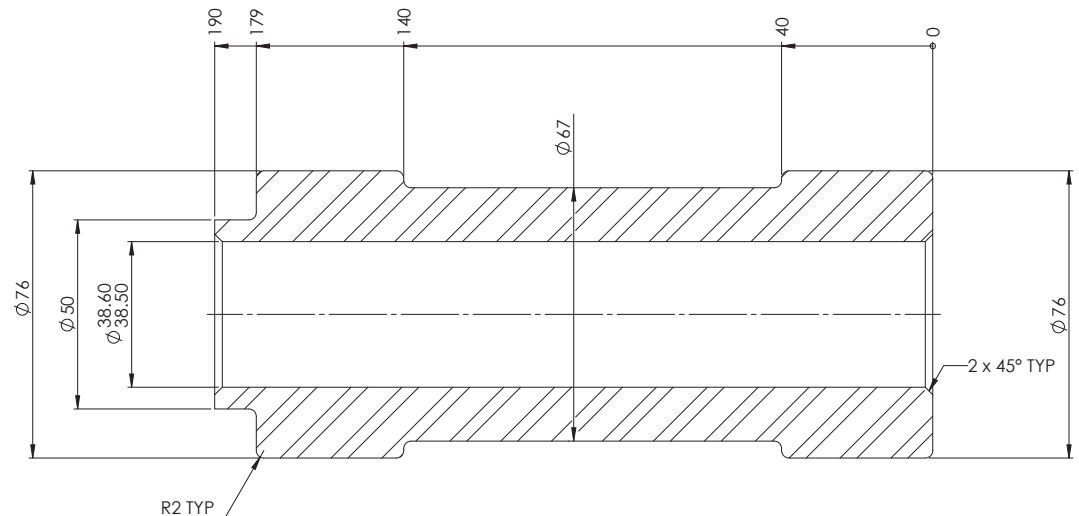
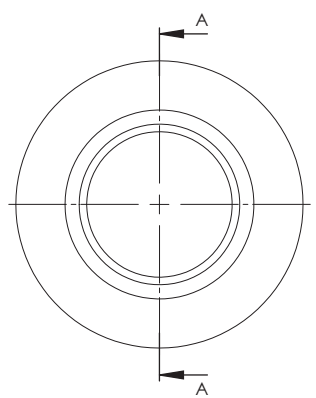
DO NOT SCALE DRAWING

THIRD ANGLE PROJECTION

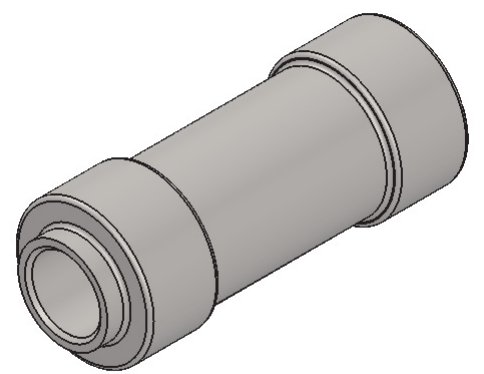


NOTES:

1. REMOVE ALL BURRS AND SHARP EDGES
2. ALL MACHINED SURFACES TO BE  $\sqrt{3.2}$ /UNLESS OTHERWISE STATED.
3. MATERIAL: AS3678-250



SECTION A-A



THE FOLLOWING CONDITIONS APPLY UNLESS OTHERWISE SPECIFIED:  
1. DIMENSIONS ARE IN MILLIMETERS  
2. SURFACE TEXTURE VALUES IN  $\mu m Ra$  (BASED ON AS1100.201)  
3. MACHINED SURFACES INDICATED AS THUS  
4. UNTOLERANCED MACHINED DIMENSIONS TO BE:-  
 $\pm 0.25$  UP TO 500,  $\pm 0.5$  OVER 500 TO 1000,  $\pm 0.8$  OVER 1000 TO 2000  
 $\pm 1.3$  OVER 2000 TO 3000,  $\pm 2.0$  OVER 3000, ANGULAR  $\pm 0^{\circ}30'$   
5. CHAMFER M/CD SHARP EDGES 1.2 TO 1.0 AT 45°.  
6. INTERNAL M/CD CORNER RADII 1.0 TO 0.7.  
7. DRAWING SYMBOLS BASED ON AS1100.201  
8. WELDING SYMBOLS BASED ON AS1100.3

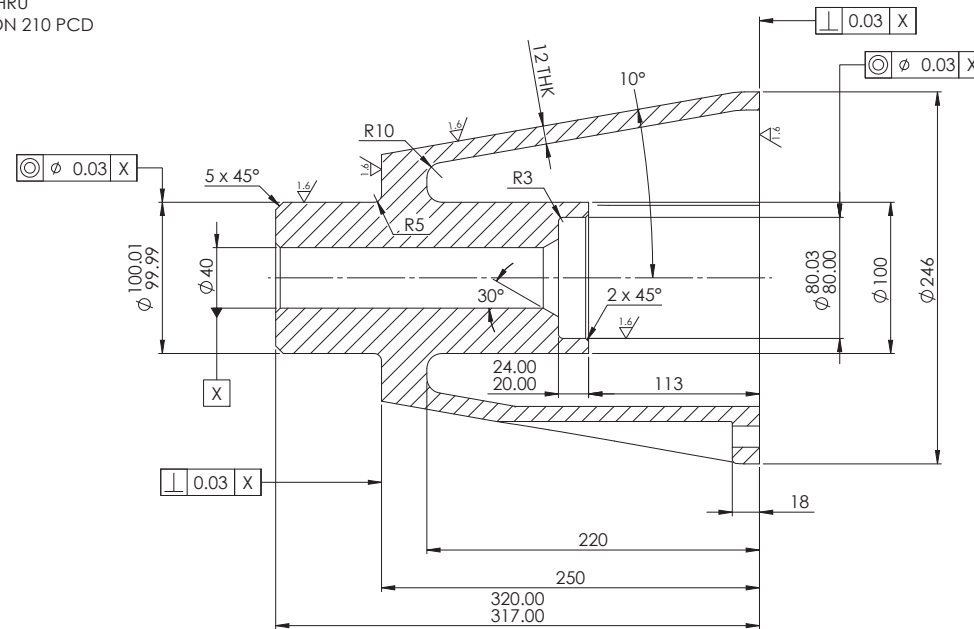
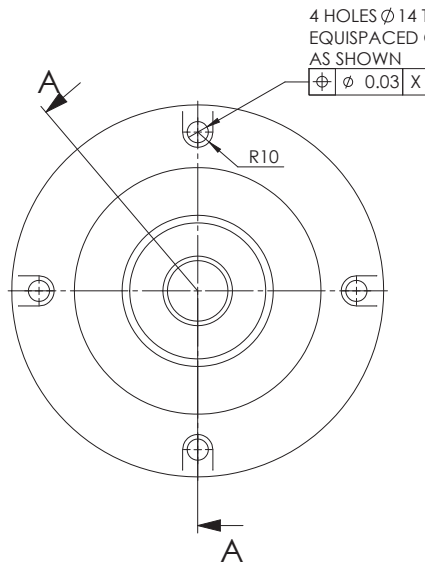
WGT	4 kg
APPV'D	
CHK'D	
DRAWN	RR
DATE	06/04/2016
SCALE:1:1	

TITLE:			COLLET DRIVE 300AX IMPELLER ASSEMBLY / DISSASSEMBLY RESEARCH - 11149580		
Faculty of Engineering & Information Technology			DWG NO.		REV
			UTS0005		0

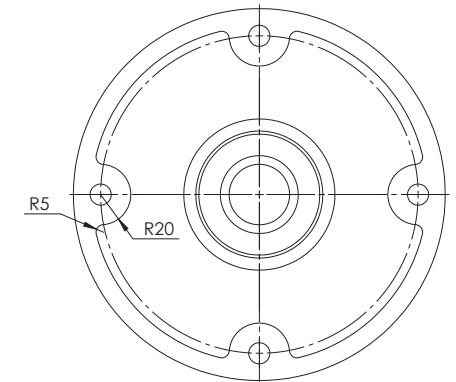
IF IN DOUBT  
ASK

DO NOT SCALE DRAWING

THIRD ANGLE PROJECTION

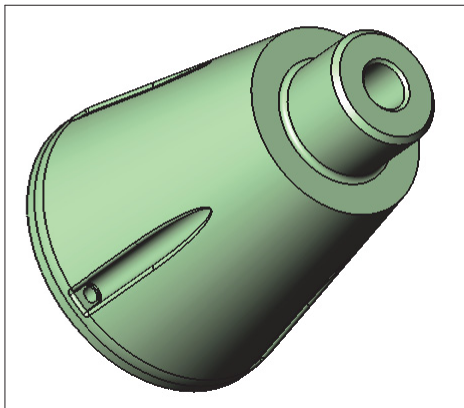
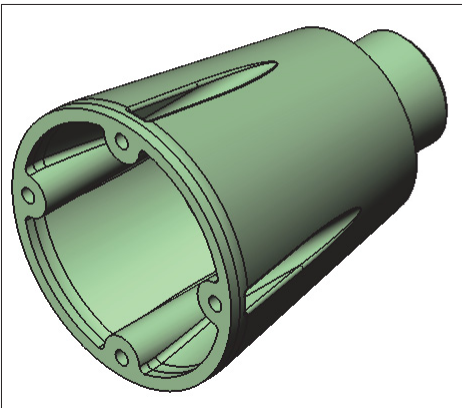


SECTION A-A



NOTES:

1. MATERIAL: ABS (ACRYLONITRILE BUTADIENE STYRENE).
2. ITEM TO BE 3D PRINTED USING THE MATERIAL OUTLINE IN NOTE 1.
3. ENSURE ALL EXTERNAL SURFACES ARE POLISHED TO BE AS SMOOTH AS POSSIBLE.



THE FOLLOWING CONDITIONS APPLY UNLESS OTHERWISE SPECIFIED:

1. DIMENSIONS ARE IN MILLIMETERS
2. SURFACE TEXTURE VALUES IN  $\mu\text{m Ra}$  (BASED ON AS1100.201)
3. MACHINED SURFACES INDICATED AS THUS
4. UNTOLERANCED MACHINED DIMENSIONS TO BE:-  
 $\pm 0.25$  UP TO 500,  $\pm 0.5$  OVER 500 TO 1000,  $\pm 0.8$  OVER 1000 TO 2000  
 $\pm 1.3$  OVER 2000 TO 3000,  $\pm 2.0$  OVER 3000, ANGULAR  $\pm 0^\circ 30'$
5. CHAMFER M/CD SHARP EDGES 1.2 TO 1.0 AT 45°.
6. INTERNAL M/CD CORNER RADII 1.0 TO 0.7.
7. DRAWING SYMBOLS BASED ON AS1100.201
8. WELDING SYMBOLS BASED ON AS1100.3

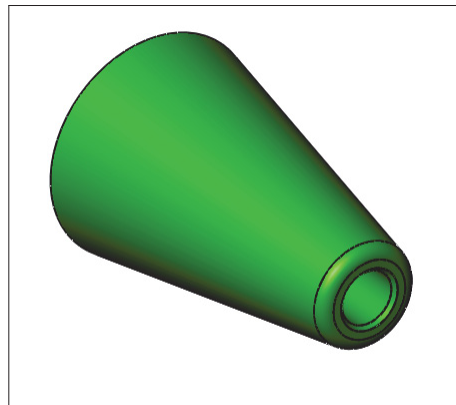
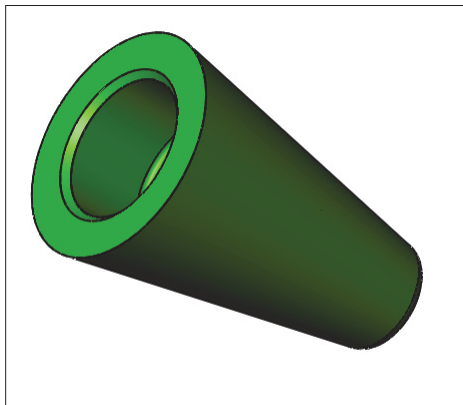
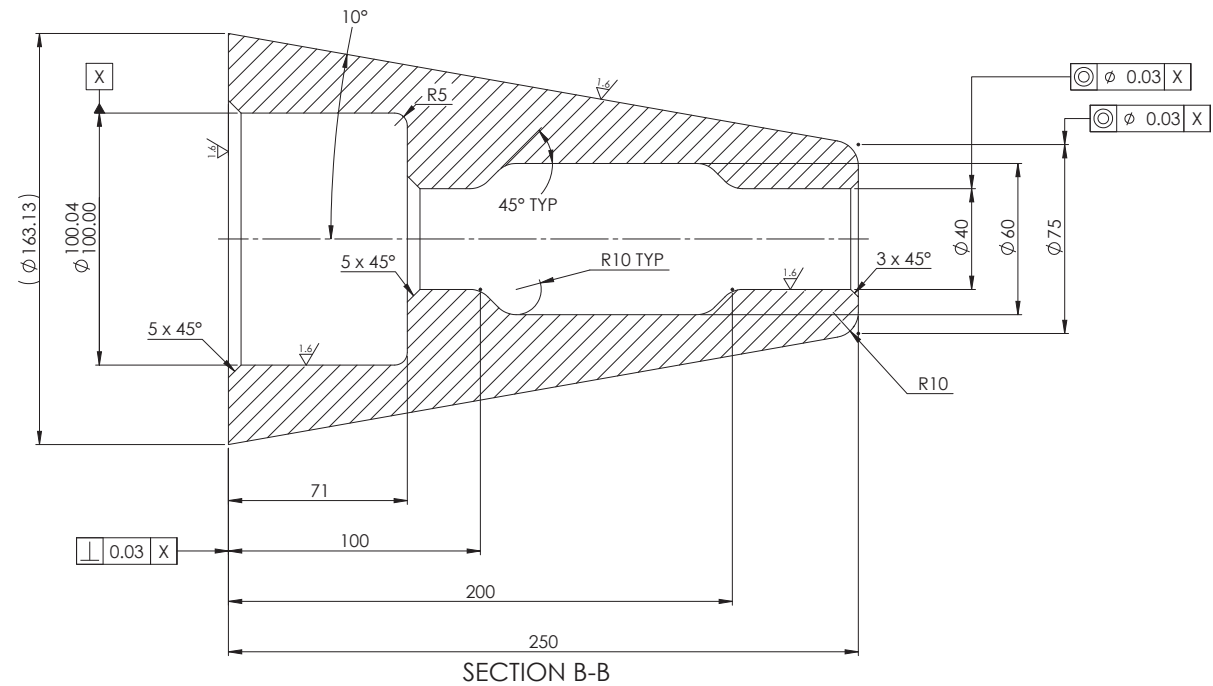
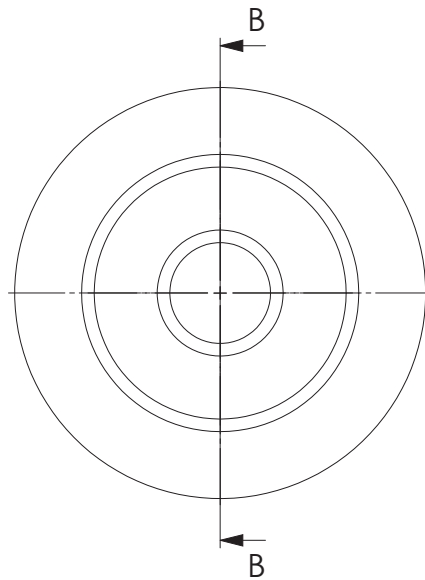
APPV'D	
CHK'D	
DRAWN	RR
DATE	19/05/2014
SCALE	1:2.5

TITLE:		DWG NO.		REV	
TAIL PIECE, BASE		UTS0006		0	
NEW DIFFUSER MODIFICATION		UTS			
RESEARCH - 11149580		Faculty of Engineering & Information Technology			

IF IN DOUBT  
ASK

DO NOT SCALE DRAWING

THIRD ANGLE PROJECTION



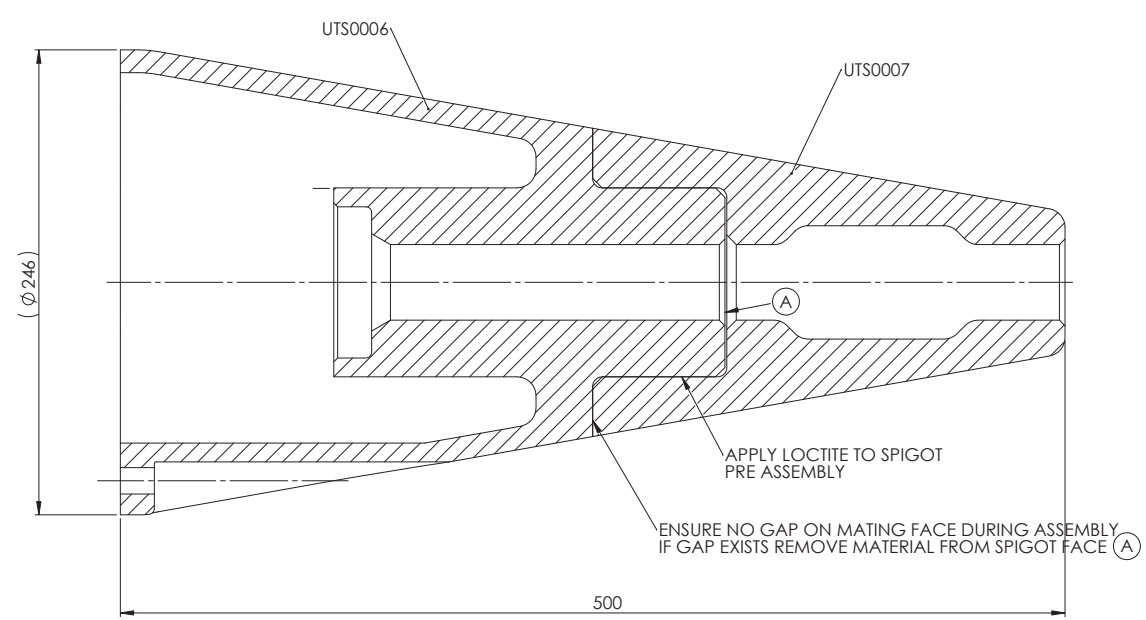
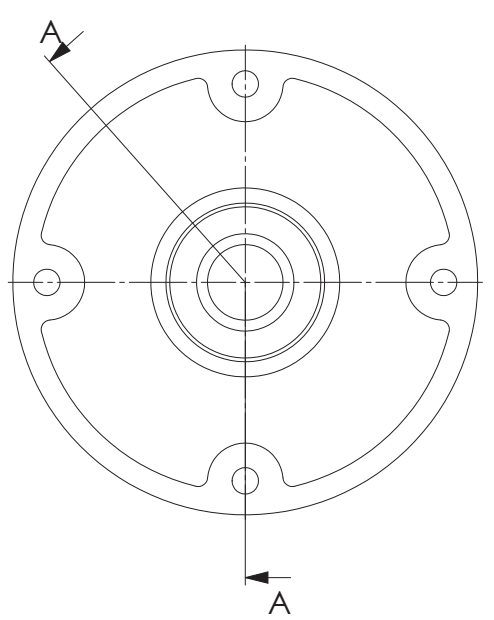
NOTES:

1. MATERIAL: ABS (ACRYLONITRILE BUTADIENE STYRENE).
2. ITEM TO BE 3D PRINTED USING THE MATERIAL OUTLINE IN NOTE 1.
3. ENSURE ALL EXTERNAL SURFACES ARE POLISHED TO BE AS SMOOTH AS POSSIBLE.

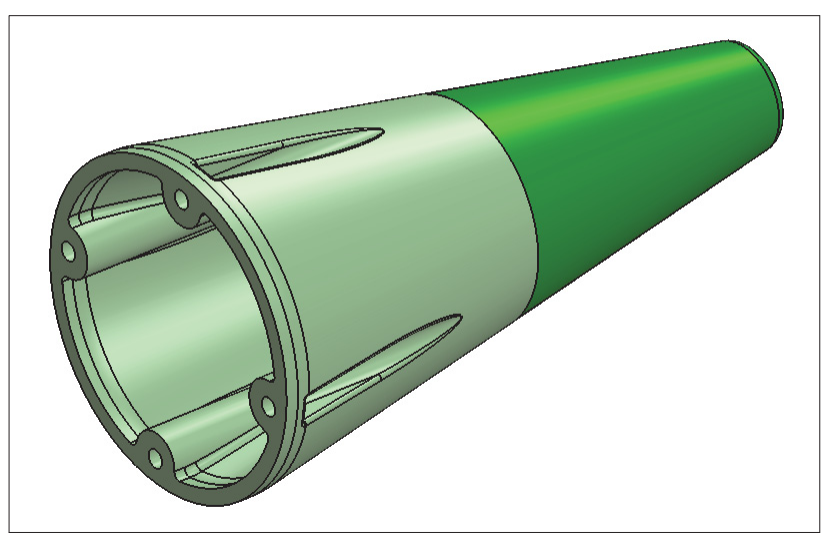
THE FOLLOWING CONDITIONS APPLY UNLESS OTHERWISE SPECIFIED:  
1. DIMENSIONS ARE IN MILLIMETERS  
2. SURFACE TEXTURE VALUES IN  $\mu m R_a$  (BASED ON AS1100.201)  
3. MACHINED SURFACES INDICATED AS THUS  
4. UNTOLERANCED MACHINED DIMENSIONS TO BE:-  
 $\pm 0.25$  UP TO 500,  $\pm 0.5$  OVER 500 TO 1000,  $\pm 0.8$  OVER 1000 TO 2000  
 $\pm 1.3$  OVER 2000 TO 3000,  $\pm 2.0$  OVER 3000, ANGULAR  $\pm 0^{\circ}30'$   
5. CHAMFER M/CD SHARP EDGES 1.2 TO 1.0 AT 45°.  
6. INTERNAL M/CD CORNER RADII 1.0 TO 0.7.  
7. DRAWING SYMBOLS BASED ON AS1100.201  
8. WELDING SYMBOLS BASED ON AS1100.3

APPV'D	
CHK'D	
DRAWN	RR
DATE	19/05/2014
SCALE	1:1.5


TITLE:		DWG NO.		REV	
TAIL PIECE, TOP		UTS0007		0	
NEW DIFFUSER MODIFICATION		UTS			
RESEARCH - 11149580		Faculty of Engineering & Information Technology			



SECTION A-A



- NOTES:
1. ENSURE ALL EXTERNAL SURFACES ARE POLISHED TO BE AS SMOOTH AS POSSIBLE.

THE FOLLOWING CONDITIONS APPLY UNLESS OTHERWISE SPECIFIED: 1. DIMENSIONS ARE IN MILLIMETERS  2. SURFACE TEXTURE VALUES IN um Ra (BASED ON AS1100:201)  3. MACHINED SURFACES INDICATED AS THUS  4. UNTOLERANCED MACHINED DIMENSIONS TO BE:- ±0.25 UP TO 500, ±0.5 OVER 500 TO 1000, ±0.8 OVER 1000 TO 2000 ±1.3 OVER 2000 TO 3000, ±2.0 OVER 3000, ANGULAR ±0°30'  5. CHAMFER M/CD SHARP EDGES 1.2 TO 1.0 AT 45°.  6. INTERNAL M/CD CORNER RADII 1.0 TO 0.7.  7. DRAWING SYMBOLS BASED ON AS1100:201  8. WELDING SYMBOLS BASED ON AS1100.3			TITLE:  TAIL PIECE,ASSEMBLY NEW DIFFUSER MODIFICATION
	APPV'D		 UTS Faculty of Engineering & Information Technology
	CHK'D		
	DRAWN	RR	
	DATE	19/05/2014	
	SCALE:1:2		DWG NO.  UTS0008
			REV  0
	6	7	8 FILE NAME: TAIL PIECE ASSEMBLY
			SHEET 1 OF 1